Pertanika Journal of

TROPICAL AGRICULTURAL SCIENCE

JTAS

VOL. 49 (S1) 2026

A Special Issue devoted to
Agricultural and Food Technologies

Guest Editors
Rosnah Shamsudin, Muhammad Hazwan Hamzah, and Maimunah Mohd Ali

PERTANIKA JOURNALS

A scientific journal published by Universiti Putra Malaysia Press

Pertanika Journal of Tropical Agricultural Science
Pertanika Journal of Tropical Agricultural Science

PERTANIKA JOURNAL OF TROPICAL AGRICULTURAL SCIENCE

About the Journal

Overview

Pertanika Journal of Tropical Agricultural Science is an official journal of Universiti Putra Malaysia. It is an open-access online scientific journal. It publishes the scientific outputs. It neither accepts nor commissions third party content.

Recognised internationally as the leading peer-reviewed interdisciplinary journal devoted to the publication of original papers, it serves as a forum for practical approaches in improving quality on issues pertaining to tropical agriculture and its related fields.

Pertanika Journal of Tropical Agricultural Science currently publishes 6 issues per year (*January, February*, *May*, *June, August*, and *November*). It is considered for publication of original articles as per its scope. The journal publishes in **English** and it is open for submission by authors from all over the world.

The journal is available world-wide.

Aims and Scope

Pertanika Journal of Tropical Agricultural Science aims to provide a forum for high quality research related to tropical agricultural research. Areas relevant to the scope of the journal include agricultural biotechnology, biochemistry, biology, ecology, fisheries, forestry, food sciences, genetics, microbiology, pathology and management, physiology, plant and animal sciences, production of plants and animals of economic importance, and veterinary medicine.

History

Pertanika was founded in 1978. Currently, as an interdisciplinary journal of agriculture, the revamped journal, *Pertanika* Journal of Tropical Agricultural Science now focusses on tropical agricultural research and its related fields.

Vision

To publish journals of international repute.

Mission

Our goal is to bring the highest quality research to the widest possible audience.

Quality

We aim for excellence, sustained by a responsible and professional approach to journal publishing. Submissions are guaranteed to receive a decision within 90 days. The elapsed time from submission to publication for the articles averages 180 days. We are working towards decreasing the processing time with the help of our editors and the reviewers.

Abstracting and Indexing of Pertanika

Pertanika Journal of Tropical Agricultural Science is now over 47 years old; this accumulated knowledge has resulted in *Pertanika* Journal of Tropical Agricultural Science being abstracted and indexed in Journal Citation Reports (JCR-Clarivate), SCOPUS (Elsevier), BIOSIS, National Agricultural Science (NAL), Google Scholar, MyCite, and ISC.

Citing Journal Articles

The abbreviation for *Pertanika* Journal of Tropical Agricultural Science is *Pertanika J. Trop. Agric. Sci*.

Publication Policy

Pertanika policy prohibits an author from submitting the same manuscript for concurrent consideration by two or more publications. It prohibits as well publication of any manuscript that has already been published either in whole or substantial part elsewhere. It also does not permit publication of manuscript that has been published in full in proceedings.

Code of Ethics

The *Pertanika* journals and Universiti Putra Malaysia take seriously the responsibility of all its journal publications to reflect the highest publication ethics. Thus, all journals and journal editors are expected to abide by the journal's codes of ethics. Refer to *Pertanika*'s **Code of Ethics** for full details, available on the official website of *Pertanika*.

Originality

The author must ensure that when a manuscript is submitted to *Pertanika*, the manuscript must be an original work. The author should check the manuscript for any possible plagiarism using any programme such as Turn-It-In or any other software before submitting the manuscripts to the Editorial Office, *Pertanika* Journal Publication Section.

All submitted manuscripts must be in the journal's acceptable **similarity index range**:
≤ 20% – *PASS*; **> 20%** – *REJECT*.

International Standard Serial Number (ISSN)

An ISSN is an 8-digit code used to identify periodicals such as journals of all kinds and on all media–print and electronic. All *Pertanika* journals have an e-ISSN.

Pertanika Journal of Tropical Agricultural Science: e-ISSN 2231-8542 (Online).

Lag Time

A decision on acceptance or rejection of a manuscript is expected within 90 days (average). The elapsed time from submission to publication for the articles averages 180 days.

Authorship

Authors are not permitted to add or remove any names from the authorship provided at the time of initial submission without the consent of the journal's Chief Executive Editor.

Manuscript Preparation

For manuscript preparation, authors may refer to *Pertanika*'s **INSTRUCTION TO AUTHORS**, available on the official website of *Pertanika*.

Editorial Process

Authors who complete any submission are notified with an acknowledgement containing a manuscript ID on receipt of a manuscript, and upon the editorial decision regarding publication.

Pertanika follows a **double-blind peer review** process. Manuscripts deemed suitable for publication are sent to reviewers. Authors are encouraged to suggest names of at least 3 potential reviewers at the time of submission of their manuscripts to *Pertanika,* but the editors will make the final selection and are not, however, bound by these suggestions.

Notification of the editorial decision is usually provided within 90 days from the receipt of manuscript. Publication of solicited manuscripts is not guaranteed. In most cases, manuscripts are accepted conditionally, pending an author's revision of the material.

The Journal's Peer Review

In the peer review process, 2 or 3 referees independently evaluate the scientific quality of the submitted manuscripts. At least 2 referee reports are required to help make a decision.

Peer reviewers are experts chosen by journal editors to provide written assessment of the **strengths** and **weaknesses** of the written research, with the aim of improving the reporting of research and identifying the most appropriate and highest quality material for the journal.

Operating and Review Process

What happens to a manuscript once it is submitted to *Pertanika*? Typically, there are 7 steps to the editorial review process:

Pertanika Journal of Tropical Agricultural Science
Pertanika Journal of Tropical Agricultural Science

1. The journal's Chief Executive Editor and Editor-in-Chief examine the paper to determine whether it is relevance to the journal's needs in terms of novelty, impact, design, procedure, language as well as presentation and allow it to proceed to the reviewing process. If it is not appropriate, the manuscript is rejected outright and the author is informed.

2. The Chief Executive Editor sends the article-identifying information having been removed, to 2 or 3 reviewers. They are specialists in the subject matter of the article. The Chief Executive Editor requests that they complete the review within 3 weeks.

   Comments to authors are about the appropriateness and adequacy of the theoretical or conceptual framework, literature review, method, results and discussion, and conclusions. Reviewers often include suggestions to strengthening of the manuscript. Comments to the editor are in the nature of the significance of the work and its potential contribution to the research field.

3. The Editor-in-Chief examines the review reports and decides whether to accept or reject the manuscript, invite the authors to revise and resubmit the manuscript, or seek additional review reports. In rare instances, the manuscript is accepted with almost no revision. Almost without exception, reviewers' comments (to the authors) are forwarded to the authors. If a revision is indicated, the editor provides guidelines to the authors to attend to the reviewers' suggestions and perhaps additional advice on how to revise the manuscript.

4. The authors decide whether and how to address the reviewers' comments and criticisms and the editor's concerns. The authors return a revised version of the paper to the Chief Executive Editor along with specific information describing how they have answered' the concerns of the reviewers and editor, usually in a tabular form. The authors may also submit a rebuttal if there is a need especially when the authors disagree with certain comments provided by the reviewers.

5. The Chief Executive Editor sends the revised manuscript out for re-review. Typically, at least 1 of the original reviewers will be asked to examine the article.

6. When the reviewers have completed their work, the Editor-in-Chief examines their comments and decides whether the manuscript is ready to be published, needs another round of revisions, or should be rejected. If the decision is to accept, the Chief Executive Editor is notified.

7. The Chief Executive Editor reserves the final right to accept or reject any material for publication, if the processing of a particular manuscript is deemed not to be in compliance with the S.O.P. of *Pertanika.* An acceptance notification is sent to all the authors.

   The editorial office ensures that the manuscript adheres to the correct style (in-text citations, the reference list, and tables are typical areas of concern, clarity, and grammar). The authors are asked to respond to any minor queries by the editorial office. Following these corrections, page proofs are mailed to the corresponding authors for their final approval. At this point, **only essential changes are accepted**. Finally, the manuscript appears in the pages of the journal and is posted online.

Pertanika Journal of

TROPICAL AGRICULTURAL SCIENCE

Vol. 49 (S1) 2026

A Special Issue devoted to
Agricultural and Food Technologies

Guest Editors
Rosnah Shamsudin, Muhammad Hazwan Hamzah, and Maimunah Mohd Ali

A scientific journal published by Universiti Putra Malaysia Press

PJTAS

***Pertanika* Journal of Tropical Agricultural Science**

AN INTERNATIONAL PEER-REVIEWED JOURNAL

Journal Section Office
Putra Science Park
1st Floor, IDEA Tower II
UPM-MTDC Technology Centre
Universiti Putra Malaysia
43400 UPM Serdang
Selangor, Malaysia

General Enquiry
Tel. No: +603 9769 1622
E-mail:
pertanika.proceeding@upm.edu.my
URL:
http://www.pertanika.upm.edu.my/

PUBLISHER
UPM Press Centre
Universiti Putra Malaysia
43400 UPM Serdang
Selangor, Malaysia
Tel: +603 9769 8855
E-mail: dir.penerbit@upm.edu.my
URL: http://penerbit.upm.edu.my

ABSTRACTING AND INDEXING OF PERTANIKA JOURNALS

The journal is indexed in Journal Citation Reports (JCR-Clarivate), SCOPUS (Elsevier), BIOSIS, National Agricultural Science (NAL), Google Scholar, MyCite and ISC.

Pertanika Journal of Tropical Agricultural Science
Vol. 49 (S1) 2026

Contents

Preface

The agricultural and food industries are undergoing rapid transformation driven by technological advancements and the increasing demand for sustainable practices. As the global population is projected to reach nearly 10 billion by 2050, food security, climate resilience, and resource efficiency have become critical concerns. The integration of cutting-edge technologies in agriculture and food production offers promising solutions to enhance productivity, reduce environmental impact, and ensure food safety. This special theme aims to explore the latest innovations in agricultural and food technologies that contribute to a more sustainable future.

This special theme will focus on recent advancements in agricultural and food technologies that support sustainable development. It will cover a wide range of topics, including but not limited to:

- Precision agriculture and smart farming
- Sustainable food production and processing
- Biotechnology and genetic advancements
- Post-harvest and food preservation technologies
- Agri-food supply chain and circular economy

Guest Editor
Rosnah Shamsudin (Prof. Ts. Dr.)
Muhammad Hazwan Hamzah (Ts. Dr.)
Maimunah Mohd Ali (Dr.)

Pertanika J. Trop. Agric. Sci. 49 (S1): 1 - 30 (2026)

PERTANIKA JOURNALS

TROPICAL AGRICULTURAL SCIENCE

Journal homepage: http://www.pertanika.upm.edu.my/

Review Article

Comparative Evaluation of Ground-based, Manual, and Remote Sensing Approaches for Crop Stress Detection: A Review between Malaysia and China

Ahmad Syafik Suraidi Sulaiman[1, 2]*, Aimrun Wayayok[2,3], Leifeng Guo[4], Samsuzana Abd. Aziz[2], and Mui Yun Wong[3]

[1]Department of Biological and Agricultural Engineering, Faculty of Engineering, Universiti Putra Malaysia, 43400 UPM Serdang, Selangor, Malaysia
[2]Smart and Precision Agriculture Programme, Engineering Research Centre, MARDI Headquarters, 43400 Serdang, Selangor, Malaysia
[3]Institute of Plantation Studies (IKP), Jalan Maklumat, 43400 Serdang, Seri Kembangan, Selangor, Malaysia
[4]Agricultural Information Institute, Chinese Academy of Agricultural Sciences (CAAS), No. 12, Zhongguancun South Street, 100081 Beijing, People's Republic of China (PRC)

ABSTRACT

This study presents a comparative evaluation of manual inspection, ground-based sensors, and UAV-based remote sensing for detecting crop stress in paddy, maize, and coconut fields across Malaysia and China. Although sensing technologies have advanced considerably, cross-country comparisons between regions with differing levels of technological maturity remain limited. China, recognised for its advanced adoption of UAV and sensor-based agriculture, provides a benchmark against Malaysia's developing digital agriculture landscape. Each method was assessed based on accuracy, responsiveness, scalability, and cost-effectiveness under field conditions. UAV-based remote sensing achieved the highest overall accuracy (mean 92%) and demonstrated superior scalability, enabling rapid large-area monitoring using vegetation indices such as NDVI and NDRE. Ground-based sensors, including soil moisture probes and chlorophyll meters, showed moderate accuracy (mean 81%) and were suitable for plot-level monitoring with real-time feedback. Manual inspection recorded the lowest accuracy (mean 68%) and limited scalability due to labour dependency and subjective assessment. UAV methods were particularly effective in early stress detection, with thermal imaging identifying canopy temperature anomalies 3–5 days before visible symptoms, especially in

ARTICLE INFO

Article history:
Received: 18 July 2025
Accepted: 18 December 2025
Published: 19 March 2026

DOI: https://doi.org/10.47836/pjtas.49.S1.01

E-mail addresses:
syafik@mardi.gov.my (Ahmad Syafik Suraidi Sulaiman)
aimrun@upm.edu.my (Aimrun Wayayok)
guoleifeng@caas.cn (Leifeng Guo)
samsuzana@upm.edu.my (Samsuzana Abd. Aziz)
muiyun@upm.edu.my (Mui Yun Wong)
* Corresponding author

maize and coconut fields. Integrating UAV and ground-based sensing provided more comprehensive and timely assessments than individual approaches. These findings support the development of scalable precision agriculture frameworks tailored to tropical and subtropical systems.

Keywords: AI, China, crop stress, ground sensing, Malaysia, manual inspection, NDVI, remote sensing

INTRODUCTION

Early and accurate detection of crop stress is critical for sustainable agriculture, efficient resource use, and stable food production, particularly under increasing climatic pressures. Crop stress, whether from pests, diseases, drought, or salinity, can significantly reduce yields if not identified and addressed promptly (Bela, 2023). In large-scale farming systems, timely monitoring remains a challenge due to limited accessibility and field size, often delaying effective management decisions (Umutoni & Samadi, 2024). Traditional methods such as manual inspection are widely used but are labour-intensive, subjective, and lack scalability (Mylonas et al., 2022).

In response, sensing technologies are gaining prominence in precision agriculture. Ground-based tools like chlorophyll meters and soil probes provide accurate, site-specific data (Soussi et al., 2024), while Unmanned Aerial Vehicles (UAVs) and satellite platforms deliver rapid, spatially extensive monitoring using indicators like Normalised Difference Vegetation Index (NDVI) and canopy temperature (Sharma et al., 2025). The integration of multispectral imaging with Artificial Intelligence (AI) analytics has further enhanced detection accuracy and decision-making efficiency (Cho et al., 2024).

Figure 1 presents a conceptual framework that outlines the integration of various sensing technologies for detecting crop stress and supporting farm-level decision-making. The process begins with environmental inputs such as climate, soil, and topography, which significantly influence crop growth and stress conditions, including water scarcity, nutrient deficiencies, pest infestations, and temperature extremes.

Monitoring these stress factors involves manual methods like visual inspections and leaf colour charts, and ground-based sensors that measure soil moisture, electrical conductivity, and chlorophyll content. These are complemented by remote sensing tools, including UAVs, satellites, and hyperspectral or thermal imaging systems, which enable large-scale and detailed monitoring.

The gathered data is transmitted through IoT networks and cloud platforms for acquisition and fusion, where it is processed using machine learning, artificial intelligence, and crop models to provide actionable insights. Ultimately, this information supports adaptive farm management strategies such as precise irrigation scheduling, fertigation, and pest control, enhancing crop productivity and sustainability through informed and timely interventions.

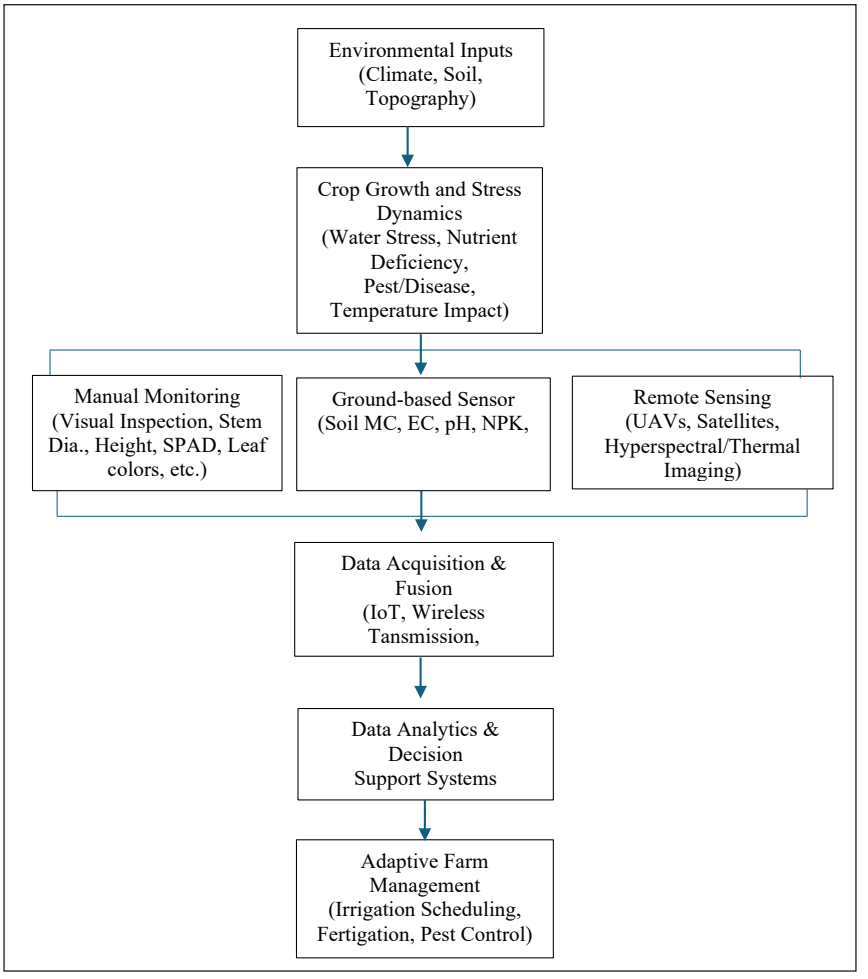

Figure 1. Conceptual framework of sensing technologies for crop stress detection

Despite rapid advancements in agricultural sensing technologies, their adoption across many parts of Asia, particularly in developing regions, remains limited (Gamage et al., 2024). Challenges such as high initial costs, insufficient technical training, and inconsistent infrastructure continue to hinder large-scale implementation. As a result, many farmers still depend on manual crop monitoring, which is labour-intensive, subjective, and often unreliable in complex field environments (Tian et al., 2020). Moreover, there is a scarcity of comparative field-based studies assessing the effectiveness and practicality of different sensing methods across diverse agroecological zones like Malaysia and China.

This study addresses that gap by evaluating the performance of manual inspection, ground-based sensors, and UAV-based remote sensing for detecting crop stress in paddy, maize, and coconut fields. It examines each method's accuracy, responsiveness, and practical

usability under real-world conditions. The research also considers limitations posed by factors such as cloud interference in Moderate Resolution Imaging Spectroradiometer (MODIS) satellite imagery and variations in sensor calibration. By highlighting both the strengths and constraints of each approach, this study aims to inform more targeted and scalable precision agriculture practices tailored to tropical and subtropical farming systems.

Crop Stress: Definition and Indicators

Crop stress can be defined as any condition that adversely affects the growth, development, and yield of crops. Stress can arise from both biotic and abiotic factors. Biotic stresses are those caused by living organisms, such as pathogens, pests, and weeds, which damage crops directly or indirectly (Kour et al., 2025). These stresses can result in diseases like fungal or bacterial infections, insect damage, and competition for resources. On the other hand, abiotic stress is caused by environmental factors like temperature extremes, drought, soil salinity, and pollution, which directly or indirectly impact plant physiology (Sanaeifer et al., 2023).

Among the various abiotic stress factors, water stress remains the most significant challenge for crop production. Water scarcity during key growth stages of crops leads to reductions in yield and quality (Guo et al., 2025). Temperature stress, particularly heat stress, can cause cellular damage, reduce photosynthesis, and compromise overall plant health (Saewong et al., 2024). Salinity stress interferes with plant water uptake and nutrient absorption, leading to stunted growth and poor productivity (Hualpa-Ramirez et al., 2024). Crops that are subjected to multiple stresses simultaneously may exhibit compounded negative effects, making early detection critical for intervention (Pascual et al., 2022).

To effectively manage crop stress, a range of indicators can be monitored, including Normalised Difference Vegetation Index (NDVI), canopy temperature, moisture levels, and chlorophyll content. NDVI is a widely used remote sensing indicator that helps assess plant health based on the reflection of sunlight from vegetation (Zhao and Qu, 2024). NDVI values typically increase with healthy vegetation, while decreases indicate stress conditions (Essaadia et al., 2022).

Canopy temperature, which can be monitored through infrared thermometers or thermal cameras, rises in response to water stress and heat stress, providing a reliable indication of crop health (González-Dugo et al., 2010).Moisture levels are essential to understanding drought stress and are often assessed through soil moisture sensors or vegetation water content measurements (Tangjialeke et al., 2024). Chlorophyll content, which can be assessed through leaf tissue analysis or optical sensors, is a key indicator of plant photosynthetic capacity and health (Wang et al., 2024). Table 1 provides a summary of various crop stress indicators and the sensing methods used for their detection.

Table 1
Summary of various crop stress indicators and the sensing methods used for their detection

Stress Indicator	Physiological Basis	Sensing Method	Sensor Type / Platform	Reference(s)
NDVI (Normalised Difference Vegetation Index)	Changes in chlorophyll content and canopy structure	Spectral reflectance	Multispectral sensors (UAV, satellite, handheld)	Zhao & Qu (2024); Essaadia et al. (2022)
Canopy Temperature	Elevated leaf temperature due to reduced transpiration	Thermal infrared imaging	Infrared thermography (ground-based, UAV)	Jones et al. (2009); Prashar & Jones (2014)
Leaf Moisture Content	Dehydration of leaf tissue under stress	NIR and SWIR spectroscopy	Proximal hyperspectral sensors	Sanaeifar et al. (2023)
Chlorophyll Fluorescence	Disruption in photosynthetic electron transport	Fluorometry	Fluorescence sensors (e.g., PAM fluorometres)	Kour et al. (2025)
Soil Moisture	Availability of water to plant roots	Dielectric sensing	TDR/Capacitive probes, IoT soil sensors	Saeed et al. (2022); Tangjialeke et al. (2024)
Relative Water Content (RWC)	Degree of cell hydration	Gravimetric and pressure chamber methods	Manual/laboratory techniques	Guo et al. (2025)
SPAD (Chlorophyll Index)	Total leaf chlorophyll content	Leaf transmittance	SPAD handheld metres	Saewong et al. (2024)
Vegetation Indices (e.g., SAVI, EVI)	Enhanced detection under sparse vegetation or varied light	Spectral reflectance	Satellite or UAV-based multispectral imaging	Essaadia et al. (2022); Li et al. (2023)
Stomatal Conductance	Closure of stomata under water stress	Porometry	Porometres (leaf-level)	Hualpa-Ramirez et al. (2024)
Leaf Colour Changes	Anthocyanin or senescence-induced discolouration	RGB imaging	Cameras (ground-based or UAV)	Pascual et al. (2022)

Manual Methods for Crop Stress Detection

While modern technologies are reshaping crop stress detection, manual methods continue to play a vital role, especially in resource-limited settings. Visual inspection remains one of the most traditional and widely used techniques, involving the direct observation of symptoms such as leaf discolouration, wilting, or reduced growth (Lau & Tov, 2023).

Although such observations are quick and inexpensive, they are often subjective and highly dependent on the observer's expertise. Nonetheless, visual assessments are still

valuable for initial stress identification and are frequently used in conjunction with more advanced diagnostic tools (Chakhvashvili et al., 2024).

Complementary manual methods include leaf and soil sampling, both of which provide deeper insights into plant health. Leaf analysis through laboratory testing can reveal nutrient deficiencies or detect pathogens, making it useful for identifying both abiotic and biotic stress factors (Kou et al., 2024; Zhang et al., 2023). For instance, low nitrogen levels in leaves may indicate nutrient stress (Francis et al., 2023).

Similarly, soil testing can identify underlying issues like pH imbalance or salinity, which often contribute to stress symptoms (Faqir et al., 2024; Tarolli et al., 2024). Despite their diagnostic accuracy, both approaches are time-consuming, require laboratory infrastructure, and lack scalability for large-scale real-time monitoring, limiting their broader application in precision agriculture.

Table 2 summarises the advantages and limitations of various manual crop management methods, highlighting their practical relevance. Manual harvesting ensures high-quality produce with minimal crop damage and environmental impact, but is labour-intensive and less scalable, making it suitable for high-value or organic crops. Manual weeding allows precise, chemical-free weed control, yet requires significant labour, limiting feasibility in large fields or regions with scarce labour.

Hand cultivation, such as hoeing, is low-cost and effective for small or irregular plots but physically demanding and inefficient at scale. Manual pruning and thinning improve plant health and yield by selectively removing diseased or crowded parts, though it demands skilled labour and time. Hand pollination is essential for controlled breeding and greenhouse environments, ensuring pollination where natural pollinators are absent, but it is impractical for large-scale operations. Collectively, these methods remain critical in specialised, smallholder, or organic farming systems where precision and crop quality are prioritised.

Table 2
The advantages and limitations of these manual methods offering insights into their relevance for crop management

Manual Method	Advantages	Limitations	Relevance for Crop Management
Manual Harvesting	• Allows precise selection of ripe produce, enhancing quality. • Reduces crop damage compared to mechanical methods. • Environmentally friendly; no fuel use.	• Labour-intensive and time-consuming. • Higher labour costs. • Limited scalability for large operations.	• Suitable for high-value crops where quality is critical. • Beneficial in regions with abundant labour. • Preferred in organic systems with minimal mechanical intervention.

Table 2 *(continued)*

Manual Method	Advantages	Limitations	Relevance for Crop Management
Manual Weeding	• Precise weed removal without harming crops. • No chemical residues; environmentally safe.	• Labour-intensive, especially for large fields. • Not feasible where labour is scarce or costly.	• Effective for small-scale or organic farming. • Useful where chemical herbicides are restricted or undesirable.
Hand Cultivation (e.g., hoeing)	• Simple tools; low cost. • Effective in small or irregular plots. • Minimal soil disturbance.	• Physically demanding. • Inefficient for large-scale operations.	• Ideal for smallholder farms and gardens. • Useful for spot treatments and hard-to-reach areas inaccessible to machinery.
Manual Pruning and Thinning	• Enhances air circulation and sunlight penetration. • Allows selective removal of diseased or damaged parts.	• Requires skilled labour. • Time-consuming.	• Important for crop health and yield optimisation. • Common in fruit orchards and vineyards.
Hand Pollination	• Ensures pollination when natural pollinators are absent. • Allows control over genetic crosses.	• Labour-intensive. • Not practical for large-scale crops.	• Essential in controlled breeding programs. • Useful in greenhouse or isolated environments.

**Source: Amanullah (2024a and 2004b)*

Ground-based Sensing Techniques

Ground-based sensing techniques have gained significant traction in recent years due to their ability to provide continuous, real-time data on crop health. Technologies such as IoT devices, handheld NDVI sensors, and soil moisture probes have become integral to precision agriculture (Zhang et al., 2024). These systems enable farmers to closely monitor crop conditions and manage resources efficiently, thus optimising productivity. IoT-based systems, for example, offer high spatial and temporal resolution, allowing continuous tracking of various environmental parameters such as soil moisture, temperature, and humidity (Dhanaraju et al., 2022). By providing real-time data, these systems allow for precise adjustments in irrigation and fertilisation, helping mitigate stress and improve crop yields (Mba et al., 2025; Rajak et al., 2023).

Handheld NDVI sensors, known for their affordability and portability, are also widely used in the field to assess plant health. These sensors measure light reflection at specific wavelengths, enabling early detection of stress before visible symptoms appear (Le et al., 2023). However, their effectiveness can be influenced by environmental factors such as light intensity and soil type, which can impact their accuracy (Zhang et al., 2024). Additionally,

soil moisture probes play a crucial role in managing water stress, one of the most common stressors in agriculture. These probes provide direct measurements of soil water content, which can be used to optimise irrigation schedules and prevent water wastage (Rasheed et al., 2022).

Figure 2 illustrates a typical setup of ground-based sensors in crop monitoring systems, including a leaf wetness sensor, which measures the duration and presence of moisture on leaf surfaces. This is critical for predicting the onset of foliar diseases, scheduling irrigation, and assessing microclimatic conditions that influence crop health. By providing real-time, site-specific information, the leaf wetness sensor enhances decision-making for disease management and irrigation planning, particularly in high-value crops where timely interventions can significantly impact yield and quality.

Table 3 compares various sensing methods based on accuracy, cost, advantages, and limitations. Soil moisture sensors offer high accuracy at a low to moderate cost but are limited to moisture measurement and require calibration. Leaf Area Index (LAI) is effective for vegetation analysis, but may need multiple sensors for larger areas. Electromagnetic Induction (EMI) is good for soil analysis, but is expensive and energy-intensive. Thermal infrared sensing provides non-invasive stress data, though it's sensitive to environmental factors. Portable chlorophyll meters are fast and non-destructive, but limited to leaf analysis. Drone-based imaging offers large-scale coverage, but requires skilled operators and has high costs. Ground Penetrating Radar (GPR) is useful for soil structure, but it is costly and specific to certain soil types.

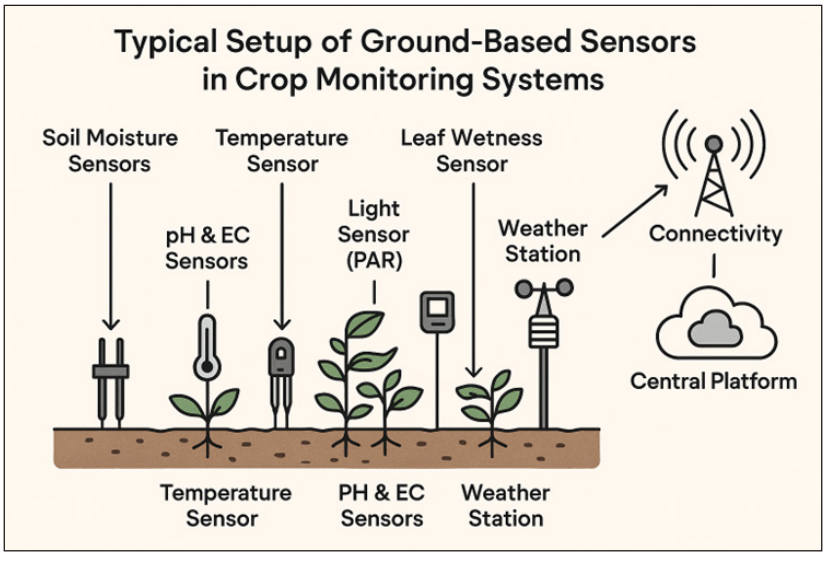

Figure 2. Typical setup of ground-based sensors used in crop monitoring systems

Table 3
Comparison of the accuracy and cost of different ground-based sensing methods

Sensing Method	Accuracy	Cost	Advantages	Limitations
Soil Moisture Sensor	± 2-5%	Low to Moderate ($50-$500)	High accuracy for moisture content measurement in soil	Limited to soil moisture; calibration required
Leaf Area Index (LAI)	± 2-3%	Moderate ($300-$2000)	Effective for vegetation analysis; non-destructive	May require multiple sensors for large areas
Electromagnetic Induction (EMI)	± 5-10%	High ($1000-$5000)	Good for soil salinity and texture analysis	Expensive; high energy consumption
Thermal Infrared Sensing	± 1-3%	Moderate ($500-$3000)	Non-invasive; provides information on plant water stress	Requires clear sky conditions; sensitive to environmental factors
Portable Chlorophyll Meter	± 1-2%	Moderate ($100-$1000)	Fast and non-destructive chlorophyll measurement	Limited to leaf analysis only
Drone-Based Imaging	± 3-5%	High ($2000-$10000)	Provides large-scale coverage with detailed imagery	Requires skilled operator; high initial cost
Ground Penetrating Radar (GPR)	± 10-15%	High ($3000-$15000)	Suitable for soil structure and depth analysis	High cost; limited to specific soil conditions

*Source: Prasad et al. (2021)

Ground Vehicle Mounted Sensing Technologies

Ground vehicle-mounted sensing platforms (GVMS) have rapidly gained attention as an intermediate approach between handheld tools and aerial remote sensing for crop stress detection. Typically mounted on tractors, ATVs, or small autonomous vehicles, GVMS integrate multispectral and hyperspectral cameras, thermal imagers, LiDAR scanners, chlorophyll meters, and soil probes to capture high-resolution data along crop rows (Sharma et al., 2025). Operating close to the canopy, these systems provide finer spatial detail and more stable signal quality than UAVs, even under cloudy, windy, or restricted-flight conditions (Unde et al., 2025).

Modern GVMS units leverage improvements in vibration damping, real-time processing, and machine learning based classification to detect subtle physiological changes such as early water stress, nutrient imbalances, canopy temperature anomalies, and biomass variations well before they are visually apparent (Wu et al., 2025). Moreover, their deployment alongside routine field operations such as fertiliser application or weeding allows continuous monitoring without additional labour, enhancing operational feasibility in large-scale and high-intensity farming systems (Mansoor et al., 2025).

Despite these strengths, practical constraints influence GVMS adoption across diverse farming systems. Field accessibility remains challenging in flooded paddy fields, steep

terrains, or perennial crop plantations with narrow inter-row spacing, while sensor fouling, vibration-induced signal noise at higher speeds, and reduced GNSS accuracy under dense canopies can limit data reliability if not carefully managed (Mat Lazim et al., 2020). International comparisons indicate that highly mechanised systems, such as those in China, achieve greater throughput and precision due to better road access, wider row spacing, and widespread use of RTK-equipped tractors (Jensen et al., 2025).

A growing consensus in the literature emphasises the benefits of integrating GVMS with UAV reconnaissance for a hybrid stress-monitoring approach, UAVs for rapid field-wide scanning and GVMS for detailed, row-level diagnostics while highlighting the ongoing need for affordable, standardised sensor modules and harmonised data-processing workflows to support broader adoption, particularly in tropical environments (Munasinghe et al., 2024).

Remote Sensing Technologies

Remote sensing technologies, such as satellite imagery and UAV-based platforms, offer powerful tools for monitoring crop stress on a large scale. Satellite systems like MODIS and Sentinel provide continuous, wide-area coverage, making them ideal for assessing crop health over large agricultural regions (Karmakar et al., 2024). MODIS, for instance, can capture data on vegetation indices such as NDVI, which provides a quantitative assessment of plant health. Sentinel satellites, with their higher spatial resolution, are particularly useful for monitoring smaller-scale agricultural areas (Heiss et al., 2025).

UAVs provide an alternative to satellite imagery, offering high-resolution, real-time data that can be tailored to specific fields (Rahman et al., 2024). UAVs are equipped with multispectral or hyperspectral cameras that capture detailed images of crop canopies, which are then analysed to assess plant health. UAVs offer the advantage of being able to capture data at a much higher frequency than satellites, providing farmers with more frequent updates on crop conditions. However, UAVs are limited by their flight range and battery life, making them suitable for smaller, more localised areas (Kramarić et al., 2025).

Vegetation indices such as NDVI, SAVI (Soil Adjusted Vegetation Index), and EVI (Enhanced Vegetation Index) are commonly used in remote sensing to assess plant health and stress (Fadl et al., 2024). These indices are calculated based on the reflectance of light at different wavelengths and are sensitive to changes in vegetation cover, chlorophyll content, and canopy structure (Gu et al., 2025). NDVI, in particular, is widely used to detect crop stress due to its simplicity and effectiveness in differentiating between stressed and healthy plants (Balasundaram et al., 2024). Figure 3 provides an example of NDVI imagery captured from satellite or UAVs, highlighting its utility in large-scale crop monitoring.

Table 4 compares different technologies for crop monitoring based on cost, spatial resolution, frequency of data acquisition, and key characteristics. Satellite imagery (e.g., Sentinel-2) is cost-effective and suitable for large-scale monitoring, with a spatial resolution

Figure 3. NDVI imagery captured from satellite or UAVs in large-scale crop monitoring

Table 4
Key characteristics of each technology, including cost, spatial resolution, and frequency of data acquisition

Technology	Cost	Spatial Resolution	Frequency of Data Acquisition	Remarks
Satellite (e.g., Sentinel-2)	Low (free access)	10-20 m	Every 5-10 days	Suitable for regional to global scale monitoring (Sothe et al., 2017).
Satellite (e.g., Planet Scope)	High (subscription)	3-5 m	Daily	Commercial service with high revisit and finer details (le Roux et al., 2021).
UAV (multispectral camera)	Medium-High (initial setup)	1-10 cm	On-demand (manual flight missions)	High flexibility and detail; limited by battery/labour (Deng et al., 2018).
Ground-based sensors (e.g., handheld NDVI, chlorophyll meters)	Low-Medium	Point-based/local	Continuous or user-defined intervals	High accuracy; useful for calibration and ground truthing (Zhao et al., 2025).
IoT soil/water sensors	Medium (installation + maintenance)	Point-based/local	Real-time/ continuous	Good for micro-environment monitoring (soil/temp/moisture) (Comegna et al., 2024).
Manned aircraft (with hyperspectral sensors)	Very high	1-5 m	Scheduled (limited due to cost/logistics)	Effective for larger farms; not cost-efficient for smallholders (Tsouros et al., 2019).

of 10-20 meters and data available every 5-10 days. In contrast, commercial services like Planet Scope offer higher spatial resolution (3-5 m) with daily data acquisition but come at a higher cost. UAVs with multispectral cameras provide high flexibility and detail with a resolution of 1-10 cm, though they are limited by battery life and manual operation.

Ground-based sensors, such as handheld NDVI and chlorophyll meters, offer high accuracy and are useful for calibration, with continuous or user-defined data intervals. IoT sensors offer real-time, continuous monitoring of micro-environmental conditions but require medium-level investment. Manned aircraft with hyperspectral sensors provide detailed data for larger farms but are costly and less suitable for small-scale operations.

Role of AI in Sensing

The role of artificial intelligence (AI) in crop stress detection has been growing rapidly, with machine learning techniques being applied to a variety of sensing data sources. AI models have shown great promise in improving the accuracy and efficiency of crop monitoring systems by integrating data from multiple sources, such as remote sensing platforms, IoT devices, and ground-based sensors (Parra-López et al., 2025). These models are capable of classifying crop conditions, predicting stress, and optimising resource management strategies, making them invaluable tools for precision agriculture (Aarif et al., 2025).

Machine learning algorithms are particularly effective in processing large datasets from various sensing technologies. For example, convolutional neural networks (CNNs) have been used for image classification, allowing for the identification of stress symptoms from UAV or satellite imagery (Upadhyay et al., 2025). These algorithms can detect subtle changes in vegetation health that may be missed by traditional methods, providing early warnings of stress conditions (Lee et al., 2025).

AI models can also integrate data from multiple sources, such as soil moisture sensors and weather data, to create predictive models for stress events (Pandey and Mishra, 2024). This allows for more proactive management of crop health, reducing the need for reactive measures like emergency irrigation or pesticide application (Taha et al., 2025).

Evaluation Criteria and Comparative Metrics

The reviewed studies were assessed based on four primary criteria: accuracy, cost, scalability, and ease of use, which are key to determining their applicability in real-world agricultural practices across diverse agro-ecological zones in Malaysia and China. Accuracy is critical in ensuring the reliability of crop stress detection methods. Vegetation indices such as NDVI and EVI, derived from satellite and UAV imagery, are commonly used to assess plant health, with strong correlations to physiological stress indicators. However, factors like atmospheric interference, sensor type, and image calibration can influence the accuracy of remote sensing data. On the other hand, ground-based IoT sensors offer high

precision at a local scale but may lack the broad spatial representation provided by remote sensing technologies.

Cost is another important factor, particularly in resource-constrained settings. While satellite imagery from open-access platforms like Sentinel is free, high-resolution UAV imagery and commercial satellite services like PlanetScope come with considerable expenses. Ground-based sensors are relatively affordable, though they incur installation and maintenance costs. The cost-effectiveness of each method depends on farm scale and the availability of technical support.

Scalability is also vital for widespread adoption; satellite imagery works well for regional monitoring but may miss small-scale stress patterns, whereas UAVs offer detailed insights but are limited by coverage area, weather conditions, and battery life. IoT sensors are modular and adaptable for both smallholder and large commercial farms. Finally, ease of use is influenced by system complexity and required user training. While manual inspections are simple, they are less effective for early detection. In contrast, IoT and remote sensing technologies require specialised knowledge for deployment and interpretation, making user-friendly interfaces and automated analytics essential for adoption by farmers with limited technical expertise.

Comparative Analysis Framework

To facilitate a structured comparison, a multi-criteria decision-making (MCDM) approach was adopted, enabling the ranking of crop stress detection methods based on predefined criteria such as accuracy, cost, scalability, and usability. Studies such as Gunawan et al. (2024) have successfully applied MCDM frameworks to identify optimal stress monitoring solutions tailored to specific cropping systems.

Additionally, regression and statistical modelling were used in select studies to quantitatively compare technologies. For instance, Zhang et al. (2019) conducted a regression-based evaluation of UAV imagery and IoT soil data to identify water stress in maize, revealing that UAVs were superior for detecting large-scale variability, while IoT sensors were better suited for identifying localised nutrient-related stress.

Figure 4 presents different crop stress detection technologies, visualising their strengths and trade-offs. The integration of multi-source data using machine learning techniques has also emerged as a promising trend. Rashid et al. (2025) combined UAV, IoT, and satellite data using a deep learning architecture to improve detection accuracy and contextual interpretation. This integrated approach enhances prediction reliability and allows a holistic view of crop health under varying climatic and soil conditions.

Ultimately, the comparative evaluation outlined in this methodology supports evidence-based decision-making for selecting suitable stress detection methods in diverse agricultural landscapes across Malaysia and China. Future studies should focus on hybrid systems that

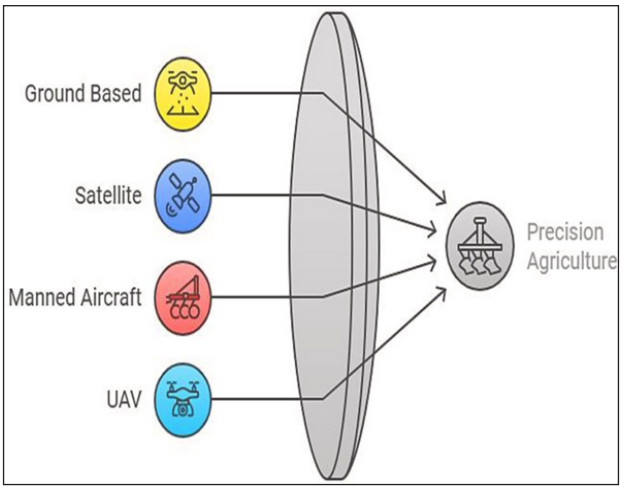

Figure 4. Different crop stress detection technologies (Rashid et al., 2025)

combine ground-based and remote sensing data within unified machine learning platforms for intelligent, real-time crop stress monitoring.

Performance of Manual Methods

Manual inspection remains one of the most commonly used methods for stress detection in crops. While this method is simple and inexpensive, it is often limited by its subjective nature and dependency on the skill of the observer. In terms of accuracy, manual observation is generally less reliable compared to more advanced technological methods. Studies have reported a high degree of variability in accuracy, with field inspectors often missing subtle signs of crop stress, particularly in the early stages (Tian et al., 2011).

The time required for manual inspection is another key consideration. Typically, manual observation can take hours or even days to cover large areas, depending on the crop type and field size (Sun et al., 2024). This is particularly challenging for large-scale farming operations, where the time and labour required can significantly impact productivity. Additionally, environmental conditions such as weather can affect the accuracy and efficiency of manual inspections, as rain, high winds, or excessive heat can obscure visual symptoms of stress.

Despite these limitations, manual inspection does have its advantages in providing a quick and relatively low-cost method for identifying overt stress symptoms, especially in cases where high-tech solutions may not be feasible (Walsh et al., 2024). Table 5 summarises the observed stress detection accuracy for manual inspection across different crop types and environments, highlighting the challenges in accuracy and the factors influencing it.

Ground-based Sensor Performance

Ground-based sensors have gained significant attention for real-time crop monitoring due to their ability to measure environmental parameters continuously. These sensors are typically placed in the field to monitor key variables such as soil moisture, temperature, and nutrient levels, which directly affect crop health (Shahab et al., 2025). In terms of real-time data quality, ground-based sensors provide a high level of reliability, with measurements that are frequently updated and capable of reflecting short-term changes in the crop environment (Velazquez-Chavez et al., 2024).

Table 5
Stress detection accuracy for manual inspection across different crop types and environments

Crop Type	Environment	Stress Detection Accuracy (%)
Wheat	Field (Dry Conditions)	85
Wheat	Field (Wet Conditions)	78
Corn	Greenhouse	92
Corn	Field (Dry Conditions)	88
Soybean	Field (Dry Conditions)	80
Soybean	Field (Wet Conditions)	76
Rice	Paddy Field	95
Rice	Greenhouse	91
Tomato	Field (Dry Conditions)	89
Tomato	Greenhouse	90

*Source: Walsh et al. (2024)

Figure 5 presents time-series data for soil moisture, NDVI, and temperature measurements collected from a set of ground sensors. The data highlights the temporal fluctuations in crop health indicators over a growing season, demonstrating how ground-based sensors can be used to track stress over time.

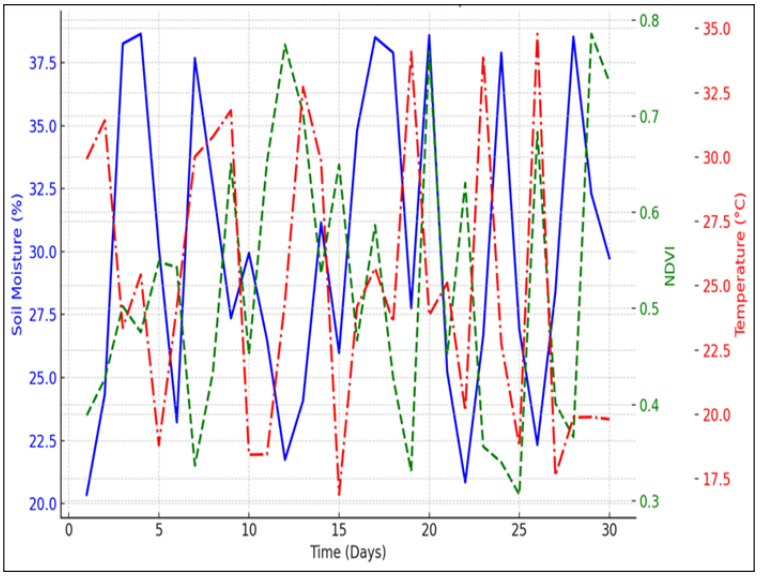

Figure 5. Time-series data for soil moisture, NDVI, and temperature measurement (Olawade et al.,2024)

Table 6 provides a comparison of sensor performance across different study locations, offering insight into how environmental factors influence the reliability and accuracy of the data.

Table 6
Comparison of sensor performance across different study locations

Country	Sensor Type	Environmental Factors	Sensor Accuracy	Reliability	Key Observations
Malaysia	Soil Moisture Sensor	High humidity, fluctuating temperatures, heavy rainfall	±2%	High	Performed well in tropical field conditions (Ahmad and Hashim, 2007).
Malaysia	Soil Temperature Sensor	High ambient temperatures, low humidity	±3%	Moderate	Performance slightly reduced due to sensor heating (Sulong et al., 2023).
China	pH Sensor	Dry inland climate, low rainfall, stable temperatures	±1.5%	Very High	Reliable for long-term deployment in drylands (Wang et al., 2024).
China	EC Sensor	Coastal zone, saline soil, high wind exposure	±5%	Low	Accuracy compromised by saline interference (Zhou et al., 2024).
Malaysia	NPK Sensor	Mixed lowland climate, moderate rainfall, occasional fog	±4%	Moderate	Sensor readings varied with environmental moisture (Ahmad and Hashim, 2007).

Remote Sensing Results

Remote sensing technologies, including UAVs and satellite imagery, have become increasingly popular for large-scale crop monitoring. These technologies provide the advantage of extensive spatial coverage, making them ideal for assessing crop stress over large agricultural areas (Dong et al., 2024). However, the resolution of the imagery plays a significant role in the effectiveness of stress detection. High-resolution imagery from UAVs allows for detailed observations of the crop canopy, enabling the detection of subtle stress symptoms that may be missed in low-resolution satellite images (Iheaturu et al., 2024).

In addition to resolution, weather conditions can also impact the reliability of remote sensing data. Cloud cover, for example, can obstruct satellite imagery, leading to incomplete data and gaps in monitoring (Chen et al., 2025). UAV-based imagery, while less affected by weather conditions, may face limitations such as reduced flight time and range, particularly when covering large areas (Yadav et al., 2024). To improve the accuracy of stress detection, artificial intelligence (AI) models have been applied to process remote sensing data, providing more accurate classifications of crop health.

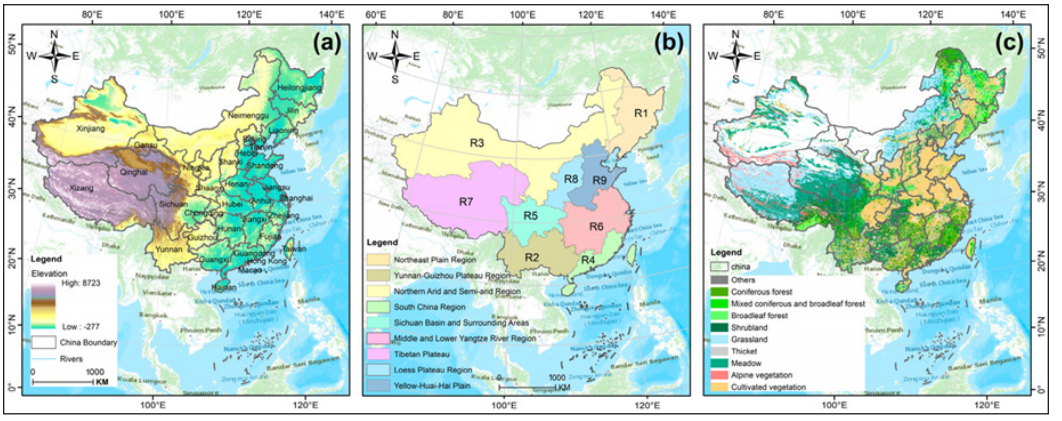

Figure 6. Spatial distribution of (a) elevation, (b) subregions of China and (c) vegetation types. (Ma et al., 2025)

Figure 6 illustrates the spatial distribution of key geographical and ecological attributes across China. Subfigure (a) presents the elevation map, highlighting topographic variations where the western regions, such as the Tibetan Plateau, feature higher elevations, while the eastern areas are characterised by lower altitudes. Subfigure (b) shows the subregional divisions of China, commonly used in environmental and agricultural studies, capturing ecological and climatic diversity across the country. Lastly, subfigure (c) depicts the distribution of vegetation types, illustrating dominant plant cover such as forests, grasslands, croplands, and barren lands.

Figure 7 illustrates remote sensing-based stress detection in four major crop types cultivated in Malaysia: paddy, oil palm, rubber, and vegetables. The multispectral or infrared satellite images show spatial patterns of crop stress, with red areas indicating stressed zones due to factors like drought, nutrient deficiency, or disease, while green areas signify healthy vegetation. In the paddy field quadrant, patchy red zones suggest irregular irrigation or pest infestations (Shaharum et al., 2020).

The oil palm quadrant displays circular plantation arrangements, with stress visible in scattered patches, possibly due to uneven soil moisture or disease. The rubber plantation appears mostly green, indicating minimal stress, likely due to uniform management and stable canopy health. In the vegetable quadrant, alternating red and green bands highlight variations in plant health across rows, which could be linked to differences in fertilisation, irrigation, or crop type diversity.

Table 7 compares AI models used for crop stress detection in Malaysia and China, showing how advanced algorithms improve detection accuracy with high-quality remote sensing data. Deep learning models (CNN) lead in accuracy (92%), while other models like Random Forest (RF) and XGBoost also perform well for large-scale monitoring.

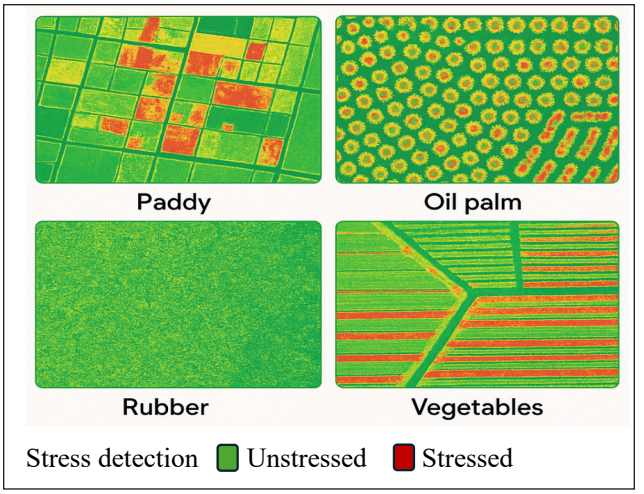

Figure 7. Stress detection in various crop types in Malaysia using remote sensing imagery

Table 7
Comparison of AI model classification accuracy for crop stress detection using remote sensing data in Malaysia and China

AI Model	Data Source	Remote Sensing Data	Region	Classification Accuracy	Notes
Support Vector Machine (SVM)	UAV (Unmanned Aerial Vehicle) imagery	High-resolution multispectral imagery	Malaysia	85%	Performs well with high-resolution data for stress detection (Zhang and Zhu, 2023)
Random Forest (RF)	Satellite imagery, field data	Landsat 8, Sentinel-2	China	88%	Robust for large-scale crop stress monitoring, with excellent feature importance handling (Zhang et al., 2022)
Deep Learning (Convolutional Neural Networks - CNN)	UAV and satellite data	Multispectral and hyperspectral data	Malaysia/ China	92%	High accuracy due to deep feature extraction and handling complex patterns (Saleh et al., 2024)
K-Nearest Neighbours (KNN)	Drone and field data	High-resolution RGB imagery	Malaysia	80%	Effective for simpler datasets but struggles with complex stress patterns (Phang et al., 2023)
Gradient Boosting Machines (GBM)	UAV and field data	High-resolution multispectral	China	89%	Highly accurate and efficient in detecting stress, especially with noise-reduced data (Bui et al., 2021)

Table 7 *(continued)*

AI Model	Data Source	Remote Sensing Data	Region	Classification Accuracy	Notes
Artificial Neural Networks (ANN)	Satellite imagery and field data	MODIS, Landsat	Malaysia/ China	87%	Performs well with non-linear relationships between remote sensing data and stress (Ni et al., 2025)
Decision Trees (DT)	Remote sensing data and field data	Sentinel-2, UAV imagery	Malaysia	83%	Simple to implement but less accurate for complex stress patterns (Xie, 2022)
XGBoost	Remote sensing data	High-resolution multispectral imagery	China	90%	Advanced boosting algorithm that offers a good balance of accuracy and computational efficiency (Samat et al., 2020)

Comparative Matrix Results

Table 8 compares manual inspection, ground-based sensors, and UAV-based remote sensing technologies for crop stress detection in Malaysia and China, highlighting their performance in terms of accuracy, scalability, and cost. UAV-based remote sensing outperforms the other methods with the highest accuracy (92%) and scalability, making it the most effective for large-scale monitoring (Su et al 2019). While manual inspection offers lower accuracy (70%) and is limited in scalability, it is cost-effective for small-scale observations. Ground-based sensors, with 80% accuracy, provide medium scalability and cost, offering a good balance between accuracy and application. UAV systems, though more expensive, are preferred for efficient, large-area coverage.

Crop stress monitoring can be achieved using ground-based, manual, and remote sensing methods, each with distinct advantages and limitations. Ground-based platforms, such as vehicle or trolley-mounted sensors, provide high-resolution, row-level data and can detect subtle physiological changes, while manual methods, including leaf sampling or SPAD measurements, are accurate but labour-intensive and limited in spatial coverage. Remote sensing approaches, such as UAV or satellite-based imaging, allow rapid, field-wide monitoring but may be affected by weather or canopy obstruction. To evaluate these approaches quantitatively, cost (C) can be calculated as:

The total system cost (C) is expressed as:

$$C = N \cdot P + L + M + E + I \quad [1]$$

where each component is defined as follows:

N = number of sensors deployed (unitless)
P = unit price per sensor (RM sensor^{-1})
L = labour cost associated with installation, calibration, operation, and data handling (RM)
M = maintenance cost, including routine servicing, sensor replacement, and system upkeep over the study period (RM)
E = energy cost, covering electrical power, batteries, charging, or fuel consumption during operation (RM)
I = installation cost, including mounting structures, wiring, communication setup, and initial system configuration (RM)

Thus, Equation (1) represents the total capital and operational cost (RM) of the monitoring system for a given deployment period.

Scalability Metric

System scalability (**S**) is defined as:

$$S = \frac{A}{T \cdot f} \quad [2]$$

where:

A area monitored (ha or m²)
T time required to complete one monitoring cycle (hours or days)
f operational constraint factor (unitless), representing limitations such as the number of field passes, sensor density, or sampling frequency

A higher **S** value indicates greater scalability, reflecting the system's ability to cover larger areas within shorter time frames under given operational constraints (Änäkkälä et al., 2022).

Table 8
Comparison of performance metrics for manual inspection, ground-based sensors, and UAV-based remote sensing technologies in crop stress detection in Malaysia and China

Method	Accuracy	Scalability	Cost	Application	Region
Manual Inspection	70%	Low	Low	Field-based observation	Malaysia/China
Ground-based Sensors	80%	Medium	Medium	Soil and plant monitoring	Malaysia/China
Remote Sensing (UAV-based)	92%	High	High	Aerial monitoring	Malaysia/China

Application and Implications

Applying these cost and scalability criteria demonstrates that mechanised Chinese farming systems achieve higher scalability and measurement precision through ground-based automated platforms. In contrast, Malaysian farms, which are typically smaller and mixed-crop, benefit more from lightweight ground sensors integrated with UAV reconnaissance.

While manual monitoring approaches incur lower initial costs, they exhibit limited scalability. Conversely, UAV-based systems provide rapid large-area coverage but involve higher operational and energy costs. Overall, this framework clarifies the trade-offs between spatial resolution, cost, and coverage, supporting the adoption of hybrid monitoring strategies according to local farm size and management conditions.

Figure 8 presents a comparison of method which include manual inspection, ground-based sensors, and UAV-based remote sensing, across three evaluation criteria: accuracy, scalability, and cost. UAV-based remote sensing stands out with the highest accuracy (92%) and scalability, while manual inspection has lower accuracy and scalability. Ground-based sensors strike a balance between cost and accuracy, with moderate scalability. Data are adapted from comparative performance metrics reported in UAV remote sensing and ground-based monitoring studies conducted in Southeast Asia and East Asia (Bui et al., 2021; Su et al., 2019; Xie, 2022).

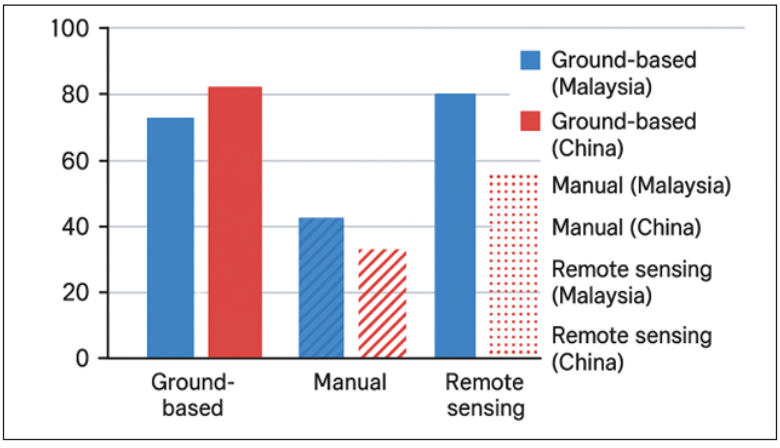

Figure 8. Comparison of methods for crop stress detection in Malaysia and China

Practical Implications for Farmers and Researchers

The practical implications of these findings depend heavily on the context of the farming operation. For smallholder farmers, the simplicity and low cost of manual inspection may make it the preferred choice, despite its limitations in accuracy (Amertet et al., 2024). However, for large-scale farms, remote sensing technologies, particularly UAV-based

systems, offer significant advantages in terms of coverage and accuracy. These methods, though costly, allow for more comprehensive monitoring of crop health, enabling farmers to detect stress across large areas in a relatively short time. Ground-based sensors, while more affordable than UAVs, provide highly reliable and accurate data on localised crop conditions. These sensors are particularly useful for monitoring variables like soil moisture, temperature, and nutrient content, which are critical for managing irrigation and fertilisation (Reza et al., 2025).

China vs Malaysia Comparison

The agricultural contexts in China and Malaysia offer unique challenges and opportunities for implementing crop stress detection technologies. China has made significant investments in agricultural infrastructure, which has facilitated the widespread adoption of advanced technologies such as UAVs and satellite-based remote sensing (Shah et al., 2024).

In contrast, Malaysia's smaller farm sizes and varying levels of infrastructure across regions may limit the widespread use of high-cost technologies like UAVs, although IoT-based sensors and manual inspection remain viable options for many farmers (Tiwari, 2022). Table 10 summarises the comparative national context of China and Malaysia, highlighting differences in infrastructure, policy support, and the availability of training for farmers.

Integration and Hybrid Systems

Recent research has emphasised the potential for integrating multiple sensing methods to improve crop stress detection. By combining remote sensing data with ground-based sensor information, it is possible to create hybrid systems that offer both broad-area monitoring and localised insights. Machine learning models can further enhance these hybrid systems by processing data from multiple sources to produce more accurate predictions of crop health.

Challenges and Limitations

Despite the advancements in crop stress detection technologies, several challenges remain. One of the primary technical barriers is the need for accurate and consistent ground truth data, which is essential for validating remote sensing and sensor-based measurements. Additionally, the cost of high-resolution sensors and UAV systems remains a significant limitation for smallholder farmers in developing regions.

Furthermore, data quality is influenced by environmental factors such as weather conditions, which can affect the accuracy of both remote sensing and ground-based sensor data. Addressing these challenges requires ongoing research and the development of more robust and affordable technologies.

CONCLUSION

This review has evaluated multiple methods for crop stress detection, including manual inspection, ground-based sensors, and remote sensing technologies. The findings indicate that remote sensing, particularly Unmanned Aerial Vehicle (UAV) based systems, provides the highest accuracy and scalability, making it most suitable for large-scale farms. Ground-based sensors offer reliable, site-specific data but require improvements in affordability and long-term reliability, especially for smallholder adoption. Manual inspection remains valuable for smallholder farms; however, it is less accurate and scalable. Consequently, manual methods and low-cost ground-based sensors are identified as needing urgent enhancement to improve usability and sustainability. Policy support, including subsidies and technical training, has been shown to significantly influence adoption rates of precision agriculture tools. For smallholder farmers, combining manual inspection with improved low-cost sensors can provide an affordable means of detecting stress, whereas larger farms benefit from integrating remote sensing with Internet of Things (IoT) sensors to achieve comprehensive, real-time crop monitoring.

Future research should focus on improving the accuracy and affordability of crop stress detection technologies. Policy support in the form of subsidies or incentives for adopting these technologies could help smallholder farmers, particularly in developing regions. Additionally, the integration of AI and machine learning models with hybrid sensing systems shows promise in improving detection accuracy and facilitating early intervention for crop stress management.

ACKNOWLEDGEMENT

The author sincerely thanks the Ministry of Higher Education (MOHE), Malaysia, for research funding (Grant No. LRGS/1/2020/UPM/01/2; Vote No. 5545202) and Universiti Putra Malaysia (UPM) for the PhD supervision. Appreciation is extended to the Malaysian Agricultural Research and Development Institute (MARDI) for the PhD scholarship and international support. Gratitude is also expressed to the Agricultural Information Institute, Chinese Academy of Agricultural Sciences (CAAS), for the research opportunity under the Talented Young Scientist Program (TYSP), China.

CONFLICTS OF INTEREST

The authors declare no conflicts of interest.

REFERENCES

Änäkkälä, M., Lajunen, A., Hakojärvi, M., & Alakukku, L. (2022). Evaluation of the influence of field conditions on aerial multispectral images and vegetation indices. *Remote Sensing, 14*(19), Article 4792. https://doi.org/10.3390/rs14194792

Aarif K. O., M., Alam, A., & Hotak, Y. (2025). Smart sensor technologies shaping the future of precision agriculture: Recent advances and future outlooks. *Journal of Sensors, 2025*, Article 2460098. https://doi.org/10.1155/js/2460098

Ahmad, S., & Hashim, N. M. (2007). Effects of soil moisture on urban heat island occurrences: Case of Selangor, Malaysia. *Humanity & Social Sciences Journal*, *2*(2), 132-138. Retrieved from https://www.researchgate.net/publication/284098159_Effects_of_Soil_Moisture_on_Urban_Heat_Island_Occurrences_Case_of_Selangor_Malaysia

Alawathugoda, C., Hinge, G., Elkollaly, M., & Hamouda, M. A. (2024). Impact of utilising high-resolution PlanetScope imagery on the accuracy of LULC mapping and hydrological modelling in an arid region. *Water, 16*(16), Article 2356. https://doi.org/10.3390/w16162356

Amanullah. (2024a). *Harvesting success: A comprehensive guide to agronomy courses*. Punjab Book Company.

Amanullah. (2024b). *Integrated agriculture: An approach for sustainable agriculture*. Walter de Gruyter. https://doi.org/10.1515/9783111448077

Amertet, S., Gebresenbet, G., & Alwan, H. M. (2024). Application of hyper-automation in farming. An analysis. *Smart Agricultural Technology, 9*, Article 100516. https://doi.org/10.1016/j.atech.2024.100516

Anam, I., Arafat, N., Hafiz, M. S., Jim, J. R., Kabir, M. M., & Mridha, M. F. (2024). A systematic review of UAV and AI integration for targeted disease detection, weed management, and pest control in precision agriculture. *Smart Agricultural Technology, 9*, Article 100647. https://doi.org/10.1016/j.atech.2024.100647

Assimakopoulos, F., Vassilakis, C., Margaris, D., Kotis, K., & Spiliotopoulos, D. (2025). AI and related technologies in the fields of smart agriculture: A review. *Information, 16*(2), Article 100. https://doi.org/10.3390/info16020100

Balasundaram, A., Sharma, A., Swaathy, K., & Kavitha, M. S. (2024). An improved Normalised difference vegetation index (NDVI) estimation using grounded Dino and segment anything model for plant health classification. *IEEE Access, 12,* 75097-75919. https://doi.org/10.1109/ACCESS.2024.3403520

Bela, K. (2023). Crop tolerance under biotic and abiotic stresses. *Agronomy*, *13*(12), Article 3024. https://doi.org/10.3390/agronomy13123024

Bui, Q.-T., Chou, T.-Y., Hoang, T.-V., Fang, Y.-M., Mu, C.-Y., Huang, P.-H., Pham, V.-D., Nguyen, Q.-H., Do, T. N. A., Pham, V.-M., & Meadows, M. E. (2021). Gradient boosting machine and object-based CNN for land cover classification. *Remote Sensing, 13*(14), Article 2709. https://doi.org/10.3390/rs13142709

Chakhvashvili, E., Machwitz, M., Antala, M., Tiemeyer, B., Bareth, G., & Conrad, C. (2024). Crop stress detection from UAVs: Best practices and lessons learned for exploiting sensor synergies. *Precision Agriculture, 25,* 2614-2642. https://doi.org/10.1007/s11119-024-10168-3

Chen, L., Hu, B., Sun, J., Xu, Y. J., Zhang, G., Ma, H., & Ren, J. (2025). Using remote sensing and machine learning to generate 100-cm soil moisture at 30-m resolution for the black soil region of China: Implication for agricultural water management. *Agricultural Water Management, 309*, Article 109353. https://doi.org/10.1016/j.agwat.2025.109353

Cho, S. B., Soleh, H. M., Choi, J. W., Hwang, W.-H., Lee, H., Cho, Y.-S., Cho, B.-K., Kim, M. S., Baek, I., & Kim, G. (2024). Recent methods for evaluating crop water stress using ai techniques: A Review. *Sensors*, *24*(19), Article 6313. https://doi.org/10.3390/s24196313

Comegna, A., Hassan, S. B. M., & Coppola, A. (2024). Development and Application of an IoT-Based System for Soil Water Status Monitoring in a Soil Profile. *Sensors*, *24*(9), Article 2725. https://doi.org/10.3390/s24092725

Deng, L., Mao, Z., Li, X., & Yan, Y. (2018). UAV-based multispectral remote sensing for precision agriculture: A comparison between different cameras. *ISPRS Journal of Photogrammetry and Remote Sensing, 146*, 124-136. https://doi.org/10.1016/j.isprsjprs.2018.09.008

Dhanaraju, M., Chenniappan, P., Ramalingam, K., Pazhanivelan, S., & Kaliaperumal, R. (2022). Smart farming: Internet of Things (IoT)-based sustainable agriculture. *Agriculture, 12*(10), Article 1745. https://doi.org/10.3390/agriculture12101745

Dong, H., Dong, J., Sun, S., Bai, T., Zhao, D., Yin, Y., Shen, X., Wang, Y., Zhang, Z., & Wang, Y. (2024). Crop water stress detection based on UAV remote sensing systems. *Agricultural Water Management, 303*, Article 109059. https://doi.org/10.1016/j.agwat.2024.109059

Essaadia, A., Abdellah, A., Ahmed, A., Abdelouahed, F., & Kamal, E. (2022). The Normalised difference vegetation index (NDVI) of the Zat valley, Marrakech: Comparison and dynamics. *Heliyon, 8*(12), Article e12204. https://doi.org/10.1016/j.heliyon.2022.e12204

Fadl, M. E., AbdelRahman, M. A. E., El-Desoky, A. I., & Sayed, Y. A. (2024). Assessing soil productivity potential in arid region using remote sensing vegetation indices. *Journal of Arid Environments, 222*, Article 105166. https://doi.org/10.1016/j.jaridenv.2024.105166

Faqir, Y., Qayoom, A., Erasmus, E., Schutte-Smith, M., & Visser, H. G. (2024). A review on the application of advanced soil and plant sensors in the agriculture sector. *Computers and Electronics in Agriculture, 226*, Article 109385. https://doi.org/10.1016/j.compag.2024.109385

Francis, B., Aravindakumar, C. T., Brewer, P. B., & Simon, S. (2023). Plant nutrient stress adaptation: A prospect for fertiliser-limited agriculture. *Environmental and Experimental Botany, 213*, Article 105431. https://doi.org/10.1016/j.envexpbot.2023.105431

Gamage, A., Gangahagedara, R., Subasinghe, S., Gamage, J., Guruge, C., Senaratne, S., Randika, T., Rathnayake, C., Hameed, Z., Madhujith, T., & Merah, O. (2024). Advancing sustainability: The impact of emerging technologies in agriculture. *Current Plant Biology, 40*, Article 100420. https://doi.org/10.1016/j.cpb.2024.100420

González-Dugo, V., Zarco-Tejada, P. J., Berni, J. A. J., Suárez, L., Goldhamer, D., & Fereres, E. (2010). Automated canopy temperature estimation via infrared thermography: A first step towards automated plant water stress monitoring. *Computers and Electronics in Agriculture, 73*(1), 74-83. https://doi.org/10.1016/j.compag.2010.04.007

Gu, C., Li, J., Liu, Q., Zhang, H., Huete, A., Fang, H., Liu, L., Mumtaz, F., Lin, S., Wang, X., Dong, Y., Zhao, J., Bai, J., Yu, W., Liu, C., & Guan, L. (2025). Deriving leaf-scale chlorophyll index from canopy reflectance by correcting for the canopy multiple scattering based on spectral invariant theory. *Remote Sensing of Environment, 322*, Article 114692. https://doi.org/10.1016/j.rse.2025.114692

Gunawan, M. I., Sitopu, J. W., & Sechan, G. (2024). Optimising crop selection: A multi-criteria decision support system for sustainable agriculture. *International Journal of Enterprise Modelling, 18*(3), 113-123. https://www.ieia.ristek.or.id.

Guo, J., Sun, Y., Rao, Z., Chen, Y., Liu, Z., Jin, H., He, X., Yang, Z., & Zhang, Q. (2025). Drought stress at different growth stages decrease dry weight and active constituent yield accumulation by inhibiting root morphology in *Scutellaria baicalensis* Georgi. *Industrial Crops and Products, 223*, Article 120280. https://doi.org/10.1016/j.indcrop.2024.120280

Heiss, N., Meier, J., Gessner, U., & Kuenzer, C. (2025). A review: Potential of Earth observation (EO) for mapping small-scale agriculture and cropping systems in West Africa. *Land, 14*(1), 171. https://doi.org/10.3390/land14010171

Hualpa-Ramirez, E., Carrasco-Lozano, E. C., Madrid-Espinoza, J., Tejos, R., Ruiz-Lara, S., Stange, C., & Norambuena, L. (2024). Stress salinity in plants: New strategies to cope with in the foreseeable scenario. *Plant Physiology and Biochemistry, 208*, Article 108507. https://doi.org/10.1016/j.plaphy.2024.108507

Iheaturu, C. J., Hepner, S., Batchelor, J. L., Agonvonon, G. A., Akinyemi, F. O., Wingate, V. R., & Speranza, C. I. (2024). Integrating UAV LiDAR and multispectral data to assess forest status and map disturbance severity in a West African forest patch. *Ecological Informatics, 84*, Article 102876. https://doi.org/10.1016/j.ecoinf.2024.102876

Jensen, T. A., Antille, D. L., & Tullberg, J. N. (2025). Improving on-farm energy use efficiency by optimising machinery operations and management: A review. *Agricultural Research, 14,* 15-33. https://doi.org/10.1007/s40003-024-00824-5

Karmakar, P., Teng, S. W., Murshed, M., Pang, S., Li, Y., & Lin, H. (2024). Crop monitoring by multimodal remote sensing: A review. *Remote Sensing Applications: Society and Environment, 33*, 101093. https://doi.org/10.1016/j.rsase.2023.101093

Kou, C., Song, F., Li, D., Xu, H., Zhang, S., Yang, W., Shi, W., & Gao, Z. (2024). A necessary considering factor for crop resistance: Precise regulation and effective utilisation of beneficial microorganisms. *New Crops, 1*, Article 100023. https://doi.org/10.1016/j.ncrops.2024.100023

Kour, S., Ahammed, G. J., & Zhou, J. (2025). Role of beneficial microorganisms in vegetable crop production and stress tolerance. In G. J. Ahammed & J. Zhou (Eds.), *Growth regulation and quality improvement of vegetable crops* (pp. 123-145). Springer. https://doi.org/10.1007/978-981-96-0169-1_10

Kramarić, L., Jelušić, N., Radišić, T., & Muštra, M. (2025). A comprehensive survey on short-distance localisation of UAVs. *Drones, 9*(3), Article 188. https://doi.org/10.3390/drones9030188

Lau, C. Y. H., & Tov, W. (2023). Effects of positive reappraisal and self-distancing on the meaningfulness of everyday negative events. *Frontiers in Psychology*, *14*, Article 1093412. https://doi.org/10.3389/fpsyg.2023.1093412

Le, T. S., Harper, R., & Dell, B. (2023). Application of remote sensing in detecting and monitoring water stress in forests. *Remote Sensing, 15*(13), Article 3360. https://doi.org/10.3390/rs15133360

Lee, K.-H., Samsuzzaman, M. N. R., Islam, S., Ahmed, S., Cho, Y. J., Noh, D. H., & Chung, S.-O. (2025). Evaluation of machine learning models for stress symptom classification of cucumber seedlings grown in a controlled environment. *Agronomy, 15*(1), Article 90. https://doi.org/10.3390/agronomy15010090

le Roux, J., Christopher, S., & Maskey, M. (2021). Exploring the use of PlanetScope data for particulate matter air quality research. *Remote Sensing, 13*(15), Article 2981. https://doi.org/10.3390/rs13152981

Ma, P., Peng, J., Zheng, J., Liu, L., Yu, X., & Li, W. (2025). Vegetation health in China is severely compromised by drought, wet and heat stress events. *Forests*, *16*(1), Article 38. https://doi.org/10.3390/f16010038

Mansoor, S., Iqbal, S., Popescu, S. M., Kim, S. L., Chung, Y. S., & Baek, J.-H. (2025). Integration of smart sensors and IoT in precision agriculture: Trends, challenges, and future prospectives. *Frontiers in Plant Science, 16,* Article 1587869. https://doi.org/10.3389/fpls.2025.1587869

Mat Lazim, S. S. R., Mat Nawi, N., Masroon, M. H., & Ishkandar, C. D. M. (2020). Adoption of IR4.0 into agricultural sector in Malaysia: Potential and challenges. *Advances in Agricultural and Food Research Journal, 1*(2). https://doi.org/10.36877/aafrj.a0000140

Mba, P. C., Njoku, J. N., & Uyeh, D. D. (2025). Enhancing resilience in specialty crop production in a changing climate through smart systems adoption. *Smart Agricultural Technology, 11*, Article 100897. https://doi.org/10.1016/j.atech.2025.100897

Munasinghe, I., Perera, A., & Deo, R. C. (2024). A comprehensive review of UAV-UGV collaboration: Advancements and challenges. *Journal of Sensor and Actuator Networks, 13*(6), Article 81. https://doi.org/10.3390/jsan13060081

Mylonas, N., Malounas, I., Mouseti, S., Vali, E., Espejo-Garcia, B., & Fountas, S. (2022). Eden Library: A long-term database for storing agricultural multi-sensor datasets from UAV and proximal platforms. *Smart Agricultural Technology, 2*, Article 100028. https://doi.org/10.1016/j.atech.2021.100028

Ni, M., Wu, Q., Li, G., & Li, D. (2025). Remote sensing technology for observing tree mortality and its influences on carbon-water dynamics. *Forests*, *16*(2), Article 194. https://doi.org/10.3390/f16020194

Pandey, D. K., & Mishra, R. (2024). Towards sustainable agriculture: Harnessing AI for global food security. *Artificial Intelligence in Agriculture, 12*, 72-84. https://doi.org/10.1016/j.aiia.2024.04.003

Parra-López, C., Ben Abdallah, S., Garcia-Garcia, G., Hassoun, A., Trollman, H., Jagtap, S., Gupta, S., Aït-Kaddour, A., Makmuang, S., & Carmona-Torres, C. (2025). Digital technologies for water use and management in agriculture: Recent applications and future outlook. *Agricultural Water Management, 309*, Article 109347. https://doi.org/10.1016/j.agwat.2025.109347

Pascual, L. S., Segarra-Medina, C., Gómez-Cadenas, A., López-Climent, M. F., Vives-Peris, V., & Zandalinas, S. I. (2022). Climate change-associated multifactorial stress combination: A present challenge for our ecosystems. *Journal of Plant Physiology, 276*, Article 153764. https://doi.org/10.1016/j.jplph.2022.153764

Phang, S. K., Chiang, T. H. A., Happonen, A., & Chang, M. M. L. (2023). From satellite to UAV-based remote sensing: A review on precision agriculture. *IEEE Access, 11*, 127057-127076. https://doi.org/10.1109/ACCESS.2023.3330886

Prasad, P., Loveson, V. J., Chandra, P., & Kotha, M. (2021). Evaluation and comparison of the earth observing sensors in land cover/land use studies using machine learning algorithms. *Science of the Total Environment, 758*, Article 143701. https://www.sciencedirect.com/science/article/pii/S1574954121003137

Olawade, D. B., Wada, O. Z., Ige, A. O., Egbewole, B. I., Olojo, A., & Oladapo, B. I. (2024). Artificial intelligence in environmental monitoring: Advancements, challenges, and future directions. *Hygiene and Environmental Health Advances, 12*, Article 100114. https://doi.org/10.1016/j.heha.2024.100114

Rahman, M. M., Siddique, S., Kamal, M., Rifat, R. H., & Gupta, K. D. (2024). UAV (Unmanned Aerial Vehicle): Diverse applications of UAV datasets in segmentation, classification, detection, and tracking. *Algorithms, 17*(12), Article 594. https://doi.org/10.3390/a17120594

Rajak, P., Ganguly, A., Adhikary, S., & Bhattachaya, S. (2023). Internet of Things and smart sensors in agriculture: Scopes and challenges. *Journal of Agriculture and Food Research, 14*, Article 100776. https://doi.org/10.1016/j.jafr.2023.100776

Rasheed, M. W., Tang, J., Sarwar, A., Shah, S., Saddique, N., Khan, M. U., Imran Khan, M., Nawaz, S., Shamshiri, R. R., Aziz, M., & Sultan, M. (2022). Soil moisture measuring techniques and factors affecting the moisture dynamics: A comprehensive review. *Sustainability, 14*(18), Article 11538. https://doi.org/10.3390/su141811538

Rashid, A. B., Kausik, A. K., Khandoker, A., & Siddque, S. N. (2025). Integration of artificial intelligence and IoT with UAVs for precision agriculture. *Hybrid Advances, 10*, Article 100458. https://doi.org/10.1016/j.hybadv.2025.100458

Saeed, I. A., Wang, M., Butt, S. L., & Wanlin, G. (2019). Development of a low-cost multi-depth real-time soil moisture sensor using time division multiplexing approach. *IEEE Access, 7*, 19688-19697. https://doi.org/10.1109/ACCESS.2019.2893680

Saewong, C., Ow, Y. X., Nualla-ong, A., & Buapet, P. (2024). Comparative effects of heat stress on photosynthesis and oxidative stress in *Halophila ovalis* and *Thalassia hemprichii* under different light conditions. *Marine Environmental Research, 199*, Article 106589. https://doi.org/10.1016/j.marenvres.2024.106589

Saleh, A., Zulkifley, M. A., Harun, H. H., Gaudreault, F., Davison, I., & Spraggon, M. (2024). Forest fire surveillance systems: A review of deep learning methods. *Heliyon, 10*(1), Article e23127. https://doi.org/10.1016/j.heliyon.2023.e23127

Sanaeifar, A., Yang, C., de la Guardia, M., Zhang, W., Li, X., & He, Y. (2023). Proximal hyperspectral sensing of abiotic stresses in plants. *Science of The Total Environment, 861*, Article 160652. https://doi.org/10.1016/j.scitotenv.2022.160652

Shah, W. U. H., Hao, G., Yasmeen, R., Yan, H., & Qi, Y. (2024). Impact of agricultural technological innovation on total-factor agricultural water usage efficiency: Evidence from 31 Chinese provinces. *Agricultural Water Management, 299*, Article 108905. https://doi.org/10.1016/j.agwat.2024.108905

Shahab, H., Naeem, M., Iqbal, M., Aqeel, M., & Ullah, S. S. (2025). IoT-driven smart agricultural technology for real-time soil and crop optimisation. *Smart Agricultural Technology, 10*, Article 100847. https://doi.org/10.1016/j.atech.2025.100847

Shaharum, N. S. N., Shafri, H. Z. M., Karim, A., Yusuf, B., & others. (2020). Oil palm mapping over Peninsular Malaysia using Google Earth Engine and machine learning algorithms. *Remote Sensing Applications: Society and Environment, 17*, Article 100287. https://doi.org/10.1016/j.rsase.2020.100287

Sharma, H., Sidhu, H., & Bhowmik, A. (2025). Remote sensing using unmanned aerial vehicles for water stress detection: A review focussing on specialty crops. *Drones, 9*(4), Article 241. https://doi.org/10.3390/drones9040241

Soussi, A., Zero, E., Sacile, R., Trinchero, D., & Fossa, M. (2024). Smart sensors and smart data for precision agriculture: A Review. *Sensors*, *24*(8), Article 2647. https://doi.org/10.3390/s24082647

Sothe, C., Almeida, C. M. d., Liesenberg, V., & Schimalski, M. B. (2017). Evaluating Sentinel-2 and Landsat-8 data to map sucessional forest stages in a subtropical forest in Southern Brazil. *Remote Sensing*, *9*(8), Article 838. https://doi.org/10.3390/rs9080838

Sulong, A. H. A., Baharun, A., Yazit, R. N. S. R. M., Bakar, R. A., & Muyandy, T. (2023). Pilot study on underground air temperature for interior thermal comfort of building in Malaysia. *IOP Conference Series: Earth and Environmental Science, 1218*(1), Article 012022. https://doi.org/10.1088/1755-1315/1218/1/012022

Sun, J., Yan, S., Alexandridis, T., Yao, X., Zhou, H., Gao, B., Huang, J., Yang, J., & Li, Y. (2024). Enhancing crop mapping through automated sample generation based on segment anything model with medium-resolution satellite imagery. *Remote Sensing, 16*(9), Article 1505. https://doi.org/10.3390/rs16091505

Taha, M. F., Mao, H., Zhang, Z., Elmasry, G., Awad, M. A., Abdalla, A., Mousa, S., Elwakeel, A. E., & Elsherbiny, O. (2025). Emerging technologies for precision crop management towards agriculture 5.0: A comprehensive overview. *Agriculture*, *15*(6), Article 582. https://doi.org/10.3390/agriculture15060582

Tangjialeke, W., Zou, J., Ding, J., Yahefujiang, H., Huang, S., & Li, J. (2024). Analysis of drought response thresholds and drought-causing factors of Central Asian vegetation. *Ecological Indicators, 169*, Article 112926. https://doi.org/10.1016/j.ecolind.2024.112926

Tarolli, P., Luo, J., Park, E., Barcaccia, G., & Masin, R. (2024). Soil salinisation in agriculture: Mitigation and adaptation strategies combining nature-based solutions and bioengineering. *iScience, 27*(2), Article 108830. https://doi.org/10.1016/j.isci.2024.108830

Tian, H., Wang, T., Liu, Y., Qiao, X., & Li, Y. (2020). Computer vision technology in agricultural automation—A review. *Information Processing in Agriculture, 7*(1), 1-19. https://doi.org/10.1016/j.inpa.2019.09.006

Tian, Y., Zhao, C., Lu, S., & Guo, X. (2011). Multiple classifier combination for recognition of wheat leaf diseases. *Intelligent Automation & Soft Computing, 17*(5), 575-583. https://doi.org/10.1080/10798587.2011.10643166

Tiwari, S. (2022). A review of Internet of Things application in Malaysia. *Borneo Journal of Sciences & Technology, 4*(1), 70-79. https://doi.org/10.3570/bjost.2022.4.1-11e

Tsouros, D. C., Bibi, S., & Sarigiannidis, P. G. (2019). A review on UAV-based applications for precision agriculture. *Information*, *10*(11), Article 349. https://doi.org/10.3390/info10110349

Umutoni, L., & Samadi, V. (2024). Application of machine learning approaches in supporting irrigation decision making: A review. *Agricultural Water Management, 294*, Article 108710. https://doi.org/10.1016/j.agwat.2024.108710

Unde, S. S., Kurkute, V. K., Chavan, S. S., Mohite, D. D., Harale, A. A., & Chougle, A. (2025). The expanding role of multirotor UAVs in precision agriculture with applications, AI integration, and future prospects. *Discover Mechanical Engineering, 4,* Article 38. https://doi.org/10.1007/s44245-025-00132-4

Upadhyay, A., Chandel, N. S., Singh, K. P., et al. (2025). Deep learning and computer vision in plant disease detection: A comprehensive review of techniques, models, and trends in precision agriculture. *Artificial Intelligence Review, 58*, Article 92. https://doi.org/10.1007/s10462-024-11100-x

Velazquez-Chavez, L. J., Daccache, A., Mohamed, A. Z., & Centritto, M. (2024). Plant-based and remote sensing for water status monitoring of orchard crops: Systematic review and meta-analysis. *Agricultural Water Management, 303*, Article 109051. https://doi.org/10.1016/j.agwat.2024.109051

Walsh, J. J., Mangina, E., & Negrão, S. (2023). Advancements in imaging sensors and AI for plant stress detection: A systematic literature review. *Plant Phenomics, 6*, Article 0153. https://doi.org/10.34133/plantphenomics.0153

Wang, L., Xiao, M., Guo, X., Yang, Y., Zhang, Z., & Lee, C. (2024). Sensing technologies for outdoor/indoor farming. *Biosensors*, *14*(12), Article 629. https://doi.org/10.3390/bios14120629

Wang, Q., Liu, H., Liang, B., Shi, L., Wu, L., & Cao, J. (2024). Will large-scale forestation lead to a soil water deficit crisis in China's drylands? *Science Bulletin (Beijing), 69*(10), 1506-1514. https://doi.org/10.1016/j.scib.2024.03.005

Wu, C., Doraisamy, V., & Rasalingam, R. R. (2025). A digital transformation framework for real-time vibration monitoring using virtual sensors and machine learning. *PaperAsia, 41*(4B). https://doi.org/10.59953/paperasia.v41i4b.601

Xie, Y. (2022). Combining CERES-Wheat model, Sentinel-2 data, and deep learning method for winter wheat yield estimation. *International Journal of Remote Sensing, 43*(2), 630-648. https://doi.org/10.1080/01431161.2022.2026521

Xue, J., & Su, B. (2017). Significant remote sensing vegetation indices: A review of developments and applications. *Journal of Sensors*, *2017*(1), 1-17. https://doi.org/10.1155/2017/1353691

Yadav, M., Vashisht, B. B., Vullaganti, N., Kumar, P., Jalota, S. K., Kumar, A., & Kaushik, P. (2024). UAV-enabled approaches for irrigation scheduling and water body characterisation. *Agricultural Water Management, 304*, Article 109091. https://doi.org/10.1016/j.agwat.2024.109091

Zhang, H., Wang, L., Jin, X., Bian, L., & Ge, Y. (2023). High-throughput phenotyping of plant leaf morphological, physiological, and biochemical traits on multiple scales using optical sensing. *The Crop Journal, 11*(5), 1303-1318. https://doi.org/10.1016/j.cj.2023.04.014.

Zhang, L., Zhang, H., Niu, Y., & Han, W. (2019). Mapping maize water stress based on UAV multispectral remote sensing. *Remote Sensing, 11*(6), Article 605. https://doi.org/10.3390/rs11060605

Zhang, X., Feng, G., & Sun, X. (2024). Advanced technologies of soil moisture monitoring in precision agriculture: A review. *Journal of Agriculture and Food Research, 18*, Article 101473. https://doi.org/10.1016/j.jafr.2024.101473

Zhang, Z., & Zhu, L. (2023). A review on unmanned aerial vehicle remote sensing: platforms, sensors, data processing methods, and applications. *Drones*, *7*(6), Article 398. https://doi.org/10.3390/drones7060398

Zhao, Q., & Qu, Y. (2024). The retrieval of ground NDVI (Normalised Difference Vegetation Index) data consistent with remote-sensing observations. *Remote Sensing, 16*(7), Article 1212. https://doi.org/10.3390/rs16071212

Zhao, P., Yan, Y., Jia, S., Zhao, J., & Zhang, W. (2025). construction and evaluation of a cross-regional and cross-year monitoring model for millet canopy phenotype based on UAV multispectral remote sensing. *Agronomy*, *15*(4), Article 789. https://doi.org/10.3390/agronomy15040789

Zhou, M., & Li, Y. (2024). Digital mapping and scenario prediction of soil salinity in coastal lands based on multi-source data combined with machine learning algorithms. *Remote Sensing*, *16*(14), Article 2681. https://doi.org/10.3390/rs16142681

Pertanika J. Trop. Agric. Sci. 49 (S1): 31 - 55 (2026)

PERTANIKA JOURNALS

TROPICAL AGRICULTURAL SCIENCE

Journal homepage: http://www.pertanika.upm.edu.my/

Modelling of Milk Kefir Fermentation for its Optimised Physicochemical and Microbiological Properties

Joyce Jen Li Lim[1], Nyuk Ling Chin[1]*, Adiratna Mat Ripen[2], and Syahmeer How[3]

[1]Department of Process and Food Engineering, Faculty of Engineering, Universiti Putra Malaysia, 43400 UPM Serdang, Selangor, Malaysia

[2]Cancer Research Centre, Institute for Medical Research, National Institutes of Health, Ministry of Health, 40170 Shah Alam, Selangor, Malaysia

[3]Food Solutions, Plant & Food Research Group, New Zealand Institute for Bioeconomy Science Limited, 4410 Palmerston North, New Zealand

ABSTRACT

Milk kefir is a tangy, probiotic-rich fermented milk drink that is underexplored, partly due to the lack of broad awareness and complexity in standardisation of processing. This research studied the milk kefir fermentation process using response surface methodology (RSM) and artificial neural network (ANN). The RSM approach has optimised milk kefir quality at pH 4.4, viscosity at 1200 mPa.s and lactic acid at 0.8% at fermentation temperature of 35.8°C for 8.8 hours. The ANN model presented predictive capabilities with a higher coefficient of determination, R^2 values and comparably lower root mean square error (RSME) and lower average absolute deviation (AAD) as compared to RSM, suggesting that the ANN model is more effective in capturing nonlinear data for predicting quality responses of milk kefir. Bacterial and fungal composition of milk kefir was measured using metagenomics via next-generation sequencing. *Firmicutes* was found as the most dominant bacterial phylum, while *Ascomycota,* the fungi phylum in both optimised and commercial milk kefir. At the genus level, *Lactobacillus* was an abundant bacterium in optimised milk kefir, while *Streptococcus* in commercial milk kefir. Both *Lactobacillus* and *Streptococcus* are recognised as probiotics that promote improvement in gut health and support immunity. For fungi, the genus *Pichia* was detected in high abundance percentage in optimised milk kefir, while *Debaryomyces* in commercial milk kefir.

Keywords: Artificial neural network, fermentation, milk kefir, optimisation, response surface methodology

ARTICLE INFO

Article history:
Received: 18 July 2025
Accepted: 10 January 2026
Published: 19 March 2026

DOI: https://doi.org/10.47836/pjtas.49.S1.02

E-mail addresses:
joylimjenli2000@gmail.com (Joyce Jen Li Lim)
chinnl@upm.edu.my (Nyuk Ling Chin)
adiratna@moh.gov.my (Adiratna Mat Ripen)
syahmeer.how@plantandfood.co.nz (Syahmeer How)
* Corresponding author

e-ISSN: 2231-8542

INTRODUCTION

The increasing global demand for sustainability has underlined the necessity of promoting resilient food production, which contributes to minimal waste and long-term food security to ensure that future generations have access to sufficient, safe, and nutritious food. Fermentation is one of the most traditional practices that has been adopted to prevent losses in highly perishable food products. Milk is known to be the third largest category of food wastage after meat and vegetable products due to its perishable nature which contributed 17% of total value loss worth $165.6 billion in the United States (Buzby et al., 2014). Although fermentation process of milk has produced products such as cheese, whey, and yoghurt (Martin et al., 2021), milk kefir is less widely known as it is primarily limited to household levels from ancient times (Alves et al., 2021). Milk kefir was discovered in the Caucasian Mountain, between Russia and Georgia, and has been passed down from one generation to another for centuries (Gentry et al., 2023). Milk kefir is a fermented beverage that is obtained from fermentation of milk commonly sourced from cow, goat, or ewe with inoculated milk kefir grains consisting of microbial communities mainly lactic acid bacteria, yeast, and acetic acid bacteria (Leite et al., 2013). The dominant genera found in the milk kefir is lactic acid bacteria, including *Lactobacillus* sp.*, Leuconostoc* sp., *Pediococcus* sp. and *Lactococcus* sp. which serve as probiotics that regulate gut microbiota and prevent dysbiosis (Fiorda et al., 2017; Garofalo et al., 2015). For yeast, *Saccharomyces cerevisiae, Candida* kefyr, and *Kluyveromyces marixanus ssp. Marxianus* are found abundantly that facilitate in acid and alcohol fermentation (Fiorda et al., 2017). However, elucidation of the beneficial microbial composition of milk kefir has remained controversial, stemming from types of substrates, fermentation time, and temperature (Gul et al., 2015). Hence, optimising processing is essential for desired and consistent milk kefir quality to establish a favourable condition that support growth of beneficial microbes.

Fermentation of milk results in the change of physicochemical properties including pH, viscosity, microbial composition, and formation of various metabolites including organic acids, ethanol, carbon dioxide, and micronutrients (Rosa et al., 2017). Fermenting milk imparts health benefits such as probiotics (Bellikci-Koyu et al., 2019), antioxidants (Yilmaz-Ersan et al., 2018), and antidiabetics (Kahraman et al., 2021). The challenges in up-scaling production and quality control of milk kefir often arise from the complexity of fermentation performance, which is influenced by the interactions of factors such as time (Hecer et al., 2019), temperature (Hecer et al., 2019), and origin of kefir grain (de Sainz et al., 2020). The complex interactions between processing factors and milk kefir properties, coupled with a general lack of fundamental knowledge of fermentation process have aggravated the quality prediction of milk kefir using a single or general mathematical models.

The Response Surface Methodology (RSM) is a practical design of experiment and mathematical tool that has been used in research and manufacturing industries to

optimise processing factors in the production of yogurt (Akhi et al., 2024) and sausage (Florence Adeola et al., 2024). Artificial Neural Network (ANN) is a powerful machine learning system which involves computational and mathematical techniques that are designed to simulate learning algorithm of the human brain (Antil et al., 2020). Within the food sector, ANN has been applied to model and predict rheological properties of dough (Razmi-Rad et al., 2007), monitoring of winemaking process (Sipos, 2020), and more recently in the spray drying of coconut milk (Ming et al., 2021). This research aims to model and optimise fermentation conditions on pH, viscosity, and lactic acid percentage using the RSM and ANN methods. The prediction capabilities of both RSM and ANN were compared by root mean square error (RMSE), absolute average deviation (AAD), and coefficient of determination (R^2). The integration between both the conventional and machine learning predictive modelling provides a more robust modelling framework for process optimisation, specifically for milk kefir which has not been implemented. This research also identified the microbial composition of milk kefir using amplicon-based sequencing via the Next Generation Sequencing to account its diverse microbial communities, hence connecting optimisation and high-resolution microbial profiling that offers a more comprehensive understanding of milk kefir dynamics beyond physicochemical properties.

MATERIALS AND METHODS

Raw Materials and Reagents

Cow's milk (Farm Fresh Milk Sdn. Bhd. Malaysia), Tibetan kefir grains purchased from Nature Brands (Nature's Recipe, Selangor, Malaysia), and commercial milk kefir (BrightCow, Malaysia).

Reactivation of Kefir Grain and Milk Kefir Production

The reactivation and preparation of kefir grain was modified from the method by Hecer et al. (2019). Kefir grains were reactivated in a container of milk for 12 hours at 25°C for three incubation cycles. In each incubation cycle, the kefir grains were separated using a sieve and transferred into a new batch of fresh milk. For milk kefir production, the reactivated kefir grains were inoculated in fresh cow milk with a ratio of 1:30 (w/v) as recommended by Gentry et al. (2023). The mixture was stirred gently before being placed in the incubator with a programmable temperature and humidity chamber (Model TMJ-9712, T Machine Technology Co., Ltd., China) for fermentation. The humidity was fixed at 60% RH throughout all experiments. Upon incubation, milk kefir grains were separated and the milk kefir obtained was left to set at room temperature for 10 minutes prior to the analysis.

pH Measurement

The pH value of milk kefir was measured using a pH meter (Milwaukee MW 100 Pro, United States). The pH meter was calibrated with pH 4 and pH 7 buffer solutions. The tip of the pH meter was immersed in 3 mL of milk kefir. The pH value was recorded once the reading remained stable. The pH value of milk kefir was obtained in triplicate.

Viscosity Measurement

Viscosity was measured using a viscometer (Model BDV-8S, Biobase, China). The spindle used was No. 2 and the speed was set at 30 rpm. A total amount of 120 mL of milk kefir was poured into a beaker, and the spindle was lowered into the milk kefir until it touched the detection level. Measurement of viscosity was performed in triplicate at a constant temperature of 25°C.

Lactic Acid Percentage Measurement

The determination of titratable acidity was performed following Triwibowo et al. (2020). Several studies have demonstrated that milk kefir is composed mainly of lactic acid, hence, measuring titratable acidity of milk has been perceived as a common quantitative method of the lactic acid percentage (Putri et al., 2020; Triwibowo et al., 2020). Based on Codex Alimentarius, the minimum titratable acidity for milk kefir is 0.6% (Food & Agriculture Organisation, 2022). A total of 5 mL of milk kefir was pipetted and transferred into the Erlenmeyer flask, followed by the addition of 2-3 drops of phenolphthalein solution. The mixture was titrated with 0.1N sodium hydroxide solution until a vibrant pink was observed. The lactic acid percentage was calculated following Eq. 1:

$$\text{Lactic acid percentage (\%)} = \frac{\text{Amount of NaOH added (ml)} * 0.009}{\text{Amount of milk kefir (ml)}} * 100\% \quad [1]$$

Response Surface Methodology (RSM) Experimental Design and Modelling

A two-factor Central Composite Design with five levels was generated using statistical software (Minitab Release 14, Minitab Inc., US). The processing factors, temperature and time are presented in Table 1, with a total of 39 runs varying temperature (X_1) from 18°C to 38°C and time (X_2) ranging from 5 hours to 9 hours. The fermentation time was set based on a preliminary experiment where milk kefir was fermented within this range of time and started to over-ferment after 9 hours based on the occurrence of whey separation. A temperature of 28°C and 7 hours were set as the centre points. To minimise variances, the experimental run was performed in triplicate. The central point was repeated five times to validate the reproducibility of the method. The responses measured included milk kefir's

pH (Y_1), viscosity (Y_2) and lactic acid percentage (Y_3). For modelling, an overall quadratic equation of the response variables as Eq. 2 was generated based on regression analysis from statistical tool (Minitab Release 14, Minitab Inc., US).

$$Y = \beta_0 + \beta_1 X_1 + \beta_2 X_2 + \beta_{11} {X_1}^2 + \beta_{22} {X_2}^2 + \beta_{12} X_{12} \quad [2]$$

where Y is the response variable, X_1 and X_2 are fermentation temperature and time respectively, β_0 is a constant coefficient, β_1, β_2 are linear regression coefficient, β_{11}, β_{22} are quadratic regression coefficient, β_{12} is interactive regression coefficient.

RSM Optimisation and Validation

The optimum incubation temperature and time were determined setting targets of pH at 4.4 based on Lengkey and Balia (2014), viscosity at 1200 mPa.s based on Setyawardani et al. (2019) and lactic acid percentage at 0.8% as recommended by Yilmaz et al. (2022). The optimised temperature and time were then used to predict values of response variables using a quadratic model (Eq. 2). A validation experiment was performed by using the optimum incubation temperature and time in the incubator to obtain responses which were then compared with those predicted using the model. The response variables' outcomes were compared with the predicted values using Eq. 3 to determine the adequacy of the mathematical model.

$$\text{Residual standard error, RSE } (\%) = \frac{\text{Experimental value} - \text{Predicted value}}{\text{Experimental value}} \times 100\% \quad [3]$$

Artificial Neural Network (ANN) Modelling

ANN modelling was performed and trained using MATLAB 2024a software (Mathworks, Natick, USA) along with the neural net fitting tool (nftool) from neuron network model to build the architecture graph. The same data collected for RSM was used in ANN modelling for similar response variable prediction. Before ANN training, data were normalised based on Eq. 4 to maintain a uniform attention during training process:

$$X_{normalised} = \frac{X_{d.v} - X_{mean}}{s} \quad [4]$$

where $X_{d.v.}$ is data value, X_{mean} is mean of dataset and s is standard deviation of dataset.

To preserve flexibility and to account for complexity in approximating nonlinear function of any desired level of accuracy, the number of neurons within a hidden layer was adjusted and a two-layer feedforward multilayer perceptron with a sigmoid transfer function was chosen as the nonlinear analysis method. The number of neurons within the

input and output layers was set based on the number of inputs and outputs respectively. The neural network topologies were built by performing adjustments on the neurons in hidden layers varying from 1 to 10. Levenberg-Marquardt backpropagation learning algorithm was employed as default to train the neural network. The dataset was segregated into 70% for training, 15% for validation and 15% for testing according following method proposed by Kantono et al. (2022). The performance of the ANN was evaluated based on mean squared error (MSE). A lower MSE was preferable when training model to obtain a minimal error in the model which was suggested by Kantono et al. (2022). The exact ANN architecture of present study consisted of one input layer with two neurons known for input factors, namely fermentation temperature and time, one hidden layer with five neurons and an output layer consisting of three neurons representing pH, viscosity and lactic acid percentage. Once the network was trained iteratively with a different number of neurons and the lowest MSE was achieved, the predicted response variables were generated and recorded. Every neuron consists of multiple inputs, multiplied by corresponding weights, total up, added extra bias and inserted into activation function to generate a single output through Eq. 5.

$$z = f(\sum_{i-1}^{n} w_i\, x_i + d) \quad [5]$$

where z is the output from neuron, x_i is the input value, w_i is the connection weight, d is the bias value and f is the activation function.

The predicted responses obtained from both RSM and ANN models were then compared in terms of prediction capabilities using RMSE, AAD and R^2 given in the Eqs. 6-8.

$$\text{Root Mean Squared Error (RMSE)} = \sqrt{\frac{1}{n}\sum_{i=1} |Y_{i,exp} - Y_{i,pred})^2} \quad [6]$$

$$\text{Absolute Average Deviation (AAD)} = \frac{100}{n}\left[\sum_{i=1}^{n}\left(\frac{|Y_{i,exp} - Y_{i,pred}|}{Y_{i,pred}}\right)\right] \quad [7]$$

$$\text{Coefficient of Determination } (R^2) = 1 - \frac{\sum_{i=1}^{n}(Y_{i,exp} - Y_{i,pred})^2}{\sum_{i=1}^{n}(Y_{i,exp} - Y_{mean})^2} \quad [8]$$

Amplicon-based Sequencing

Microbiological composition of optimised and commercial milk kefir was identified and compared by performing amplicon sequencing which includes 16S sequencing for bacterial diversity and ITS sequencing for fungal diversity. Prior to sequencing, microbial DNA of milk kefir samples was isolated using DNeasy Powerfood Microbial Kit (Qiagen, Hilden,

Germany) in accordance with protocol stated in Qiagen's handbook. Extracted DNA was processed for clean-up utilising AMPure XP beads (Beckman Coulter®, Brea, CA, USA) to purify the product. Then, extracted DNA was amplified specifically targeting the 16S V3-V4 regions and the ITS 2-region. Successful amplification was determined by presence of desired band in positive control and absence band in negative control. DNA amplicons were read and sequenced using Illumina Miseq System (Illumina, San Diego, California) at 2x250bp configuration, which generates approximately 100,000 raw reads per sample. Raw sequencing data collected were pre-processed using DADA2 in Rstudio (Version 2024.12.0-467) for bioinformatics analysis. Steps of pre-processing raw data involve checking sequencing quality to identify and trim low-quality regions, learning error rate, merging the contigs, defining taxonomy, collating number of sequences at different stages and creating phyloseq object. Bar plot featuring microbial composition of optimised and commercial milk kefir were constructed and their abundance percentage of dominant taxa was compared.

RESULTS AND DISCUSSION

Regression Modelling Analysis using RSM

Table 1 shows the experimental results of CCD with experimental responses including pH, viscosity and lactic acid percentage. Table 2 lists the regression coefficients, β and respective p-value from regression modelling using Eq. 2 yielding prediction models for each response (Eqs. 9-11) obtained from Minitab. It was found that all linear terms of temperature (X_1) and time (X_2) and the interaction term of temperature and time (X_{12}) were giving significant impacts to the responses. The quadratic term of temperature (X_1^2) was not significant towards pH and viscosity ($P > 0.05$) while for quadratic term of time (X_2^2) was not significant for the pH and lactic acid percentage.

Table 1
Experimental runs generated from CCD for collected milk kefir responses. Responses with subscript RSM and ANN are both predicted values from modelling using Eqs. 2 and 5

Run	X_1	X_2	Y_1			Y_2			Y_3		
			Y_{exp}	Y_{rsm}	Y_{ann}	Y_{exp}	Y_{rsm}	Y_{ann}	Y_{exp}	Y_{rsm}	Y_{ann}
1	28	7	5.55	5.47	5.52	1448.6	1536.3	1438.6	0.43	0.43	0.43
2	28	8	5.31	5.36	5.38	1395.3	1367.1	1424.6	0.45	0.48	0.47
3	28	7	5.53	5.47	5.52	1477.8	1536.3	1438.6	0.43	0.43	0.43
4	28	7	5.53	5.47	5.52	1528.3	1536.3	1438.6	0.41	0.43	0.43
5	28	7	5.46	5.47	5.52	1489.1	1536.3	1438.6	0.47	0.43	0.43
6	18	9	6.23	6.25	6.22	567.4	571.2	567.6	0.36	0.35	0.36
7	28	8	5.31	5.36	5.38	1375.0	1367.1	1424.6	0.43	0.48	0.47

Table 1 *(continued)*

Run	X_1	X_2	Y_1			Y_2			Y_3		
			Y_{exp}	Y_{rsm}	Y_{ann}	Y_{exp}	Y_{rsm}	Y_{ann}	Y_{exp}	Y_{rsm}	Y_{ann}
8	18	9	6.24	6.25	6.22	568.9	571.2	567.6	0.36	0.35	0.36
9	28	7	5.45	5.47	5.52	1485.0	1536.3	1438.6	0.47	0.43	0.43
10	23	7	5.72	5.75	5.72	1623.2	1469.6	1629.1	0.34	0.36	0.32
11	28	7	5.45	5.47	5.52	1477.8	1536.3	1438.6	0.47	0.43	0.43
12	23	7	5.74	5.75	5.72	1634.0	1469.6	1629.1	0.32	0.36	0.32
13	23	7	5.74	5.75	5.72	1647.1	1469.6	1629.1	0.34	0.36	0.32
14	28	6	5.51	5.63	5.56	1416.3	1206.0	1465.1	0.40	0.37	0.41
15	18	5	5.94	5.96	5.97	360.2	413.1	361.1	0.25	0.29	0.28
16	18	5	5.97	5.96	5.97	361.0	413.1	361.1	0.31	0.29	0.28
17	38	9	4.22	4.21	4.19	1209.2	1178.8	1184.6	0.92	0.91	0.90
18	33	7	4.97	5.14	5.01	1746.9	1691.3	1740.5	0.58	0.56	0.59
19	28	7	5.40	5.47	5.52	1427.3	1536.3	1438.6	0.43	0.43	0.43
20	33	7	4.98	5.14	5.01	1746.6	1691.3	1740.5	0.56	0.56	0.59
21	38	5	5.62	5.58	5.62	700.3	692.3	669.6	0.50	0.52	0.51
22	28	7	5.44	5.47	5.52	1421.1	1536.3	1438.6	0.43	0.43	0.43
23	28	7	5.40	5.47	5.52	1413.7	1536.3	1438.6	0.43	0.43	0.43
24	28	7	5.38	5.47	5.52	1412.8	1536.3	1438.6	0.54	0.43	0.43
25	38	5	5.62	5.58	5.62	654.2	692.3	669.6	0.50	0.52	0.51
26	28	7	5.38	5.47	5.52	1445.5	1536.3	1438.6	0.47	0.43	0.43
27	38	5	5.61	5.58	5.62	651.1	692.3	669.6	0.50	0.52	0.51
28	28	6	5.51	5.63	5.56	1408.7	1206.0	1465.1	0.41	0.37	0.41
29	33	7	4.98	5.14	5.01	1727.3	1691.3	1740.5	0.59	0.56	0.59
30	38	9	4.23	4.21	4.19	1197.3	1178.8	1184.6	0.92	0.91	0.90
31	28	7	5.37	5.47	5.52	1412.3	1536.3	1438.6	0.47	0.43	0.43
32	18	5	5.98	5.96	5.97	359.6	413.1	361.1	0.31	0.29	0.28
33	28	7	5.88	5.47	5.52	1498.9	1536.3	1438.6	0.38	0.43	0.43
34	18	9	6.22	6.25	6.22	568.4	571.2	567.6	0.36	0.35	0.36
35	28	7	5.87	5.47	5.52	1493.1	1536.3	1438.6	0.36	0.43	0.43
36	38	9	4.23	4.21	4.19	1208.3	1178.8	1184.6	0.92	0.91	0.90
37	28	8	5.31	5.36	5.38	1353.0	1367.1	1424.6	0.45	0.48	0.47
38	28	6	5.51	5.63	5.56	1413.0	1206.0	1465.1	0.40	0.37	0.41
39	28	7	5.86	5.47	5.52	1490.0	1536.3	1438.6	0.34	0.43	0.43

Note. where Y_{exp} is experimental value, Y_{rsm} is value predicted by RSM model, Y_{ann} is value predicted by ANN model

Table 2
Regression coefficients, β *and their p-value for responses, pH (Y_1), viscosity (Y_2) and lactic acid percentage (Y_3) for processing factors temperature (X_1) and time (X_2)*

Term	Y_1		Y_2		Y_3	
	β	p-value	β	p-value	β	p-value
Constant	4.848	0.000	-9698	0.000	0.874	0.000
X_1	0.1374	0.000	-105.5	0.000	-0.0706	0.000
X_2	0.006	0.000	3462	0.000	0.020	0.000
X_1^2	-0.00095	0.576*	1.77	0.144*	0.001081	0.023
X_2^2	0.0313	0.461*	-249.8	0.000	-0.0060	0.600*
X_{12}	-0.02071	0.000	4.11	0.008	0.004275	0.000

Note. $*P > 0.05$

$$Y_1 = 4.848 + 0.1374\,X_1 + 0.006\,X_2 - 0.00095{X_1}^2 + 0.0313\,{X_2}^2 - 0.02071\,X_{12} \quad [9]$$

$$Y_2 = -9698 - 105.5\,\mathrm{X}_1 + 3462\,\mathrm{X}_2 + 1.77\,{X_1}^2 - 249.8\,{X_2}^2 + 4.11\,\mathrm{X}_{12} \quad [10]$$

$$Y_3 = 0.874 - 0.0706\,\mathrm{X}_1 + 0.020\,\mathrm{X}_2 + 0.001081\,{X_1}^2 - 0.0060\,{X_2}^2 + 0.004275\,\mathrm{X}_{12} \quad [11]$$

The goodness of fit of the models was determined by the coefficient of determination, R^2. The R^2 values of pH, viscosity and lactic acid percentage were 92.19%, 95.03%and 94.51%, respectively. The results are much higher than the R^2 obtained by a parallel study by Abadl et al. (2023) on optimising coconut milk kefir, with R^2 value of 75%. Ghasemlou et al. (2012) explained that a high value of R^2 above 90% shows a close agreement between the experimental and predicted values proposed by the modelling equations, suggesting that the models are considered valid and highly reliable.

Response Surface Analysis using RSM

Figure 1a shows a sharp decrease in milk kefir pH with an increase in both fermentation temperature and time. Milk kefir pH incubated for 9 hours at a higher temperature of 38°C resulted in a lower pH of 4.23 compared to a pH of 5.96 when incubated at a lower temperature of 18°C for 9 hours. Milk kefir fermented at 38°C for 9 hours had the lowest pH which was sufficient to inhibit growth of undesirable spoilage microorganisms and preserve shelf life of the product. Alegbeleye et al. (2022) explained that maintaining a pH range between 4.2 and 4.6 was important in maintaining safety quality of food product.

The trend was in agreement with Abadl et al. (2023) who reported a gradual decrease in pH when increasing temperature of coconut milk kefir fermentation from 25°C to 35°C. In terms of fermentation time, Kivanc & Yapici (2019) observed a pH drop from 6 to 4.5 after 24 hours of milk kefir fermentation. The pH reduction is due to increased lactic acid bacteria (LAB) and its metabolism activity (Ribeiro et al., 2020). Higher fermentation temperature and longer fermentation time encourage the microorganism to proliferate rapidly and favourably, thereby increasing the LAB population which metabolises lactose into lactic acids aided by β-galactosidase enzyme. The presence of lactic acids contributes to a higher concentration of H^+ ions which drastically decreases milk kefir pH drastically (Divayanti et al., 2023).

Figure 1b shows that milk kefir viscosity gradually increased with fermentation temperature from 18°C to 38°C. With fermentation time, milk kefir viscosity also increased rapidly, reaching a peak at 7 hours, beyond which there was a gradual decline. A maximum viscosity of 1746.9 m.Pas was achieved when milk kefir was fermented at 33°C for 7 hours. Milk kefir viscosity of 1200-1600 m.Pas has been recommended by Putri et al. (2020) and it has been set as a reference for quality control as it dictates the organoleptic properties including texture, mouthfeel and cohesiveness. The increasing trend of milk kefir viscosity was consistent with Putri et al. (2020), who found that milk kefir fermented at 37°C resulted in a higher viscosity than at room temperature of 25°C. The increase of viscosity when raising fermentation temperature is attributed to the increase of kinetic energy in the molecules of milk kefir, encouraging casein coagulation and intermolecular interaction between the carbohydrate and proteins, which leads to the formation of a well-structured and stronger gel matrix (Khubber et al., 2021; Putri et al., 2020). The non-linear increase of viscosity with fermentation time was similar to that of Kivanc & Yapici (2019), who conducted a prolonged fermentation time at 22°C, where milk kefir viscosity reached its peak at 48 hours before decreasing as they focused on the formation of gel network between carbohydrate-protein network and how the gel network led to changes in viscosity during fermentation. The increase in viscosity over fermentation time is due to more and stronger molecular interactions and cross-linkages between molecules such as polysaccharides and protein (Akhi et al., 2024). The decrease in viscosity after the peak is due to whey separation when the protein network starts to denature and destabilise as a result of the growth of an extremely acidic environment from the continuous fermentation (Rekha et al., 2012).

Figure 1c shows that the lactic acid percentage increased with fermentation temperature and time due to favourable conditions for the growth and multiplication of lactic acid bacteria (Triwibowo et al., 2020). Milk kefir fermented at 38°C for 9 hours at 0.918% was the highest in terms of lactic acid percentage, and it was three times of that fermented at 18°C for 5 hours at 0.316%. The Codex Alimentarius regulated by Food and Agriculture

Organisation (2022) requires milk kefir to have at least 0.6% of lactic acid. The increase of lactic acid percentage with fermentation temperature and time is consistent with the work by Ribeiro et al. (2020), who reported that a significant increase in lactic acid percentage by a 12.17-fold higher in titratable acidity rate when kefir incubation temperature was increased from 17°C to 32°C. Kivanc & Yapici (2019) showed a gradual increase in lactic acid percentage from 0.14% to 1.0% in an extended fermentation of milk kefir from 2 to 24 hours. Hecer et al. (2019) showed that milk kefir incubated at 30°C consisted of higher *Lactobacillus* spp. count at 6.37 $\log_{10}$ CFU/mL compared to milk kefir incubated at 20°C at 6.04 $\log_{10}$ CFU/mL. The advantage of high lactic acid percentage is that it inhibits spoilage microorganisms as the acidification process drives a low pH and enhances food safety. The inverse relationship between lactic acid percentage and pH is reported in various studies (Moonga et al., 2019).

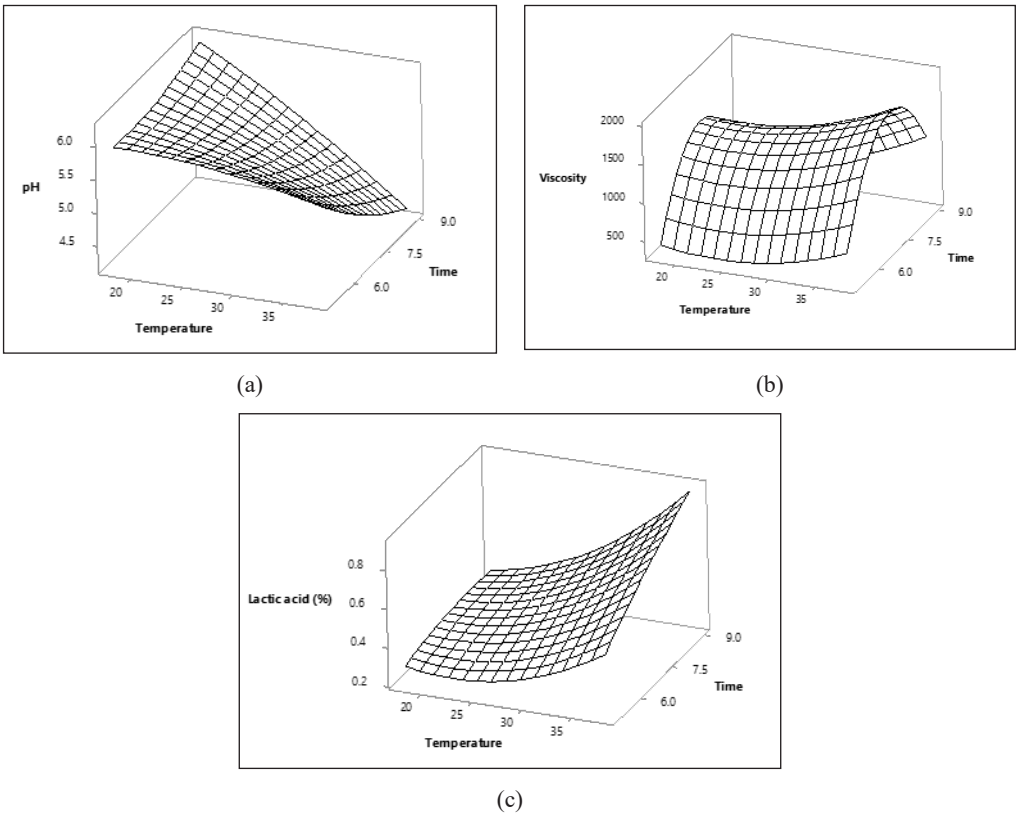

Figure 1. Response surface plot illustrating interaction effect of fermentation temperature and time on (a) pH, (b) viscosity, and (c) lactic acid percentage of milk kefir

Optimisation using RSM

The optimisation of milk kefir at a targeted pH 4.4, viscosity 1200 m.Pas and lactic acid percentage 0.8% yielded fermentation temperature at 35.78°C and fermentation time at 8.84 hours. The composite desirability obtained was 0.9717, indicating that the setting optimally achieved a favourable outcome for all responses as a whole as the result is close to one with individual desirability of pH, viscosity and lactic acid percentage at 0.9464, 0.9742 and 0.9950, respectively (Table S1). Composite and individual desirability are essential for evaluating how well the combination of processing variables satisfies the targeted response values. The validation experiment performed at the suggested optimum conditions was compared with the predicted. The residual standard error (RSE) shows that all errors were lower than 10%, where predicted and actual values are in agreement (McLaughlin & Magee, 1998), which also suggests that predictions made from models (Eqs. 9-11) are accurate and valid. Figure 2 also shows the behaviour of actual responses generated from the optimised factors demonstrated that as fermentation temperature and time increased, the lactic acid percentage and viscosity increased while the pH decreased. For viscosity, it increased with temperature, but over time, it trends up before down at around 7 hours, as seen in the response surface plot, Figure 1b.

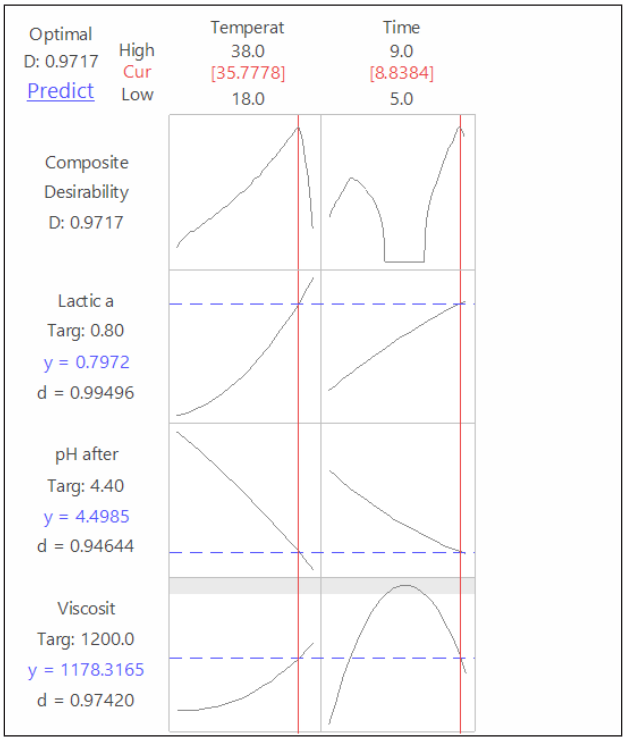

Figure 2. Response behaviour of lactic acid percentage, pH and viscosity predicted from the processing conditions

Comparison of the Predictive Capability between ANN and RSM Models

The neural network model (ANN) was established through training, validation, and testing. In constructing ANN modelling, the feedforward multilayer perceptron and 70% data were used as the training set, while the remaining 30% data was used for validation and testing set, each at 15%. One hidden layer with five neurons was chosen to construct ANN model where fermentation temperature and fermentation time were input parameters, while pH, viscosity and lactic acid percentage were the output parameters. During the training of neurons, it was found that the accuracy of the model declined after five neurons within the hidden layer. The increase of neurons beyond 5 caused the model to become overly complex and overfit the training data, leading to a high predictive error. The response values predicted by ANN model using the same dataset of RSM are presented in Table 1 as Y_{ann}.

RSM and AAN models' predictive capability were compared using statistical parameters including RMSE, AAD and R^2 which were calculated following Eqs. 6-8 as shown in Table 3. The RMSE and AAD values for all predicted responses of pH, viscosity and lactic acid percentage from the ANN model were lower when compared to the RSM model, suggesting the ANN model was more accurate in terms of smaller predictive errors and smaller absolute average deviations. For the coefficient of determination, R^2, the ANN model also presented a higher R^2 value than the RSM model by 1.92%, 4.26% and 0.70% for pH, viscosity and lactic acid percentage respectively. Achieving a low RMSE, low AAD and high R^2 are the criteria that are generally sought to define a highly accurate model as lower RMSE implies a minimal average prediction error, a lower AAD reflects consistency and minimal average deviation from actual values while a high R^2 indicates the goodness of fit of the model (Kantono et al., 2022). Prior research also agreed that ANN model provided a better predictive and generalisation ability with lower percentage error as compared to RSM in the prediction of solubility, colour change, antioxidant activity and total anthocyanin content of spray-dried pomegranate juice by Youssefi et al. (2009). The superiority of the predictive accuracy of ANN which yielded lower RMSE, lower AAD and higher R^2 values across all predicted response values can be explained by its universal capability in approximating nonlinearity of the system while the RSM is limited to second-order polynomial (Youssefi et al., 2009). The RSM, however, can provide

Table 3
Comparison of predictive capabilities of RSM and ANN modelling on responses

	pH			Viscosity			Lactic Acid Percentage		
Parameters	**RSM**	**ANN**	**Difference**	**RSM**	**ANN**	**Difference**	**RSM**	**ANN**	**Difference**
RMSE	0.046	0.035	- 0.011	0.073	0.026	- 0.47	0.00261	0.00258	- 0.00003
AAD (%)	0.116	0.056	- 0.06	1.121	0.089	- 1.032	0.692	0.008	- 0.684
R^2 (%)	92.19	94.11	+ 1.92	95.03	99.29	+ 4.26	94.51	95.21	+ 0.70

information such as individual and interaction effects of processing variables. Modelling milk kefir fermentation using both RSM and ANN methods has helped to bridge traditional fermentation practices to a more systematic and scientific approach of producing consistent and quality milk kefir product.

Comparison of Bacterial Composition

Figure 3a shows abundance percentage of phyla across optimised and commercial milk kefir. Among phyla, *Firmicutes* were found as the most dominant phylum in both optimised and commercial milk kefir. Commercial milk kefir exhibited a higher abundance percentage of *Firmicutes* than optimised milk kefir, where both accounted for 99.99% and 94.86%, respectively. *Proteobacteria* was also found in optimised milk kefir at abundance percentage of 5.09% while only a small amount was detected in commercial milk kefir which was 0.002%. A similar finding was reported recently by Sumarmono et al. (2023) who indicated *Firmicutes* and *Proteobacteria* were the dominant phyla that were found in milk kefir. *Actinobacteria* and *Bacteroidetes* were other phyla that were identified in optimised milk kefir despite in small percentages, which contributed for less than 0.001% of abundance (Table S2). *Firmicutes* as the dominant phylum serves a significant role in regulating dietary fibre uptake and colonise intestinal mucosa which leads to homeostasis that promote health promoting function for gut (Sun et al., 2023). *Firmicutes* is also known as short-chain fatty acid-producing bacteria which assist in regulating glucose metabolism and insulin sensitivity, relieving inflammatory conditions among diabetic patients (Cifuentes

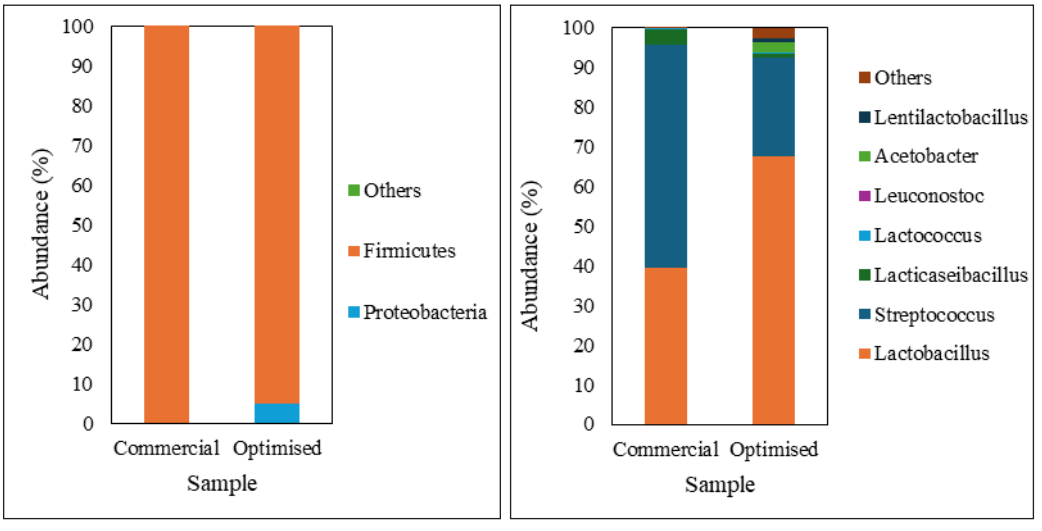

(a) (b)

Figure 3. Abundance percentage of bacterial composition in commercial and optimised milk kefir. (a) Phylum level and (b) Genus level

et al., 2024). *Proteobacteria* as the second dominant phylum in optimised milk kefir are mainly responsible for serving carbohydrate digestion in human body and trigger immune response (Hou et al., 2022).

Figure 3b shows abundance percentage of genera composition in commercial and optimised milk kefir. At genus level, optimised and commercial milk kefir consisted of a total of up to 14 and 6 genera respectively (Table S2), suggesting that optimised milk kefir exhibited a higher diversity of genera in microbial community, providing a wider range of beneficial genera with health potential. *Streptococcus*, *Lactobacillus*, *Lacticaseibacillus*, *Lactococcus* and *Leuconostoc* were the top five dominant genera found in commercial milk kefir. Optimised milk kefir comprised five dominant genera namely, *Lactobacillus*, *Streptococcus*, *Acetobacter*, *Lentilactobacillus* and *Lacticaseibacillus*. A similar finding was established in a study by Sumarmono et al. (2023), who have noted that *Lactobacillus* were predominantly detected in cow and goat milk kefir at high abundance percentage. The abundance percentage of *Lactobacillus* and *Lentilactobacillus* were observed to be higher in optimised milk kefir as compared to commercial milk kefir by a difference of 28.12% and 0.97% while abundance percentage of *Streptococcus*, *Lacticaseibacillus*, *Lactococcus,* and *Leuconostoc* were found higher in commercial milk kefir as compared to optimised milk kefir, by a difference by 31.11%, 2.95%, 0.01% and 0.1% respectively. *Lactobacillus, Streptococcus*, *Lentilactobacillus, Lacticaseibacillus, Leuconostoc,* and *Lactococcus* are recognised as probiotics as they are mainly associated with maintaining gut health and preventing pathogen invasion (Ajibola et al., 2023; Garcia et al., 2020). In fermentation, they are also a lactic-acid producing bacteria which facilitate fermentation process by lowering the pH during fermentation process that aim to preserve and extend shelf life (Ajibola et al., 2023). 16S amplicon sequences have effectively revealed the presence of other genera in optimised milk kefir that was accounted in relatively small abundance percentages. Of these, *Pseudomonas, Klebsiella, Acinetobacter,* and *Bacillus* were detected in optimised milk kefir and are typically associated with gut microbiota (Karaliute et al., 2022; Lee et al., 2019). Optimised milk kefir can serve as a potential candidate as a health-boosting product due to its high diversity in potential genera and consisting of relatively high abundance percentage of *Lactobacillus* which is often associated with mounting clinical evidences in supporting health benefits such as strengthening immunity (Rastogi et al., 2022), enhancing gut health (Huynh & Zastrow, 2023) and controlling blood glucose level (Kumari et al., 2023)

Comparison of Fungal Composition

Figure 4a shows bar plot featuring abundance percentage of fungal phyla across optimised and commercial milk kefir. Two phyla namely *Ascomycota* and *Basidiomycota* were detected in both milk kefir. *Ascomycota* was the dominant phylum in both milk kefir,

accounting for more than 90%. This was consistent with the results of both Sumarmono et al. (2023) and Marsh et al. (2013) who found that *Ascomycota* was detected abundantly in milk kefir originating from Ireland and the United Kingdom. In the present study, commercial milk kefir exhibited a higher relative abundance percentage of *Ascomycota* as compared to optimised milk kefir by a difference of 8.77%. Meanwhile, *Basidiomycota*, another phylum was found to be more abundant in optimised milk kefir as compared to commercial milk kefir by a difference of 8.76%. *Ascomycota* serves a vital role in fermented beverages in fermenting sugars and breaking down anti-nutritive factors (Cason et al., 2020). In medical field, members of *Ascomycota* also exhibit anti-diabetic properties, regulate lipid levels and serve as alpha-amylase inhibitors (Jiang et al., 2025). *Basidiomycota* also exhibit multiple roles, from decomposers in soil to enzyme development and bioremediation. *Basidiomycota* has been extensively reviewed recently due to its bioactive compounds that contribute to antimicrobial, anticancer and anti-inflammatory activities (Oliveira et al., 2024).

Figure 4b shows bar plot featuring abundance percentage of fungal genera for optimised and commercial milk kefir. The most abundant genus in commercial milk kefir was *Debaryomyces* (91.81%) but only a small amount was found in optimised milk kefir (3.84%). In optimised milk kefir, *Pichia* (83.66%) was found dominantly while commercial milk kefir consisted of less than 1% of *Pichia*. A similar finding was found in a study by Rahmani et al. (2022) who detected *Pichia* abundantly in milk kefir. In contrast, research by Sumarmono et al. (2023) reported *Kazachstania* and *Kluyveromyces* as the dominant genus in cow milk kefir. *Pichia* serves an important role in fermentation where it acts as a biofilm

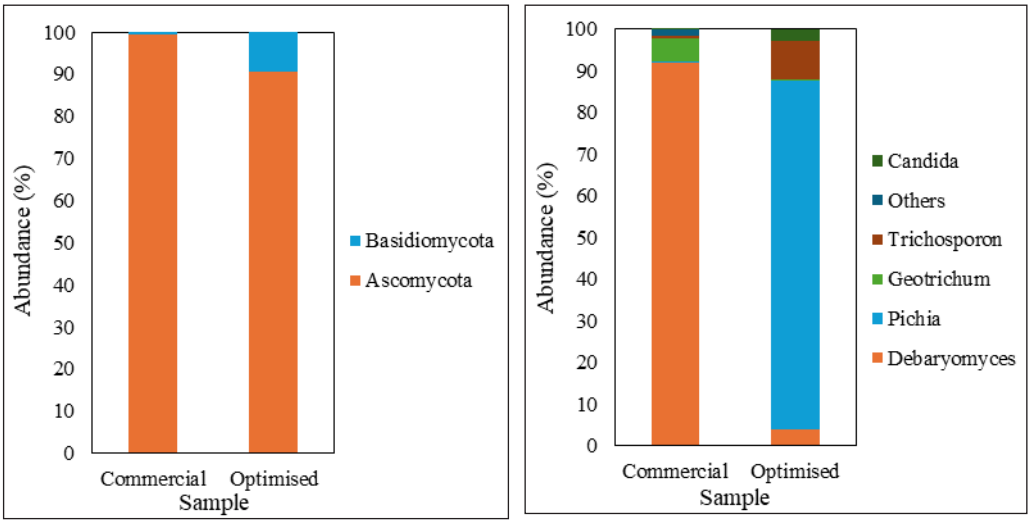

(a) (b)

Figure 4. Abundance percentage of fungal composition in commercial and optimised milk kefir. (a) Phylum level and (b) Genus level

producer that adheres to kefir grain surface and establishes a symbiotic relationship with *Lactobacillus* where they utilise bioproducts as energy and microbial growth factors, which also have the role of contributing to lactic and alcohol fermentation (Hamet et al., 2013; Wang et al., 2012). Referring to Table S3, *Geotrichum* was found in a higher percentage in commercial milk kefir compared to optimised milk kefir by a difference of 5.23%. Meanwhile, optimised milk kefir showed a higher percentage of *Trichosporon* and *Candida* by 8.79% and 2.65% respectively when compared to commercial milk kefir. Other genera with abundance percentage less than 1% in commercial milk kefir include *Cyberlindnera*, *Gyoerffyella*, *Aspergillus*, *Dipodacus, Wickerhamiella,* and *Cutaneotrichosporon* while *Mycoaciella* and *Clasdosporium* were found in small percentages in optimised milk kefir. This showed that the optimum processing parameters have also helped provide favourable conditions that encouraged the growth of beneficial bacteria such as *Pichia* as the dominant fungal species which facilitates microbial growth for successive lactic and alcohol fermentation.

CONCLUSION

Modelling milk kefir fermentation using both RSM and ANN methods has helped bridge traditional fermentation practices to a more systematic and scientific approach to producing consistent and quality milk kefir product. By optimising processing parameters using RSM, target physicochemical qualities such as pH, viscosity and lactic acid percentage can be achieved. It also allows determination of combinations of processing parameters that provide a critical impact on changes of qualities. The recommended fermentation temperature of 35.78°C and fermentation time of 8.84 hours according to the definition of desired milk kefir quality with targeted values of 4.4 pH, 0.8% lactic acid and 1200 mPa.s. While the ANN gave a better modelling predictive capability, the RSM has provided more information, including interaction effects of processing factors and the optimal conditions to produce targeted milk kefir quality. The optimisation approach has not only helped in determining optimal processing parameters for desired quality of milk kefir but also created favourable conditions that promote the enhanced growth of beneficial bacteria including probiotics *Lactobacillus. Pichia* was found to be the dominant fungal which serves as an important bioproduct and microbial growth factor in successive lactic and alcohol fermentation. This validated modelling framework ultimately enables manufacturers to adapt for industrial manufacturing with targeted physicochemical quality in a more efficient and low-cost manner. Scaling-up to a pilot-scale level and more research on product shelf life and stability integrated with consumer sensory studies will be helpful in commercialisation validation of milk kefir.

ACKNOWLEDGEMENT

This work was supported by the Ministry of Education (MOE) Malaysia, through the Fundamental Research Grant Scheme with Project No. FRGS/1/2022/TK05/UPM/01/3. We thanked Dr. Chun Wie Chong from the School of Pharmacy and Monash Malaysia Microbiome Centre of Microbiome Research Centre, Monash University Malaysia for his advice in this research.

REFERENCES

Abadl, M. M. T., Marzlan, A. A., Sulaiman, R., Abas, F., & Meor Hussin, A. S. (2023). Optimisation of coconut milk kefir beverage by RSM and screening of its metabolites and peptides. *Fermentation*, *9*(5), 430. https://doi.org/10.3390/FERMENTATION9050430/S1

Ajibola, O. O., Thomas, R., & Bakare, B. F. (2023). Selected fermented indigenous vegetables and fruits from Malaysia as potential sources of natural probiotics for improving gut health. *Food Science and Human Wellness*, *12*(5), 1493-1509. https://doi.org/10.1016/J.FSHW.2023.02.011

Akhi, A., Ahmed, T., Ara, R., & Rana, M. R. (2024). Response surface optimisation of thermo-sonication conditions and taro mucilage concentrations for the preparation of soy yoghurt. *Journal of Agriculture and Food Research*, *15*, Article 100918. https://doi.org/10.1016/J.JAFR.2023.100918

Alegbeleye, O., Odeyemi, O. A., Strateva, M., & Stratev, D. (2022). Microbial spoilage of vegetables, fruits and cereals. *Applied Food Research*, *2*(1), Article 100122. https://doi.org/10.1016/J.AFRES.2022.100122

Alves, E., Ntungwe, E. N., Gregório, J., Rodrigues, L. M., Pereira-Leite, C., Caleja, C., Pereira, E., Barros, L., Aguilar-Vilas, M. V., Rosado, C., & Rijo, P. (2021). Characterisation of kefir produced in household conditions: Physicochemical and nutritional profile, and storage stability. *Foods, 10*(5), Article 1057. https://doi.org/10.3390/FOODS10051057

Antil, S. K., Antil, P., Singh, S., Kumar, A., & Pruncu, C. I. (2020). Artificial neural network and response surface methodology based analysis on solid particle erosion behaviour of polymer matrix composites. *Materials*, *13*(6), Article 1381. https://doi.org/10.3390/MA13061381

Bellikci-Koyu, E., Sarer-Yurekli, B. P., Akyon, Y., Aydin-Kose, F., Karagozlu, C., Ozgen, A. G., Brinkmann, A., Nitsche, A., Ergunay, K., Yilmaz, E., & Buyuktuncer, Z. (2019). Effects of regular kefir consumption on gut microbiota in patients with metabolic syndrome: A parallel-group, randomised, controlled study. *Nutrients*, *11*(9). https://doi.org/10.3390/NU11092089

Buzby, J. C., Wells, H. F., & Hyman, J. (2014). The estimated amount, value, and calories of postharvest food losses at the retail and consumer levels in the United States. *Food Loss in the United States: Selected Analyses*, 1-42. https://doi.org/10.2139/SSRN.2501659

Cason, E. D., Mahlomaholo, B. J., Taole, M. M., Abong, G. O., Vermeulen, J. G., de Smidt, O., Vermeulen, M., Steyn, L., Valverde, A., & Viljoen, B. (2020). Bacterial and fungal dynamics during the fermentation process of Sesotho, a traditional beer of Southern Africa. *Frontiers in Microbiology*, *11*, 1451. https://doi.org/10.3389/FMICB.2020.01451/FULL

Cifuentes, M. P., Chapman, J. A., & Stewart, C. J. (2024). Gut microbiome derived short chain fatty acids: Promising strategies in necrotising enterocolitis. *Current Research in Microbial Sciences*, *6*, Article 100219. https://doi.org/10.1016/J.CRMICR.2024.100219

de Sainz, I., Redondo-Solano, M., Solano, G., & RamÃ, L. (2020). Short communication: Effect of different kefir grains on the attributes of kefir produced with milk from Costa Rica. *Journal of Dairy Science*, *103*, 215-219. https://doi.org/10.3168/jds.2018-15970

Divayanti, F., Maruddin, F., Malaka, R., & Dagong, M. I. A. (2023). Investigating the effects of fermentation time on physicochemical properties of commercial liquid milk kefir. *AIP Conference Proceedings*, *2628*. https://doi.org/10.1063/5.0144008/17962871/050014_1_5.0144008.PDF

Fiorda, F. A., de Melo Pereira, G. V., Thomaz-Soccol, V., Rakshit, S. K., Pagnoncelli, M. G. B., Vandenberghe, L. P. de S., & Soccol, C. R. (2017). Microbiological, biochemical, and functional aspects of sugary kefir fermentation - A review. *Food Microbiology*, *66*, 86-95. https://doi.org/10.1016/J.FM.2017.04.004

Florence Adeola, A., Olajide Philip, S., Abdul-Razaq Adesola, A., Henry Adegoke, B., & Adebukola Tolulope, O. (2024). Response surface methodology for the optimisation of process parameters during hot-air frying of chicken sausages incorporated with corn bran. *Sustainable Food Technology*. https://doi.org/10.1039/D3FB00204G

Food and Agriculture Organisation. (2022). *Standard for fermented milks* (CXS 243-2003). Codex Alimentarius.

Garcia, C., Guerin, M., Souidi, K., & Remize, F. (2020). Lactic fermented fruit or vegetable juices: Past, present and future. *Beverages, 6*(1), Article 8. https://doi.org/10.3390/BEVERAGES6010008

Garofalo, C., Osimani, A., Milanović, V., Aquilanti, L., De Filippis, F., Stellato, G., Di Mauro, S., Turchetti, B., Buzzini, P., Ercolini, D., & Clementi, F. (2015). Bacteria and yeast microbiota in milk kefir grains from different Italian regions. *Food Microbiology, 49*(1), 123-133. https://doi.org/10.1016/J.FM.2015.01.017

Gentry, B., Cazón, P., & O'Brien, K. (2023). A comprehensive review of the production, beneficial properties, and applications of kefiran, the kefir grain exopolysaccharide. *International Dairy Journal, 144*, Article 105691. https://doi.org/10.1016/J.IDAIRYJ.2023.105691

Ghasemlou, M., Khodaiyan, F., Jahanbin, K., Gharibzahedi, S. M. T., & Taheri, S. (2012). Structural investigation and response surface optimisation for improvement of kefiran production yield from a low-cost culture medium. *Food Chemistry*, *133*(2), 383-389. https://doi.org/10.1016/J.FOODCHEM.2012.01.046

Gul, O., Mortas, M., Atalar, I., Dervisoglu, M., & Kahyaoglu, T. (2015). Manufacture and characterisation of kefir made from cow and buffalo milk, using kefir grain and starter culture. *Journal of Dairy Science, 98*(3), 1517-1525. https://doi.org/10.3168/JDS.2014-8755

Hamet, M. F., Londero, A., Medrano, M., Vercammen, E., Van Hoorde, K., Garrote, G. L., Huys, G., Vandamme, P., & Abraham, A. G. (2013). Application of culture-dependent and culture-independent methods for the identification of Lactobacillus kefiranofaciens in microbial consortia present in kefir grains. *Food Microbiology, 36*(2), 327-334. https://doi.org/10.1016/J.FM.2013.06.022

Hecer, C., Ulusoy, B., & Kaynarca, D. (2019). Effect of different fermentation conditions on composition of kefir microbiota. *International Food Research Journal*, *26*(2), 401-409.

Hou, K., Wu, Z.-X., Chen, X.-Y., Wang, J.-Q., Zhang, D., Xiao, C., Zhu, D., Koya, J. B., Wei, L., Li, J., & Chen, Z.-S. (2022). Microbiota in health and diseases. *Signal Transduction and Targeted Therapy*, *7*. https://doi.org/10.1038/s41392-022-00974-4

Huynh, U., & Zastrow, M. L. (2023). Metallobiology of Lactobacillaceae in the gut microbiome. *Journal of Inorganic Biochemistry*, *238*, Article 112023. https://doi.org/10.1016/J.JINORGBIO.2022.112023

Jiang, Y., Song, H., Zhang, G., & Ling, J. (2025). The application of medicinal fungi from the subphylum Ascomycota in the treatment of type 2 diabetes. *Journal of Future Foods*, *5*(4), 361-371. https://doi.org/10.1016/J.JFUTFO.2024.07.014

Kahraman, M., Ertekin, Y. H., & Satman, İ. (2021). The effects of kefir on kidney tissues and functions in diabetic rats. *Probiotics and Antimicrobial Proteins, 13*(2), 375-382. https://doi.org/10.1007/S12602-020-09698-9/METRICS

Kantono, K., How, M. S., & Wang, Q. J. (2022). Design of experiments meets immersive environment: Optimising eating atmosphere using artificial neural network. *Appetite, 176*, Article 106122. https://doi.org/10.1016/J.APPET.2022.106122

Karaliute, I., Ramonaite, R., Bernatoniene, J., Petrikaite, V., Misiunas, A., Denkovskiene, E., Razanskiene, A., Gleba, Y., Kupcinskas, J., & Skieceviciene, J. (2022). Reduction of gastrointestinal tract colonisation by Klebsiella quasipneumoniae using antimicrobial protein KvarIa. *Gut Pathogens, 14*(1), 1-11. https://doi.org/10.1186/S13099-022-00492-2/FIGURES/4

Khubber, S., Chaturvedi, K., Thakur, N., Sharma, N., & Yadav, S. K. (2021). Low-methoxyl pectin stabilises low-fat set yoghurt and improves their physicochemical properties, rheology, microstructure and sensory liking. *Food Hydrocolloids, 111*, Article 106240. https://doi.org/10.1016/J.FOODHYD.2020.106240

Kivanc, M., & Yapici, E. (2019). Survival of escherichia coli o157:H7 and Staphylococcus aureus during the fermentation and storage of kefir. *Food Science and Technology (Brazil)*, *39*, 225-230. https://doi.org/10.1590/FST.39517

Kumari V. B, C., Huligere, S. S., Alotaibi, G., Al Mouslem, A. K., Bahauddin, A. A., Shivanandappa, T. B., & Ramu, R. (2023). Antidiabetic activity of potential probiotics Limosilactobacillus spp., Levilactobacillus spp., and Lacticaseibacillus spp. isolated from fermented sugarcane juice: A comprehensive in vitro and in silico study. *Nutrients, 15*(8). https://doi.org/10.3390/NU15081882

Lee, N. K., Kim, W. S., & Paik, H. D. (2019). Bacillus strains as human probiotics: characterisation, safety, microbiome, and probiotic carrier. *Food Science and Biotechnology, 28*(5), Article 1297. https://doi.org/10.1007/S10068-019-00691-9

Leite, A. M. de O., Miguel, M. A. L., Peixoto, R. S., Rosado, A. S., Silva, J. T., & Paschoalin, V. M. F. (2013). Microbiological, technological, and therapeutic properties of kefir: A natural probiotic beverage. *Brazilian Journal of Microbiology, 44*(2), 341-349. https://doi.org/10.1590/S1517-83822013000200001

Lengkey, H. A. W., & Balia, R. L. (2014). The effect of starter dosage and fermentation time on pH and lactic acid production. *Biotechnology in Animal Husbandry*, *30*(2), 339-347. https://doi.org/10.2298/BAH1402339L

Marsh, A. J., O'Sullivan, O., Hill, C., Ross, R. P., & Cotter, P. D. (2013). Sequencing-based analysis of the bacterial and fungal composition of kefir grains and milks from multiple sources. *PLOS ONE, 8*(7), Article e69371. https://doi.org/10.1371/JOURNAL.PONE.0069371

Martin, N. H., Torres-Frenzel, P., & Wiedmann, M. (2021). Invited review: Controlling dairy product spoilage to reduce food loss and waste. *Journal of Dairy Science*, *104*(2), 1251-1261. https://doi.org/10.3168/JDS.2020-19130

McLaughlin, C. P., & Magee, T. R. A. (1998). The determination of sorption isotherm and the isosteric heats of sorption for potatoes. *Journal of Food Engineering*, *35*(3), 267-280. https://doi.org/10.1016/S0260-8774(98)00025-9

Ming, J. L. K., Anuar, M. S., How, M. S., Noor, S. B. M., Abdullah, Z., & Taip, F. S. (2021). Development of an artificial neural network utilising particle swarm optimisation for modelling the spray drying of coconut milk. *Foods, 10*(11), Article 2708. https://doi.org/10.3390/FOODS10112708

Moonga, H. B., Schoustra, S. E., Linnemann, A. R., Kuntashula, E., Shindano, J., & Smid, E. J. (2019). The art of mabisi production: A traditional fermented milk. *PLOS ONE*, *14*(3), Article e0213541. https://doi.org/10.1371/JOURNAL.PONE.0213541

Oliveira, R. S., Preto, M., Santos, G., Silva, A. M., Vasconcelos, V., & Martins, R. (2024). Exploring the bioactive potential of Pisolithus (Basidiomycota): Comprehensive insights into antimicrobial, anticancer, and antioxidant properties for innovative applications. *Microorganisms, 12*(3), 450. https://doi.org/10.3390/MICROORGANISMS12030450

Putri, Y. D., Setiani, N. A., & Warya, S. (2020). The effect of temperature, incubation, and storage time on lactic acid content, pH, and viscosity of goat milk kefir. *Current Research on Biosciences and Biotechnology, 2*(1), 101-104. https://doi.org/10.5614/CRBB.2020.2.1/HPMQ5042

Rahmani, B., Alimadadi, N., Attaran, B., & Nasr, S. (2022). Yeasts from Iranian traditional milk kefir samples: Isolation, molecular identification, and their potential probiotic properties. *Letters in Applied Microbiology*, *75*(5), 1264-1274. https://doi.org/10.1111/LAM.13794

Rastogi, S., Singh, A., De, S., Soares, C., & Bezirtzoglou, E. (2022). Gut microbiome and human health: Exploring how the probiotic genus Lactobacillus modulate immune responses. *Frontiers in Pharmacology, 13*, Article 1042189. https://doi.org/10.3389/FPHAR.2022.1042189

Razmi-Rad, E., Ghanbarzadeh, B., Mousavi, S. M., Emam-Djomeh, Z., & Khazaei, J. (2007). Prediction of rheological properties of Iranian bread dough from chemical composition of wheat flour by using artificial neural networks. *Journal of Food Engineering*, *81*(4), 728-734. https://doi.org/10.1016/J.JFOODENG.2007.01.009

Rekha, R., V, U., Dharaiya, C. N., & Bhopal, S. (2012). Factors affecting syneresis in yoghurt: A review. *Indian Journal of Dairy and Bioscience, 23*, 1-11.

Ribeiro, A. C., Lemos, Á. T., Lopes, R. P., Mota, M. J., Inácio, R. S., Gomes, A. M. P., Sousa, S., Delgadillo, I., & Saraiva, J. A. (2020). The combined effect of pressure and temperature on kefir production—A case study of food fermentation in unconventional conditions. *Foods*, *9*(8). https://doi.org/10.3390/FOODS9081133

Rosa, D. D., Dias, M. M. S., Grześkowiak, Ł. M., Reis, S. A., Conceição, L. L., & Peluzio, M. D. C. G. (2017). Milk kefir: Nutritional, microbiological, and health benefits. *Nutrition Research Reviews*, *30*(1), 82-96. https://doi.org/10.1017/S0954422416000275

Setyawardani, T., Sumarmono, J., Rahardjo, A. H. D., Widayaka, K., & Santosa, R. S. S. (2019). Texture profile and sensory characteristics of kefir with colostrum addition. *IOP Conference Series: Earth and Environmental Science*, *372*(1). https://doi.org/10.1088/1755-1315/372/1/012036

Sipos, A. (2020). A knowledge-based system as a sustainable software application for the supervision and intelligent control of an alcoholic fermentation process. *Sustainability, 12*(23), Article 10205. https://doi.org/10.3390/SU122310205

Sumarmono, J., Kusuma, R. J., Rahayu, N., Sukarno, A. S., & Wulansari, P. D. (2023). Metagenomic analysis of the microbial community in kefir grains from different milk sources. *Biodiversitas, 24*(10), 5302-5308. https://doi.org/10.13057/BIODIV/D241011

Sun, Y., Zhang, S., Nie, Q., He, H., Tan, H., Geng, F., Ji, H., Hu, J., & Nie, S. (2023). Gut firmicutes: Relationship with dietary fibre and role in host homeostasis. *Critical Reviews in Food Science and Nutrition, 63*(33), 12073-12088. https://doi.org/10.1080/10408398.2022.2098249

Triwibowo, B., Wicaksono, R., Antika, Y., Ermi, S., Jarmiati, A., Ari Setiadi, A., & Syahriar, R. (2020). The effect of kefir grain concentration and fermentation duration on characteristics of cow milk-based kefir. *Journal of Physics: Conference Series, 1444*(1), 012001. https://doi.org/10.1088/1742-6596/1444/1/012001

Wang, S. Y., Chen, K. N., Lo, Y. M., Chiang, M. L., Chen, H. C., Liu, J. R., & Chen, M. J. (2012). Investigation of microorganisms involved in biosynthesis of the kefir grain. *Food Microbiology, 32*(2), 274-285. https://doi.org/10.1016/J.FM.2012.07.001

Yilmaz, B., Sharma, H., Melekoglu, E., & Ozogul, F. (2022). Recent developments in dairy kefir-derived lactic acid bacteria and their health benefits. *Food Bioscience, 46*, 101592. https://doi.org/10.1016/J.FBIO.2022.101592

Yilmaz-Ersan, L., Ozcan, T., Akpinar-Bayizit, A., & Sahin, S. (2018). Comparison of antioxidant capacity of cow and ewe milk kefirs. *Journal of Dairy Science, 101*(5), 3788-3798. https://doi.org/10.3168/JDS.2017-13871

Youssefi, S., Emam-Djomeh, Z., & Mousavi, S. M. (2009). Comparison of Artificial Neural Network (ANN) and Response Surface Methodology (RSM) in the prediction of quality parameters of spray-dried pomegranate juice. *Drying Technology, 27*(7), 910-917. https://doi.org/10.1080/07373930902988247

SUPPLEMENTARY DATA

Table S1
Response optimisation and desirability

Responses	Goal	Target	Predicted Result	Experimental Result	RSE (%)	Desirability
Y_1	Target	4.4	4.4985	4.51	0.25	0.9464
Y_2	Target	1200	1178.32	1296.6	9.12	0.9742
Y_3	Target	0.8	0.7972	0.792	0.66	0.9950

Table S2
Bacterial composition of optimised and commercial milk kefir

Sample	Commercial	Optimised_R1	Optimised_R2	Optimised_R3
Phylum				
Firmicutes	99.99754	96.45881	93.05435	95.1441
Proteobacteria	0.002457	3.518859	6.918533	4.830824
Spirochaetes	0	0	0	0
Bacteroidetes	0	0.00072	0	0
Candidatus_Saccharibacteria	0	0	0	0
Actinobacteria	0	0	0.001731	0
Fusobacteria	0	0	0	0
Genus				
Streptococcus	56.06486	24.95623	23.06716	26.81051
Lactobacillus	39.57859	69.22007	67.80139	66.08603
Lacticaseibacillus	3.952579	1.262293	0.768405	0.980652
Lactococcus	0.224704	0.151302	0.263635	0.233323
Leuconostoc	0.135068	0.034583	0.047304	0.043182
Pseudomonas	0.002456	0.016571	0.029421	0.022288
Acetobacter	0	1.464030	3.376484	2.505955
Lentilactobacillus	0	0.831442	1.101843	0.990402
Klebsiella	0	0.744984	1.192990	0.697879
Moraxella	0	0.010087	0.017306	0.019502
Acinetobacter	0	0.006484	0.008076	0.009054
Bacillus	0	0.002882	0.007499	0.004615
Brachybacterium	0	0	0.001731	0
Massilia	0	0	0.001731	0

Table S3
Fungal composition of optimised and commercial milk kefir

Sample	Commercial	Optimised_R1	Optimised_R2	Optimised_R3
Phylum				
Ascomycota	99.3535	99.7347	92.7599	79.2698
Basidiomycota	0.64647	0.26529	7.24009	20.7302
Genus				
Debaryomyces	91.8081	3.76292	4.12425	3.65451
Geotrichum	5.52877	0.80983	0.08234	0
Cyberlindnera	0.77788	0.04887	0	0
Trichosporon	0.62359	0.23736	7.24551	20.7512
Gyoerffyella	0.41948	0	0	0
Pichia	0.34394	92.5929	85.9132	72.4812
Aspergillus	0.17679	0	0	0
Dipodascus	0.13822	0	0	0
Candida	0.10447	2.52025	2.63473	3.09196
Wickerhamiella	0.04982	0	0	0
Cutaneotrichosporon	0.02893	0	0	0
Mycoaciella	0	0.02793	0	0
Cladosporium	0	0	0	0.02115

Pertanika J. Trop. Agric. Sci. 49 (S1): 57 - 81 (2026)

PERTANIKA JOURNALS

TROPICAL AGRICULTURAL SCIENCE

Journal homepage: http://www.pertanika.upm.edu.my/

Physicochemical and Microstructural Properties of Buffalo Meat Batter Incorporated with Ultrasound-treated Coconut Flesh as a Meat Substitute

Nur Shahira Shaifulamri[1], Abu Bakar Asyrul-Izhar[1], Nurul Izzah Khalid[1], Rabiha Sulaiman[1], and Mohammad Rashedi Ismail-Fitry[1, 2]*

[1]Department of Food Technology, Faculty of Food Science and Technology, Universiti Putra Malaysia, 43400 UPM Serdang, Selangor, Malaysia
[2]Halal Products Research Institute, Universiti Putra Malaysia, 43400 UPM Serdang, Selangor, Malaysia

ABSTRACT

Coconut flesh exhibits potential as a meat substitute due to its physicochemical properties (pH, cooking yield, and water-holding capacity (WHC)), which can be further enhanced through ultrasound treatment. This study aimed to evaluate the effects of ultrasound treatment and varying concentrations of coconut flesh on the physicochemical, rheological, and microstructural properties of buffalo meat batter. Five formulations were formulated, which are: a control (100% buffalo meat), 50% buffalo meat with 50% untreated coconut flesh (50%C), 100% untreated coconut flesh (100%C), 50% buffalo meat with 50% ultrasound-treated coconut flesh (50%USC), and 100% ultrasound-treated coconut flesh (100%USC). The results indicated that the 50%USC formulation effectively replaced buffalo meat without inducing significant (p>0.05) alterations in the physicochemical properties. This formulation exhibited a more stable emulsion and superior moisture retention compared to the control, as well as lower fat content and higher protein levels than the other treated samples (p<0.05). Furthermore, the texture profile of the 50%USC formulation was acceptable and comparable to the control formulation (100% buffalo meat). Notably, 50%USC also outperformed the control in terms of rheological and microstructural characteristics. Additionally, the 50%C formulation emerged as a viable alternative, displaying physicochemical, textural, and water-holding capacity (WHC) properties comparable to the control, with no statistically significant (p>0.05) deterioration in these quality attributes. These findings suggest that substituting buffalo meat with coconut flesh, particularly when subjected to ultrasound

ARTICLE INFO

Article history:
Received: 18 July 2025
Accepted: 31 December 2025
Published: 19 March 2026

DOI: https://doi.org/10.47836/pjtas.49.S1.03

E-mail addresses:
shahirashaifulamri@gmail.com (Nur Shahira Shaifulamri)
asyrul@upm.edu.my (Abu Bakar Asyrul-Izhar)
nurulizzah@upm.edu.my (Nurul Izzah Khalid)
rabiha@upm.edu.my (Rabiha Sulaiman)
ismailfitry@upm.edu.my (Mohammad Rashedi Ismail-Fitry)
* Corresponding author

treatment, may enhance the quality and structural integrity of meat batter while maintaining desirable functional properties.

Keywords: Emulsion stability, healthier meat products, meat analogue, meat emulsion, meat replacement

INTRODUCTION

Meat substitutes are food materials that replace animal protein with plant-based sources like grains, beans, or cereals (Sze Wei et al., 2024). Cristina et al. (2021) classified non-animal meat products into three main types: meat extenders, which are non-meat ingredients with high protein content; meat substitutes, which replicate the texture, appearance and functionality of meat; and total protein products, which are entirely free from animal-derived proteins. Meat substitutes are formulated to act as direct analogues to conventional meat, enabling their incorporation into food products that traditionally rely on animal-derived meat components. Traditions used tempeh, wheat gluten, and tofu as protein sources to replace meat consumption (Jiang et al., 2020). Meat substitutes may be made from a variety of protein sources, including soy protein, cereal protein, and mycoprotein (Ismail et al., 2020). According to Riaz (2005), they were successful in providing the desired quality of the meat-replacement product compared to the meat-based product. The consumption of meat substitutes is associated with several health benefits, including improved quality of life, reduced risk of obesity, cardiovascular protection, lower blood cholesterol levels, decreased risk of cancer, and enhanced bone mass development. The ingredients commonly used in plant-based meat alternatives can improve the nutritional profile of the final product (Tuso et al., 2013). This recognition has led to growing consumer demand for meat substitutes.

Coconut, scientifically known as *Cocos nucifera* L., may be employed in its entirety, from the tree's trunk to its leaves. Coconut ranks as the fourth most important industrial crop in Malaysia, following palm, rubber, and paddy cultivation (Rozhan & Rohany, 2021). The flesh is the white, meaty component of a coconut seed. Coconut flesh is classified into two types: matured coconut kopyor (water with meat particles floating in it) and immature coconut. Wynn (2017) observed slight variations in the macronutrient composition between mature and immature coconut meat. In the matured coconut meat, a decrease in crude fat was observed alongside a reciprocal increase in total carbohydrates (calculated by difference). The protein found in coconut flesh is certainly derived from the oilseeds; nevertheless, it is lacking in methionine, lysine and threonine (Tenda et al., 2021). The proportion of essential amino acids in coconut flesh is naturally lower than that found in animal proteins. Nevertheless, proteins derived from mature coconut possess a generally favourable amino acid composition and exhibit comparatively good nutritional quality (Ching et al., 2015; Wynn, 2017). Fresh coconut flesh has been shown to have excellent

protein-emulsifying properties, suggesting its potential applicability in the formulation of meat products (Onsaard et al., 2006). In addition, it has an aromatic flavour and odour (Jangchud et al., 2007), and the sweet taste of regular coconut is mainly due to sucrose (Wynn, 2017), which could beneficially affect the sensory acceptance of the final product.

An ultrasound homogeniser, also known as a sonicator, is a device equipped with a vibrating probe that generates shear forces, inducing cavitation within liquid samples. This instrument is essential for sample homogenisation, cell lysis, particle size reduction in suspensions, extraction of biological materials, and the enhancement of chemical processes (O'Sullivan et al., 2017). Aside from that, they may be used to produce an emulsion. The structure of proteins can be altered by utilising ultrasound techniques. Ultrasound treatment enhances the solubility and viscosity of soy protein isolate dispersions, thereby improving subsequent processing steps (Hu et al. 2013). This discovery was supported by Tian et al. (2020), who found that ultrasound exerted a substantial influence on the protein's structural and physicochemical characteristics, promoting the breakdown of peptide aggregates by disrupting non-covalent interactions. Various studies have reported that high-frequency ultrasound can improve protein solubility, reduce protein particle size, and enhance their functional properties (Arzeni et al. 2012; Jambrak et al. 2008). Jambrak et al. (2008) examined the impact of low-intensity, high-energy ultrasound (20-40 kHz) applied for 15 to 30 minutes on whey protein and found that the treatment improved both its solubility and hydrolysis. These improvements were attributed to conformational changes in the globular structure of proteins, which exposed hydrophilic regions to water. Similarly, Arzeni et al. (2012) examined the impact of high-frequency ultrasound on protein degradation, aggregation formation and solubility. Their findings suggested that increasing the temperature could facilitate the dissociation of small protein aggregates and reduce particle formation. Concurrently, ultrasound treatment promoted protein-water interactions, further enhancing protein solubility.

As coconut flesh has potential as a meat substitute, pre-treatment with ultrasound could enhance its physicochemical properties compared with untreated samples. Therefore, this study aimed to evaluate the use of ultrasound-treated and untreated coconut flesh as substitutes for meat in the production of buffalo meat batter. The output could benefit the food industry and future research in finding a suitable meat substitute.

MATERIALS AND METHODS

Meat Batter Preparation

Fresh tenderloin, buffalo meat, and animal fats were acquired from the Pasar Borong Selangor, Seri Kembangan, Selangor, Malaysia. The dry ingredients, including semi-matured grated coconut flesh, salt, cornstarch, sodium tripolyphosphate (STPP), sugar, and garlic powder, were sourced from the Sri Serdang local market in Seri Kembangan,

Table 1
Formulation of buffalo meat batter with different amounts of coconut flesh or ultrasound-treated coconut flesh as meat substitutes

Ingredients %	Control	50%C	100%C	50%USC	100%USC
Meat	70	35	-	35	-
Coconut	-	35	70	-	-
Ultrasound-treated coconut	-	-	-	35	70
Animal fats	15	15	15	15	15
Corn starch	5	5	5	5	5
Salt	1.2	1.2	1.2	1.2	1.2
STPP	0.3	0.3	0.3	0.3	0.3
Garlic powder	1.0	1.0	1.0	1.0	1.0
Sugar	1.0	1.0	1.0	1.0	1.0
Ice water	6.5	6.5	6.5	6.5	6.5
Total	**100**	**100**	**100**	**100**	**100**

Selangor, Malaysia. The sample preparation for the meat batter emulsion followed the steps described by Ismail et al. (2021a), with several modifications. First, the lean meat and fat were ground separately in a mincer (Model 4822, Hobart, Offenburg, Germany) through an 8 mm plate, then stored at -18°C.

The ultrasound treatment on the coconut flesh was adapted from Sui et al. (2017) and Sun et al. (2019) with a few modifications. The shredded coconut flesh was soaked in deionised water, then homogenised at 5,000 rpm for 5 minutes in a chilled microcentrifuge (Kubota 3740, Japan). The goal of pre-homogenising is to produce a coarse o/w emulsion. The shredded coconut was then treated for 10 minutes in an ice bath using an ultrasound homogeniser set to 25% power (the full power is 500 W) with a Φ6 mm ultrasound probe. The basic formulation for the meat batter consisted of 70% minced meat, 15% fat, 6.5% ice water, 5% corn flour, 1.2% salt, 1% garlic powder, 1% sugar, and 0.3% STPP. Five formulations were prepared with 100% meat (control), 50% meat + 50% coconut flesh (50%C), 100% coconut flesh (100%C), 50% meat + 50% ultrasound-treated coconut flesh (50%USC), and 100% ultrasound-treated coconut flesh (100%USC) (Table 1). All samples were set up for three replications.

Emulsion Stability Analysis

Emulsion stability was assessed as described by Ismail et al. (2021a). A 10 g sample of meat batter was weighed and placed in a centrifuge tube. The sample was then centrifuged at 3000 rpm for 15 minutes at 4°C, resulting in the separation of a transparent upper layer and an optically 'creamy' bottom layer. Subsequently, the tube was incubated in a water bath at 75°C for 30 minutes. To determine the total expressible fluid (TEF) and expressible

fat (EFAT), the centrifuge tube lids were left open and inverted over marked crucibles for 1 hour to allow the expressible fluid to drip. The pelleted samples were then weighed, and the collected supernatants were oven-dried overnight at 105°C. The quantities of TEF and EFAT were calculated using the Equations 1, 2, and 3.

$$TEF = (Weight\ of\ centrifuge\ tube + Weight\ of\ the\ sample) - (Weight\ of\ centrifuge\ tube + Weight\ of\ the\ pellet) \quad [1]$$

$$\%TEF = \frac{TEF}{Weight\ of\ sample} \times 100 \quad [2]$$

$$\%EFAT = \frac{(Weight\ of\ crucible + Weight\ of\ dried\ supernatant) - (Weight\ of\ empty\ crucible)}{TEF} \times 100 \quad [3]$$

Proximate Analysis

Proximate analysis was conducted to determine the contents of protein, fat, moisture, ash, carbohydrates, and fibre in the samples. The samples were chopped into smaller pieces, minced through a 2 cm sieve three times to ensure homogeneity, and chemically analysed according to the AOAC (2012) method. AOAC procedures were used to calculate the total proportion of carbohydrates, protein, fat, fibre, moisture, and ash (AOAC, 2012).

pH Analysis

A cooked sample weighing 5 g was homogenised with 45 mL of distilled water, and the pH was measured using a handheld pH meter (Jenway, U.K.) and evaluated according to the manufacturer's instructions.

Cooking Yield Measurement

A 5 g portion of meat batter was weighed, placed in a centrifuge tube, and centrifuged at 1000 g for 15 seconds (Kubota 3740, Japan) to remove air bubbles. The samples were then submerged in a warmed water bath at 50°C, with the temperature steadily raised until the sample reached an internal temperature of 72°C, as detected by a thermocouple. The centrifuge tubes were cooled in a cold-water bath for 5 minutes before the exudates were expelled; the cooked samples were then removed and wiped dry with filter paper. The cooking yield was calculated based on Ismail et al. (2021b) using the Equations 4 and 5.

$$Cooking\ loss\ (\%) = \frac{Weight\ of\ the\ uncooked\ \ sample\ - Weight\ of\ the\ pellet}{Weight\ of\ the\ uncooked\ \ sample} \times 100 \quad [4]$$

$$Cooking\ yield\ (\%) = 100\% - Cooking\ loss \quad [5]$$

Water Holding Capacity Analysis

The water-holding capacity (WHC) was determined according to the method described by Ming-Min and Ismail-Fitry (2023). In a centrifuge tube, 5 g of raw material were manually mixed with 32 mL of distilled water and left for 10 minutes. The material was then centrifuged for 25 minutes at 2900 rpm in a chilled microcentrifuge (Kubota 3740, Japan). The supernatant was discarded, and the sample was dried for 20 minutes at 50°C with a 10 to 20° downward tilt. The following Equation 6 was used to determine the WHC.

$$WHC = \frac{(b-a)-(c-a)}{b-a} \times 100\% \quad [6]$$

Where,
a = weight of empty centrifuge
b = weight of centrifuge with supernatant
c = weight of the dried centrifuge

Colour Measurement

A hand-held colourimeter (CR-40, Minolta Camera Co., Japan) with an aperture of 8 mm was used to measure CIELAB L*, a*, and b* values, which were used as indicators of samples' lightness, redness, and yellowness, respectively. The colour measurements for uncooked and cooked samples were examined according to Ismail et al. (2021b). The uncooked sample was evenly spread in a 5 cm-diameter transparent plastic container, while the cooked sample was thinly sliced and arranged in a similar round container. For each sample, the colour was recorded at 3 different points, and the mean value was used for analysis

Warner-Bratzler Shear Force Test

The measurement of the shear force was conducted according to Faridah et al. (2023) with minor modifications. The cooked sample was sliced horizontally, measuring 25 mm in length and 15 mm in diameter, using a texture analyser (TA-XT2i, Stable Micro System, UK) fitted with a Warner-Bratzler (WB) shear blade that features a triangular slow cutting edge (1 mm thickness) at a cutting speed of 1.5 mm/s. The maximum shear force (N) and shear work (N.sec) were measured according to Faridah et al. (2023).

Rheological Test

The dynamic rheological properties of the meat emulsion were estimated using a rheometer (Anton Paar Rheometer, MCR 302 Series, Austria) fitted with a 35 mm diameter stainless steel plate and a 1 mm gap. To determine the limit of the linear viscoelastic range, an oscillatory strain sweep (0.1-100%, frequency = 1 Hz) was performed (LVR). In addition, a frequency sweep test (0.1-100 Hz) was conducted at LVR (= 1%). The samples were tested for 5 minutes at 25 °C. The storage modulus (G') and loss modulus (G") were determined, and the phase angle (tan = G″/G′) was calculated according to the method of Faridah et al. (2023).

Texture Profile Analysis

The texture profile analysis was performed using the TA-XT2 texture analyser (Stable Micro Systems, Surrey, UK). The cooked sample was compressed twice to 75% of its original height using a P/75 probe connected to a 30 kg weight. During the measurement, the texture analyser was set with a test speed of 1.5 mm/s and a post-test speed of 1.5 mm/s.

Microstructure Analysis

The microstructure of the meat emulsion sample was observed using a variable-pressure scanning electron microscope (Leo / Zeiss 1455 VPSEM, UK). The sample, measuring 5 mm in thickness, was fixed with 0.1 mol/L phosphate buffer (pH 7.0) containing 2.5% glutaraldehyde at 4°C for 24 h and dehydrated in incremental concentrations of ethanol solutions (50, 70, 90, 95, and three times with 100%) for 10 mins per solution. Subsequently, the sample was freeze-dried in acetone, cooled in liquid nitrogen, and mounted onto the stubs using double-sided carbon tape. It was then sputter-coated with gold for 3 minutes using an automated sputter coater. The specimen was observed at 250× magnification (Ismail et al., 2021b).

Statistical Analysis

Minitab 19 (MiniTab Inc., United States of America) was used to conduct a one-way analysis of variance (ANOVA) at the 95% confidence level ($p<0.05$) to evaluate the significant differences between the collected data.

RESULTS AND DISCUSSION

Proximate Composition of Buffalo Meat Batter

Table 2 presents the proximate composition of cooked meat batter incorporating coconut flesh as a meat substitute. No significant differences ($p>0.05$) in moisture content were observed between the control and other samples. These findings indicate that coconut flesh

has a water content comparable to that of meat, which is a crucial factor in its potential as a meat substitute. Furthermore, moisture content may significantly influence the water-holding capacity of the product (Serdaroğlu et al., 2017).

No significant changes ($p>0.05$) in protein contents were observed in the treated samples compared to the control. However, when combined with buffalo meat, 50%USC exhibited a higher ($p<0.05$) protein content than the other treated samples, indicating the effectiveness of ultrasound treatment in releasing protein. This may be due to modifications in protein structure during ultrasound processing. High-energy ultrasound is a complementary technique for studying the structural and biochemical characteristics of proteins. Evidence suggests that ultrasonic exposure can enhance protein foaming capacity by stabilising the foam structure, increasing foam expansion, and promoting particle size reduction. Jambrak et al. (2008) tested the foaming characteristics of whey protein concentrates (WPC), whey protein isolate (WPI), and whey protein hydrolysate (WPH) at 10% (w/v) using ultrasound. They concluded that 15 min of ultrasonic pulses to protein systems at 10% (w/w) improves foaming. A reduction in particle size was observed, attributed to the likely disruption of protein aggregates during sonication, thereby enhancing protein adsorption at the system interface. Overall, sonication improved the particle size, volume, and hydrophobicity of the protein isolate, thereby enhancing foaming behaviour

Substituting the meat with coconut flesh significantly reduced the fat content ($p<0.05$) for 50%C and 50%USC. Although the fat content for 100%C and 100%USC was not significantly different from the control ($p>0.05$), both were still lower than the control. The observed reduction in fat content may be linked to the quantity of intermuscular and intramuscular fat present in the meat, which remained inseparable during processing. Additionally, the measured fat content could also be influenced by the coconut flesh itself, as it has been reported to contain approximately 60% fat (U.S. Department of Agriculture,

Table 2
Proximate composition of buffalo meat batter with different amounts of coconut flesh or ultrasound-treated coconut flesh as meat substitutes

Samples	Moisture (%)	Protein (%)	Fat (%)	Ash (%)	Carbohydrate (%)	Crude fibre (%)
Control	65.02±0.16^{a}	15.76±0.82^{ab}	14.06±1.02^{a}	2.38±0.11^{a}	3.74±0.71^{b}	0.03±0.21^{c}
50%C	66.57±0.37^{a}	14.06±1.32^{b}	7.68±1.48^{b}	1.66±0.08^{b}	9.34±0.56^{a}	0.68±0.06^{b}
100%C	65.56±0.40^{a}	13.77±0.86^{b}	10.29±1.00^{ab}	1.66±0.13^{b}	8.00±0.60^{a}	0.92±0.60^{a}
50%USC	64.71±0.10^{a}	18.82±0.75^{a}	5.56±0.33^{c}	2.40±0.08^{a}	7.78±0.57^{ab}	0.72±0.87^{ab}
100%USC	66.02±0.29^{a}	14.52±2.70^{b}	8.81±1.85^{ab}	1.49±0.11^{b}	8.20±0.48^{a}	0.86±0.48^{a}

All values are mean ± SD
$^{a-c}$Means in the same column with different uppercase superscripts are significantly different ($p<0.05$). 100% meat (control), 50% meat + 50% coconut flesh (50%C), 100% coconut flesh (100%C), 50% meat + 50% ultrasound-treated coconut flesh (50%USC), and 100% ultrasound-treated coconut flesh (100%USC)

2019). Cofrades et al. (2000) demonstrated that adding fibre to meat products could increase fat retention. Kim et al. (2013) and Ktari et al. (2014) reported that adding fibre to meat products enhanced fat binding. All samples substituted with coconut flesh showed significantly higher fibre content than the control ($p<0.05$), consistent with the presence of dietary fibre in coconut flesh (Trinidad et al., 2006).

The ash content of all treated samples was reduced ($p<0.05$) compared with the control, except for 50%USC. The naturally lower ash content of coconut compared to animal meat likely contributes to the lower ash levels observed in samples using coconut flesh as a substitute (Slavin, 2008). The carbohydrate content of all treated samples was higher, particularly for 100%C and 100%USC ($p<0.05$), although 50%C also showed a significant difference. The higher carbohydrate values are expected because coconut flesh contributes carbohydrates mainly in the form of dietary fibre (non-starch polysaccharides), with smaller amounts of soluble sugars (U.S. Department of Agriculture, 2019); moreover, total carbohydrate was calculated by difference, which includes fibre, thereby increasing the apparent carbohydrate fraction in the coconut-substituted meat batter.

Emulsion Stability, Water Holding Capacity (WHC), Cooking Yield, and pH of Buffalo Meat Batter

Table 3 presents the emulsion stability, water-holding capacity (WHC), cooking yield, and pH values of the buffalo meat batter incorporated with coconut flesh as a meat substitute. The emulsion stability of the raw batter and the overall emulsifying quality of the meat substitute emulsion were evaluated using the percentages of TEF and EFAT. Evaluating emulsion stability is essential for determining the ability of a meat emulsion to maintain its structural integrity when subjected to potential variations in physicochemical properties. According to Serdaroğlu et al. (2016), a higher percentage suggests a less stable emulsion. Except for the 100% substitution samples (100%C and 100%USC), there was no significant difference ($p>0.05$) between the treatments and the control. These findings are likely linked to the sample protein concentration, as neither 100%C nor 100%USC contained any meat and had low crude protein levels. Strong interactions between proteins can hold lipid droplets in place, strengthening the protein matrix and enhancing emulsion stability (Smith, 1988). Myosin is the main protein in meat that binds it together. It also acts as a natural emulsifier and plays a crucial role in maintaining a stable meat emulsion structure (Álvarez et al., 2007). This is supported by Zorba and Kurt (2006), who reported that increasing the amount of chicken meat in the meat mixture effectively enhanced emulsion stability. This finding aligns with Kamani et al. (2019), who found that partial replacement of meat with a soy-based ingredient with a high protein content improved the emulsion of chicken sausage. Although there was no significant difference among the other four samples, the 50%USC exhibited the highest emulsion stability, with the lowest %TEF and

%EFAT values. Ultrasound plays a significant role in promoting the gelation of polymer residues. Arzeni et al. (2012) reported a positive effect on the elasticity of the resulting gel network, attributing this enhancement to protein polymer aggregation facilitated by hydrophobic interactions.

Water holding capacity serves as an indicator of the meat batter's ability to bind water with external influences, a crucial parameter for determining emulsion stability (Serdaroğlu et al., 2016). A strong water-retention capacity is essential not only for maintaining product quality but also for minimising exudation during storage and distribution, and for preserving juiciness after cooking before consumption. Substituting the meat with coconut flesh reduced the WHC for 100%C samples ($p<0.05$) (Table 3). This may be attributed to the most abundant proteins in coconut flesh being globulin and albumin, which are soluble in NaCl and water (Patil & Benjakul, 2017). Coconut flesh treated with ultrasound exhibited no changes ($p>0.05$) in WHC compared to the control. Hagenmaier et al. (1975) reported that some proteins present in the aqueous phase of the coconut milk emulsion have the potential to act as emulsifiers and stabilise fat globules. Ultrasound application can disrupt small protein aggregates, reduce particle size, enhance protein-water interactions, and increase protein solubility (Arzeni et al., 2012). These factors contributed to a better-emulsified coconut flesh solution, in which the addition of ultrasound-treated coconut flesh to the batter stabilised the WHC. A more stable protein matrix results in reduced water and fat release, thereby improving the binding properties of meat products (Pietrasik & Shand, 2003).

One of the most relevant measures used to rate the quality of comminuted meat products is cooking yield, which reflects moisture and fat losses during heating (Aaslyng et al., 2003). Cooking yield is strongly influenced by the formation of a heat-induced gel matrix from myofibrillar proteins that immobilise water and stabilise the fat phase (Varga-Visi

Table 3
The emulsion stability (%TEF and %EFAT), water holding capacity (WHC), cooking yield, and pH values of buffalo meat batter with different amounts of coconut flesh or ultrasound-treated coconut flesh as meat substitutes

Samples	%TEF	%EFAT	WHC	Cooking yield (%)	pH Raw	pH Cooked
Control	5.36±1.02^{b}	15.76±0.82^{ab}	86.05±0.90^{a}	96.93±3.17^{a}	6.33±0.06^{a}	6.53±0.06^{a}
50%C	6.68±0.48^{b}	17.82±0.75^{a}	87.91±0.41^{a}	96.12±7.21^{a}	6.17±0.00^{a}	6.27±0.06^{a}
100%C	21.81±0.80^{a}	13.77±0.86^{b}	78.38±0.83^{b}	86.22±6.86^{b}	6.00±0.06^{a}	6.20±0.00^{a}
50%USC	4.38±1.48^{b}	14.06±1.02^{ab}	91.60±0.20^{a}	98.95±2.92^{a}	5.71±0.00^{b}	6.37±0.06^{a}
100%USC	22.29±1.00^{a}	15.52±0.70^{ab}	88.55±0.90^{a}	91.87±3.03^{b}	5.56±0.00^{b}	6.20±0.00^{a}

All values are mean ± SD

$^{a-c}$Means in the same column with different uppercase superscripts are significantly different ($p<0.05$). 100% meat (control), 50% meat + 50% coconut flesh (50%C), 100% coconut flesh (100%C), 50% meat + 50% ultrasound-treated coconut flesh (50%USC), and 100% ultrasound-treated coconut flesh (100%USC)

& Toxanbayeva, 2017). In the present study, 100%C and 100%USC showed significantly lower (p<0.05) cooking yield than the control and other treatments. This reduction is likely due to the complete replacement of buffalo meat, which decreases the availability of myofibrillar proteins required for gelation and emulsification, resulting in poorer entrapment of water and fat during cooking. In contrast, partial substitution preserved cooking yield because the remaining meat proteins could still form a cohesive gel network capable of retaining moisture and fat (Abdul Wahab et al., 2024).

Establishing the pH is essential for determining meat-eating quality, as water-holding capacity (WHC) is strongly pH-dependent and, in turn, influences tenderness, juiciness, and microstructure. In this study, pH decreased significantly (p<0.05) as the concentration of coconut flesh increased. This may be linked to the organic acids profile; malic acid, one of the principal organic acids reported in coconut, contributes to acidity and can lower batter pH, thereby affecting protein charge and water retention. During coconut maturation, the concentrations of organic acids—particularly malic acid—are reported to change, with pH generally increasing from early developmental stages toward full maturity as acids are metabolised (Jackson et al., 2004; Santoso et al., 1996). After cooking, pH increased slightly, and no significant differences (p>0.05) were observed among samples, likely because thermal processing reduces moisture and shifts the acid-base balance, making the cooked product less acidic (Li et al., 2022). This reduction in acidity after cooking is important because an excessively low pH can increase cooking losses by moving proteins closer to their isoelectric point, weakening water binding; in contrast, a less acidic (higher pH) cooked product generally supports better WHC, improved juiciness/tenderness, and a milder, less sour flavour perception.

Texture Profile and Shear Force of Buffalo Meat Batter

The texture profile analysis and shear force test of the cooked batter with coconut flesh as a meat substitute are presented in Table 4. Samples with a 100% substitute formulation (100%C and 100%USC) exhibited lower values (p<0.05) for all texture parameters, shear force, and work of shearing than the control. A trend towards reduced value was observed across all parameters as the quantity of coconut flesh increased. The hardness results may be linked to the moisture-retention properties of coconut protein. Bernasconi et al. (2020) also reported that the beef patty was softer when soybean protein was used as a meat substitute, possibly due to enhanced moisture retention induced by soybean protein. This may account for the reduced hardness observed in the substituted samples, which likely contributed to the decreased resistance of the cooked batter to shredding, thus lowering both the maximum shear force and the work needed for shearing. Furthermore, the significant reduction in hardness in samples containing plant-based ingredients could be due to their high fibre content, which may interfere with the protein gel matrix, consequently softening the meat

Table 4
Texture profiles and Warner Bratzler shear force of buffalo meat batter with different amounts of coconut flesh or ultrasound-treated coconut flesh as meat substitutes

Samples	Hardness (g)	Springiness	Cohesiveness	Gumminess	Chewiness (g/m^3)	Resilience	Maximum Shear Force (N/mm)	Work of shearing (N/mm)
Control	11124.93±835.17^{a}	0.87±0.06^{a}	0.48±0.06^{a}	7966.53±336.12^{a}	5510.94±319.98^{a}	0.18±0.06^{a}	15.36±1.02^{a}	15.76±0.82^{ab}
50%C	9525.12±547.21^{ab}	0.71±0.06^{b}	0.37±0.01^{a}	5326.27±572.66^{b}	4513.69±380.81^{a}	0.12±0.01^{ab}	10.68±0.48^{b}	17.82±0.75^{a}
100%C	5525.22±626.86^{c}	0.40±0.02^{c}	0.10±0.02^{b}	4816.20±457.46^{c}	2220.51±388.48^{b}	0.08±0.00^{b}	4.81±0.10^{c}	13.77±0.86^{b}
50%USC	9022.46±592.92^{b}	0.84±0.02^{a}	0.43±0.02^{a}	5766.30±384.14^{b}	4083.18±211.26^{a}	0.13±0.00^{ab}	13.38±1.48^{ab}	14.06±1.02^{ab}
100%USC	5920.95±732.92^{c}	0.47±0.06^{c}	0.11±0.02^{b}	4766.37±402.16^{c}	1731.45±267.45^{b}	0.08±0.00^{b}	2.29±1.00^{c}	15.52±0.70^{ab}

All values are mean ± SD
$^{a-c}$Means in the same column with different uppercase superscripts are significantly different (p<0.05). 100% meat (control), 50% meat + 50% coconut flesh (50%C), 100% coconut flesh (100%C), 50% meat + 50% ultrasound-treated coconut flesh (50%USC), and 100% ultrasound-treated coconut flesh (100%USC)

texture (Han et al., 2018). Wan Rosli et al. (2015) reported that frankfurters substituted with oyster mushroom powder showed a significant reduction in hardness compared to the control samples, while Kamani et al. (2019) reported that meat-free sausages displayed a noticeably softer texture than their meat-based counterparts. These reductions in hardness, gumminess, and chewiness may be attributed to the lower levels of insoluble muscle fibres and connective tissue present in the emulsion system (Ismail et al., 2021b; Ming-Min & Ismail-Fitry, 2023). This could be due to the myofibrillar protein network in buffalo meat being more resilient than plant fibre, thereby providing the flesh with greater compressive resistance.

Cohesiveness is defined as the extent to which a product withstands subsequent deformation relative to its resistance during the initial deformation. Springiness is characterised by the ability of the cooked meat batter to recover its original dimensions after experiencing compressive deformation (Nishinari et al., 2013). Fat and protein exert a synergistic effect on the springiness of meat products, as the protein matrix can bind lipid and water droplets, which may fill the air gaps within the emulsion matrix and reduce springiness as fat content increases (Ismail et al., 2021a; Youssef & Barbut, 2010). This finding generally aligns with previous research connecting meat texture to the incorporation of plant fibre. Song et al. (2016) found that the springiness of the frankfurter decreased significantly (p<0.05) as the amount of citrus fibre added into the product increased. Similarly, the addition of sea spaghetti and sugarcane dietary fibre to meat emulsion systems significantly reduced the cohesiveness (Fernández-Martín et al., 2009; Zhuang et al., 2016).

Texture profile is critical in developing plant-based meat alternatives, as replicating the textural properties of conventional patties is one of the most significant challenges in this field. Consequently, a meat emulsion with a complete (100%) substitution of animal components with plant-based ingredients may not achieve satisfactory final product quality. However, when the meat fraction was reduced to 50%, most parameters (cohesiveness, chewiness, and resilience) did not change significantly (p>0.05) compared to the control, and the significant differences (p<0.05) observed in hardness and gumminess remained within the range value of commercial meat products. Thus, it can be expected that coconut can replace up to 50% of buffalo meat in meat products without sacrificing textural qualities.

Colour Properties of Buffalo Meat Batter

Colour is often the first criterion that consumers consider when selecting a cut of meat. L* refers to lightness or darkness, a* refers to red and green and b* refers to blue and yellow. Buffalo meat is generally darker and redder than beef due to its higher myoglobin content, and therefore typically shows lower L* and higher a* values (Yie et al., 2023). Table 5 displays the colour properties of buffalo meat batter with varying amounts of coconut flesh or ultrasound-treated coconut flesh as meat substitutes. No significant difference (p>0.05)

Table 5
The colour properties of buffalo meat batter with different amounts of coconut flesh or ultrasound-treated coconut flesh as meat substitutes

Samples	Raw			Cooked		
	L*	a*	b*	L*	a*	b*
Control	56.10±1.41^{a}	4.63±0.10^{a}	13.65±1.35^{a}	53.10±1.41^{b}	3.63±0.10^{a}	10.05±0.35^{a}
50%C	56.34±1.00^{a}	3.52±0.70^{ab}	14.09±0.11^{a}	56.73±1.20^{ab}	2.74±0.14^{b}	9.85±0.50^{a}
100%C	56.57±0.67^{a}	3.06±0.32^{b}	13.96±0.08^{a}	58.39±0.53^{ab}	2.24±0.14^{b}	10.08±0.16^{a}
50%USC	55.71±0.10^{a}	3.62±0.75^{ab}	14.19±0.08^{a}	62.60±0.43^{a}	2.42±0.13^{b}	10.97±0.66^{a}
100%USC	55.68±0.54^{a}	2.90±2.30^{c}	13.91±0.20^{a}	62.85±0.80^{a}	2.07±0.16^{b}	10.12±0.14^{a}

All values are mean ± SD
$^{a-c}$Means in the same column with different uppercase superscripts are significantly different (p<0.05). 100% meat (control), 50% meat + 50% coconut flesh (50%C), 100% coconut flesh (100%C), 50% meat + 50% ultrasound-treated coconut flesh (50%USC), and 100% ultrasound-treated coconut flesh (100%USC)

was observed in the raw L* values of the samples. Although non-meat additives, particularly flour, can cause a pale tint in beef products, it was demonstrated that using coconut flesh did not affect the lightness of the samples. Similarly, Selani et al. (2015) found no changes in L* values of beef burgers when these were flavoured with either pineapple, passion fruit, or mango by-products. However, for the cooked samples, significant differences in L* values were observed between the treated and control samples. Incorporating passion fruit albedo into pork patties also increased their L* values, suggesting that the L* behaviour of cooked burgers with fruit albedo was due to the white parts in the raw material (López-Vargas et al., 2014). Another potential explanation is that myoglobin denaturation, changes in the heme group structure, and redox reactions involving myoglobin species have been hypothesised to contribute to the observed loss of redness (Carlez et al., 1995).

The a* values of the raw samples were influenced by the addition of coconut flesh, particularly for the 100%C and 100%USC (p<0.05). This was likely due to the control sample containing only minced buffalo meat, which has a high myoglobin concentration, as well as to the colour of the coconut flesh itself. All the cooked samples showed lower a* values than the control. The a* values of the cooked batter were also lower compared to the raw samples. This may be attributed to myoglobin denaturation or heme displacement under heat. In fact, heat treatment reduced the redness of the meat emulsion compared to raw sausages (Carlez et al., 1995). There were no significant differences (p>0.05) observed in b* values for raw and cooked samples, irrespective of the amount of coconut flesh added. Nonetheless, the yellowness b* value significantly decreased when the samples were cooked. This may relate to the implication of the grey-brown colour alongside the low a* value.

Viscoelastic Properties of Buffalo Meat Batter

G' and G" are two indicators commonly used to characterise gel properties. G' measures the elastic energy stored in a material, indicating its elasticity, while G" represents the viscous component of the emulsion, evaluated from the energy dissipated during deformation. According to Campo-Deaño et al. (2009) and Hrynets et al. (2010), an increased G' value correlates with greater rigidity and a denser network structure, resulting in enhanced gel strength. Moreover, samples that exhibit greater frequency dependence tend to display more fluid-like behaviour than elastic behaviour (Campo-Deaño et al., 2009). The 50%USC sample, which achieved the highest texture profile analysis score, also exhibited the highest G′ and G″ values among all formulations (Figure 1a). Owing to its well-organised

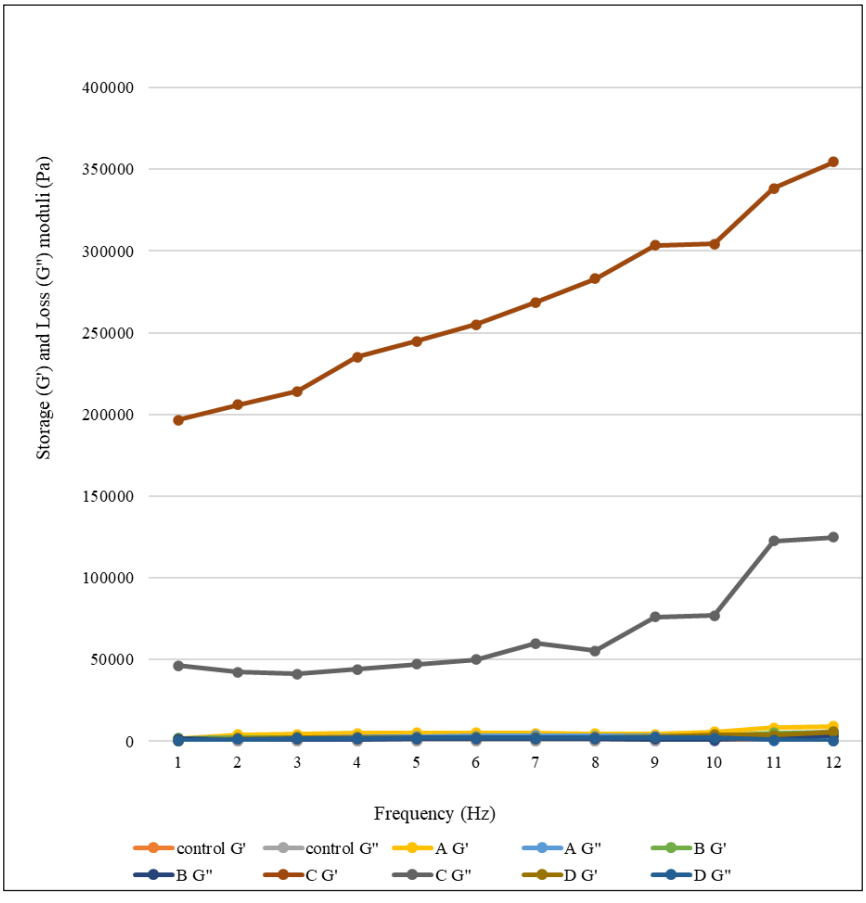

Figure 1a. The storage and loss moduli of buffalo meat batter with different amounts of coconut flesh or ultrasound-treated coconut flesh as meat substitutes

Note. 100% meat (control), 50% meat + 50% coconut flesh (sample A: 50%C), 100% coconut flesh (sample B: 100%C), 50% meat + 50% ultrasound-treated coconut flesh (sample C: 50%USC), and 100% ultrasound-treated coconut flesh (sample D: 100%USC)

matrix structure (Kumar et al., 2017), this sample showed only minimal changes in G′ and G″ across the 1 to 10 Hz frequency range, suggesting a more stable emulsion network. Compared with other samples, the 50% USC showed higher G' at lower frequencies and a greater discrepancy between G' and G", suggesting the strongest network structure among all samples. Additionally, with increased moisture, texturisation occurs, leading to a degradation of the material's textural qualities.

The viscoelastic properties of the samples may also relate to their water-holding capacity (WHC) and moisture content. Kumar et al. (2017) reported that decreases in G' and G" with increased aloe gel incorporation were attributed to enhanced WHC and elevated moisture levels. A noticeable link exists between the texture profile analysis (TPA) value and the dynamic rheological characteristics of these samples. Increased moisture content promotes texturisation, resulting in a reduction of specific textural attributes. While it is established that ultrasonic treatments encourage protein unfolding, denaturation, aggregation, and gelation, protein gels induced by coconut shreds exhibit enhanced glossiness, smoothness, softness and elasticity compared to heat-induced gels. These properties are particularly significant in the context of meat product formulation (Chambale et al., 2014; Famelart et al., 1998; McClements et al., 2021; Messens et al., 1997; Supavititpatana & Apichartsrangkoon, 2007). A greater storage modulus implies a more potent gel and a more rigid structure (Campo & Tovar, 2008), resulting from the establishment of stable network structures or strong particle-particle interactions (Acevedo et al., 2014).

Figure 1b shows that, in the frequency analysis, all samples except the control exhibited a gel-like behaviour, as their loss factor values were less than 1. According to Agafonkina et al. (2019), larger tan δ values resulted in a more stable matrix. Although the control sample has the highest tan δ value ≈ 1.10, the 50%USC was still declared a stable matrix emulsion due to the small (p>0.05) variation in tan δ values relative to the control sample.

Microstructure of Buffalo Meat Batter

Figure 2 depicts the microstructure of a cross-section of buffalo meat emulsion incorporated with coconut flesh at different percentages. The control exhibits a homogenised protein matrix with few to no pores. Samples 100%C and 100%USC exhibit a less-dense matrix structure, with the most prominent pores and spaces. The larger pores and less dense matrix observed in the sample with 100% substitution were most likely caused by a lack of protein content, which destabilises the emulsion matrix as protein plays a significant role in the 3-D structure of emulsion (Alvarez et al., 2007; Devatkal et al., 2014). The proteins in coconuts are primarily water-soluble, enhancing the food's emulsifying potential. Moreover, the larger aggregate size of coconut protein is associated with a substantial hydrophobic surface, thereby indicating the most prominent matrix pores observed in samples 100%C

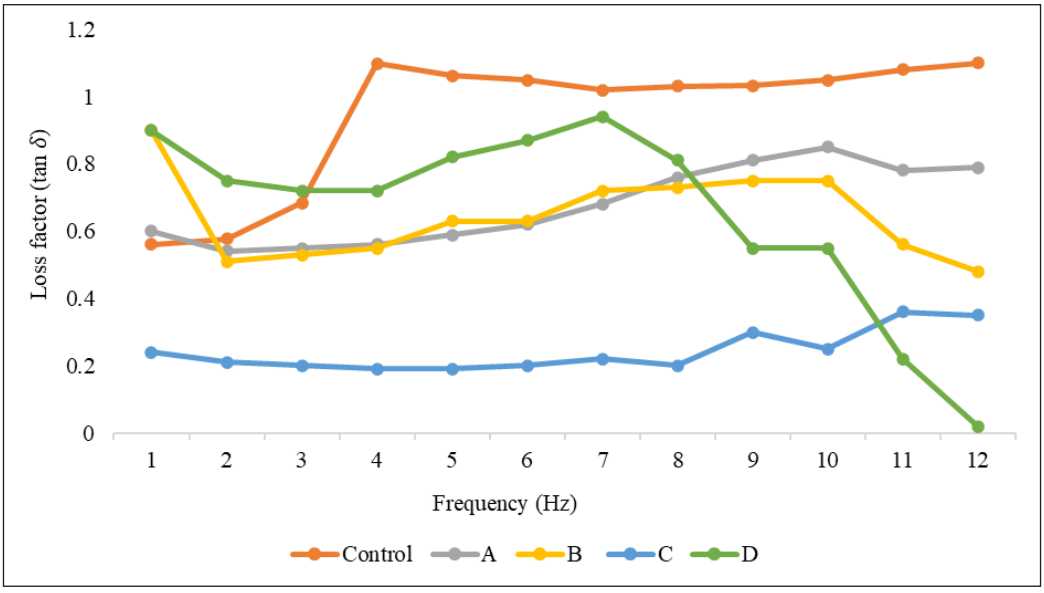

Figure 1b. Loss factor (tan δ) of buffalo meat batter with different amounts of coconut flesh or ultrasound-treated coconut flesh as meat substitutes
Note. 100% meat (control), 50% meat + 50% coconut flesh (sample A: 50%C), 100% coconut flesh (sample B: 100%C), 50% meat + 50% ultrasound-treated coconut flesh (sample C: 50%USC), and 100% ultrasound-treated coconut flesh (sample D: 100%USC)

and 100%USC. The 50%USC sample exhibits a spongy appearance due to dense protein aggregates. Ultrasound-treated coconut flesh samples display a protein network appearance similar to that of the control, but denser and more homogeneous. Overall, the gels appeared to have smaller pores than the controls, which supports the findings of increased elastic modulus.

This finding aligns with Liu et al. (2016), who investigated the effect of protein aggregates of varying sizes on the textural and microstructural features of fat-free acidified milk model systems. Nanoparticulated whey protein was found to produce acid gels exhibiting increased firmness, accelerated gelation, reduced whey separation, and a denser microstructure. Consequently, the intrinsic properties of protein aggregates emerge as a key factor influencing the extent to which the rheological characteristics of emulsion gels are modified. Similarly, our study showed that the addition of treated coconut yielded comparable outcomes, including improved texture, enhanced emulsion stability, and more organised protein networks. Moreover, it was observed that the textural modifications of protein aggregates were mainly due to interactions with other proteins within the continuous phase.

Microstructural analysis of the meat batter samples also revealed a slightly porous, coarse structure with minimal voids, consisting of finely suspended meat particles and fat

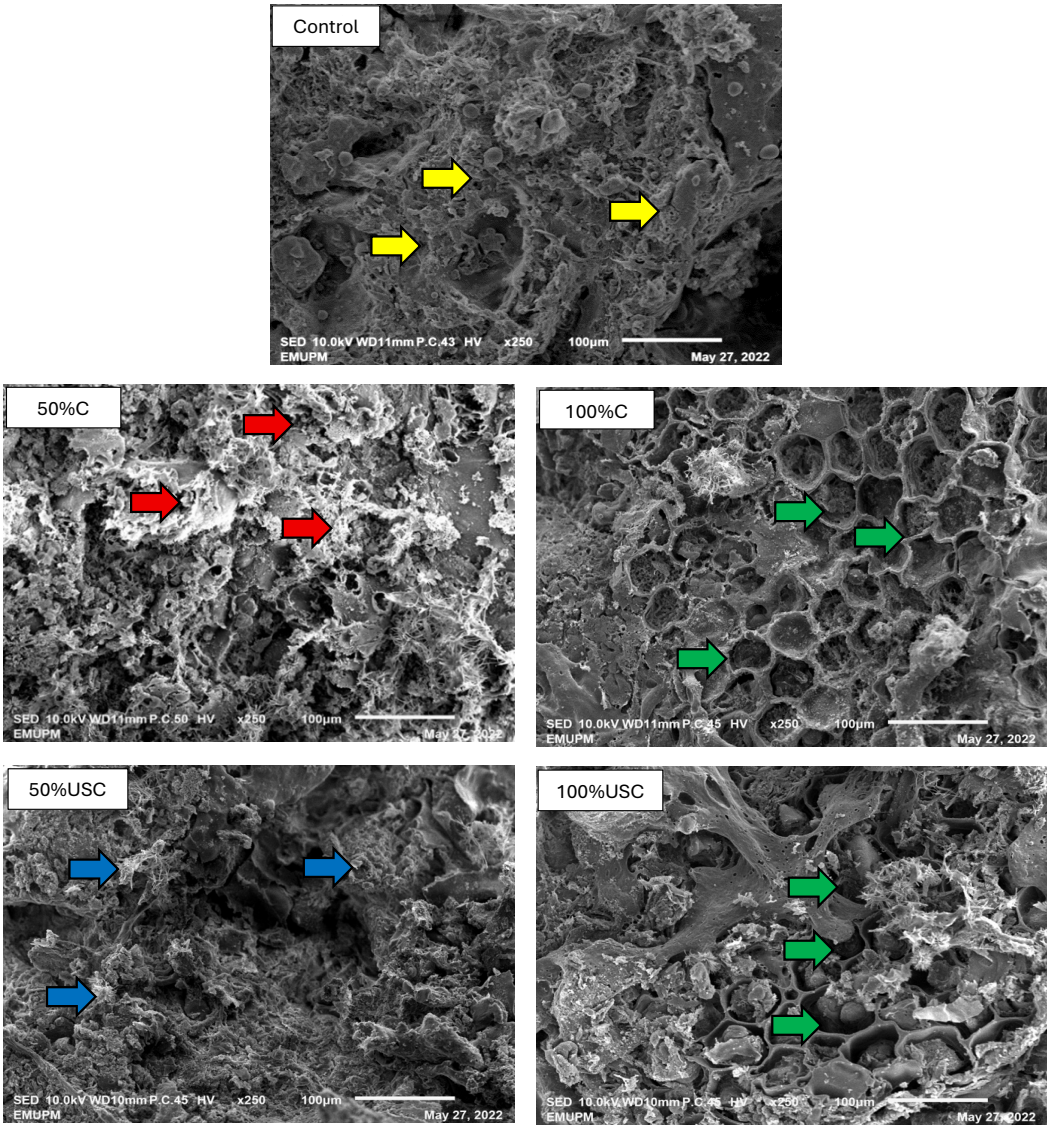

Figure 2. Scanning Electron Micrograph (250× magnification) of buffalo meat batter with different amounts of coconut flesh or ultrasound-treated coconut flesh as meat substitutes

Note. 100% meat (control), 50% meat + 50% coconut flesh (50%C), 30% meat, 100% coconut flesh (100%C), 50% meat + 50% ultrasound-treated coconut flesh (50%USC), 30% meat and 100% ultrasound-treated coconut flesh (100%USC)

Yellow arrows: homogenised meat matrices; Red arrows: coconut flesh with meat; Blue arrows: disrupted coconut flesh homogenised with meat; Green arrows: pores of coconut flesh batters

globules dispersed within a continuous protein matrix. This indicates that fat appeared to be interconnected with the protein network in the gel, as in the control. It has already been shown that as protein concentration increases, gel holes shrink and protein distribution

becomes more uniform throughout the gel. In line with comparable structures from previous investigations, Jiménez et al. (2010) and Tahmasebi et al. (2016) identified that the size of fat globules decreases as the globulin-stabilised emulsion exhibits a lower coalescence index and flocculation factor. The fat globule shrinks as emulsion stability rises. This was corroborated by Kang et al. (2022), who partially replaced beef with soybean protein and found that increasing the soybean protein substitution ratio reduced pore size, thereby decreasing fat globule size. Thus, the addition of treated coconut flesh impacted the formation of the protein network and, consequently, the final texture of the batter emulsion.

CONCLUSION

This study shows that ultrasound-treated coconut flesh (50%USC) is a promising partial meat replacer in emulsified buffalo sausages. The 50%USC formulation produced the most stable emulsion, with improved moisture retention and higher fibre, while maintaining acceptable physicochemical and textural properties within the range of commercial products. Rheological and microstructural results further confirmed that ultrasound treatment improved the incorporation of coconut flesh without compromising product integrity. Untreated coconut flesh (50%C) also performed comparably to the control and may serve as a secondary option. Overall, using ultrasound-treated coconut flesh can support the development of healthier, lower-fat meat products and offers a sustainable approach for valorising coconut by-products.

ACKNOWLEDGEMENT

This research project was supported by Universiti Putra Malaysia through the GPB - Geran Putra Berimpak with grant number 9817700. Authors also acknowledge support from the University Driven Research Programme (UDRP), “Functional Food Development and Future Food”, under the Faculty of Food Science and Technology, UPM.

CONFLICTS OF INTEREST

The authors have declared no conflict of interest.

REFERENCES

Aaslyng, M. D., Bejerholm, C., Ertbjerg, P., Bertram, H. C., & Andersen, H. J. (2003). Cooking loss and juiciness of pork in relation to raw meat quality and cooking procedure. *Food Quality and Preference*, *14*(4), 277-288. https://doi.org/10.1016/S0950-3293(02)00086-1

Abdul Wahab, N. Q., Pangestika, L. M. W., & Ismail-Fitry, M. R. (2024). Partial incorporation of black jelly mushroom (*Auricularia polytricha*) as a plant-based ingredient in the production of hybrid patties using meat from different species. *International Journal of Food Science and Technology*, *59*(11), 8786-8795. https://doi.org/10.1111/ijfs.17516

Acevedo, D., Montero, P. M., & Marrugo, Y. A. (2014). Rheological characterisation of artisanal and technical unctuous pastes of sesame (*Sesamum indicum*) cultivated in Zambrano-Bolivar (Colombia). *Information Technology*, *25*(4), 73-78. https://doi.org/10.4067/S0718-07642014000400010

Agafonkina, I. V., Korolev, I. A., & Sarantsev, T. A. (2019). The study of thermal denaturation of beef, pork, chicken and turkey muscle proteins using differential scanning calorimetry. *Theory and Practice of Meat Processing*, *4*(3), 19-23. https://doi.org/10.21323/2414-438x-2019-4-3-19-23

Álvarez, D., Castillo, M., Payne, F. A., Garrido, M. D., Bañón, S., & Xiong, Y. L. (2007). Prediction of meat emulsion stability using reflection photometry. *Journal of Food Engineering*, *82*(3), 310-315. https://doi.org/10.1016/j.jfoodeng.2007.02.031

Alvarez, S., Fresno, M., Darmanin, N., Briggs, H. R., Mendez, P., & Castro, N. (2007). Native forages assessment for the improvement of milk production in goats. *Journal of Animal and Veterinary Advances*, *6*(1), 94-98.

AOAC International. (2012). *Official methods of analysis of AOAC International* (G. W. Latimer Jr., Ed.; 19th ed.). AOAC International.

Arzeni, C., Martinez, K., Zema, P., Arias, A., Perez, O. E., & Pilosof, A. M. R. (2012). Comparative study of high intensity ultrasound effects on food proteins functionality. *Journal of Food Engineering*, *108*(3), 463-472. https://doi.org/10.1016/j.jfoodeng.2011.08.018

Bernasconi, A., Szerman, N., Vaudagna, S. R., & Speroni, F. (2020). High hydrostatic pressure and soybean protein addition to beef patties: Effects on the formation of mixed aggregates and technological parameters. *Innovative Food Science and Emerging Technologies*, *66*, Article 102503. https://doi.org/10.1016/j.ifset.2020.102503

Campo, L., & Tovar, C. (2008). Influence of the starch content in the viscoelastic properties of surimi gels. *Journal of Food Engineering*, *84*(1), 140-147. https://doi.org/10.1016/j.jfoodeng.2007.05.011

Campo-Deaño, L., Tovar, C. A., Pombo, M. J., Solas, M. T., & Borderías, A. J. (2009). Rheological study of giant squid surimi (*Dosidicus gigas*) made by two methods with different cryoprotectants added. *Journal of Food Engineering*, *94*(1), 26-33. https://doi.org/10.1016/j.jfoodeng.2009.02.024

Carlez, A., Veciana-Nogues, T., & Cheftel, J. C. (1995). Changes in colour and myoglobin of minced beef meat due to high pressure processing. *LWT - Food Science and Technology*, *28*(5), 528-538. https://doi.org/10.1006/fstl.1995.0088

Chambale, B., Bergenståhl, B., & Dejmek, P. (2014). Heat induced gels from coconut press cake proteins. *Food and Nutrition Sciences*, *5*(6), 562-570. https://doi.org/10.4236/fns.2014.56066

Ching, N., Mohammad, A., Law, Y. N., & Jahim, J. (2015). Sequential fractionation of value-added coconut products using membrane processes. *Journal of Industrial and Engineering Chemistry*, *25*, 162-167. https://doi.org/10.1016/j.jiec.2014.10.028

Cofrades, S., Guerra, M. A., Carballo, J., Fernández-Martín, F., & Colmenero, F. J. (2000). Plasma protein and soy fibre content effect on bologna sausage properties as influenced by fat level. *Journal of Food Science*, *65*(2), 281-287. https://doi.org/10.1111/j.1365-2621.2000.tb15994.x

Cristina, P. S., Munekata, P. E. S., Pateiro, M., Domínguez, R., Misihairabgwi, J. M., & Lorenzo, J. M. (2021). Modern food production: Fundaments, sustainability, and the role of technological advances. In *Sustainable production technology in food* (pp. 1-22). Elsevier. https://doi.org/10.1016/B978-0-12-821233-2.00003-4

Devatkal, S. K., Manjunatha, M., Narsaiah, K., & Patil, R. T. (2014). Evaluation of quality characteristics of chicken meat emulsion/nuggets prepared by using different equipment. *Journal of Food Science and Technology*, *51*(3), 511-518. https://doi.org/10.1007/s13197-011-0518-6

Famelart, H., Chapron, L., Piot, M., Brulé, G., & Durier, C. (1998). High pressure-induced gel formation of milk and whey concentrates. *Journal of Food Engineering*, *36*(2), 149-164. https://doi.org/10.1016/S0260-8774(98)00048-X

Faridah, M. R., Yusoff, M. M., Rozzamri, A., Ibadullah, W. Z. W., Hairi, A. N. A., Daud, N. H. A., Huda, N., & Ismail-Fitry, M. R. (2023). Effect of palm-based shortenings of various melting ranges as animal fat replacers on the physicochemical properties and emulsion stability of chicken meat emulsion. *Foods*, *12*(3), Article 597. https://doi.org/10.3390/foods12030597

Fernández-Martín, F., López-López, I., Cofrades, S., & Colmenero, F. J. (2009). Influence of adding sea spaghetti seaweed and replacing the animal fat with olive oil or a konjac gel on pork meat batter gelation. *Meat Science*, *83*(2), 209-217. https://doi.org/10.1016/j.meatsci.2009.04.020

Hagenmaier, R., Lopitakwong, R., & Verasestakul, S. (1975). Nutritive value and food use of coconut skim milk solids (a research note). *Journal of Food Science*, *40*(6), 1324-1325. https://doi.org/10.1111/j.1365-2621.1975.tb01081.x

Han, M., Clausen, M. P., Christensen, M., Vossen, E., Van Hecke, T., & Bertram, H. C. (2018). Enhancing the health potential of processed meat: The effect of chitosan or carboxymethyl cellulose enrichment on inherent microstructure, water mobility and oxidation in a meat-based food matrix. *Food & Function*, *9*(7), 4017-4027. https://doi.org/10.1039/C8FO00835C

Hrynets, Y., Omana, D. A., Xu, Y., & Betti, M. (2010). Effect of acid- and alkaline-aided extractions on functional and rheological properties of proteins recovered from mechanically separated turkey meat (MSTM). *Journal of Food Science*, *75*(7), E477-E486. https://doi.org/10.1111/j.1750-3841.2010.01736.x

Hu, H., Wu, J., Li-Chan, E. C. Y., Zhu, L., Zhang, F., Xu, X., & Pan, S. (2013). Effects of ultrasound on structural and physical properties of soy protein isolate (SPI) dispersions. *Food Hydrocolloids*, *30*(2), 647-655. https://doi.org/10.1016/j.foodhyd.2012.08.001

Ismail, I., Hwang, Y. H., & Joo, S. T. (2020). Meat analog as future food: A review. *Journal of Animal Science and Technology*, *62*(2), 111-120. https://doi.org/10.5187/jast.2020.62.2.111

Ismail, M. A., Chong, G. H., & Ismail-Fitry, M. R. (2021a). Comparison of the microstructural, physicochemical and sensorial properties of buffalo meat patties produced using bowl cutter, universal mixer and meat mixer. *Journal of Food Science and Technology*, *58*(12), 4703-4710. https://doi.org/10.1007/s13197-020-04960-y

Ismail, N. A., Bakar, J., Sazili, A. Q., & Ismail-Fitry, M. R. (2021b). Effect of different levels of fat, sodium chloride, and sodium tripolyphosphate on the physicochemical and microstructure properties of Jamnapari goat meat emulsion modelling system. *International Food Research Journal*, *28*(5), 916-925. https://doi.org/10.47836/ifrj.28.5.04

Jackson, J. C., Gordon, A., Wizzard, G., McCook, K., & Rolle, R. (2004). Changes in chemical composition of coconut (*Cocos nucifera*) water during maturation of the fruit. *Journal of the Science of Food and Agriculture*, *84*(10), 1049-1052. https://doi.org/10.1002/jsfa.1783

Jambrak, A. R., Mason, T. J., Lelas, V., Herceg, Z., & Herceg, I. L. (2008). Effect of ultrasound treatment on solubility and foaming properties of whey protein suspensions. *Journal of Food Engineering*, *86*(2), 281-287. https://doi.org/10.1016/j.jfoodeng.2007.10.004

Jangchud, K., Puchakawimol, P., & Jangchud, A. (2007). Quality changes of burnt aromatic coconut during 28-day storage in different packages. *LWT - Food Science and Technology*, *40*(7), 1232-1239. https://doi.org/10.1016/j.lwt.2006.08.014

Jiang, H., Natasha, M. E., Liu, H., & Shao, S. (2020). A review of research on plant-based meat alternatives: Driving forces, history, manufacturing, and consumer attitudes. *Comprehensive Reviews in Food Science and Food Safety*, *19*(5), 2639-2656. https://doi.org/10.1111/1541-4337.12610

Jiménez-Colmenero, F., Cofrades, S., López-López, I., Ruiz-Capillas, C., Pintado, T., & Solas, M. T. (2010). Technological and sensory characteristics of reduced/low-fat, low-salt frankfurters as affected by the addition of konjac and seaweed. *Meat Science*, *84*(3), 356-363. https://doi.org/10.1016/j.meatsci.2009.09.002

Kamani, M. H., Meera, M. S., Bhaskar, N., & Modi, V. K. (2019). Partial and total replacement of meat by plant-based proteins in chicken sausage: Evaluation of mechanical, physico-chemical and sensory characteristics. *Journal of Food Science and Technology*, *56*(5), 2660-2669. https://doi.org/10.1007/s13197-019-03754-1

Kang, K. M., Lee, S. H., & Kim, H. Y. (2022). Effects of using soybean protein emulsion as a meat substitute for chicken breast on physicochemical properties of Vienna sausage. *Food Science of Animal Resources*, *42*(1), 73-83. https://doi.org/10.5851/kosfa.2021.e63

Kim, H. W., Hwang, K. E., Song, D. H., Lee, S. Y., Choi, M. S., Lim, Y. B., Choi, J. H., Choi, Y. S., Kim, H. Y., & Kim, C. J. (2013). Effects of dietary fibre extracts from brewer's spent grain on quality characteristics of chicken patties cooked in convective oven. *Korean Journal for Food Science of Animal Resources*, *33*(1), 45-52. https://doi.org/10.5851/kosfa.2013.33.1.45

Ktari, N., Smaoui, S., Trabelsi, I., Nasri, M., & Salah, R. B. (2014). Chemical composition, techno-functional and sensory properties and effects of three dietary fibres on the quality characteristics of Tunisian beef sausage. *Meat Science*, *96*(1), 521-525. https://doi.org/10.1016/j.meatsci.2013.07.038

Kumar, Y., Tyagi, S. K., Vishwakarma, R. K., & Kalia, A. (2017). Textural, microstructural, and dynamic rheological properties of low-fat meat emulsion containing aloe gel as potential fat replacer. *International Journal of Food Properties*, *20*(1), 132-144. https://doi.org/10.1080/10942912.2017.1336721

Li, J., Shi, A., Liu, H., Hu, H., Wang, Q., Adhikari, B., Jiao, B., & Pignitter, M. (2022). Effect of hydrothermal cooking combined with high-pressure homogenisation and enzymatic hydrolysis on the solubility and stability of peanut protein at low pH. *Foods*, *11*(9), Article 1289. https://doi.org/10.3390/foods11091289

Liu, G., Buldo, P., Greve, M. T., Nielsen, S. B., Nielsen, J. H., & Ipsen, R. (2016). Effects of added whey protein aggregates on textural and microstructural properties of acidified milk model systems. *International Dairy Journal*, *62*, 43-52. https://doi.org/10.1016/j.idairyj.2016.07.006

López-Vargas, J. H., Fernández-López, J., Pérez-Álvarez, J. Á., & Viuda-Martos, M. (2014). Quality characteristics of pork burger added with albedo-fibre powder obtained from yellow passion fruit (*Passiflora edulis* var. *flavicarpa*) co-products. *Meat Science*, *97*(2), 270-276. https://doi.org/10.1016/j.meatsci.2014.02.010

McClements, D. J., Weiss, J., Kinchla, A. J., Nolden, A. A., & Grossmann, L. (2021). Methods for testing the quality attributes of plant-based foods: Meat- and processed-meat analogs. *Foods*, *10*(2), Article 260. https://doi.org/10.3390/foods10020260

Messens, W., Van Camp, J., & Huyghebaert, A. (1997). The use of high pressure to modify the functionality of food proteins. *Trends in Food Science & Technology*, *8*(4), 107-112. https://doi.org/10.1016/S0924-2244(97)01015-7

Ming-Min, W., & Ismail-Fitry, M. R. (2023). Physicochemical, rheological and microstructural properties of chicken meat emulsion with the addition of Chinese yam (*Dioscorea polystachya*) and arrowroot (*Maranta arundinacea*) as meat substitutes. *Future Foods*, *7*, Article 100221. https://doi.org/10.1016/j.fufo.2023.100221

Nishinari, K., Kohyama, K., Kumagai, H., Funami, T., & Bourne, M. C. (2013). Parameters of texture profile analysis. *Food Science and Technology Research*, *19*(3), 519-521. https://doi.org/10.3136/fstr.19.519

O'Sullivan, J. J., Park, M., Beevers, J., Greenwood, R. W., & Norton, I. T. (2017). Applications of ultrasound for the functional modification of proteins and nanoemulsion formation: A review. *Food Hydrocolloids*, *71*, 299-310. https://doi.org/10.1016/j.foodhyd.2016.12.037

Onsaard, E., Vittayanont, M., Srigam, S., & McClements, D. J. (2006). Comparison of properties of oil-in-water emulsions stabilized by coconut cream proteins with those stabilised by whey protein isolate. *Food Research International*, *39*(1), 78-86. https://doi.org/10.1016/j.foodres.2005.06.003

Patil, U., & Benjakul, S. (2017). Characteristics of albumin and globulin from coconut meat and their role in emulsion stability without and with proteolysis. *Food Hydrocolloids*, *69*, 220-228. https://doi.org/10.1016/j.foodhyd.2017.02.006

Pietrasik, Z., & Shand, P. J. (2003). The effect of quantity and timing of brine addition on water binding and textural characteristics of cooked beef rolls. *Meat Science*, *65*(2), 771-778. https://doi.org/10.1016/S0309-1740(02)00280-2

Riaz, M. (2005). *Soy applications in food: Textured soy protein utilization in meat and meat analogue products*. CRC Press. https://doi.org/10.1201/9781420037951

Rozhan, A., & Rohany, M. (2021). *Strengthen coconut industry in Malaysia*. FFTC Agriculture Policy Platform (FFTC-AP). https://ap.fftc.org.tw/article/2938

Santoso, U., Kubo, K., Ota, T., Tadokoro, T., & Maekawa, A. (1996). Nutrient composition of kopyor coconuts (*Cocos nucifera* L.). *Food Chemistry*, *57*(2), 299-304. https://doi.org/10.1016/0308-8146(95)00237-5

Selani, M. M., Margiotta, G. B., Piedade, S. M. S., Contreras-Castillo, C. J., & Canniatti-Brazaca, S. G. (2015). Physicochemical, sensory, and cooking properties of low fat beef burgers with addition of fruit byproducts and canola oil. *International Proceedings of Chemical, Biological and Environmental Engineering*, *81*, 58-65.

Serdaroğlu, M., Nacak, B., & Karabıyıkoğlu, M. (2017). Effects of beef fat replacement with gelled emulsion prepared with olive oil on quality parameters of chicken patties. *Korean Journal for Food Science of Animal Resources*, *37*(3), 376-385. https://doi.org/10.5851/kosfa.2017.37.3.376

Serdaroğlu, M., Öztürk, B., & Urgu, M. (2016). Emulsion characteristics, chemical and textural properties of meat systems produced with double emulsions as beef fat replacers. *Meat Science*, *117*, 187-195. http://dx.doi.org/10.1016/j.meatsci.2016.03.012

Slavin, J. L. (2008). Position of the American Dietetic Association: Health implications of dietary fibre. *Journal of the American Dietetic Association*, *108*(10), 1716-1731. https://doi.org/10.1016/j.jada.2008.08.007

Smith, D. M. (1988). Meat proteins: Functional properties in comminuted meat products. *Food Technology*, *42*(4), 116-121.

Song, J., Pan, T., Wu, J., & Ren, F. (2016). The improvement effect and mechanism of citrus fibre on the water-binding ability of low-fat frankfurters. *Journal of Food Science and Technology*, *53*(12), 4197-4204. https://doi.org/10.1007/s13197-016-2407-5

Sui, X., Bi, S., Qi, B., Wang, Z., Zhang, M., Li, Y., & Jiang, L. (2017). Impact of ultrasonic treatment on an emulsion system stabilised with soybean protein isolate and lecithin: Its emulsifying property and emulsion stability. *Food Hydrocolloids*, *63*, 727-734. https://doi.org/10.1016/j.foodhyd.2016.10.024

Sun, Y., Zhang, M., Bhandari, B., & Yang, C. H. (2019). Ultrasound treatment of frozen crayfish with chitosan nano-composite water-retaining agent: Influence on cryopreservation and storage qualities. *Food Research International*, *126*, Article 108670. https://doi.org/10.1016/j.foodres.2019.108670

Supavititpatana, T., & Apichartsrangkoon, A. (2007). Combination effects of ultra-high pressure and temperature on the physical and thermal properties of ostrich meat sausage (yor). *Meat Science*, *76*(3), 555-560. https://doi.org/10.1016/j.meatsci.2007.01.007

Sze Wei, A., Brishti, F. H., Sani, M. S. A., Ishamri, I., Sarbon, N. M., & Ismail-Fitry, M. R. (2024). Methylcellulose replacement with different enzymatically treated plant fibres as a binder in the production of plant-based meat patties. *LWT*, *201*, Article 116231. https://doi.org/10.1016/j.lwt.2024.116231

Tahmasebi, M., Labbafi, M., Emam-Djomeh, Z., & Yarmand, M. S. (2016). Manufacturing the novel sausages with reduced quantity of meat and fat: The product development, formulation optimisation, emulsion stability, and textural characterisation. *LWT - Food Science and Technology*, *68*, 76-84. https://doi.org/10.1016/j.lwt.2015.12.011

Tenda, E., Miftahorrachman, & Kumaunang, J. (2021). Profile of amino acids and fatty acids of some Indonesia tall coconut varieties. *IOP Conference Series: Earth and Environmental Science*, *974*(1), Article 012133. https://doi.org/10.1088/1755-1315/974/1/012133

Tian, R., Feng, J., Huang, G., Tian, B., Zhang, Y., Jiang, L., & Sui, X. (2020). Ultrasound driven conformational and physicochemical changes of soy protein hydrolysates. *Ultrasonics Sonochemistry*, *68*, Article 105202. https://doi.org/10.1016/j.ultsonch.2020.105202

Trinidad, T. P., Mallillin, A. C., Valdez, D. H., Loyola, A. S., Askali-Mercado, F. C., Castillo, J. C., Encabo, R. R., Masa, D. B., Maglaya, A. S., & Chua, M. T. (2006). Dietary fibre from coconut flour: A functional food. *Innovative Food Science & Emerging Technologies*, *7*(4), 309-317. https://doi.org/10.1016/j.ifset.2004.04.003

Tuso, P. J., Ismail, M. H., Ha, B. P., & Bartolotto, C. (2013). Nutritional update for physicians: Plant-based diets. *The Permanente Journal*, *17*(2), 61-66. https://doi.org/10.7812/TPP/12-085

U.S. Department of Agriculture. (2019). *Arrowroot, raw*. FoodData Central. https://fdc.nal.usda.gov/fdc-app.html#/food-details/168490/nutrients

Varga-Visi, É., & Toxanbayeva, B. (2017). Application of fat replacers and their effect on quality of comminuted meat products with low lipid content: A review. *Acta Alimentaria*, *46*(2), 181-186. https://doi.org/10.1556/066.2016.0008

Wan Rosli, W. I., Nor Maihiza, M. S., & Raushan, M. (2015). The ability of oyster mushroom in improving nutritional composition, β-glucan and textural properties of chicken frankfurter. *International Food Research Journal*, *22*(1), 311-317.

Wynn, T. (2017). Nutrition studies on mature and immature coconut meat and coconut water. *Yadanabon University Research Journal*, *8*(1), 1-8.

Youssef, M. K., & Barbut, S. (2010). Physicochemical effects of the lipid phase and protein level on meat emulsion stability, texture, and microstructure. *Journal of Food Science*, *75*(2), S108-S114. https://doi.org/10.1111/j.1750-3841.2009.01475.x

Yie, L. J., Khalid, N. I., & Ismail-Fitry, M. R. (2023). Quality evaluation of buffalo meatballs produced at different comminution process temperatures. *Malaysian Journal of Fundamental and Applied Sciences*, *19*(4), 573-582. https://doi.org/10.11113/mjfas.v19n4.2946

Zhuang, X., Han, M., Kang, Z. L., Wang, K., Bai, Y., Xu, X. L., & Zhou, G. H. (2016). Effects of the sugarcane dietary fibre and pre-emulsified sesame oil on low-fat meat batter physicochemical property, texture, and microstructure. *Meat Science*, *113*, 107-115. https://doi.org/10.1016/j.meatsci.2015.11.007

Zorba, Ö., & Kurt, Ş. (2006). Optimisation of emulsion characteristics of beef, chicken and turkey meat mixtures in model system using mixture design. *Meat Science*, *73*(4), 611-618. https://doi.org/10.1016/j.meatsci.2006.02.017

Pertanika J. Trop. Agric. Sci. 49 (S1): 83 - 100 (2026)

PERTANIKA JOURNALS

TROPICAL AGRICULTURAL SCIENCE

Journal homepage: http://www.pertanika.upm.edu.my/

Design and Performance Evaluation of an Off-Grid Solar Powered LED Lighting System for Tower Hydroponic Cultivation

Renny Eka Putri*, Siti Nurhaliza, and Omil Charmyn Chatib

Department of Agriculture Engineering and Biosystem, Universitas Andalas, Padang, 25163 West Sumatera, Indonesia

ABSTRACT

The rapid increase in urbanisation has led to a reduction in productive agricultural land, driving the need for modern agricultural innovations that are efficient and environmentally friendly. This study aims to design an LED grow light system using solar power to support the growth of pak choy (*Brassica rapa* L.) plants using the hydroponic tower system (HTS) method in a greenhouse. This solar power system utilises the potential of solar energy in the Lubuk Alung area, Padang, West Sumatra, Indonesia. The study was conducted by comparing plant growth between the LED grow light system treatment and control plants without an LED. The parameters observed included plant height, leaf length, leaf width, and number of leaves. This system integrates natural light with artificial lighting from LEDs for 3 hours at night to extend the duration of plant photosynthesis. The maximum sunlight intensity is 1180.26W/m² with an electrical power generated around 3045.07 watts. The average solar panel efficiency reaches 20% with peak power occurring at 11:00-12:00 WIB. The results showed that plants supplemented with LED lighting exhibited significantly better growth than control plants. Analysis indicated that this system requires a relatively high initial investment but has potential benefits through increased productivity and pesticide-free crop quality. This research proves that the use of renewable energy in modern agricultural systems can be a practical, efficient, and sustainable solution to meet food needs in urban areas.

Keywords: Energy efficiency, *greenhouse,* hydroponics, LED grow light, pak choy, solar panel

ARTICLE INFO

Article history:
Received: 18 July 2025
Accepted: 05 January 2026
Published: 19 March 2026

DOI: https://doi.org/10.47836/pjtas.49.S1.04

E-mail addresses:
rennyekaputri@ae.unand.ac.id (Renny Eka Putri)
siti_nurhaliza@gmail.com (Siti Nurhaliza)
omilcchatib@ae.unand.ac.id (Omil Charmyn Chatib)
* Corresponding author

INTRODUCTION

The rapid increase in the world's population has put increasing pressure on natural resources. (Abu Hatab et al., 2019). By 2050, it is estimated that around 68% of the population will live in urban areas, with

Indonesia projected to reach an urbanisation rate of 66.6% by 2035 (United Nations, 2019). This increase in urbanisation creates various problems in several food sectors, one of which is an increase in food demand that is faster than the increase in production (Arifin et al., 2019). Therefore, one solution that can help overcome this challenge is the development of efficient and environmentally friendly agricultural technology (Abu Hatab et al., 2019). Hydroponics is a growing method that is increasingly being applied due to its ability to increase the efficiency of water and nutrient use, as well as minimise the use of pesticides (Chatterjee et al., 2025; Putri et al., 2023). The use of greenhouses can control environmental conditions that are suitable for optimising plant growth, while hydroponic techniques minimise land use and maximise water and nutrient efficiency (Putri et al., 2025; Yusuf et al., 2025). The cultivation system with the hydroponic tower system (HTS) allows the cultivation of pak choy on a vertical scale, thus maximising the use of limited land in urban areas (Al-Kodmany, 2018). The Tower Hydroponic system offers advantages, including efficient water and nutrient use, improved aeration of plant roots, and increased planting density per unit area (Putri et al., 2025). Due to its vertical configuration, this system is particularly suitable for controlled environments and limited land conditions. In this study, the tower hydroponic system was employed as the plant cultivation platform to evaluate system performance under controlled nutrient delivery and environmental conditions (Barbosa et al., 2015).

Pakcoy (*Brassica rapa L.*) is a vegetable with high protein and vitamin content that is suitable for cultivation using hydroponic systems. However, plant growth in greenhouses is greatly influenced by light availability (Xin et al., 2019). Indonesia, located in a tropical region with natural sunlight varying seasonally and daily, is often below the optimal requirements for continuous photosynthesis (Parker et al., 2019). Insufficient light intensity or duration can inhibit the rate of photosynthesis, reducing biomass accumulation and overall crop yields (Zou et al., 2025). LED grow light is one of the effective and efficient artificial lighting solutions for hydroponic plants. (Bantis et al., 2020). Full-spectrum LEDs with a Photosynthetically Active Radiation (PAR) range of 400-700nm can replace sunlight as a production source for plants (Huché-Thélier et al., 2016). However, the use of LED grow lights requires high electrical energy consumption. To overcome this problem, in this study, the electricity needs from the State Electricity Company (PLN) of Indonesia were replaced by the use of solar panels to meet electricity needs. The integration of LED grow lights with solar power represents a sustainable approach to reducing dependency on fossil fuels and minimising operational costs in greenhouse agriculture. Indonesia, as a tropical country, has significant solar energy potential that can be harnessed to support agricultural systems, especially in regions with high solar irradiance such as West Sumatra. The utilisation of solar-powered LED lighting not only enhances plant growth but also contributes to environmentally friendly and low-emission agricultural practices (Al-Shamani et al., 2016).

To address energy consumption challenges in controlled-environment agriculture, the application of solar photovoltaic systems in greenhouse operations has emerged as a sustainable and environmentally friendly solution. Indonesia, located in the tropical region, has significant solar energy potential with an average solar radiation ranging from 4.5 to 5.1 kWh/m²/day, making it suitable for solar-based agricultural applications (Gholami et al., 2025). Previous studies have demonstrated that greenhouse systems powered by solar photovoltaic energy can substantially reduce dependence on grid electricity while maintaining stable microclimatic conditions necessary for plant growth (Al-Shamani et al., 2016; Hassanien et al., 2016). The integration of renewable energy into greenhouse systems also contributes to reduced operational costs and lower carbon emissions, supporting long-term agricultural sustainability. Therefore, this study aims to design and evaluate a solar panel-powered LED grow light system integrated with a Hydroponic Tower System (HTS) to enhance the growth of pak choy (*Brassica rapa* L.) under tropical greenhouse conditions. The proposed system combines natural sunlight with supplemental LED lighting powered by solar energy to extend the daily photoperiod and improve photosynthetic activity. This research is expected to contribute to the development of sustainable urban agriculture by providing a replicable and energy-efficient vertical farming model that supports increased crop productivity while minimising reliance on conventional grid electricity.

MATERIALS AND METHODS

The materials and methods of this study were carried out through a series of well-defined research stages to ensure systematic implementation and reliable results. The experiment was conducted at a specific experimental location under greenhouse conditions, which served as the controlled environment for the study. The first stage involved the setup of the hydroponic tower system (HTS) as the primary plant cultivation unit, followed by the installation of LED grow lights to provide supplemental artificial lighting. Subsequently, a solar photovoltaic system was designed and integrated to supply electrical power for the LED lighting system and supporting components. Pak choy (Brassica rapa L.) plants were selected as the plant material and cultivated under controlled growing conditions, including nutrient solution composition, irrigation scheduling, and photoperiod management. The final stage consisted of data collection and analysis, where plant growth parameters such as plant height, leaf length, leaf width, and number of leaves were measured and statistically analysed to evaluate the effects of the integrated hydroponic, lighting, and solar energy systems.

Experimental Location

This experiment was conducted in a greenhouse located in Lubuk Alung District, West Sumatra, Indonesia, with the coordinates -00°67'8122”, 100°28'043”. This research was

conducted from November to December 2024. In that month, the DNI data recorded in the Lubuk Alung area were 78.3 kwh /m² and 85.8 kwh/m². The DNI value this month is relatively low compared to the data in the previous month. This is influenced by the large number of clouds covering the area. The greenhouse is constructed using a light steel frame with UV-resistant polyethylene sheets for the roof and walls, combined with insect-proof netting. This series was made in a greenhouse (GH). The greenhouse measures 5.85 meters long, 4.30 meters wide, and 2 meters high. Its roof is triangular, measuring 5.85 meters long, 4.60 meters at the base, and 1.05 meters high (Figure 1).

Hydroponic Tower System (HTS) Setup

The HTS system was built using a hydroponic tower system made of 4-inch PVC pipe and a height of 125 cm. The pipe has 26 holes on the sides, and the holes are spaced 15 cm apart. The pipe is positioned vertically. A nutrient film technique (NFT) recirculation system is used, where a submersible pump flows the nutrient solution from the storage tank to the top of each tower, allowing the solution to drip through the plant roots before returning to the tank, as shown in Figure 2.

LED Grow Light Installation

The duration of LED exposure to plants can be determined by first calculating the average photosynthetic photon flux density (PPFD), which represents the amount of photosynthetically active radiation received by the plant canopy per unit time. The relationship between light intensity and exposure duration is expressed using the Daily Light Integral (DLI), which quantifies the cumulative number of photosynthetically active photons received per unit area per day. As shown in Equation (1), DLI is obtained by multiplying the

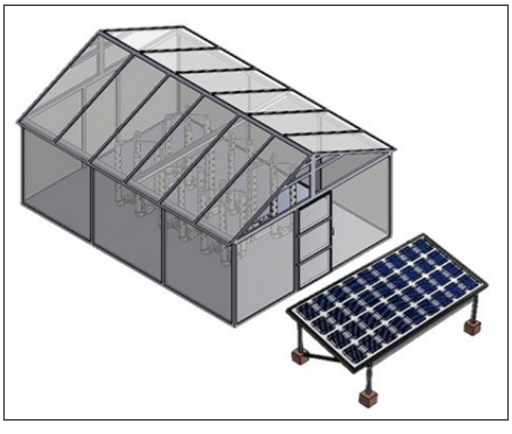

Figure 1. Greenhouse and hydroponic tower

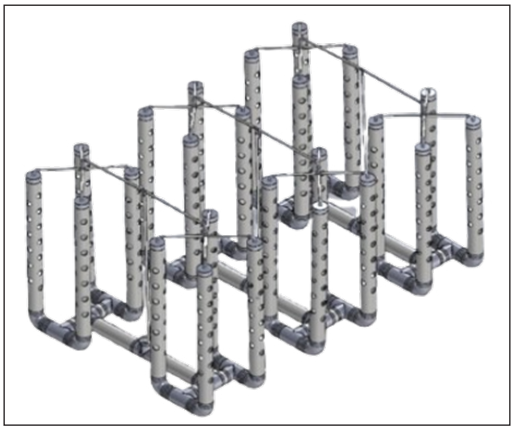

Figure 2. Overview of tower hydroponic system

average PPFD by the light exposure time, providing a practical metric for evaluating whether plants receive sufficient light for optimal photosynthesis (Faust, Logan, & Heins, 2005). This approach is widely applied in controlled-environment and greenhouse agriculture to optimise artificial lighting strategies, particularly when using LED systems. By adjusting the photoperiod based on measured PPFD values, the target DLI for leafy vegetable growth can be achieved while avoiding excessive light input and unnecessary energy consumption (Mitchell et al., 2015; Pennisi et al., 2019).

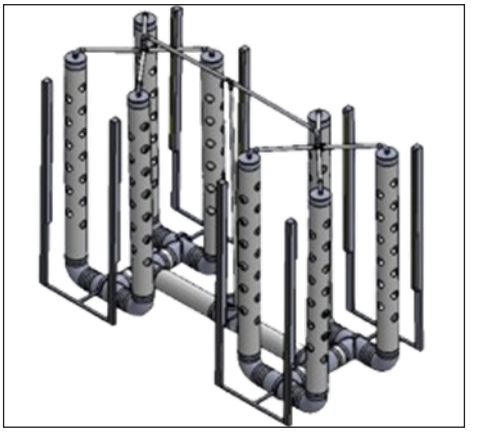

Figure 3. LED position on HTS

The selection of the type of LED lamp is based on the light spectrum that suits the photosynthesis needs of plants. The specifications of the lamp used are *full-spectrum LED* grow light strips or LEDs with a complete spectrum because they cover the entire PAR (*Photosynthetically Active Radiation*) light spectrum. The full spectrum LED used has white light with a CCT (Correlated Colour Temperature) of 5700K with a power of 15watts. This LED lamp has a light beam range of 120 × 30 cm. Positioning greatly influences the results of the study (Pereira, 2025). The optimal LED exposure time for pakcoy plants is 14 hours. LED calibration testing was carried out using four lamps placed at a distance of 15 cm from the plants with a grid size of 22.5 cm × 15 cm (Figure 3).

The duration of LED exposure to plants can be determined by first finding the average PPFD value. To find the average PPFD value, use the following Equation 1:

$$DLI = Average\ PPFD \times exposure\ time \quad [1]$$

where:
DLI = Daily Light Integral (mol m^{-2} day^{-1})
PPFD = Photosynthetic photon flux density (μmol m^{-2} s^{-1})

Solar Photovoltaic System Design

Solar panels are the main element in a solar power plant system which plays a role in converting solar energy into direct current (DC) electricity (Putri et al., 2025). In this design, the PLTS system is designed using an *Off-Grid configuration.* This *Off-Grid* System aims to supply electrical power needs, both in the form of direct current (DC) and alternating current (AC). This system consists of a 550 Wp monocrystalline solar panel, a 100 Ah

VRLA battery, a 20 A solar charge controller, and a pure sine wave inverter. Daily electrical energy requirements (Et) are calculated using the following Equation 2.

$$Et = (P \times t) \quad [2]$$

where:
P = Load power consumption (W)
t = Operational time (hours)

Table 1
Daily electrical energy requirements for greenhouse operations

Electrical Load	Amount	Load Capacity (watts)	Operating Hours (Hours)	Power Requirement (Wh)
Pump	4	36	12	1728
Spraying	1	60	0.23	13.8
Exhaust Fan	1	45	6	270
Light	8	15	3	360
Total Power Requirement (Wh)				2371.8

The required solar panel capacity is estimated using Equation 3.

$$SP = Et/Tmax \quad [3]$$

where:
SP = Solar panel capacity (Wp)
Tmax = Effective sunshine hours (hours)

Based on the calculation of daily energy requirements and an average of 5 hours of sunlight/day, the minimum capacity required is 474.36Wp; therefore, a panel with a capacity of 550Wp was selected.

Plant Materials and Growing Conditions

Pakcoy (*Brassica rapa L.*) was germinated in rockwool cubes for 10 days before being transferred to the HTS. The nutrient solution was prepared using the AB Mix formula, with electrical conductivity (EC) maintained at 1.5-2.0mS /cm and pH adjusted to 6.0-6.5. Two treatments were established: LED-assisted system - plants receiving supplemental LED lighting and Control - plants receiving only natural sunlight.

Data Collection and Analysis

Plant growth parameters (height, leaf length, leaf width, and number of leaves) were measured every 3 days for 27 days after planting (DAP). Statistical analysis was performed using a two-tailed independent t-test at a 95% confidence level ($p < 0.05$). Environmental parameters inside and outside the greenhouse (temperature, relative humidity, light intensity) were recorded using a data logger.

RESULTS

The results present and interpret the performance of the integrated hydroponic tower system equipped with solar-powered LED lighting. The discussion begins with the results of LED light and photoperiod calibration, which are critical for ensuring appropriate light intensity, spectral suitability, and photoperiod duration to support optimal photosynthesis in leafy vegetables (Bantis et al., 2018; Pennisi et al., 2019). This is followed by an analysis of the solar panel energy potential, focusing on solar irradiance availability, power generation characteristics, and system reliability in meeting nighttime lighting demands, as commonly evaluated in photovoltaic-powered greenhouse systems (Duffie & Beckman, 2013; Hassanien et al., 2016). Finally, plant growth observations are discussed based on measured vegetative parameters to assess the response of pak choy growth to supplemental LED lighting and renewable energy integration, as reported in previous hydroponic and controlled-environment agriculture studies (Mitchell et al., 2015; Resh, 2013).

LED Light and Photoperiod Calibration

The LED light and photoperiod calibration were performed to ensure uniform light distribution and adequate light intensity for optimal pak choy growth. Based on previous studies, the optimal daily light exposure for pak choy plants is approximately 14 hours; therefore, the photoperiod in this study was set accordingly. Calibration tests were conducted prior to the experiment to verify that the LED system delivered consistent and sufficient illumination across the plant canopy. Four LED lamps were installed at a distance of 15 cm above the plants to achieve effective light penetration and minimise shading effects. Light intensity measurements were carried out using a lux meter arranged in a measurement grid with a spacing of 22.5 cm × 15 cm to represent the planting layout. The recorded illuminance values were used to evaluate the spatial uniformity of light distribution across the hydroponic tower system. Since lux values do not directly represent photosynthetically active radiation, the measured data were converted into photosynthetic photon flux density (PPFD) values using the Waveform Lighting conversion tool (www.waveformlighting.com). The resulting PPFD values, presented in Figure 4 and 5, were used to confirm that the LED lighting system met the light requirements for vegetative growth of pokcoy.

271 1.1	246 2.1	211 3.1	203 4.1
1863 1.2	2208 2.2	3735 3.1	2973 4.2
2689 1.3	3250 2.3	6235 3.3	7190 4.3
2739 1.4	4858 2.4	7180 3.4	7681 4.4
2550 1.5	4550 2.5	7246 3.5	8070 4.5
3218 1.6	6018 2.6	7220 3.6	7878 4.6
2522 1.7	5040 2.7	7659 3.7	6890 4.7

Figure 4. LED lux meter measurement data at a distance of 15 cm from the plant

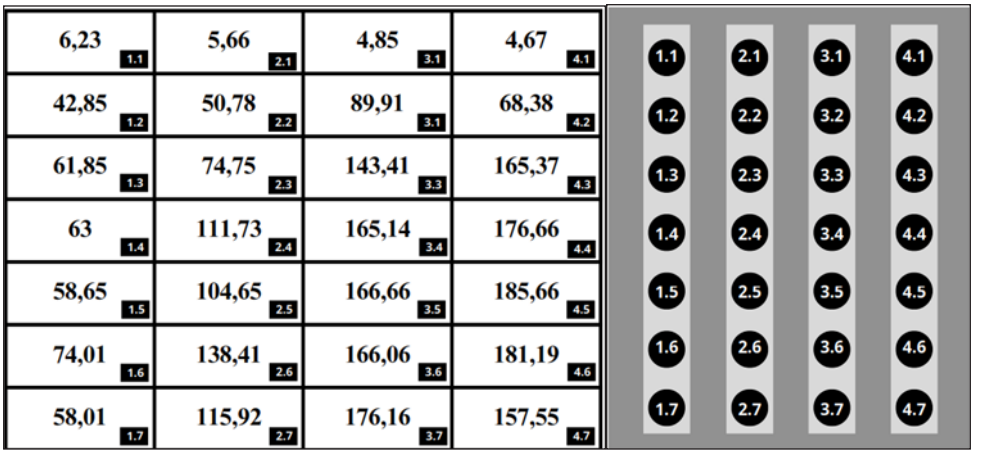

Figure 5. PPFD values from LED calibration tests

The duration of LED exposure for plants can be determined by first calculating the average PPFD value using the following Equation 4.

$$\bar{x} = \Sigma \frac{xi}{n}$$

$$\bar{x} = \frac{2.827{,}81 \frac{umol}{s} / m^2}{35} \quad [4]$$

$$= 80.79 \text{ µmol /s/m}^2$$

where:
$\bar{x}$: Average PPFD (µmol/s/m²)
Xi : PPFD value at each grid point
N : total number of grid points

After obtaining the average PPFD value, the Daily Light Integral (DLI) can be calculated using the following Equation 5.

$$\begin{aligned} &\text{DLI} = \text{Average PPFD} \times \text{exposure time} \\ &\text{DLI} = 80.79\ \mu\text{mol/s/m}^2 \times 3600\ \text{s/hour} \\ &= 290.844\ \mu\text{mol/m}^2\text{/hour} \times 1/1{,}000{,}000 \\ &= 0.290844\ \text{mol/m}^2\text{/hour} \times 14\ \text{hours} \\ &= 4.0718\ \text{mol/m}^2\text{/day} \end{aligned} \quad [5]$$

Based on the calculated DLI value, the LED lighting photoperiod can then be determined using the following Equation 6.

$$\begin{aligned} \text{Fp} &= \frac{DLI}{PPFD \times 0{,}0036} \\ \text{Fp} &= \frac{4{,}0718}{80{,}79 \times 0{,}0036} \\ \text{Fp} &= \frac{4{,}0718}{0{,}290844} \\ &= 13{,}999 \approx 14\ hours \end{aligned} \quad [6]$$

Calibration of the LED grow light at a distance of 15 cm from the plant canopy resulted in an average PPFD of 80.79 µmol m^{-2} s^{-1}. Based on Equation 1, the Daily Light Integral (DLI) achieved was 4.07 µmol m^{-2} day^{-1} for the LED supplementation period. When combined with natural sunlight, this extended the photoperiod to 14 hours/day, allowing for longer photosynthetic activity outside of daylight hours. Figure 6 show procedure using sunlight and LED lighting. From 07.00 to 18.00, plants rely exclusively on natural

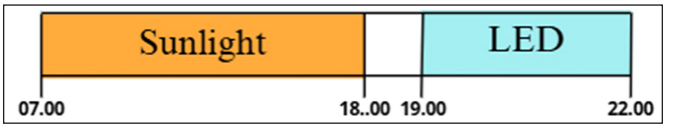

Figure 6. Supplemental lighting schedule showing the combination of natural sunlight and LED grow light periods

sunlight as the primary light source. During this period, the LED lighting system remains switched off, allowing photosynthesis to occur under natural solar radiation while reducing electrical energy consumption. From 18.00 to 19.00, a transition period without lighting is applied. This interval represents a gradual shift from daylight to darkness, simulating natural conditions. The transition phase helps prevent sudden changes in light intensity that could induce physiological stress in plants and supports a more stable photoperiodic response. From 19.00 to 22.00, LEDs are activated to provide supplemental artificial lighting. The additional illumination extends the daily light exposure and supports photosynthetic activity during the evening. After 22:00, all lighting sources are turned off to allow a complete dark period, which is essential for maintaining normal plant photoperiodism and growth regulation. This lighting strategy integrates the efficient use of natural sunlight with controlled LED supplementation to optimise plant growth while maintaining energy efficiency and a balanced light-dark cycle.

Results of Solar Panel Energy Potential Analysis

This research was conducted from November to December 2024. During those months, the recorded DNI data for the Lubuk Alung area were 78.3 kWh /m² and 85.8 kWh/m². The DNI values for these months were relatively low compared to the data from the previous month. This was influenced by the large amount of cloud covering the area. The average daily light intensity outside *the greenhouse* during the study was approximately 331.13 W /m². This figure is relatively low compared to the average normal sunlight intensity of approximately 800-1,200 W/m². Monitoring of light intensity in a greenhouse environment can be seen in Figure 7.

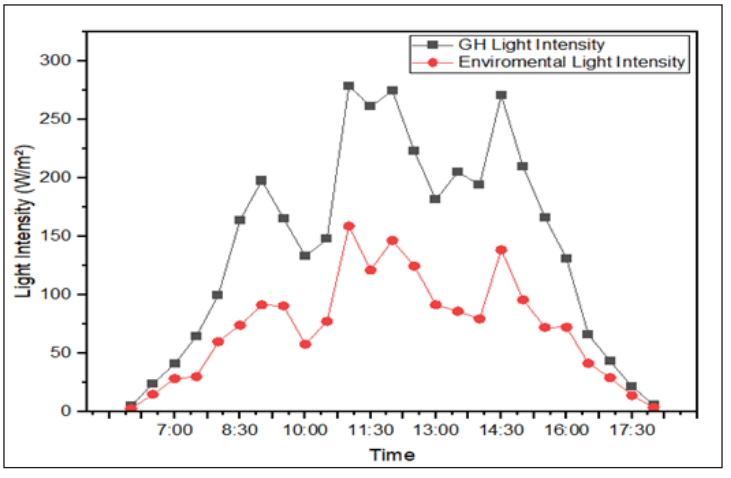

Figure 7. Greenhouse light intensity monitoring and the environment

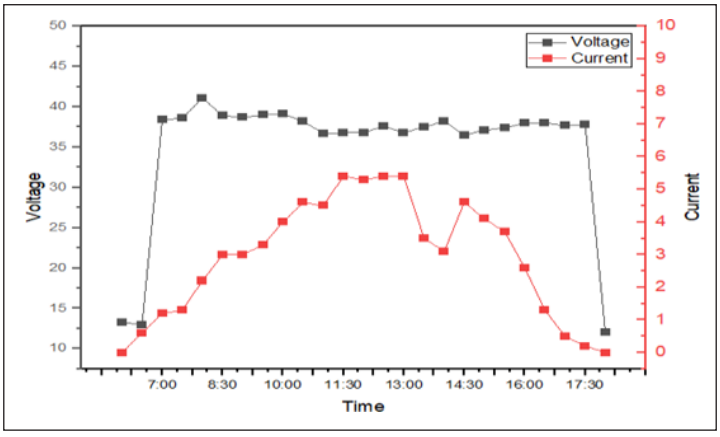

Figure 8. Hourly voltage and current output from solar panels

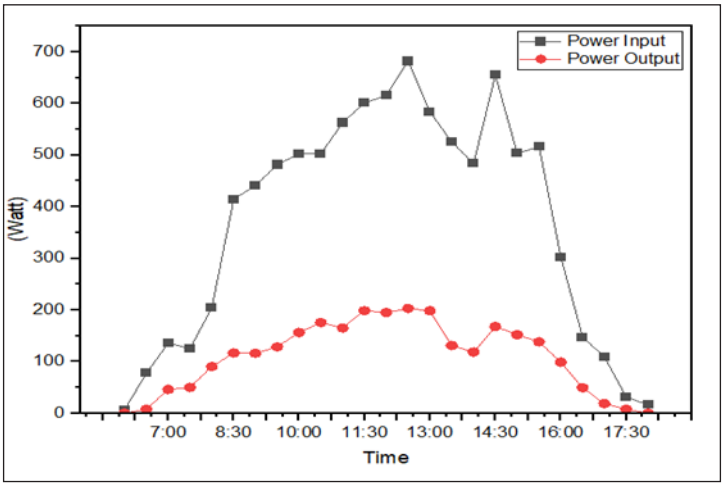

Figure 9. Daily power input and output of the solar photovoltaic system

Monitoring of the solar photovoltaic system was carried out from 06:00 to 18:00 during which time the peak output occurred between 11:00 and 12:00, this coincided with the maximum level of solar irradiation. The average charging efficiency of the solar photovoltaic system was 82 %, with a maximum instantaneous efficiency of 89% during optimal sunlight conditions. Monitoring of the solar photovoltaic input and output power can be seen in Figure 8 and 9.

Based on the three graphs above, it can be seen that there are differences in current and voltage values for each period. Voltage tends to appear more stable than current because current is primarily influenced by sunlight intensity (irradiance), while voltage is more sensitive to changes in temperature and load conditions (Figure 10). The 100 Ah VRLA

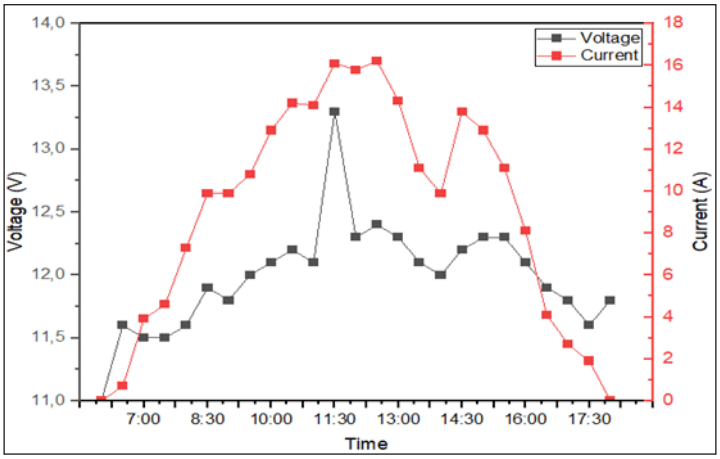

Figure 10. Monitoring of battery voltage and current during a 24- hour cycle

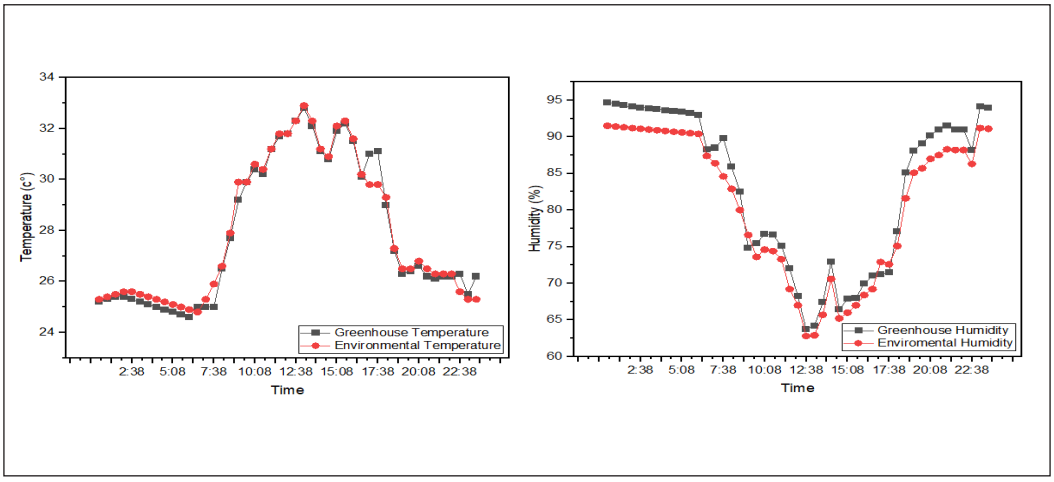

Figure 11. Humidity inside and outside the greenhouse

battery maintained a stable discharge, enabling the LED system to operate at night. The State of Charge (SOC) remained above 60% throughout the test, demonstrating sufficient capacity for the designed load (Skoplaki, E., & Palyvos, J. A.,2009; Villalva et al., 2009).

The average temperature monitoring inside the greenhouse during the experiment was at 27.5 ± 1.3°C, with an average relative humidity of 75.2 ± 4.8%. These values remain within the optimal growth range for *Brassica rapa L. This* occurs because the *greenhouse* is equipped with *an exhaust fan* and *misting* which function to control the temperature and humidity conditions *of the greenhouse.* Temperature and humidity monitoring can be seen in Figure 11.

Plant Growth Observation

Observations of pak choy plants involved two treatments (plants in the system with LED lighting for 3 hours at night and control plants without LED lighting). The LED lighting was applied to the plants in the system from 7:00 PM to 10:00 PM WIB. The purpose of this LED lighting was to compare the growth of the plants in the system with the LED lighting compared to the control plants. Lighting is one of the environmental factors that influences photosynthesis and plant growth. In hydroponic systems, especially those used indoors or in locations with limited natural light, supplemental lighting such as LEDs is often used to support optimal plant growth. Therefore, it's important to determine whether adding LEDs for 3 hours per day can have an impact. significantly on plant growth compared to the control system. This hypothesis can be proven by the results of the plant t-test analysis in Table 10. Measurement parameters for plants include plant height, leaf length, leaf width, and number of leaves. The average values for height, leaf length, leaf width, and number of leaves at 27 DAP are summarised in Table 4. A comparative graph of the growth of Pak choy can be seen in Figure 12.

Table 2
Comparison of plant growth parameters between LED-assisted treatment and control treatment at 27 days after planting

Observed Parameters	Treatment	Average	Standard Deviation	*t* value	*t* table	Significance (p-value)
Plant Height	System	13,419	1,034	4.163	1,985	0,000
	Control	12,581	0.934			
Leaf Length	System	8,226	0.703	5,479	1,985	0,000
	Control	7,450	0.683			
Leaf Width	System	5,450	0.451	5.141	1,985	0,000
	Control	4,961	0.480			
Number of Leaves	System	12,268	1,305	10,097	1,985	0,000
	Control	10,178	0.592			

The comparison of plant growth parameters between the LED-assisted treatment and the control at 27 days after planting (DAP) was evaluated using an independent t-test, as presented in Table 4. The results indicate that all observed growth parameters, plant height, leaf length, leaf width, and number of leaves, were significantly higher in plants grown under the LED-assisted system compared to the control treatment without LED supplementation. For plant height, the LED-assisted treatment showed a higher average value (13.419 cm) than the control (12.581 cm). The calculated t value (4.163) exceeded the critical t table value (1.985), with a p-value of 0.000, indicating a statistically significant difference. Similar trends were observed for leaf length and leaf width, where

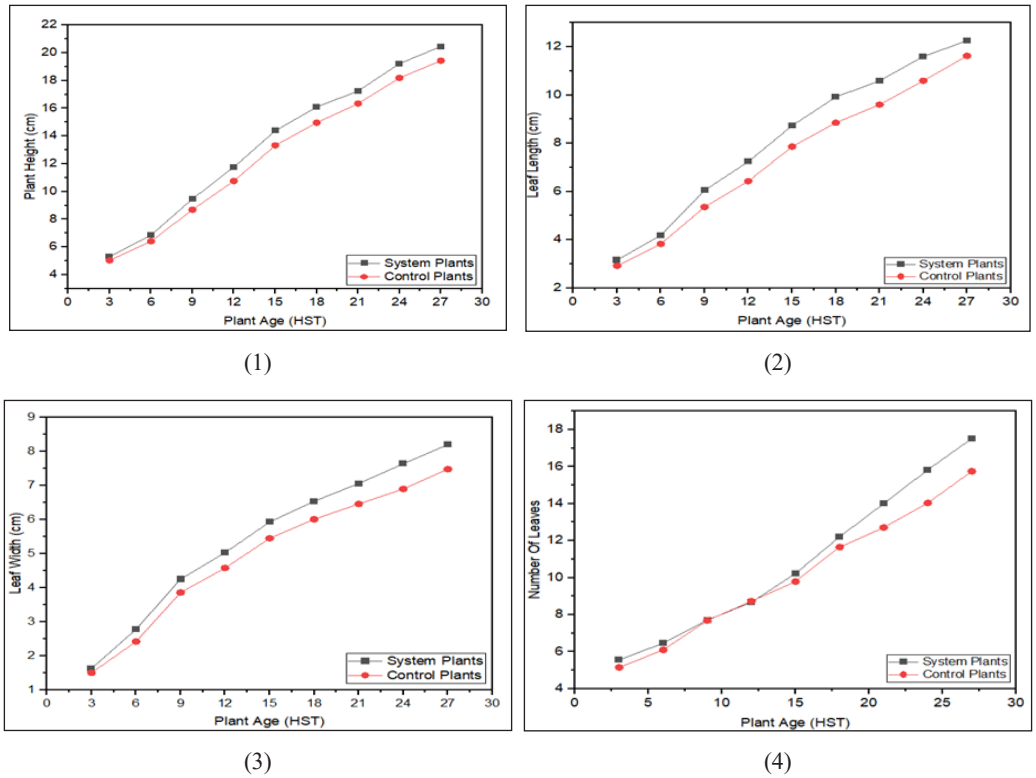

Figure 12. Graph (1) leaf length (2) number leaves (3) leaf width (4) Number of leaves during the cultivation period

the LED-assisted system produced longer and wider leaves, with t values of 5.479 and 5.141, respectively, both exceeding the critical value and resulting in highly significant differences ($p < 0.05$). The most pronounced effect of LED supplementation was observed in the number of leaves, where plants under the LED-assisted system achieved an average of 12.268 leaves compared to 10.178 leaves in the control. The corresponding t value of 10.097, far above the t table value, confirms a very strong statistical significance ($p = 0.000$). Overall, these results demonstrate that supplemental LED lighting significantly enhanced vegetative growth of pak choy at 27 HST, likely due to extended photoperiod and improved photosynthetic activity, thereby validating the effectiveness of the LED-assisted hydroponic tower system (Fan et al., 2019).

In the graph of the average plant height at 27 days after planting (DAP), the system plant reached a height of 20.45 cm and the average height of the control plant was 19.43 cm. The average length of pak choy leaves at 27 DAP planting age, the average leaf length of the system plant was 12.55 cm and the control plant was 11.62 cm. The average leaf width of the plant at 27 DAP, the system plant had a larger leaf width than the control

plant, which was 8.20 cm, while the control plant was 7.48 cm. The average number of leaves on the 27th day of DAP for the system plant and the control plant was 17.52 and 15.75 leaves, respectively. Based on these data, it can be seen that the system plant had a longer leaf length than the control plant.

Figure 13. Plants with LED lighting

Based on the plant growth data above, it can be seen that plants given additional light with LED grow lights experience faster growth than plants without LEDs. This occurs because LED grow lights are able to replace sunlight at night for photosynthesis. According to Huché-Thélier et al. (2016) , leafy plants require wavelengths for photosynthesis in the visible light spectrum of 500-600 nm. This light spectrum wavelength can be obtained from LED grow lights. In theory, pak choy plants with additional lighting from LEDs will experience faster growth than plants without LEDs. LED plants experience a longer photosynthesis period because the light spectrum from LEDs can replace sunlight as the main component of the photosynthesis process in plants (Figure 13). The LED light spectrum refers to the electromagnetic wavelength of light produced by a light source to encourage plant growth. For photosynthesis, plants use light in the PAR (photosynthetically active radiation) region with wavelengths (400nm-700nm) measured in nanometers (nm) (Wu et al., 2024) .

CONCLUSION

This research successfully designed a solar panel-based LED grow light system for application in *greenhouses* with *Hydroponic Tower System* (HTS), effectively providing additional lighting at night. The solar panels used have an average energy conversion efficiency of 20%, with stable peak power achieved between 11:00-12:00 WIB. The maximum input power produced by the solar panels is 3045.07watts with a maximum light intensity of 1180.26W/m², indicating good solar panel performance in supporting the system's energy needs. The addition of LED grow lights has been shown to increase the growth of pak choy plants, indicated by significant T-test results on the parameters of plant height, leaf length, leaf width, and number of leaves compared to control plants. Overall, this system has great potential to be implemented in urban agriculture as part of a sustainable agricultural solution based on renewable energy.

ACKNOWLEDGEMENT

The authors would like to express their gratitude to the Laboratory of Instrumentation and Control, Department of Agricultural and Biosystems Engineering, Faculty of Agricultural Technology, for providing laboratory facilities and technical support during this research.

REFERENCES

Abu Hatab, A., Cavinato, M. E. R., Lindemer, A., & Lagerkvist, C. J. (2019). Urban sprawl, food security, and agricultural systems in developing countries: A systematic review of the literature. *Cities, 94*, 129-142. https://doi.org/10.1016/j.cities.2019.06.001

Al-Kodmany, K. (2018). The vertical farm: A review of developments and implications for the vertical city. *Buildings*, *8*(2). https://doi.org/10.3390/buildings8020024

Al-Shamani, A. N., Alghoul, M. A., Elbreki, A. M., Ammar, A. A., Abulkhair, H. A., & Sopian, K. (2016). Design and performance evaluation of a photovoltaic powered greenhouse system. *Renewable and Sustainable Energy Reviews,* 59, 873-884. https://doi.org/10.1016/j.rser.2016.01.021

Arifin, B., Achsani, N.A., Martianto, D., Sari, L.K., & Firdaus, A.H. (2019). The future of Indonesian food consumption. *Indonesian Journal of Economics, 8*(1), 71-102. https://doi.org/10.52813/jei.v8i1.13

Barbosa, G. L., Gadelha, F. D. A., Kublik, N., Proctor, A., Reichelm, L., Weissinger, E., Wohlleb, G. M., & Halden, R. U. (2015). Comparison of land, water, and energy requirements of lettuce grown using hydroponic vs. conventional agricultural methods. *International Journal of Environmental Research and Public Health*, *12*(6)*,* 6879-6891. https://doi.org/10.3390/ijerph120606879

Bantis, F., Koukounaras, A., Siomos, A. S., Fotelli, M. N., & Kintzonidis, D. (2020). Bichromatic red and blue LEDs during healing enhance the vegetative growth and quality of grafted watermelon seedlings. *Scientia Horticulturae, 261*, Article 109000. https://doi.org/10.1016/j.scienta.2019.109000

Chatterjee, A., Ghosh, P., Winkler, B., V, V., Debnath, S., Cichocki, J., Trenkner, M., Vanicela, B., Riethmueller, C., Walz, M., Chandra, S., & Pal, H. (2025). Demystifying the integration of the hydroponics cultivation system, reinforcing bioeconomy and sustainable agricultural growth. *Scientia Horticulturae, 341,* Article 113973. https://doi.org/10.1016/j.scienta.2025.113973

Fan, X.-X., Xu, Z.-G., Liu, X.-Y., Tang, C.-M., Wang, L.-W., & Han, X.-L. (2013). Effects of light intensity on the growth and leaf development of young tomato plants grown under a combination of red and blue light. *Scientia Horticulturae, 153*, 50-55. https://doi.org/10.1016/j.scienta.2013.01.017

Faust, J. E., Logan, J., & Heins, R. D. (2005). Daily light integral: A research review and high-resolution maps of the United States. *HortScience, 40*(7), 1825-1829. https://doi.org/10.21273/HORTSCI13144-18

Gholami, M., Arefi, A., Hasan, A., Li, C., & Muyeen, S. M. (2025). Enhancing energy autonomy of greenhouses with semi-transparent photovoltaic systems through a comparative study of battery storage systems. *Scientific Reports, 15*(1), Article 2213. https://doi.org/10.1038/s41598-025-85418-z

Hassanien, R. H. E., Li, M., & Dong Lin, W. (2016). Advanced applications of solar energy in agricultural greenhouses. *Renewable and Sustainable Energy Reviews, 54*, 989-1001. https://doi.org/10.1016/j.rser.2015.10.095

Huché-Thélier, L., Crespel, L., Gourrierec, J. Le, Morel, P., Sakr, S., & Leduc, N. (2016). Light signalling and plant responses to blue and UV radiations: Perspectives for applications in horticulture. *Environmental and Experimental Botany, 121*, 22-38. https://doi.org/10.1016/j.envexpbot.2015.06.009

Mitchell, C. A., Both, A. J., Bourget, C. M., Burr, J. F., Kubota, C., Lopez, R. G., Morrow, R. C., & Runkle, E. S. (2015). LEDs: The future of greenhouse lighting. *Chronica Horticulturae, 55*(2), 6-12.

United Nations. (2019). *World urbanisation prospects: The 2018 revision* (ST/ESA/SER.A/420). https://population.un.org/wup/assets/WUP2018-Report.pdf

Parker, G. G., Fitzjarrald, D. R., Cibelle, I., & Sampaio, G. (2019). Consequences of environmental heterogeneity for the photosynthetic light environment of a tropical forest. *Agricultural and Forest Meteorology, 278*, Article 107661. https://doi.org/10.1016/j.agrformet.2019.107661

Pereira, J. (2025). Lighting strategies in vertical urban farming for enhancement of plant productivity and energy consumption. *Applied Energy*, 378, Article 124669. https://doi.org/10.1016/j.apenergy.2024.124669

Pennisi, G., Orsini, F., Landolfo, M., Pistillo, A., Crepaldi, A., Nicola, S., De Pascale, S., & Gianquinto, G. (2019). Optimal photoperiod and light intensity for indoor cultivation of leafy vegetables. *Scientia Horticulturae, 249,* 96-104. https://doi.org/10.1016/j.scienta.2019.01.013

Putri, R. E., Putri, I., & Hasan, A. (2025). Design and performance testing of a solar power generation system (SPGS) for a smart greenhouse with tower hydroponic support. *International Journal of Energy Production and Management, 10*(2), 165-173. https://doi.org/10.18280/ijepm.100201

Putri, R. E., & Jatiarum, S. A. (2025). Optimising pakcoy (*Brassica rapa* L.) growth in a smart greenhouse: Harnessing IoT for temperature and humidity control through tower farming systems. *IOP Conference Series: Earth and Environmental Science, 1477*(1), Article 012047. https://doi.org/10.1088/1755-1315/1477/1/012047

Putri, R. E., & Agus, N. P. (2025). Development of automatic watering system using verticulture method on pakcoy (*Brassica rapa* L.) based Internet of Things (IoT). *AIP Conference Proceedings, 3223*(1). https://doi.org/10.1063/5.0243748

Putri, I., Putri, R. E., & Pramana, F. A. (2023, June). Performance test of solar power plant as a source of electricity in mini greenhouse. *IOP Conference Series: Earth and Environmental Science, 1182*(1), Article 012021. https://doi.org/10.1088/1755-1315/1182/1/012021

Skoplaki, E., & Palyvos, J. A. (2009). On the temperature dependence of photovoltaic module electrical performance: A review of efficiency/power correlations. *Solar Energy*, *83*(5), 614-624. https://doi.org/10.1016/j.solener.2008.10.008

Villalva, M. G., Gazoli, J. R., & Filho, E. R. (2009). Comprehensive approach to modelling and simulation of photovoltaic arrays. *IEEE Transactions on Power Electronics*, *24*(5), 1198-1208. https://doi.org/10.1109/TPEL.2009.2013862

Wu, B. S., Mansoori, M., Schwalb, M., Islam, S., Naznin, M. T., Addo, P. W., MacPherson, S., Orsat, V., & Lefsrud, M. (2024). Light emitting diode effect of red, blue, and amber light on photosynthesis and plant growth parameters. *Journal of Photochemistry and Photobiology B: Biology, 256*, Article 112939. https://doi.org/10.1016/j.jphotobiol.2024.112939

Xin, P., Li, B., Zhang, H., & Hu, J. (2019). Optimisation and control of the light environment for greenhouse crop production. *Scientific Reports, 9*(1), 1-13. https://doi.org/10.1038/s41598-019-44980-z

Yusuf, A. G., Al-Yahya, F. A., & Saleh, A. A. (2025). Optimising greenhouse microclimate for plant pathology: Challenges and cooling solutions for pathogen control in arid regions. *Frontiers in Plant Science, 16*, 1-15. https://doi.org/10.3389/fpls.2025.1492760

Zou, J., Luo, S., Shi, M., Wang, D., Liu, W., Shen, Y., Ding, X., & Jiang, Y. (2025). Effects of different light intensities on lettuce growth, yield, and energy consumption optimisation under uniform lighting conditions. *PeerJ*, *13*(3), 1-17. https://doi.org/10.7717/peerj.19229

Pertanika J. Trop. Agric. Sci. 49 (S1): 101 - 118 (2026)

PERTANIKA JOURNALS

TROPICAL AGRICULTURAL SCIENCE

Journal homepage: http://www.pertanika.upm.edu.my/

Moisture Sorption Isotherms and Thermodynamic Characterisation of *Averrhoa bilimbi* (L.) Fruit

La Choviya Hawa[1]*, Mochamad Bagus Hermanto[1], Ubaidillah Ubaidillah[1], Rosnah Shamsudin[2], Lita Puspita R. Perdana[1], Ishika Cherry Nafisa[1], and Nabila Intan Milania[1]

[1]Department of Biosystems Engineering, Faculty of Agricultural Technology, Universitas Brawijaya, Malang, 65145 East Java Province, Indonesia

[2]Department of Process and Food Engineering, Faculty of Engineering, Universiti Putra Malaysia, 43400 UPM Serdang, Selangor, Malaysia

ABSTRACT

This study investigates the moisture sorption isotherms and thermodynamic properties of *Averrhoa bilimbi* (L.) fruit at the temperature of 25, 35, and 45°C using a gravimetric static method. The equilibrium moisture content (EMC) was measured under adsorption and desorption conditions, and five sorption models (GAB, BET, Peleg, Chung–Pfost, and Halsey) were applied to fit the experimental data. Among these, The BET model exhibited best predictive accuracy based on statistical parameters (R^2, χ^2, RMSE, and mean relative error). This study further evaluated critical water boundaries and calculated the net isosteric heat and sorption entropy using the Clausius–Clapeyron equation. Results demonstrated significant hysteresis between adsorption and desorption isotherms, with higher energy requirements during adsorption due to capillary condensation and bound water dynamics. The findings provide essential insights into the drying behaviour and stability of *A. bilimbi*, which can inform optimised postharvest processing and storage strategies for this highly perishable fruit.

ARTICLE INFO

Article history:
Received: 18 July 2025
Accepted: 29 December 2025
Published: 19 March 2026

DOI: https://doi.org/10.47836/pjtas.49.S1.05

E-mail addresses:
la_choviya@ub.ac.id (La Choviya Hawa)
mbhermanto@ub.ac.id (Mochamad Bagus Hermanto)
ubaidillah88@ub.ac.id (Ubaidillah)
rosnahs@upm.edu.my (Rosnah Shamsudin)
litapuspita@ub.ac.id (Lita Puspita R. Perdana)
cherrynafisa@ student.ub.ac.id (Ishika Cherry Nafisa)
nabila_nia@student.ub.ac.id (Nabila Intan Milania)
* Corresponding author

Keywords: Averrhoa *bilimbi*, moisture sorption isotherms, sorption modelling, isosteric heat, thermodynamic properties

INTRODUCTION

Averrhoa bilimbi (L.) is a fruit species widely cultivated in tropical regions such as Indonesia, Malaysia, Sri Lanka, India, Myanmar, Bangladesh, and parts of Central and South America (Mokhtar & Aziz, 2017).

e-ISSN: 2231-8542

The fruit is characterised as small in size, green in colour, and has a sour flavour due to its high oxalic acid contain (Garg et al., 2022). The bilimbi fruit is commonly used in folk medicine due to its medicinal properties (Sarker & Chowdhruy, 2024). The fruit has rich dietary fibre, protein, minerals, anthocyanins, tannins, and vitamin C (Madiha et al., 2024). The fruit is considered as a promising commodity for functional food product.

The fruit has been reported previously processed into various derivative products, including jams, pickles, jellies, vinegar, wine, and beverages (Prasad et al., 2021). Eaten raw or served as traditional dishes such as *bilimbir daal* or bilimbi soup are very common in Sri Lanka and Bangladesh (Bhuiyan et al., 2022; Waisundara, 2020). The fruit also fermented and utilised as traditional seasoning locally known as *asam sunti* in Aceh Province, Indonesia (Istiqamah et al., 2019). Anuar and Salleh (2019) reported research of bilimbi fruit with focus on preserving the fruit through processing techniques such as jam production. The utilisation of bilimbi fruit for beverages has also been reported in previous studies, e.g., bilimbi fruit tea (Juanda et al., 2022), black tea added with bilimbi fruit extract (Anggraini et al., 2016), bilimbi fruit wine (Caoli et al., 2017), and bilimbi fruit juice (Astillo, 2022). The bilimbi juice can also be used as natural acid coagulant for tofu production (Sitanggang et al., 2020). These developments highlight the growing potential of bilimbi fruit in the food industry, particularly as a health-oriented and consumer goods product.

Bilimbi fruit in Indonesia predominantly used as flavouring agent in local cuisine and is seldom consumed raw. Unlike other sour-source flavour such as tamarind, pineapple, and citrus, bilimbi fruit has limited attention in terms of postharvest research and derivative product development. The high moisture content of bilimbi fruit (>80%) make it highly perishable and typically has a shelf life of less than 24 h after harvest (Alhassan & Ahmed, 2017). Product diversification through postharvest processing, such as drying, is essential to extend utilisation and promote broader consumption.

The drying process not only improves product stability but also enables the availability of product all year long. However, the drying process can impact product quality by causing nutritional and physicochemical alteration. Therefore, optimised drying process is critical to balance food safety and product quality. In order to optimise the drying process, the fundamental data such as moisture sorption isotherms (MSI) and thermal properties of the fruit are necessary. MSI are fundamental in designing drying process and determining suitable packaging and storage conditions for dried products (Hssaini et al., 2022a). The MSI described the relationship between equilibrium moisture content and water activity at a constant temperature are unique to each product, depending on its composition and structure (Li & Ramaswamy, 2025). Accurate MSI data enable manufacturers to control drying endpoints, minimise deterioration, and ensure product safety. MSI behaviour has been studied previously for food products, e.g., muntries, finger lime, cabya, butterfly-pea

flower, cassava flour, fig, yacon, cheese-puri, and corn starch jelly candy (Bernstein and Noreña, 2013; Efendi, 2024; Hawa et al., 2020, 2021; Hssaini et al., 2022; Michalski et al., 2025; Thanuja & Ravindra, 2014).

The present study aims to determine the MSI of bilimbi fruit at three temperatures (25, 35, 45°C) using standard gravimetric method. Additionally, the experimental data are modelled using established sorption equations, and the thermodynamics properties, including net isosteric heat of sorption and the critical water activity boundaries during adsorption and desorption, are evaluated.

METHODS

Sample Preparation

The fresh bilimbi fruits as raw materials were obtained from local farmers in Malang, East Java Province, Indonesia. The fruits were collected at the green edible maturity stage with approximately 95% (wb) of moisture content depict in Figure 1. The fruit then cleaned from excessive peduncles and dust then sliced with sharp knife. A single fruit of bilimbi has approximately 6 cm in length and then sliced into eight parts with a thickness of 3 mm each. The sample then grouped into desorption and adsorption sample. For both group of samples, the sliced fruit dehydrated using laboratory hot air dryer (Memmert UFE550, Memmert GmbH, made in Germany) at 50°C for 48 h as adsorption and at 50°C for 12 h as desorption. Five saturated salt solutions (KOH, MgCl2, CaCl2, NaCl, and KCl) were utilised to obtain water activity values ranging from 0.063 to 0.843, as presented in Table 1.

Figure 1. The green edible maturity stage of bilimbi

Table 1
The selected salt used for preparing salt solutions and their corresponding water activities (a_w)

Saturated Salt Solution	a_w (25°)	a_w (35°)	a_w (45°)
KOH	0.082	0.074	0.063
$MgCl_2$	0.328	0.324	0.311
$CaCl_2$	0.640	0.625	0.571
NaCl	0.754	0.752	0.745
KCl	0.843	0.826	0.817

*Source: Bell & Labuza (2000); Rizvi (2005)

Moisture Sorption Isotherm Determination

Moisture sorption isotherms analysis of bilimbi using the gravimetric static method refers to research conducted by Hawa et al. (2020) at three subjected temperatures (25±2ºC, 35±2ºC, and 45±2ºC). The experimental procedure includes fifteen hermetic jars of 350 ml for each sample. Triplicate bilimbi samples for both adsorption and desorption experiments. Two cups were inserted into the hermetic jar. The first cup was plastic with 20 ml of salt solution, and the second cup was an aluminium foil cup filled with a bilimbi sample (1±0.1 g). The identical process is applied to adsorption and desorption. Each sample was placed in a hermetic jar alongside the saturated salt solution. Subsequently, the hermetic jars were placed at constant temperatures (25, 35, and 45 °C) in the incubator (Memmert E07086, Memmert GmbH, Germany). The incubator was previously allowed to be run empty for 2 hours to enable it to stabilise at the target temperature (25±2ºC, 35±2ºC, and 45±2ºC) to maintain a constant relative humidity corresponding to a constant water activity (aw) for respective temperatures (Hawa et al., 2020). Figure 2 illustrates for collecting

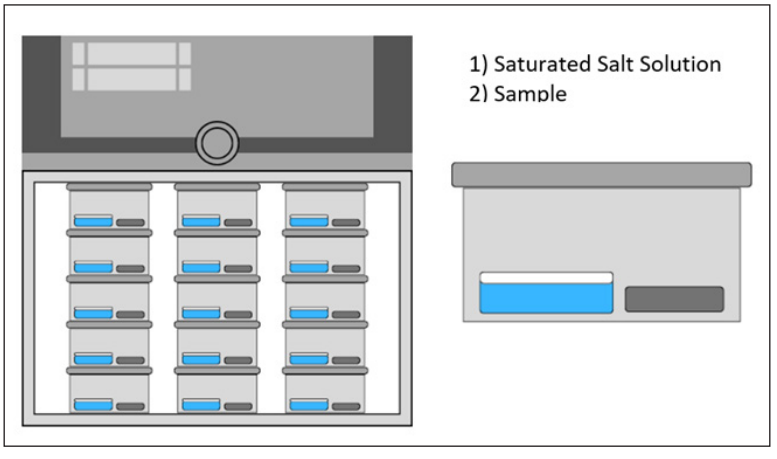

Figure 2. The illustration of hermetic jars placed in the incubator

moisture sorption on bilimbi incubation. The samples were weighed at the sixth hour and subsequently every 24 hours using a digital balance with ±0.001 g of accuracy. The experiment was stopped until the mass remained constant if there is a difference of less than 2% in three consecutive weight measurements. To determine the equilibrium moisture content (EMC), the samples were dried at 105°C for 4 hours.

Mathematical Modelling of Sorption Isotherms

A semi-empirical sorption model was used to predict the equilibrium moisture content of bilimbi (Oduola et al., 2022). The research used five models to predict moisture sorption phenomena, namely GAB, BET, Peleg, Chung-pfost, and Halsey. The summarised of five models showed in Table 2 were fitted using Microsoft Excel 365 for Windows. Where a_w is the water activity, a, b, n, K, and C are dimensionless constants, and *Mo* is the monolayer water content in wet basis.

Each model was evaluated using statistical analysis. It is essential to recognise the parameters of model accuracy in order to identify the suitability of the model used by established standards. Statistical analysis was used to determine water activity, on changes in equilibrium moisture content. To evaluate the model performance, the coefficient of determination (R^2), chi square (χ^2), mean relative percent error (P), and root mean square error ($RMSE$) between the experimental and the predicted data were used. The value of R^2 is the main criterion for initial model selection, where χ^2, RMSE, and P are the second, the third, and the supplementary criterion, respectively (Hawa et al., 2021; Hawa et al., 2021; Hawa et al., 2020).

Table 2
The mathematical models for fit the sorption isotherms of bilimbi

Semi-empirical Sorption Model	Equation
GAB	$EMC = \frac{\bar{M}_o CKa_w}{(1-Ka_w)(1-Ka_w+CKa_w)}$
BET	$EMC = \frac{M_o Ca_w}{(1-a_w)(1+(C-1)a_w}$
Peleg	$EMC = a{a_w}^b + C{a_w}^n$
Chung-pfost	$EMC = a - b\ ln[-(T+c)\ ln(a_w)]$
Halsey	$EMC = \left(-\frac{C}{ln\ a_w}\right)^{1/n}$

*Source: Andrade & Hensel (2013)

$$R^2 = \frac{\left(\sum_{i=1}^{N}\left(EMC_{exp} - \overline{EMC}_{exp}\right)\left(EMC_{pre} - \overline{EMC}_{pre}\right)\right)^2}{\sum_{i=1}^{N}\left(EMC_{exp} - \overline{EMC}_{exp}\right)^2 \sum_{i}^{N}\left(EMC_{pre} - \overline{EMC}_{pre}\right)^2} \quad [1]$$

$$\chi^2 = \frac{\sum_{i}^{N}\left(EMC_{exp} - EMC_{pre}\right)^2}{N-n} \quad [2]$$

$$P = \frac{100}{n}\sum_{i=1}^{n}\left|\frac{EMC_{exp} - EMC_{pre}}{EMC_{exp}}\right| \quad [3]$$

$$RMSE = \left[\frac{1}{N}\sum_{i=1}^{N}(EMC_{exp} - EMC_{pre})^2\right]^{\frac{1}{2}} \quad [4]$$

Thermodynamics Properties Determination

Determination of the Sorption Heat

The differential enthalpy commonly termed isosteric heat of sorption Q_{st} (kJ mol^{-1}) and defined as the sum of the net isosteric heat of adsorption (q_{st}) and the latent heat of condensation of pure water (Q_c) at the average experimental temperature. To determine the isosteric heat os sorption, moisture sorption data obtained from the best fitting isotherm model at three distinct temperatures were employed. The values were calculated through the linearised form of the Clausius–Clapeyron equation as below (Hssaini et al., 2022; Sahu et al., 2018), where a_w is the water activity, T (K) is the temperature, q_{st} is the net isosteric heat of sorption, and R is the ideal gas constant (8.314×10^3 kJ mol^{-1} K^{-1}).

$$q_{st} = -R\left[\frac{d[ln\ a_w]}{d\left(\frac{1}{T}\right)}\right]_M \quad [5]$$

To estimate the net isosteric heat of sorption (q_{st}), a specific moisture content (M) was assumed. The corresponding water activity (a_w) values were predicted using the best-fitting sorption isotherm model. A linear relationship between $ln\ a_w$ and $1/T$ was established, and the slope of the resulting plot was used to calculate the value of q_{st}. In this analysis, the assumed moisture content was set to the monolayer moisture content (Mm), as determined from the selected sorption model. The required a_w values for the given moisture contents were computed using Microsoft Excel 365. The value of the isosteric heat of sorption (Q_{st}) was determined from the following relationship, where Q_c is the heat of condensation of pure water (43.65 kJ mol^{-1}) at the mean temperature (308.15 K) used in this study.

$$Q_{st} = q_{st} + Q_c \quad [6]$$

Determination of the Sorption Entropy

Sorption entropy was determined by applying equation to the sorption data predicted by the best-fitting sorption model as below (Hssaini et al., 2022; Sahu et al., 2018), where ΔS is the entropy (kJ mol^{-1}). The value ΔS was computed from the intercept ($\Delta S/R$) value of the plot between *ln* a_w and *1/T* for definite values of moisture content.

$$-ln\, a_w = \frac{Q_{st}}{RT} - \frac{\Delta S}{R} \quad [7]$$

Determination of Critical Water Boundary

Primary Bound Water

The critical limit of primary bound water was calculated using the BET (Brunauer-Emmett-Teller) equation by plotting a graph of a_w data against [$a_w/(1-a_w)\ X_e$] (Jamaluddin et al., 2014).

$$\frac{a_w}{(1-a_w)\,Xe} = \left(\frac{1}{X_m\ .C}\right) + \left(\frac{a_w(C-1}{X_m\ .C}\right) \quad [8]$$

Secondary Bound Water

Logarithmic analysis can be used to determine the limit of secondary bound water. *Log(1-a_w)* data plotted against X_e results in a straight line that splits into two. The coordinates expressed as *Log(1-a_w)* which is the relationship between *Log(1-a_w)* and water will produce two straight line curves. The first line represents the position of the secondary bound water, while the second line represents the tertiary bound line. The intersection of the two lines indicates the maximum amount of secondary bound water capacity (Jamaluddin et al., 2014).

$$log\ (1 - a_w) = b\ (X_e) + a \quad [9]$$

Tertiary Bound Water

The tertiary bound water was determined using a second-order polynomial model, with the value of tertiary bound water limited to a_w values greater than the fraction of secondary bound water (Jamaluddin et al., 2014).

$$y = ax^2 + bx + c \quad [10]$$

RESULTS AND DISCUSSION

Equilibrium Moisture Content of Dried Bilimbi

The equilibrium moisture content of samples during adsorption and desorption at temperatures of 25°C , 35°C , and 45°C are shown in Figure 3. The equilibrium moisture content of the adsorption samples rises with elevated relative humidity at a constant temperature and diminishes with reduced relative humidity (Figure 3) (Yadav & Mishra, 2023). At elevated temperatures, the kinetic energy of water molecules will increase, hence diminishing the intermolecular forces of attraction among them. As temperature increases, the water activity of the saturated salt solution and the equilibrium moisture content decrease (Arslan-Tontul, 2020).

Similar to the adsorption samples, the desorption samples exhibited a linear correlation between equilibrium water content and water activity. As illustrated in Figure 3, the equilibrium moisture content of bilimbi increased as water activity at a constant temperature condition (Fadimu et al., 2019). At a constant water activity, the desorption equilibrium moisture content was observed to be lower than the adsorption equilibrium moisture content. This illustrates the reversed phenomenon of hysteresis frequently observed. The phenomenon of capillary condensation results in a swift escalation of the adsorption sample prior to the attainment of pressure equilibrium. This process transpires when water vapor persistently adsorbs in many layers within porous solids until the pore space is saturated with water. This anomalous phenomenon is explained in the study by Shen et al. (2023) which references to the hypothesis proposed by Broekhoff and de Boer in 1973, asserting that the filling of open holes results from an unstable adsorption layer intricately

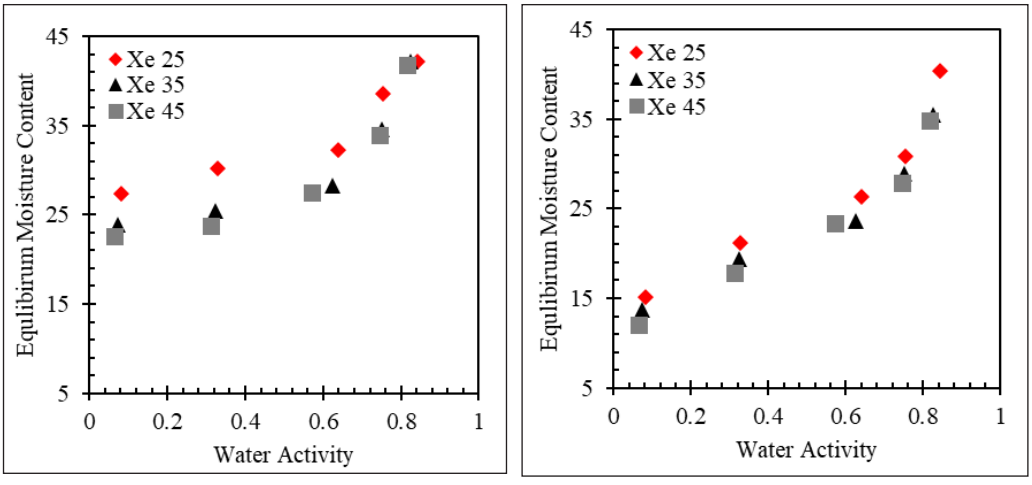

Figure 3. Equilibrium moisture content of bilimbi: (a) adsorption sample, (b) desorption sample

linked to the pore radius. The desorption pressure is inferior to the adsorption pressure. The configuration of the closed space is a primary element influencing the elevation of adsorption hysteresis beyond desorption hysteresis. The anomalous behavior observed in adsorption samples is affected by the development of multimolecular adsorption layers until the constricted regions of the pores are obstructed, resulting in the creation of a meniscus that induces capillary condensation (Broekhoff & de Boer, 1967).

Mathematical Modelling of the Moisture Sorption Isotherm

The fittest model to represent moisture sorption isotherms of bilimbi was chosen based on the predicted value that most closely aligns with experimental value. In order to evaluate the model performance, the statistical parameters, i.e., R^2, χ^2, RMSE, and P values. Table 3 summarises the statistical parameters based on fitting results of experimental data to the selected models used. Based on the main criterion, it can be seen that BET model consistently gives the highest R^2 with lowest χ^2 and RMSE values in all tested temperature. The BET model also provides the same performance in both adsorption and desorption samples within tested water activity range (0.063 to 0.843).

Table 3
Moisture sorption statistical performance

Model	T (°C)	Adsorption				Desorption			
		R^2	χ^2	RMSE	P	R^2	χ^2	RMSE	P
GAB	25	0.9170	0.0338	0.1163	28.8	0.9401	0.0093	0.0609	25.9
	35	0.8645	0.0247	0.0993	28.2	0.9533	0.0077	0.0557	25.5
	45	0.8899	0.0222	0.0942	24.1	0.9710	0.0059	0.0486	23.9
BET	25	0.9768	0.0290	0.1318	25.8	0.9842	0.0078	0.0685	21.5
	35	0.9945	0.0152	0.0953	19.9	0.9843	0.0056	0.0578	19.7
	45	0.9984	0.0128	0.0875	21.2	0.9729	0.0046	0.0524	21.3
Peleg	25	0.8460	0.0014	0.0292	7.8	0.9075	0.0022	0.0363	12.5
	35	0.7752	0.0030	0.0426	12.2	0.9188	0.0015	0.0298	11.5
	45	0.7900	0.0032	0.0439	13.7	0.9410	0.0012	0.0270	12.1
Chung-pfost	25	0.9501	0.0007	0.0171	4.1	0.9702	0.0011	0.0208	6.5
	35	0.9040	0.0021	0.0288	8.5	0.9759	0.0007	0.0164	5.5
	45	0.9190	0.0020	0.0281	9.2	0.9851	0.0005	0.0135	5.1
Halsey	25	0.9788	0.0450	0.1643	47.5	0.9873	0.0153	0.0957	39.9
	35	0.9927	0.0273	0.1281	40.0	0.9877	0.0117	0.0837	38.1
	45	0.9971	0.0248	0.1221	40.3	0.9780	0.0103	0.0786	38.0

The Brunauer-Emmett-Teller (BET) model is the foundational mathematical model used to describe the relationship between equilibrium moisture content and water activity in food products, including bilimbi. It is especially important for understanding and

predicting how food interact with moisture during storage, processing, and packaging. The BET model is based on the theory of multilayer adsorption, where water molecules first form a monolayer on the food surface and then additional layers at higher water activities. The BET model also allows the determination of two key parameters, i.e., the monolayer moisture content (M_o) and BET energy constant (C). The monolayer moisture content (M_o) represents the amount of water strongly bound to the food surface (Staudt et al., 2013). Below the M_o value, the food is most stable with minimal chemical and microbial changes. BET constant (C) reflects the energy of adsorption in the first layer compared to subsequent layers. The M_o value from BET model is used to determine optimal moisture levels for storage stability. Foods stored at or below this moisture content are less prone to spoilage and quality loss (Abdullah et al., 2020). Based on the results, it can be seen than dried bilimbi fruit will safe at below 0.087 (d.b.) if stored at room temperature (approx. 25-35°C).

The BET model is universally accepted mathematical models to describe the sorption behaviour of various fruit, e.g. banana, mango, and pineapple (Talla et al., 2005), apple with PEF treatment (Castagnini et al., 2020), green and red peppers (Kaymak-Ertekin & Sultanoglu, 2001), and green chilli (Getahun et al., 2020). In addition, (Andrade & Hensel, 2013) mentioned that BET model also found to suitable for dried tomato, apple, and blueberry.

Hysteresis Curve of Moisture Sorption Isotherm

The hysteresis curve observed for dried bilimbi at all tested temperatures depicted in Figure 4. It was a convincing confirmation that the experimental adsorption and desorption data display a clear sigmoidal trend. The curve corresponding to a Type II moisture sorption isotherm typically associated with multilayer adsorption in food system (Al-Muhtaseb et al., 2002). The sigmoidal profile characteristics reflects multilayer adsorption driven by Raoults's law, capillary effect, and surface moisture interactions (Labuza & Altunakar, 2020). The results also showed that the sigmoidal pattern is clearly observed across all temperatures, confirming that the moisture binding mechanism conforms to multilayer formation typical of high-moisture fruit matrices. The hysteresis loop in the bilimbi isotherms also reveals two distinct regions of equilibrium moisture variation, i.e., at water activities of approximately 0.2–0.4 and 0.6–0.7, which correspond to multilayer adsorption and progressive pore filling. These features mirror trends reported previously for other starchy and high-carbohydrate foods.

Hysteresis is a well-documented phenomenon in food and fruit moisture sorption isotherms, where the desorption curve (drying) lies above the adsorption curve (rehydration) at the same water activity. This means that, for a given water activity, the equilibrium moisture content is higher during desorption than during adsorption. This pattern is observed in a wide range of foods, including bananas and tamarind (Pandian et al., 2025; Yan et al.,

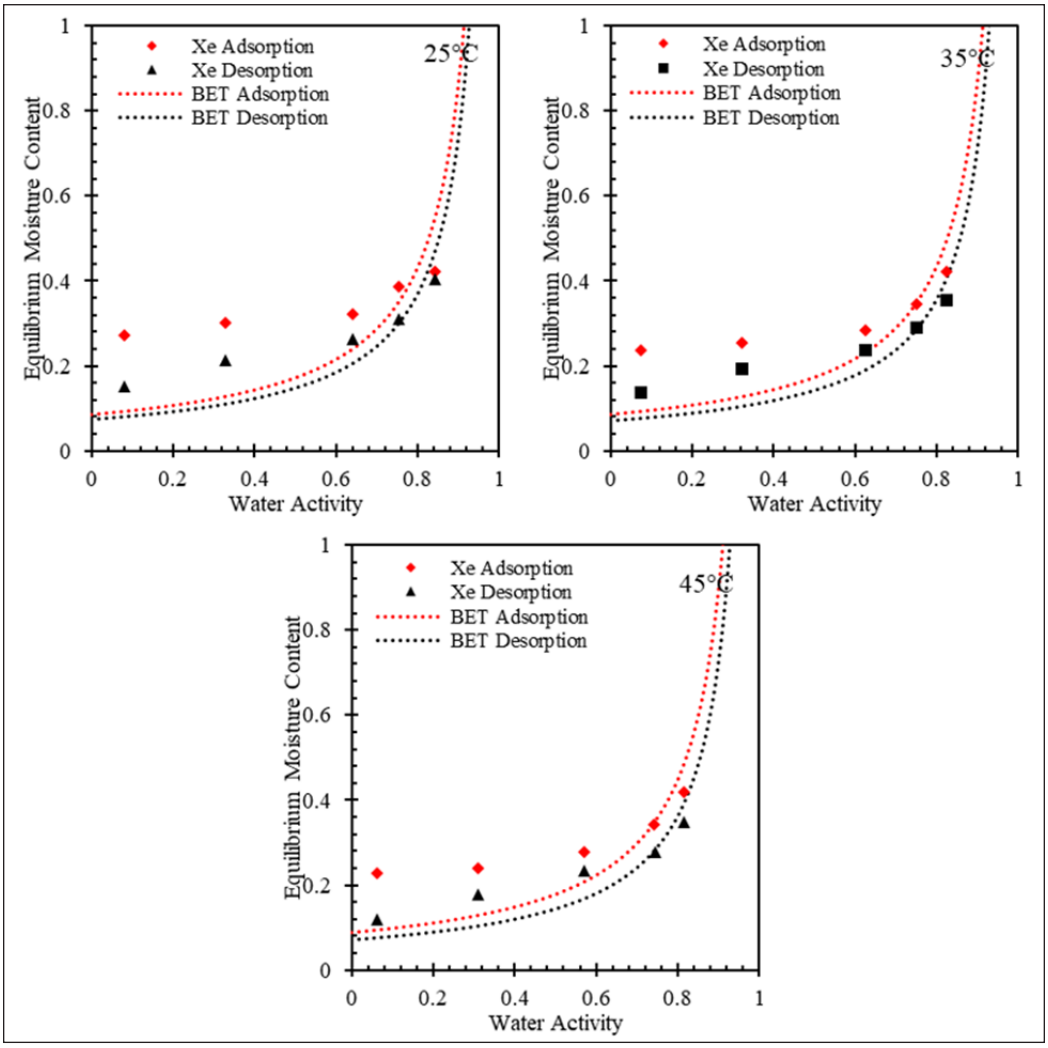

Figure 4. Sorption isotherms of bilimbi at different temperatures fitted with the BET model

2008). The higher desorption curve is attributed to structural and physicochemical changes in the food matrix during drying, such as pore collapse, capillary effects, and strong binding of water in small pores, which make it harder for water to leave during desorption than to enter during adsorption (Fikry et al., 2025). However, the hysteresis magnitude in bilimbi, where adsorption values consistently exceed desorption values, aligns with the pattern noted by (Shen et al., 2023). While the vast majority of studies report the desorption curve above the adsorption curve, crossing or overlap can occur at very high-water activities or under specific conditions as previously reported for whole black peppercorns (Yogendrarajah et al., 2015) and four-finger threadfin (Saniso et al., 2025).

Critical Water Boundary

Figure 5 shows the position of the bound water fraction in the adsorption and desorption samples at the three storage temperatures used. The position of the bound water fraction in bilimbi is influenced by the condition of water activity and equilibrium water content at constant storage temperature conditions. (Thanuja & Ravindra, 2014) stated that the sorption isothermal phenomenon in materials can be divided into three zones based on the observed decrease in equilibrium moisture content. Zone I is primary bound water (a_w 0 - 0.35), Zone II is secondary bound water (a_w 0.35 - 0.80), and Zone III is tertiary bound water (a_w > 0.8).

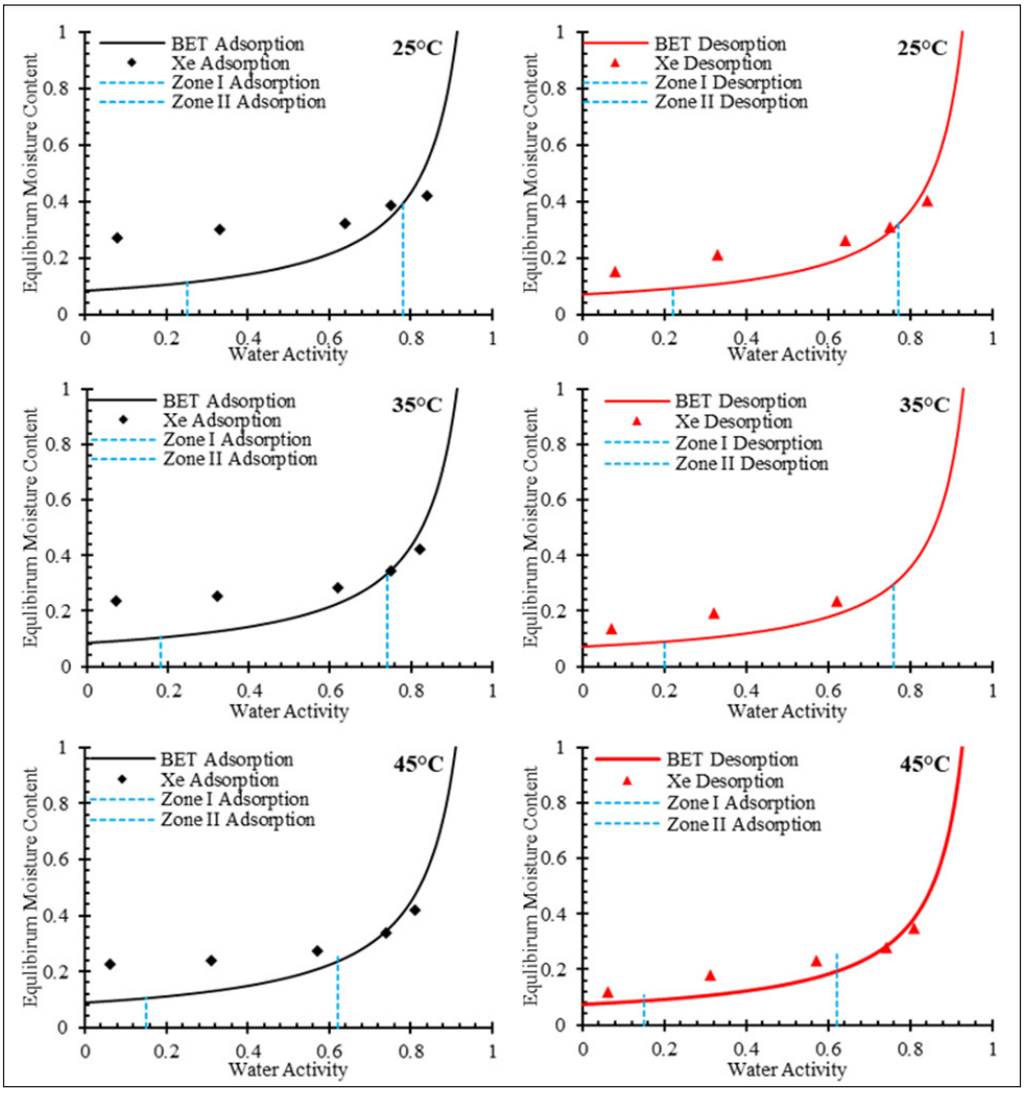

Figure 5. Bound water fraction for adsorption and desorption at different temperatures

Across all temperatures, the bilimbi sorption isotherms show the typical three-zone pattern of a Type II curve. In Zone I ($a_w \approx$ 0-0.2), the equilibrium moisture content remains low and increases only slightly, indicating the presence of strongly bound water associated with hydrophilic sites on the solid matrix. This water is tightly held and cannot be easily removed due to strong interactions with polar constituents. In Zone II ($a_w \approx$ 0.2-0.7), the moisture content increases gradually and almost linearly, corresponding to the formation of multilayer water held by weaker intermolecular forces. This region reflects the adsorption of water beyond the primary sorption sites, and its slope matches the behaviour shown in the graphs. In Zone III ($a_w >$ 0.7), the equilibrium moisture content rises sharply as free or capillary water accumulates within macropores. This rapid increase reflects water that is only weakly bound and is readily available to support microbial growth and enzymatic activity, consistent with the steep curvature observed in the plotted bilimbi adsorption and desorption data. The similar findings have been reported previously on fruit products, e.g., fig (Hssaini et al., 2022) and sweet cherry (Ouaabou et al., 2022).

Isosteric and Net Isosteric Heat

The experimental results for bilimbi showed that the maximum net isosteric heat of sorption reached 96.43 kJ/mol, while the highest isosteric heat reached 140.08 kJ/mol (Figure 6 and 7). The net isosteric heat represents the energy required to evaporate water bound within the food matrix, and in case of bilimbi, the adsorption consistently exhibited higher value than desorption. This trend aligns with (Koua et al., 2012), who reported that, at a constant equilibrium moisture content, the net isosteric heat of desorption generally exceeds that of absorption. It was due to water removal requires greater energy than capillary condensation. A positive net isosteric heat reflects the release of energy during sorption.

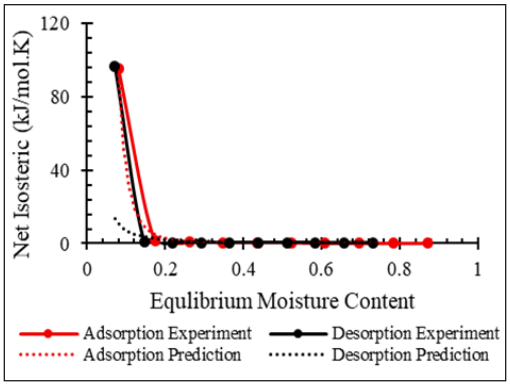

Figure 6. Sorption net isosteric of bilimbi at different moisture content

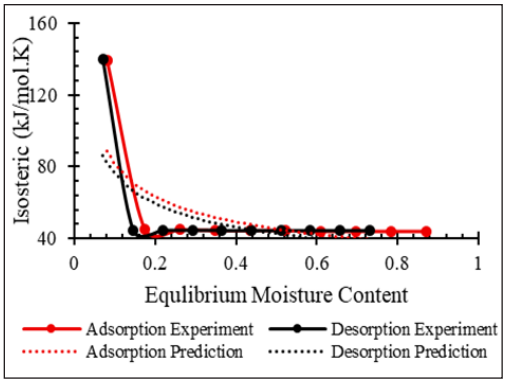

Figure 7. Sorption isosteric of bilimbi at different moisture content

The higher energy demand during adsorption compared with desorption is consistent with the findings of Shen et al. (2023), who associated this difference with the presence of energy barriers during transitions between metastable states in adsorption–desorption processes. (Desgranges & Delhommelle, 2019) further demonstrated that the free energy required to initiate capillary condensation decreases as surface moisture increases.

Isosteric heat provides important insight into liquid–solid interactions during storage. In bilimbi, the isosteric heat is highest at low equilibrium moisture content and decreases as moisture content increases. At low moisture levels, water molecules are strongly bound to hydrophilic components such as carbohydrates and proteins, requiring more energy for evaporation. Conversely, at higher moisture contents, water behaves more like free water, reducing the energy needed for phase change. This pattern is consistent with the results of Barati et al. (2016), who observed that net isosteric heat is greatest at low water content and diminishes as equilibrium moisture content increases due to the shift from tightly bound water to weaker bound or free water.

CONCLUSION

This study successfully characterised the moisture sorption behaviour and thermodynamic properties of Averrhoa bilimbi fruit. Moisture sorption isotherms were significantly affected by temperature and showed typical sigmoidal (Type II) hysteresis behaviour. The BET model provided the most accurate prediction of equilibrium moisture content across the tested temperature range and sorption conditions. Thermodynamic analysis revealed that net isosteric heat and entropy decreased with increasing moisture content, indicating stronger water–solid interactions at lower moisture levels. The identification of critical water activity zones (primary, secondary, and tertiary bound water) contributes to understanding the fruit's moisture retention and stability during drying and storage.

ACKNOWLEDGEMENT

This research received financial support from Universitas Brawijaya, in the framework of Hibah Guru Besar Universitas Brawijaya Fakultas Teknologi Pertanian funding scheme (No. 01213/UN.F1001/B/PT0103.2/2024).

REFERENCES

Abdullah, S., Keoh, S. C., Johar, H. M., Razak, N. A., Shaari, A. R., & Rukunudin, I. H. (2020). Mathematical modelling of moisture sorption isotherms by using BET and GAB models. *IOP Conference Series: Materials Science and Engineering*, *932*(1). https://doi.org/10.1088/1757-899X/932/1/012037

Alhassan, A., & Ahmed, Q. (2016). Averrhoa bilimbi Linn.: A review of its ethnomedicinal uses, phytochemistry, and pharmacology. *Journal of Pharmacy & Bioallied Sciences*, *8*(4), 265. https://doi.org/10.4103/0975-7406.199342

Al-Muhtaseb, A. H., McMinn, W. A. M., & Magee, T. R. A. (2002). Moisture sorption isotherm characteristics of food products: A review. *Food and Bioproducts Processing*, *80*(2), 118–128. https://doi.org/10.1205/09603080252938753

Andrade, S. P. C., & Hensel, O. (2013). Experimental determination and mathematical fitting of sorption isotherms for Lemon Balm (Melissa officinalis L.). *Agricultural Engineering International: CIGR Journal*, *15*(1), 139–145. https://cigrjournal.org/index.php/Ejounral/article/view/2146

Anggraini, T., Febrianti, F., Aisman, & Ismanto, S. D. (2016). Black tea with averrhoa bilimbi L extract: A healthy beverage. *Agriculture and Agricultural Science Procedia*, *9*, 241–252. https://doi.org/10.1016/j.aaspro.2016.02.141

Anuar, N. A., & Salleh, R. M. (2019). Development of fruit jam from Averrhoa bilimbi L. *Journal of Food Processing and Preservation*, *43*(4). https://doi.org/10.1111/jfpp.13904

Arslan-Tontul, S. (2020). Moisture sorption isotherm, isosteric heat, and adsorption surface area of whole chia seeds. *LWT*, *119*, 108859. https://doi.org/10.1016/j.lwt.2019.108859

Astillo, J. D. (2020). Bilimbi fruit (Averrhoabilimbi) juice. *International Journal of Environment, Agriculture and Biotechnology*, *5*(3). https://doi.org/10.22161/ijeab.53.12

Barati, M., Zare, D., & Zomorodian, A. (2016). Moisture sorption isotherms and thermodynamic properties of safflower seed using empirical and neural network models. *Journal of Food Measurement and Characterisation*, *10*(2), 236–246. https://doi.org/10.1007/S11694-015-9298-4

Bernstein, A., & Noreña, C. P. Z. (2013). Study of thermodynamic, structural, and quality properties of Yacon (Smallanthus sonchifolius) during drying. *Food and Bioprocess Technology 2013*, *7*(1), 148–160. https://doi.org/10.1007/s11947-012-1027-y

Bhuiyan, M. H. R., Hossain, M. A., & Yeasmen, N. (2022). Local-traditional foods of Bangladesh: A treasure to be preserved. *International Journal of Gastronomy and Food Science*, *30*. https://doi.org/10.1016/j.ijgfs.2022.100602

Broekhoff, J. C. P., & de Boer, J. H. (1967). Studies on pore systems in catalysts: IX. Calculation of pore distributions from the adsorption branch of nitrogen sorption isotherms in the case of open cylindrical pores A. Fundamental equations. *Journal of Catalysis*, *9*(1), 8–14. https://doi.org/10.1016/0021-9517(67)90174-1

Caoli, M. A., Arenillo, S. A., & Magsino, R. F. (2017). Acceptability of Kamias (Averrhoabilimbi) wine. *Asia Pacific Journal of Multidisciplinary Research*, *5*(2), 85–88.

Castagnini, J. M., Iaccheri, E., Tylewicz, U., Dalla Rosa, M., & Rocculi, P. (2020). Pulsed electric fields effect on mechanical and sorption properties of dried apple tissue. *Innovative Food Science & Emerging Technologies*, *65*, 102442. https://doi.org/10.1016/j.ifset.2020.102442

Desgranges, C., & Delhommelle, J. (2019). Nucleation of Capillary Bridges and Bubbles in Nanoconfined CO2. *Langmuir*, *35*(47), 15401–15409. https://doi.org/10.1021/acs.langmuir.9b01744

Efendi, M. (2024). Influence of glazing type on the drying kinetics and thermal performance of indirect solar dryer for jelly candy. *Renewable Energy*, *231*. https://doi.org/10.1016/j.renene.2024.120950

Fadimu, G. J., Sanni, L. O., Adebowale, A. R. A., Kareem, S. O., Sobukola, O. P., Kajihausa, O. E., Saghir, A., Siwoku, B., Akinsanya, A., & Adenekan, M. K. (2018). Effect of drying methods on the chemical composition, colour, functional and pasting properties of plantain (*Musa Parasidiaca*) Flour. *Hrvatski Časopis Za Prehrambenu Tehnologiju Biotehnologiju I Nutricionizam*, *13*(1–2), 38–43. https://doi.org/10.31895/hcptbn.13.1-2.2

Fikry, M., Al-Ghamdi, S., Alfaifi, B., Ibrahim, M. N., Alqahtani, N., Umar, M., & Assatarakul, K. (2025). Mathematical modelling of sorption isotherms and the thermodynamic properties of vacuum-dried and freeze-dried Barhi dates. *Scientific Reports 2025 15:1*, *15*(1), 19781-. https://doi.org/10.1038/s41598-025-01935-x

Garg, M., Chaudhary, S. K., Kumari, S., & Goyal, A. (2022). Phytochemical, biological and traditional claims on Averrhoa bilimbi: An Overview. *Indian Journal of Pharmaceutical Sciences*, *84*(3), 532–542. https://doi.org/10.36468/pharmaceutical-sciences.947

Getahun, E., Gabbiye, N., Delele, M. A., Fanta, S. W., Gebrehiwot, M. G., & Vanierschot, M. (2020). Effect of maturity on the moisture sorption isotherm of chili pepper (Mareko Fana variety). *Heliyon*, *6*(8), e04608. https://doi.org/10.1016/j.heliyon.2020.e04608

Hawa, L. C., Efendi, M., Ubaidillah, Razak, A. A., & Wibisono, Y. (2021). Moisture sorption isotherm and isosteric heat of butterfly-pea flowers (*Clitoria ternatea*). *IOP Conference Series: Earth and Environmental Science*, *757*(1), 012028. https://doi.org/10.1088/1755-1315/757/1/012028

Hawa, L. C., Efendi, M., Ubaidillah, U., & Yulianingsih, R. (2021). Determination and modelling moisture sorption isotherms of dehydrated butterfly-pea (Clitoria ternatea L.) flower powder. *IOP Conference Series: Earth and Environmental Science*, *924*(1), 012010. https://doi.org/10.1088/1755-1315/924/1/012010

Hawa, L. C., Ubaidillah, U., Damayanti, R., & Hendrawan, Y. (2020). Moisture sorption isotherms of modified cassava flour during drying and storage. *Heat and Mass Transfer/Waerme- Und Stoffuebertragung*, *56*(8), 2389–2396. https://doi.org/10.1007/S00231-020-02866-1

Hssaini, L., Ouaabou, R., Charafi, J., Idlimam, A., Lamharrar, A., Razouk, R., & Hanine, H. (2022). Hygroscopic proprieties of fig (Ficus carica L.): Mathematical modelling of moisture sorption isotherms and isosteric heat kinetics. *South African Journal of Botany*, *145*, 265–274. https://doi.org/10.1016/j.sajb.2020.11.026

Istiqamah, A., Lioe, H. N., & Adawiyah, D. R. (2019). Umami compounds present in low molecular umami fractions of asam sunti – A fermented fruit of Averrhoa bilimbi L. *Food Chemistry*, *270*, 338–343. https://doi.org/10.1016/j.foodchem.2018.06.131

Jamaluddin, J., Molenaar, R., & Tooy, D. (2014). Kajian isotermi sorpsi air dan fraksi air terikat kue pia kacang hijau asal kota Gorontalo [Study on moisture sorption isotherm and bound water fractions of green beans taste of pia cake from Gorontalo]. *Jurnal Ilmu dan Teknologi Pangan*, *2*(1), 27–36.

Juanda, Agustina, R., & Hartuti, S. (2022). Optimisation of sensory characteristics of bilimbi tea drink (Averrhoa Tea). *IOP Conference Series: Earth and Environmental Science*, *1116*(1). https://doi.org/10.1088/1755-1315/1116/1/012066

Kaymak-Ertekin, F., & Sultanoglu, M. (2001). Moisture sorption isotherm characteristics of peppers. *Journal of Food Engineering*, *47*(3), 225–231. https://doi.org/10.1016/S0260-8774(00)00120-5

Koua, B. K., Koffi, P. M. E., Gbaha, P., & Toure, S. (2012). Thermodynamic analysis of sorption isotherms of cassava (Manihot esculenta). *Journal of Food Science and Technology*, *51*(9), 1711. https://doi.org/10.1007/S13197-012-0687-y

Labuza, T. P., & Altunakar, B. (2020). Water activity prediction and moisture sorption isotherms. *Water Activity in Foods: Fundamentals and Applications*, 161–205. https://doi.org/10.1002/9781118765982.ch7

Li, H., & Ramaswamy, H. S. (2025). Influence of osmotic dehydration conditions and finish air drying on the adsorption isotherms of cylindrical apple slices. *Drying Technology*, *43*(1–2), 321–330. https://doi.org/10.1080/07373937.2024.2440803

Michalski, P., Nur-A-Tomal, M. S., Crawford, S., Rudman, M., & van 't Hag, L. (2025). Advancement in fruit drying through the analysis of moisture sorption isotherms: processing effects on Australian native fruits in comparison to apple. *Journal of Food Engineering*, *395*. https://doi.org/10.1016/j.jfoodeng.2025.112526

Mokhtar, S. I., & Abd Aziz, N. A. (2016). Antimicrobial Properties of Averrhoa bilimbi extracts at different maturity stages. *Journal of Medical Microbiology & Diagnosis*, *5*(3). https://doi.org/10.4172/2161-0703.1000233

Oduola, A. A., Luthra, K., & Atungulu, G. G. (2022). Determination of moisture sorption isotherms of industrial hemp (Cannabis sativa L.) flower and leaf composite powders. *Industrial Crops and Products*, *186*, 115201. https://doi.org/10.1016/j.indcrop.2022.115201

Ouaabou, R., Ennahli, S., Hssaini, L., Nabil, B., Idlimam, A., Lamharrar, A., Mahrouz, M., & Hanine, H. (2022). Moisture sorption isotherms of sweet cherry (*Prunus Avium* L.): Comparative study of kinetics and thermodynamic modelling of five varieties. *International Journal of Food Science*, *2022*(1), 6786590. https://doi.org/10.1155/2022/6786590

Pandian, N. K. S., Naveenkumar, M., Arulkumar, M., Kamaleeswari, K., Ramkumar, R., Karuppuchamy, V., Kishore, S. G., & Pandiselvam, R. (2025). Adsorption and desorption kinetics of deseeded tamarind (*Tamarindus indica* L.) fruit and its modelling approach. *Journal of Food Process Engineering*, *48*(4), e70092. https://doi.org/10.1111/jfpe.70092

Prasad, S. C., K, V. K., & Reghu, R. (2021). international journal of research in pharmaceutical sciences consumption of bilimbi cause acute kidney injury production and hosted by. *Int. J. Res. Pharm. Sci*, *2021*(1), 653–655. https://doi.org/10.26452/ijrps.v12i1.4146

Sahu, S. N., Tiwari, A., Sahu, J. K., Naik, S. N., Baitharu, I., & Kariali, E. (2018). Moisture sorption isotherms and thermodynamic properties of sorbed water of chironji (Buchanania lanzan Spreng.) kernels at different storage conditions. *Journal of Food Measurement and Characterisation*, *12*(4), 2626–2635. https://doi.org/10.1007/S11694-018-9880-7

Saniso, E., Hayibaka, M., Chaidana, H., & Techo, J. (2025). Moisture sorption isotherm and isosteric heat of sorption of four-finger threadfin (Eleutheronema tetradactylum). *Food Biophysics*, *20*(2). https://doi.org/10.1007/S11483-025-09961-y

Sarker, M. A. M., & Chowdhury, A. Y. S. F. U. A. (2024). Estimation of total phenolic content and antioxidant activity of methanolic extracts of leaf, bark and fruit of Averrhoa bilimbi Linn. *Bangladesh Medical Research Council Bulletin*, *50*(1), 10–14. https://doi.org/10.3329/bmrcb.v50i1.68855

Shen, J. F., Wu, C. M., Song, J., Yu, J. J., & Li, Y. R. (2023). Adsorption and capillary condensation transitions on nanostructures: Mechanisms of atomic evolution and meniscus growth. *International Communications in Heat and Mass Transfer*, *148*, 107064. https://doi.org/10.1016/j.icheatmasstransfer.2023.107064

Sitanggang, A. B., Alexander, R., & Budijanto, S. (2020). The utilisation of bilimbi (Averrhoa bilimbi) and lime (Citrus aurantifolia) juices as natural acid coagulants for tofu production. *Journal of Food Science and Technology*, *57*(12), 4660–4670. https://doi.org/10.1007/S13197-020-04503-5

Staudt, P. B., Kechinski, C. P., Tessaro, I. C., Marczak, L. D. F., De, R., & Cardozo, N. S. M. (2013). A new method for predicting sorption isotherms at different temperatures using the BET model. *Journal of Food Engineering*, *114*(1), 139–145. https://doi.org/10.1016/j.jfoodeng.2012.07.016

Talla, A., Jannot, Y., Nkeng, G. E., & Puiggali, J. R. (2005). Experimental determination and modelling of sorption isotherms of tropical fruits: Banana, mango, and pineapple. *Drying Technology*, *23*(7), 1477–1498. https://doi.org/10.1081/DRT-200063530

Thanuja, D., & Ravindra, M. R. (2014). Thermodynamic analysis of moisture sorption characteristics of cheese-puri mix. *Journal of Food Processing and Preservation*, *38*(1), 420–429. https://doi.org/10.1111/j.1745-4549.2012.00790.x

Waisundara, V. Y. (2020). Traditional functional food of Sri Lanka and their health significance. *Nutritional and Health Aspects of Food in South Asian Countries*, 143–158. https://doi.org/10.1016/B978-0-12-820011-7.00020-4

Yadav, S., & Mishra, S. (2023). Moisture sorption isotherms and storage study of spray-dried probiotic finger millet milk powder. *Journal of Stored Products Research*, *102*. https://doi.org/10.1016/j.jspr.2023.102128

Yan, Z., Sousa-Gallagher, M. J., & Oliveira, F. A. R. (2008). Sorption isotherms and moisture sorption hysteresis of intermediate moisture content banana. *Journal of Food Engineering*, *86*(3), 342–348. https://doi.org/10.1016/j.jfoodeng.2007.10.009

Yogendrarajah, P., Samapundo, S., Devlieghere, F., De Saeger, S., & De Meulenaer, B. (2015). Moisture sorption isotherms and thermodynamic properties of whole black peppercorns (Piper nigrum L.). *LWT - Food Science and Technology*, *64*(1), 177–188. https://doi.org/10.1016/j.lwt.2015.05.045

Yusoff, I. M., Azelee, N. I. W., Chua, L. S., & Mustafa, R. R. (2024). A comparison of phytoconstituent and functional loaded low moisture food from Averrhoa bilimbi using freeze drying and oven drying methods. *Journal of Food Measurement and Characterisation*, *18*(9), 7468–7479. https://doi.org/10.1007/S11694-024-02741-1

Pertanika J. Trop. Agric. Sci. 49 (S1): 119 - 143 (2026)

PERTANIKA JOURNALS

TROPICAL AGRICULTURAL SCIENCE

Journal homepage: http://www.pertanika.upm.edu.my/

Enhancing Tomato Market Quality Standard through Light-emitting Diodes Technology

Ubong David Offiong[1], Diyana Jamaludin[1]*, Juju Nakasha Jaafar[2], Khairudin Nurulhuda[1], and Samsuzana Abd Aziz[1]

[1]Department of Biological and Agricultural Engineering, Faculty of Engineering, Universiti Putra Malaysia, 43400 UPM Serdang, Selangor

[2]Department of Crop Science, Faculty of Agriculture, Universiti Putra Malaysia, 43400 UPM Serdang, Selangor

ABSTRACT

Light-emitting diode (LED) is an emerging technology with a high application prospect as a preservation technique for fruits and vegetables at the postharvest phase. This study investigates the effect of different LED wavelengths on the quality attributes of tomatoes during market-display conditions. Tomatoes were illuminated with different sets of LED treatments during the 5 days of storage: white, red-blue (5R:1B), and blue-red (5B:1R) LEDs before placing them in a market-displayed condition. Key quality indices, including colour, firmness, pH, brix, and weight, were monitored throughout the display period. Functional regression models of the quality index for the displayed period were established. Compared to the control, the 5B:1R LED treatment reduced tomato redness and overall colour change by 17.9%, suggesting a delayed ripening effect. Acid strength increased with a pH drop of 0.6, 0.5, and 0.1 units for 5B:1R, 5R:1B, and white LEDs relative to the control. Firmness improved by 43.1%, 31.4%, and 18.3% for 5B:1R, white, and 5R:1B treatments. Additionally, weight was retained more effectively, with increases of 30% and 4.9% for 5B:1R and 5R:1B LEDs over the control. A quadratic regression model effectively described changes and trends in the tomato market quality indices investigated. These findings provide a foundation for predictive modelling of tomato shelf-life and quality under LED treatments in market-displayed environments.

ARTICLE INFO

Article history:
Received: 18 July 2025
Accepted: 26 December 2025
Published: 19 March 2026

DOI: https://doi.org/10.47836/pjtas.49.S1.06

E-mail addresses:
offiongubong42@gmail.com (Ubong David Offiong)
diyana_upm@upm.edu.my (Diyana Jamaludin)
k_nurulhuda@upm.edu.my (Khairudin Nurulhuda)
jujunakasha@upm.edu.my (Juju Nakasha Jaafar)
samsuzana@upm.edu.my (Samsuzana Abd Aziz)
* Corresponding author

Keywords: Tomatoes qualities, market-displayed condition, postharvest management, LED treatment

INTRODUCTION

The Food and Agriculture Organisation (FAO) has identified tomatoes as one of the first four fruits that can lower the risk of prostate cancer and other cardiovascular

ailments (Zhao et al., 2023). Their nutritional profile makes them an essential vegetable for a healthy diet. Due to their low calories and high fibre content, they are considered an excellent choice for digestive health and weight management (Clark & Slavin, 2013). Huang et al. (2018) also cited other benefits, including improving the immune system and reducing inflammation and age-related degeneration. These benefits are rarely obtained from tomatoes due to their quick progression to senescence, due to respiration and ethylene-associated activities. Panebianco et al. (2024) identified the factors affecting tomato quality and shelf life, including storage conditions, techniques, and ripening stages. Essential measures must be implemented to reduce losses during storage and on-the-market shelf conditions.

After harvest, tomatoes spend a longer duration of their postharvest life in the market. Extending shelf life and preservation of quality in this environment should be prioritised to ensure consumers receive the needed health benefits from tomatoes. At the same time, retailers also benefit economically by extending the shelf life and retaining the nutritional quality of their products. This calls for a robust preservation method that can uphold the effect of treatment for a longer period while tomatoes thrive in the market environment.

Common preservation techniques for tomato storage, such as cold room storage, modified atmosphere packaging (MAP), pulse light, ultrasonic wave, and coating, have limitations such as chilling injuries, high energy consumption, low efficiency, high-performance requirement, high cost of investment, and problem of adjusting to processing parameters (Salehi, 2022; Venkatachalam et al., 2024). In addition, an 18.96% average worldwide loss in tomatoes was attributed to storage conditions and techniques (Costa et al., 2022). Light-emitting diodes (LEDs) can overcome these limitations as they consume low energy when in operation, have a lifespan of 70,000-100,00 operating hours, are compact and portable, and their wavelength can be adjusted to suit specific plant requirements (Craver et al., 2019; Elliott & Lee, 2020; Gupta & Agarwal, 2017).

Plants harness the blue and red wavelengths of visible light for their growth and development (Chan et al., 2024). These wavelengths are crucial for the synthesis of chlorophyll and carotenoid pigments as shown in Fig. 1. The blue wavelength (400-500 nm) is absorbed by the cryptochrome receptor and can suppress gene expression for chlorophyll degradation while the red wavelength (600-700 nm) is absorbed by phytochrome receptor which accelerate the production of carotenoid pigment by activating the enzymes and transcriptional factors for its production (Liu & van Iersel, 2021). LED quality characteristics, including wavelengths, photoperiod, and intensity, influence plant morphology and functionality by eliciting responses at physiological and biochemical levels, enhancing bioactive compounds and physiological properties, and inducing resistance to ripening and cell wall degradation processes (Khan et al., 2022).

The application of LED technology in the postharvest management of tomatoes has gained increasing attention, yet key aspects of its effectiveness remain under investigation.

Martínez-Zamora et al. (2023) investigated the impact of LED illumination on the quality and bioactive compounds of tomatoes during cold storage and reported a reduction in firmness loss by 30–35% and an enhancement in redness by 27%. These findings suggest that LED treatments may contribute to quality retention under low-temperature storage; however, their applicability to ambient or retail display conditions has not been sufficiently addressed. In a related study, Panjai et al. (2019) examined the influence of LED lighting on tomato ripening and quality development. While the study confirmed positive effects on physiological parameters, it did not provide detailed insight into the specific roles of different spectral combinations or treatment durations. De Bruijn et al. (2023) developed models to study its impact on tomatoes' postharvest life. Interestingly, Nájera et al. (2018) reported that even short, daily exposures to LED light (one hour) could enhance organoleptic qualities by up to 60%, suggesting that intermittent lighting may be a viable strategy. However, the mechanisms underlying these sensory improvements remain poorly understood and warrant further investigation. Offiong et al. (2023) obtained a reduced pH value in tomatoes (2.81) when illuminated with blue/red LED light, comparable with tomatoes with no light treatment (3.05), and an increase in the brix value when exposed to red/blue LED light (4.06) compared to darkness (3.84). Furthermore, de Bruijn et al. (2023) took a more modelling-based approach to understanding LED effects on postharvest dynamics, which provides a useful framework but lacks integration with experimental validation. Finally, Nassarawa et al. (2021) broadly endorsed LEDs as a promising tool for enhancing quality and extending shelf life, though their review primarily summarised existing findings rather than critically assessing inconsistencies or limitations.

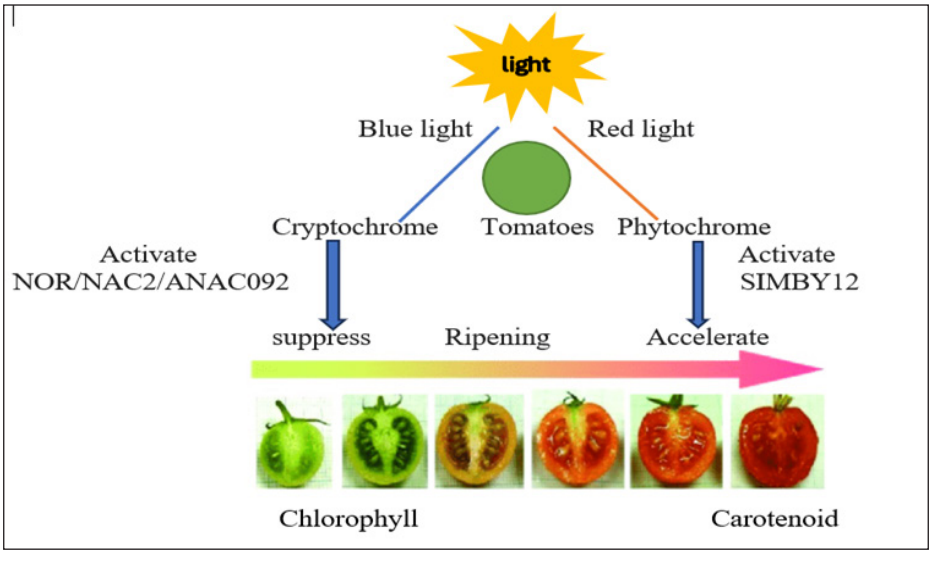

Figure 1. Schematic diagramme showing the effect of light on tomato ripening

During market-displayed environments, tomato quality indices hasten to senescence due to physicochemical reactions. Previous studies have shown that the changes in tomato fruit quality are associated with complex physical and chemical reactions that can be modelled with different empirical approaches, such as linear, power, logarithmic, and polynomial regression models (Kabaş et al., 2024; Qin et al., 2024). The Linear Regression model reveals a direct assessment of the relationship between the LED treatments and the quality index of tomatoes over time. It can reveal the improvement or degradation in quality metrics due to increasing exposure to LED wavelengths. The logarithm regression model assesses changes in quality indices over time and can reveal if the benefits of LED treatment are increasing or diminishing over a prolonged display time. Power regression can capture relationships when LED treatment varies with time in a non-linear pattern. The polynomial regression model allows flexibility, accommodating curvilinear relationships, and can identify optimal LED wavelengths that can maximise quality indices, revealing the nonuniformity of LED treatment effect across all levels of exposure.

Although some previous studies have investigated the treatment of tomatoes with different LED wavelengths, no attention was given to the effects of LED wavelengths on the quality of tomatoes in market environments after LED pre-treatment during storage. Prolonging the shelf life in the market environment and reducing the frequency of waste and spoilage is a major setbacks in the tomato supply chain. Studies on tomato preservation treatment in the market environment are scarce, as most studies focus on storage conditions. To describe the preservation impact of LED treatment on tomatoes and forecast the changes in the quality of tomatoes during display, the key objectives of this study were to (1) evaluate the impact of LED pretreatment on quality indices of tomatoes in market-displayed conditions, (2) established the corresponding regression models to study the quality changes in tomatoes which will provide the conceptual framework for modelling shelf-life predictions.

METHODS

Materials in the Study

Freshly harvested tomatoes acquired from the Lojing Highland farm in Malaysia were used for the study. A pre-selection was done to ensure uniform sizes and proper maturity stages, where tomatoes were grouped into the breaker and turning stages. Only those free from mechanical and physiological damage, with no infection and microbial growth, were used for the study. A total of 480 samples were randomly divided into four groups representing the control and LED treatments, with 120 samples in each group.

Light-emitting Diodes (LED) Treatment System

The LED multilayer treatment system (120 × 35 × 120 cm) primarily consists of four layers, with each layer housing each of the treatments (white, 5R:1B, 5B:1R LEDs, and the control group). The white LED represents a combination of red and blue light in equal proportions, creating a balanced spectrum. The 5R:1B LED provided a red-dominant environment with five parts red to one part blue, while the 5B:1R LED created a blue-dominant environment with five parts blue to one part red. A control group was included as a baseline reference. Together, these treatments allowed for a comparison of balanced, red-enriched, and blue-enriched spectra against standard conditions to evaluate their effects on tomatoes. The LED (T8, SMD 2835, China) of 15W, with wavelengths ranging from 400-750 nm, was 100 cm in length, and 2 lamps with the same wavelengths were installed in each layer. Each layer was subdivided into 6 units, with each unit measuring 20 × 35 cm. Measurement of light intensity was carried out using a light spectrum meter (Spectrum Technologies Inc. 3415F USA) in each of the units to ensure all units had uniform light intensity with no significant differences. These units were used for the display of samples, as no variability was expected to occur in these units due to light intensities. The LEDs were fixed 10 cm apart from each other in each layer.

Sample Treatment

The study comprises two phases: the storage phase and the market display phase. These two phases represent the conventional method of tomato handling after harvest, where tomatoes are stored for some days in cold chambers before being taken to the market for display. To mimic the conventional way of tomato handling after harvest, the storage and the market display phases were replicated in the study.

Storage Condition

At the storage phase, the treatments had a photoperiod of 16 hours of light and 8 hours of darkness. Tomato samples were pretreated for 5 days and later moved to the market-displayed environment, where they were kept for 24 days, and tomato quality indices were measured every 3 days. The temperature and relative humidity of the storage phase were adjusted to 5 °C and 90% to prevent fluctuations of these factors, which might introduce variability. This environmental condition was quoted by Martinez-Zamora (2023) as the condition suited for tomato storage.

Market Display Condition

The market display phase had a temperature and relative humidity of 24°C and 78%, which were average conditions obtained after careful measurement of the environmental

conditions of the fruits and vegetables retail outlets in Malaysia using the Elitech Data logger (Gsp-6 USA). A 100-W white bulb illuminated the tomato samples throughout the display period to replicate the market environment. The arrangement of each replicate follows the same setting as under storage conditions.

480 sample of tomatoes were used in the study, which consisted of four replicates in each treatment, and 30 samples in each replicate. Three samples were randomly withdrawn from each replicate every 3 days, resulting in 12 samples for each treatment used for data collection for each measurement day. Five quality indices were chosen for investigation, which are colour, firmness, pH, total soluble solids (TSS), and weight, because these indices influence consumer preferences in the market, and these quality indices were obtained from each tomato samples.

Statistical Methods

Analysis of variance (ANOVA) and Duncan Multiple Range Test (DMRT) were used in analysing data that follows the Gaussian distribution. In contrast, the Kruskal-Wallis and the Bonferroni Post Hoc analyses were used to analyse data that did not conform to the Gaussian distribution theory.

Procedures for Quality Index Determination

Colour Measurement

A colourimeter (3nh NR-145, China) assessed the specimens' colour measurements. The colourimeter was calibrated using the manufacturer's instructions with the colourimeter white tiles. After warming up the colourimeter for 5 minutes, it was placed on the surface of each sample and activated to take the reading with no gap between the instrument and the surface of the specimen. The L (lightness), a* (redness), b* (yellowness), and $\Delta\varepsilon$ (differences in colour changes) values were measured. Figure 2 shows the visual description of the colour parameters (L*, a* and b*). Colour changes ($\Delta\varepsilon$) were calculated using the equation.

$$\Delta\varepsilon = [(L_1 - L_0)^2 + (a_1^* - a_0^*)^2 + (b_1^* - b_0^*)^2]^{1/2} \quad [1]$$

where $\Delta\varepsilon$are the changes in the colour of the tomato samples. The subscripts “0” and “1" are the initial (before treatment and the final (after treatment) measurement of colour.

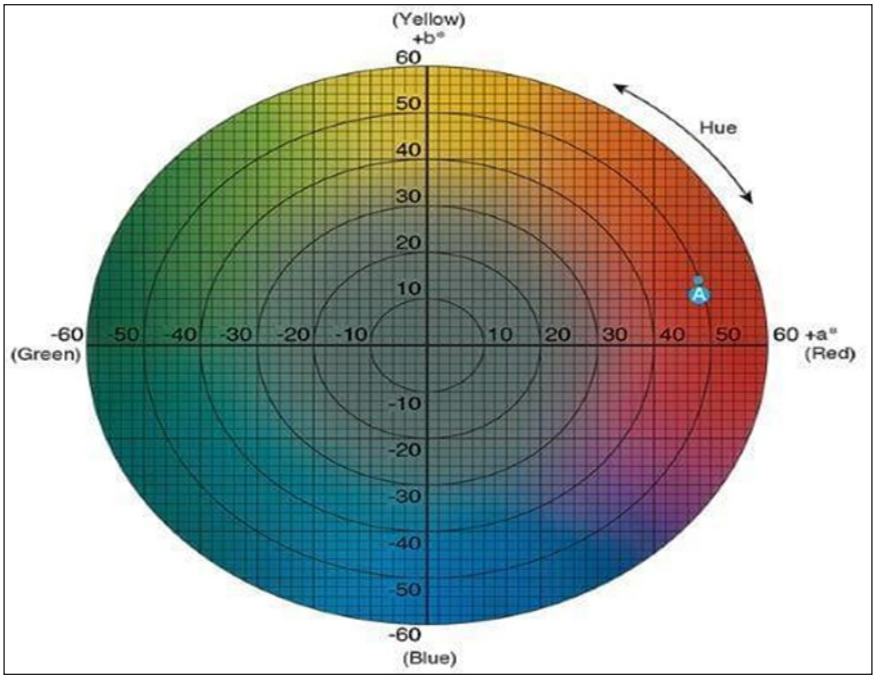

Figure 2. Colour wheel showing changes in colour and brightness for L, a*, and b* colour parameters. The a* value is represented by the horizontal axis measurement where it increases from -60 to +60 showing the degradation of green pigment and accumulation of red colour, while the vertical axis measurement represents the progression of colour from blue to yellow which represents the b* value, while hue established the relationship between the a* and b* values

Firmness Measurement

The puncture test, with a handheld penetrometer (Tianpeng GY-1 12228, China, of 15 kg/m^2 capacity and a cylindrical probe diametre of 3.5 mm), was conducted to measure the firmness of the specimen. The test was carried out at two opposite sides of the equatorial plane randomly selected in each specimen, and the probe was inserted to a depth of 10 mm. The maximum force was recorded as the firmness of each specimen expressed as kg/m^2 (Zhao et al., 2023).

pH Measurement

The pH meter was first calibrated using a 4, 7, and 10 buffer solution to ensure accurate measurements. Each sample was subdivided into three parts and squeezed to obtain the juice; the combined juices were stirred for uniformity. The solution obtained was measured with a digital pH meter (Extech, pH100 China).

Total Soluble Solids Measurement

A digital refractometer (model PAL-BX/A3590, Atago, Tokyo, Japan) was employed to measure the concentration of total soluble solids in the tomato samples. Each sample was sliced into three portions, and each portion was squeezed to release juice greater than 2 drops and placed in the refractometer to obtain the Brix value. The average readings from the three slices were used as the soluble solids of each tomato expressed as a percentage.

Weight Measurement

A tree (HRB-103, USA) high precision scale milligram lab balance of 0.1 mg readability was used to measure the weight of tomatoes. Tomatoes were measured before treatment, after treatment, and every 3 days in a market display condition. Weight loss was calculated using the equation below

$$\text{Weight loss (\%)} = \frac{W_1 - W_2}{W_1} \times 100 \quad [2]$$

where $W_1 - W_2$ are the initial and weight loss before and after treatment (g)

Regression Models of Different Quality Indicators during Market Display

Regression models are powerful mathematical tools for establishing relationships between parameters and their predicted outcomes. It captures the fundamental trends and can be used to explain underlying mechanisms in associated data, To identify the best model for fitting the data, four functional regression models were employed in analysing the data such as; the linear regression model: Data were fitted into this model to establish the relationship between the various variables exposed to different LED treatments over time in the Market displayed environment. The model assumes a steady rate of change and is given by the equation:

$$y = \beta_0 + \beta_1 x + \varepsilon \quad [3]$$

Logarithmic regression: A logarithmic model was used to assess the suitability of nonlinear relationships between the dependent and non-dependent variables. The model is expressed as:

$$y = \beta_0 + \beta_1 log(x) + \varepsilon \quad [4]$$

Polynomial regression: Polynomial regression, which involves the use of higher-order terms, was employed to capture potential nonlinear relationships. Different degrees of

polynomials were tested to determine the optimal fit. The second-order term was used, which is represented by

$$y = \beta_0 + \beta_1 x + \beta_2 x^2 + \varepsilon \quad [5]$$

Power regression Model: Data were fitted into the power model to analyse the relationships between the dependent variable and the independent variable when raised to power. This model is represented by

$$y = \beta_0 x^{\beta_1} + \varepsilon \quad [6]$$

where

Y = Tomato variables influenced by different LED treatments,
X = Time of display (days),
B_0 = intercept,
β_1 =is the slope, and
ε = error term.

Each of these models was fitted to the data of each treatment for each variable, and the coefficient of determination (R^2) was obtained. The adjusted R^2, which explains the magnitude of variance captured by the model based on the number of predictors, was computed as shown in Equation 7. The model with the highest Adjusted R^2 was chosen for each treatment and subjected to evaluation to determine the treatment that best fits the data and can describe the dynamics of tomato quality in the market-displayed environment. The model's performances were evaluated using two metrics, including the coefficient of determination (R^2), mean absolute error (MAE), which measures the average absolute differences between predicted and actual values, and the root mean squared error (RMSE), which measures the average proportion of errors between observed and predicted values. These metrics are widely used in assessing regression problems (Han et al, 2022). These metrics were calculated according to Equations 8 and 9.

$$Adjusted\ R^2 = 1 - \left(\frac{(1-R^2)(n-1)}{n-k-1}\right) \quad [7]$$

where

R^2 = Coefficient of Determination
n = Number of observations
k = Number of predictors

$$\text{MAE} = \frac{1}{Z}\sum_{i=1}^{z} \quad (x_i - y_i) \qquad [8]$$

$$\text{RMSE} = \sqrt{\frac{1}{Z}\sum_{i=1}^{z} \quad (x_i - y_i)^2} \qquad [9]$$

where

Z = Number of observations

x = Predicted values

y = Actual values

The arithmetic mean of the absolute error (MAE) assesses the regression models. An MAE value closer to zero indicates the most accurate regression. The root mean square error (RMSE), which is also employed in regression model evaluation, shows sensitivity to outliers (Kabaş et al., 2024). Both metrics take values from 0 to infinity, with lower values close to 0 indicating higher accuracy of the model. The coefficient of determination (R^2) measures the goodness of fit and explains the variance in the predicted variable relative to the observed variables. It takes values between 0 and 1, and the closer the R^2 is to 1, the higher the accuracy of the model. The model with the highest R^2 values, lowest MAE, and RMSE was chosen as the best fit for the data, which explains the phenomenon of the variables.

RESULTS AND DISCUSSION

Light Intensities of LED Treatments

Table 1 shows the light intensities of the LED treatments used in the study. it could be seen that across the 6 sections of each treatment compartment, sections B, C, D, and E show no significant differences with each other across all treatments. This shows that the light intensities across these sections will ensure even distribution of light to the samples.

Table 1
Average LED intensities from the multi-layer rack where tomatoes were placed for treatment, with the significant differences of each section

Light	Average intensity in each section ($\mu mol^{-2}s^{-1}$)					
	A	B	C	D	E	F
White LED	102^{b}	112^{a}	118^{a}	119^{a}	117^{a}	100^{b}
5R:1B LED	58^{c}	87^{a}	101^{a}	95^{a}	85^{ab}	48^{c}
5B:1R LED	57^{b}	94^{a}	107^{a}	107^{a}	101^{a}	58^{b}

Effect of LED Wavelengths on the Quality Index of Market-displayed Tomatoes

Effect of LED Pretreatment on the Colour of Market-displayed Tomatoes

Colour is a vital factor that influences consumers' preferences and purchasing decisions, as the perception of colour can affect the evaluation of the quality and appeal of tomatoes (Jürkenbeck et al., 2020). Fig. 3 visualises the tomato samples after treatment and how the treatments delayed ripening in tomatoes during the 24 days of market display. Before treatment, all the samples were relatively at the same maturity stage. After treatment, the control samples reached the deep red maturity stage on day 9 of the display, the 5R:1B LED-treated samples extended till day 15 of the display, while the white and the 5B:1R LEDs extended till day 21 and 24, respectively.

An increase in the a-value leads to more red colour accumulation as brightness diminishes; likewise, an increase in the b-value leads to higher accumulation in yellow colour on the tomato's surface. Fig. 4a shows that the brightness (L*) value of tomatoes decreases continuously as the display period increases, indicating that the colour becomes darker with time. 3.5, 8.3, and 7.5 % increases in brightness over the control for 5R:1B, 5B:1R, and white LEDs, respectively, were observed, showing that the different LED treatments delayed the darkening of tomatoes' colour as displayed time increases. A significant difference was observed between the treatments and the control, but none was observed between the three LED treatments. Choi & Park (2023) submit that ripening in tomatoes corresponds with the decrease in brightness of the pigment as the accumulation of various colours darkens the colour of the tomatoes.

The trend for a-value (Fig. 4b) shows significant increases within the first 6 days and a moderate increase in subsequent days of market display. A percentage decrease over the control of 9.8, 19, 9, and 13.8 % in a-value was observed for 5R:1B, 5B:1R, and white LEDs, showing that LED treatments can delay redness on the surface of tomatoes, with 5B:1R LED being the most effective. The trend for b* value (Fig. 4c) shows an increase in the yellowness of tomatoes from days 1-3, a constant rate from days 3-9, a further increase from days 9-15 and a decrease in subsequent days of display. On its peak day of accumulation, percentage increases of 8.4,k 20.3 and 5.8 % were observed over the control for 5R:1B, 5B:1R, and white LEDs, respectively, indicating that LED treatment maintained the yellowness in tomatoes over time, while 5B:1R LED reflected the most effective treatment as market-display time increases. Significant differences were observed between the treatments and the control ($P < 0.05$).

Delta E (ΔE) measures the quantifiable difference between two colours within the colour space, assessing how these colours differ in the human eye. The initial ΔE values (before treatment) show relatively close differences between the tomatoes in each treatment. The ΔE trend (Fig. 4d) increases for all treatments over time, suggesting that the colour differences become more pronounced as display time progresses. The control had the

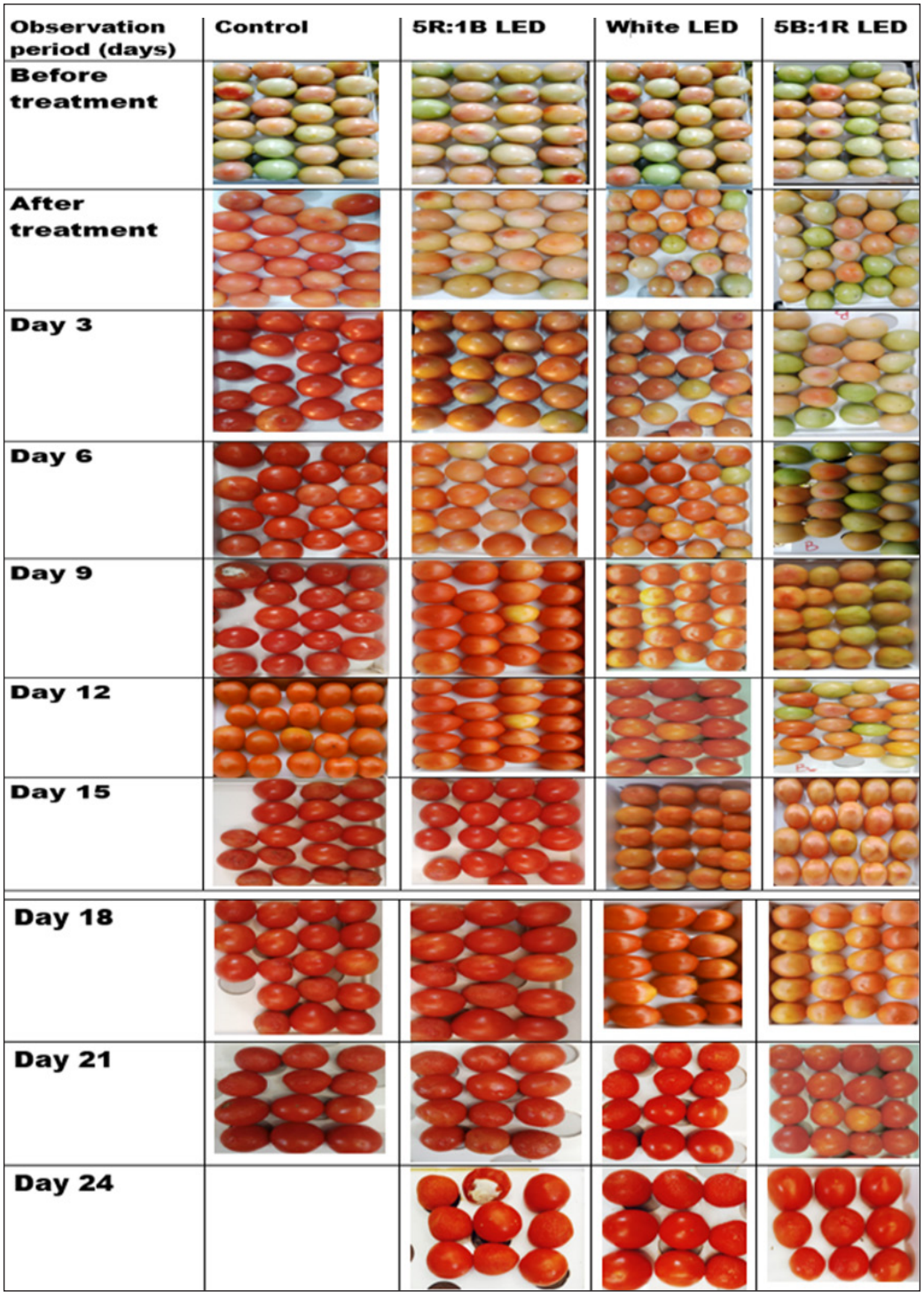

Figure 3. Visual changes in tomatoes pretreated with different LED wavelengths during the 24 days of market display

highest ΔE values with peak values of 67.962 on day 15, indicating that tomatoes without LED treatment may undergo accelerated colour changes due to ripening processes. This was closely followed by the 5R:1B LED treatment with a peak value of 66.892, which also promoted colour changes significantly, while the 5B:1R and white LEDs treatment showed less colour changes with peak values of 63.974 on day 18 and 62.903 on day 21. Significant differences were observed ($p<0.05$).

The colour of tomatoes depends on the concentration of various pigments, including chlorophyll, hydroxylated carotenoids, xanthophylls, carotene, and lycopene, as ripening progresses. (Khoo et al., 2011). Zhao et al. (2023) obtained less colour variation when treating tomatoes with high-voltage electrostatic fields. Nassarawa et al. (2022) reported on delayed ripening when treating grapefruit with red LED light. Blue light activates cryptochrome receptors through the absorption of photons by the flavin adenine dinucleotide (FAD) chromophore, which triggers conformational changes that cause the repression of ethylene biosynthesis and signalling, thereby delaying the onset of ripening (Xu et al., 2018). For this study, white and 5B:1R LEDs delayed changes in tomato colour.

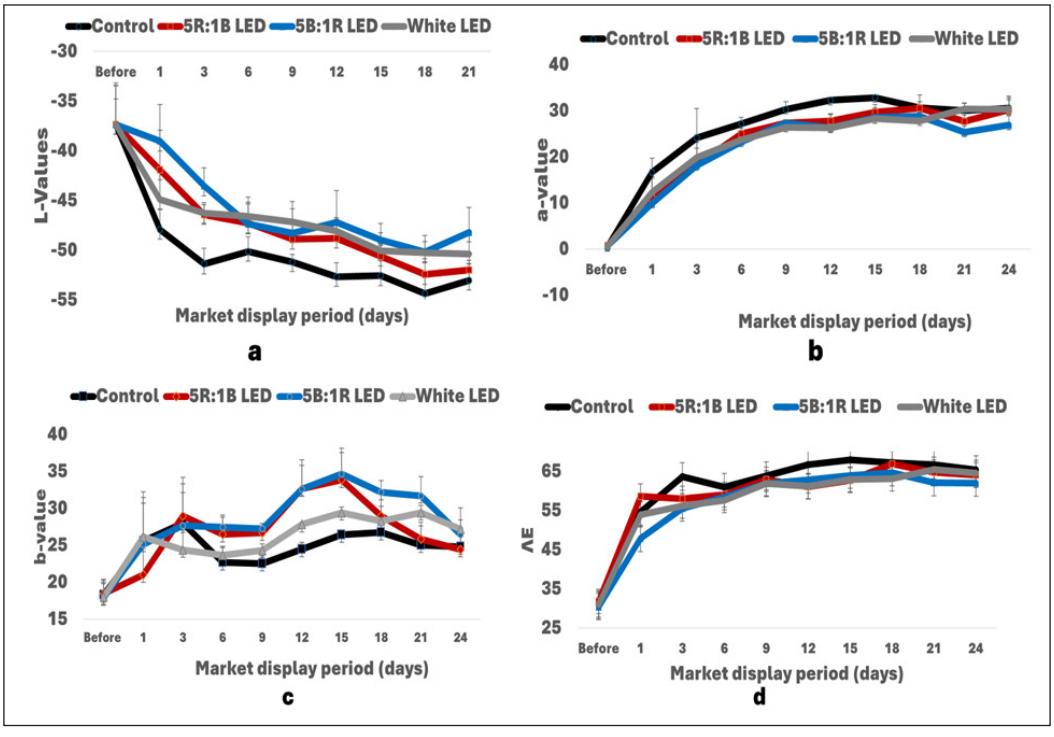

Figure 4. Changes in: a) lightness (L*), b) redness (a*), c) yellowness (b*) and d) colour change (ΔE) in tomatoes pretreated with LED wavelengths (white, 5R:1B, 5B:1R) and the control group at different display periods for 24 days

Effect of LED Pretreatment on the Firmness of Market-displayed Tomatoes

The firmness of the control specimen and different LED-treated specimens at various times was analysed (Figure 5). A downward trend in firmness was observed for all treatments. In the first interval (Days 1 - 3), relatively moderate declines were obtained. The second interval (Days 3 -15) was marked by significant reductions, especially in the Control and 5R:1B treatments, signifying increased deterioration. This shows that this period may be the critical period for firmness and stability when displayed in the market. During this period, the control lost 9.182 kg/m^2, 5R:1B LED lost 8.358 kg/m^2, 5B:1R LED lost 7.881kg/m^{2,} while white LED lost 8.177 kg/m^2. This shows that 5B:1R LED produces the lowest firmness loss during this critical period, signifying the effectiveness of the treatment in resisting firmness loss more than other treatments and the control. In the third interval (Days 15-21), the rate of losses decreased, but observable differences among treatments remained noticeable.

In comparison with the control, 18.3, 43.1, and 31.4 % increases in firmness for 5R:1B, 5B:1R, and white LEDs were obtained. Figure 5 shows that significant differences were observed for the different LED treatments and the control ($P < 0.05$). This indicates that the softening rate in tomatoes during market-displayed conditions was slower with LED-treated samples than with the control samples. This result is in line with the study of Nájera et al. (2018). Blue light-activated cryptochrome receptors stimulate the expression

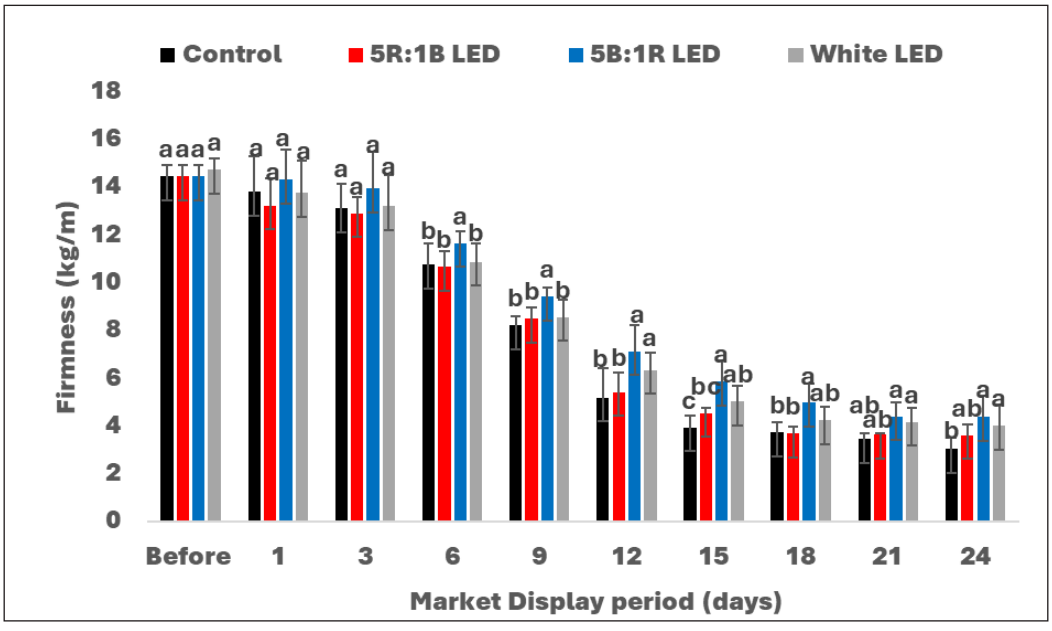

Figure 5. Changes in firmness of tomato pretreated with different LED wavelengths at different display times for 24 days with significant differences in the different display days ($p<0.5$)

of microRNAs, which in turn silence genes associated with the galacturonate pathway, and inhibit the activities of cell wall degradation enzymes, delaying starch hydrolysis (Wang et al., 2014; Wang et al., 2018).

Effect of LED Pretreatment on the pH of Market-displayed Tomatoes

The change in pH value is a vital indicator of tomato quality; lowering the pH value results in a slow respiration rate and enhanced quality in tomatoes. (Tigist et al., 2013). Figure 6 shows the pH curves of tomatoes pretreated with different LED wavelengths during market-displayed conditions. The trend shows a decrease from days 1-15, and the curves slightly increase from days 15-24 across all treatments. In comparison with the untreated tomatoes (control), 0.6, 0.5, and 0.1 units drop in pH were obtained relative to the control for 5R:1B. 5B:1R, and white LEDs on day 24 of display, signifying an increase in acid strength of LED-treated tomatoes over the control. Significant differences were observed from days 1-6 for the 5B:1R LED with other treatments. Studies have shown that citrate and malate acids are substrates used in respiration processes. They contribute to energy production during ripening (Batista-Silva et al., 2018), and an increase is always observed in the pH of tomatoes after harvest (Tolesa & Workneh, 2017). However, using LED during preservation and marketability, specifically 5B:1R LED, may maintain a low pH value by retaining organic acid in the fruits through suppression of the catabolic rate, preventing

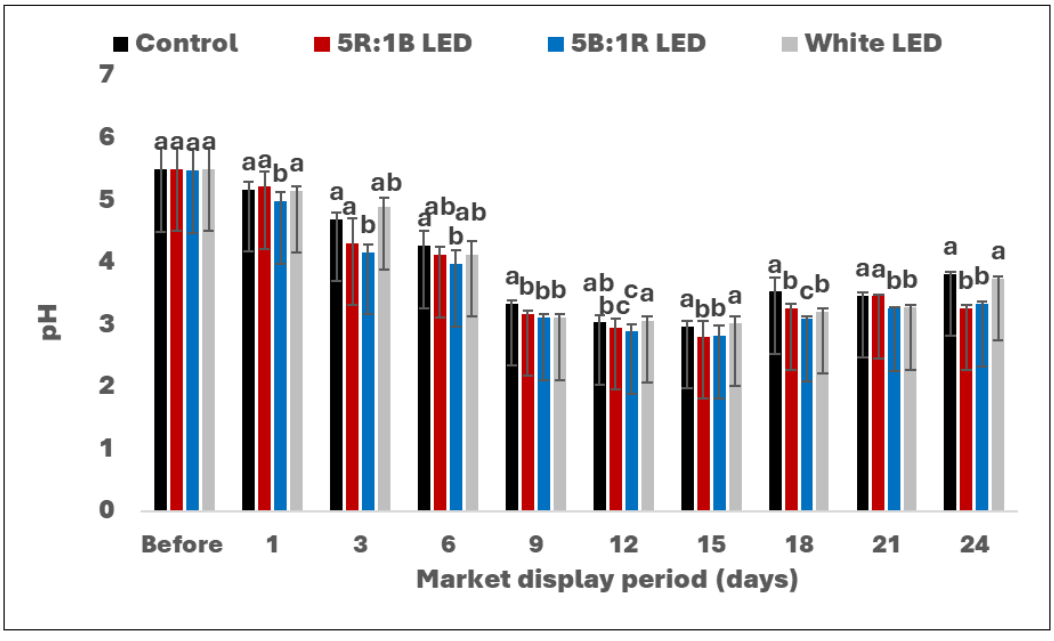

Figure 6. Changes in pH value of tomato pretreated with different LED wavelengths at different display times for 24 days with the significant differences obtained during the display period ($p<0.5$)

the breakdown of these acids and ensuring they remain in the fruit for an extended period (Wang et al., 2023).

Tomatoes free from microbial growth or defects influenced purchasing decisions in the market environment. Higher acidity prevents microbial growth in tomatoes since neutral or slightly alkaline conditions favour pathogens (Zheng et al., 2023). Therefore, increasing acidity in tomatoes through LED treatments can reduce microbial spoilage, extend shelf life, and reduce the risk of foodborne illnesses. The growing consumer demand for natural food products has intensified interest in natural preservation methods since synthetic methods are linked to health-threatening issues (Teshome et al., 2022). The increasing acidity with the LED treatment method replaces the need for synthetic preservatives, as it aligns with consumer demand, favouring minimal processed and organic products and offering an edge in a health-conscious market.

Effect of LED Pretreatment on Total Soluble Solid (TSS) Concentration of Market-displayed Tomatoes

The variation trend of TSS concentration in tomatoes pretreated with different LED wavelengths, with an increase in the market display time, is displayed in Figure 7. The TSS concentration in the untreated samples (control) reached its peak at 9 days with a value of 4.908% before decreasing gradually. The peak concentration of TSS for 5R:1B and white

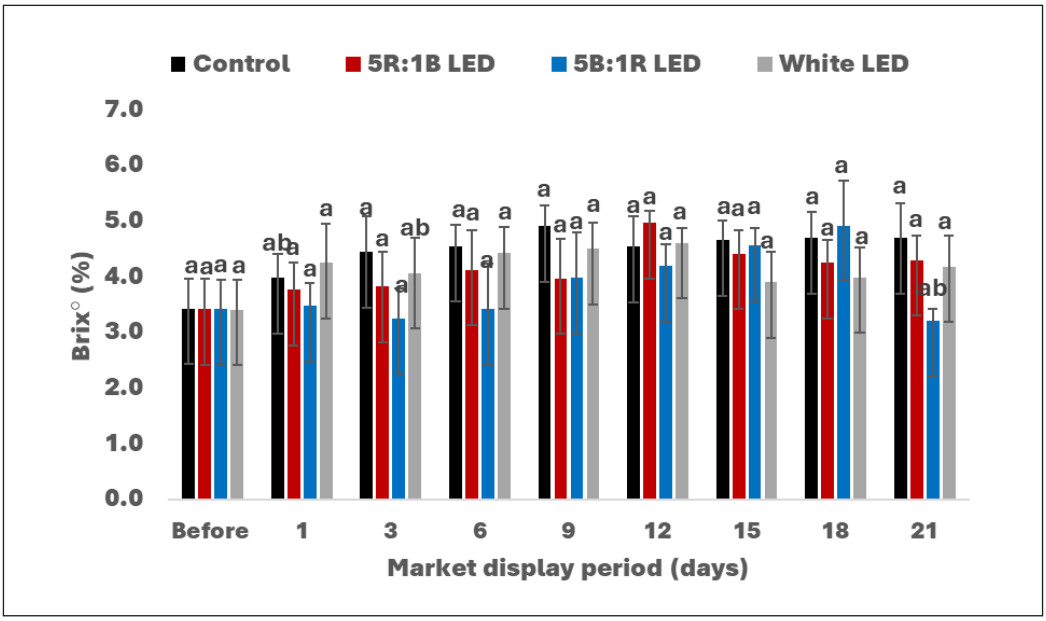

Figure 7. Changes in TSS of tomato pretreated with different LED wavelengths at different display times for 24 days with the significant differences obtained during the display period ($p<0.5$)

LED treatments occurred on the 12th day with values of 4.966 and 4.611 %, while the 5B:1R LED treatment attained its peak accumulation at 18 days with a value of 4.922%. The result shows that 5R:1B LED accumulated more TSS, though with a short duration (12 days), as compared to 5B:1R LED, with a value of 4.922%, but with a prolonged duration of market display (18 days). 5R:1B and 5B:1R LEDs recorded an increase of 1.2 and 0.2 % over the control, while the white LED lagged by 6.1%. Figure 7 reveals that 5B:1R LED treatment shows significant differences with other treatments from days 1-6, as it maintained a low brix value ($p<0.05$). The result of the study aligns with that of Xiang et al. (2021), with an increase of 4.86, 4.92, 4.98, and 5.08% for the treated groups, while the untreated group had a TSS of 4.76%. This study agrees with Nassarawa et al. (2022b) report on higher concentration of soluble solids in grapefruit when treated with red LED light over the control and blue LED Light.

Relationship between Acidity, Sugar Levels, and the Flavour Profile of Tomatoes

The flavour profile of tomatoes depends on the balance between sourness (acids) and sweetness (sugars). The soluble sugars contribute to sweetness, while organic acids contribute to their acidity, producing sourness (Li et al., 2023). It is a necessity to achieve a balance of these quality markers for enhanced flavour in tomatoes. An 8.7% increase in acid concentration produces a 0.2% increase in sugar level for 5B:1R LED, whereas a 4.2% increase in acidity level yields a 1.2% enhancement in sugar level for 5R:1B LED. The 5R:1B LED treatment produces a balanced flavour profile for LED-treated tomatoes.

Effect of LED Pretreatment on the Weight of Market-displayed Tomatoes

Weight loss in tomatoes is caused by transpiration, where water evaporates from the tomato, resulting in a weight reduction. Figure 8 shows that after treatment, the weight loss of tomato samples across the different treatments was relatively the same. On days 6-12, the control samples recorded more losses. On days 15-18, 5R:1B LED shows slightly higher losses than the control samples. Days 18-21 reveal a high percentage of losses for control, white and 5R:1B LEDs. Throughout the display period, the 5B:1R LED maintained a lower percentage of weight loss. 30% and 4,9% of weight were observed with 5B:1R and 5R:1B LEDs over the control at the end of the display period, indicating that these treatments significantly reduce weight loss in tomatoes during market display conditions. Significant differences were observed with 5B:1R LED over other treatment conditions.

Establishment of Regression Models on Tomato Market Quality Indicators

Functional regression models were used to obtain changes in the quality index of tomatoes in market-displayed conditions after pretreatment with varying LED wavelengths. The

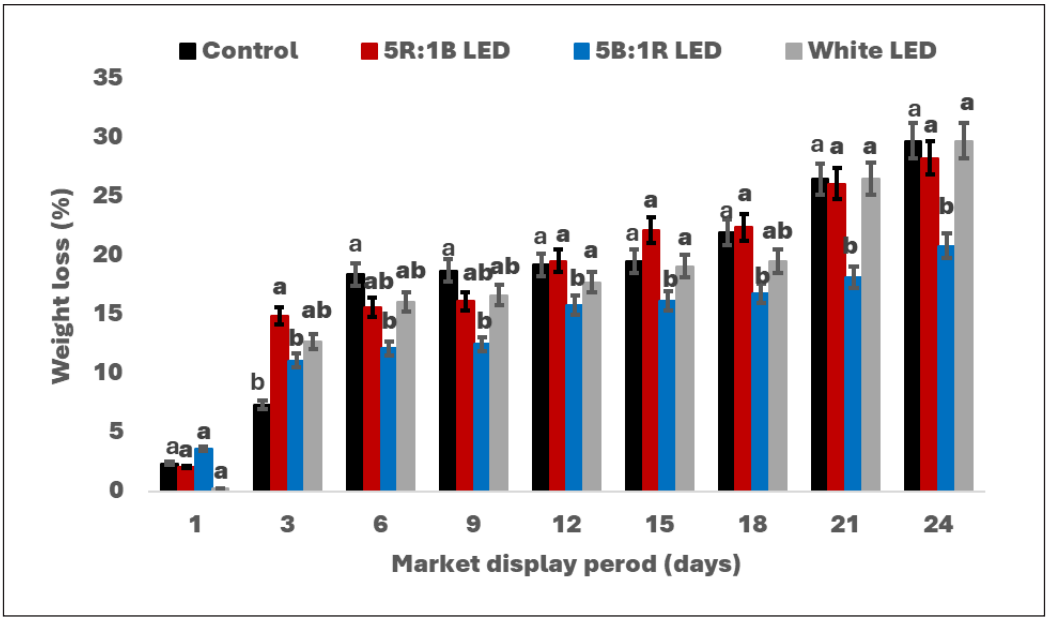

Figure 8. Changes in weight of tomato pretreated with different LED wavelengths at different display times for 24 days, with the significant differences obtained during the display period ($p<0.5$)

regression models were estimated based on R^2 values from the changes in tomato quality indices as a function of market display time (days) to obtain the variation curves of various quality indicators (Table 1). The model with the best R^2 value was chosen as the best model that fit the trend of each quality index. Evaluation of the models with the highest R^2 value involves metrics such as MAE and RMSE.

Regression Analysis on LED Pretreatment on the Colour of Market-displayed Tomatoes

The quadratic regression model had the highest R^2 values compared to other treatments on a-values (degree of redness), showing that the model explains a greater portion of the variance, which explains light inhibition of red colour accumulation in tomatoes (a-value), and the variances in colour distinction (ΔE). Table 2 reveals that the 5B:1R LED had the lowest MAE and RMSE values for both a* and ΔE, showing that the treatment model has higher reliability and accuracy and can also explain a larger portion of the variances than other treatment models. This aligns with the empirical results, affirming that 5B:1R LED delays ripening and also produces a model to describe the influence of LED on colour dynamics in tomatoes during market-displayed conditions.

Regression Model Analysis on LED Pretreatment on the Firmness of Market-displayed Tomatoes

The quadratic regression model produces the highest $R^{2,}$ indicating that the model best captures the data describing the dynamics of firmness in tomatoes. Adjusted R^2 values of 0.980, 0.975, 0.987, and 0.987 for the control, 5R:1B, 5B:1R and white LED, respectively, indicate that this model explains a greater portion of the variance for each treatment (Table 2). However, further metrics showed that the 5B:1R LED had the lowest MAE and RMSE values compared to other treatments, indicating that the magnitude of error between the predicted and the actual values is small compared to other treatments, and the accuracy is high.

Regression Model Analysis on LED Pretreatment on the pH of Market-displayed Tomatoes

pH, a measure of the acidity and alkalinity in tomatoes which serves as an important quality check shows that the pH data fitted into the quadratic regression model, as the model produces higher R^2 values compared to other regression models. Table 2 shows

Table 2
Model selection using the coefficient of determination

Treatment	Regression Models	R^2		R^2	R^2	R^2
		Colour		Firmness	pH	Weight loss
		a*	ΔE			
Control	Linear	0.518	0.426	0.900	0.423	0.861
	Log	0.856	-	0.902	0.704	0.877
	Power	0.817	-	0.743	0.723	0.862
	Quadratic	0.917	0.681	0.981	0.938	0.894
5R:1B LED	Linear	0.674	0.426	0.92	0.465	0.569
	Log	0.937	-	0.887	0.738	0.895
	Power	0.872	-	0.914	0.753	0.869
	Quadratic	0.960	0.592	0.976	0.906	0.901
5B:1R LED	Linear	0.775	0.515	0.935	0.501	0.877
	Log	0.919	-	0.899	0.802	0.900
	Power	0.913	-	0.764	0.826	0.912
	Quadratic	0.944	0.820	0.988	0.944	0.915
White LED	Linear	0.552	0.533	0.913	0.745	0.846
	Log	0.874	-	0.909	0.811	0.847
	Power	0.786	-	0.776	0.887	0.787
	Quadratic	0.910	0.699	0.988	0.958	0.858

that white LED had lower MAE and RMSE values, which indicate higher reliability and accuracy than other treatment models. Although the empirical data identify 5B:1R LED as the treatment that enhances firmness with a 43.1% increase in firmness over the control, the model shows that the treatment is more likely to produce a less accurate model with higher MAE and RMSE values.

Alternatively, the white LED had higher reliability and accuracy with higher predictive power than the 5B:1R LED and also performed well empirically with a 31.4% increase in firmness over the control. These differences between the empirical data and model output raise concerns about the relationship between empirical data and the model's predictive ability. Whereas 5B:1R LED can offer an immediate effect on pH, the modelling result suggests that white LED treatment may provide a more detailed framework for understanding pH dynamics across varying days of tomatoes in the market environment. This variation lies in the model's ability to capture the variability in the data more than the empirical observation shown in the average output. This highlights the essence of empirical measurements and modelling approaches in understanding the impact of LED treatments.

Regression Model Analysis on LED Pretreatment on the Weight of Market-displayed Tomatoes

The quadratic regression model produces the highest R^2 values, indicating that the model best captures the data describing the dynamics of weight loss in tomatoes. Table 3 shows that the 5B:1R LED had the lowest MAE and RMSE values compared to other treatments. This 5B:1R LED pretreatment produces less weight loss in tomatoes and can explain the changes in tomato weight across the market display period.

None of these models could describe the changes in the b-component of the colour variable and total soluble solids, as these variables were not included in the modelling.

With this study, the overall quality and flavour profile of tomatoes can be improved, making them more desirable to consumers. Retailers can manage inventory better, reducing the frequency of markdowns on unsold produce and improving overall profitability. This efficiency can also lead to better pricing strategies and reduced logistical costs. Conducting consumer preference studies will provide valuable insights into how LED treatments influence purchasing decisions and understanding consumer perceptions can inform targeted marketing strategies and product positioning in the marketplace.

Comparative Evaluation of the LED Treatment Method with other Tomato Preservation Methods

Comparing the effect of LEDs with other tomato preservation techniques, Paulsen et al. (2019) reported an 18 % reduction in red colouration and a 37 % increase in firmness on tomatoes preserved with modified atmosphere packaging (MAP). The coating technique

Table 3
Fitting model and parameters of quality indices of LED-treated tomato fruit during market display condition

Quality Indicators	Treatment	MAE	RMSE	Adjusted R^2	Fitting Equation
Colour (a*)	Control	1.893	1.376	0.917	$y = -0.062x^2 + 1.991x + 16.901$
	5R:1B	5.964	2.442	0.960	$y = -0.089x^2 + 2.707x + 9.980$
	White	3.030	1.741	0.910	$y = -0.073x^2 + 2.349x + 10.169$
	5B:1R	0.590	0.768	0.979	$y = -0.042x^2 + 1.663x + 13.421$
ΔE	Control	36.032	6.003	0.680	$y = -0.102x^2 + 3.212x + 45.505$
	5R:1B	36.627	6.052	0.591	$y = -0.073x^2 + 2.456x + 45.661$
	White	27.799	5.272	0.698	$y = -0.074x^2 + 2.583x + 43.266$
	5B:1R	18.856	4.342	0.819	$y = -0.105x^2 + 3.324x + 40.08$
Firmness	Control	0.328	0.573	0.980	$y = 0.024x^2 - 1.078x + 15.696$
	5R:1B	0.351	0.593	0.975	$y = 0.021x^2 - 1.001x + 15.141$
	White	0.180	0.425	0.987	$y = 0.021x^2 - 0.984x + 15.460$
	5B:1R	0.171	0.413	0.987	$y = -0.018x^2 - 0.924x + 16.0$
pH	Control	0.051	0.226	0.937	$y = 0.011x^2 - 0.320x + 5.541$
	5R:1B	0.051	0.226	0.905	$y = 0.001x^2 - 0.303x + 5.352$
	White	0.030	0.174	0.956	$y = 0.011x^2 - 0.343x + 5.623$
	5B:1R	1.751	1.323	0.943	$y = 0.009x^2 - 0.291x + 5.147$
Weight Loss	Control	87.893	9.375	0.897	$y = 0.211x^2 - 5.344x + 0.791$
	5R:1B	72.869	8.536	0.901	$y = -0.228x^2 + 4.916x + 1.203$
	White	83.830	9.156	0.858	$y = -0.144x^2 + 4.225x + 0.880$
	5B:1R	30.628	5.534	0.915	$y = -0.158x^2 + 3.297x + 2.634$

**Note.* The table shows the model evaluation metrics (MAE, RMSE, and R^2), and their equations

shows a 20 % decrease in red colouration, a 31.6 % increase in firmness, and an increase in pH from 4.4 with the control to 4.6 with chitosan coating (Venkatachalam et al., 2024). The result obtained from 5B:1R LED of 19.9 % red colour reduction, an increase in acid strength, a 43.1 % increase in firmness over the control, and a 30% weight loss reduction qualifies the LED treatment as a more reliable technique for the preservation of tomatoes to lengthen their shelf life and improve the quality**.** Additionally, it is cost-effective, compact, produces high efficiency, and its parameters can be regulated to suit the properties of any crop under investigation.

CONCLUSION

This study investigated the effects of LED pretreatment during storage on the postharvest quality of tomatoes during market display over 24 days, assessing key parameters including colour, firmness, total soluble solids (TSS), pH, and weight loss. The results demonstrate that 5B:1R LED pretreatment effectively delayed the progression of lightness and red colour development, moderated overall colour changes, preserved firmness, increased acid strength, and significantly reduced weight loss. In contrast, the 5R:1B LED configuration notably enhanced TSS content. The beneficial effects of the pretreatments were maintained for up to 15 days under market conditions before significant changes in ripening, firmness, and pH increase were observed. Regression analysis revealed that the dynamics of the quality indices followed nonlinear trends: quadratic models best described changes in the quality parameters. Overall, these findings highlight the potential of LED light pretreatments, particularly specific red-blue light ratios, as an effective postharvest strategy for maintaining tomato quality and extending shelf life in market environments. This research offers a foundation for the development of predictive models to monitor and optimise the quality of LED-treated tomatoes during retail display.

ACKNOWLEDGEMENT

This research was conducted in the Department of Biological and Agricultural Engineering, Universiti Putra Malaysia, and supported by the Fundamental Research Grant Scheme (FRGS) from the Ministry of Higher Education, Malaysia (MOHE), under the code project FRGS/1/2023/TK08/UPM/02/05.

REFERENCES

Batista-Silva, W., Nascimento, V. L., Medeiros, D. B., Nunes-Nesi, A., Ribeiro, D. M., Zsögön, A., & Araújo, W. L. (2018). Modifications in organic acid profiles during fruit development and ripening: Correlation or causation? *Frontiers in Plant Science*, *9*, Article 1689. https://doi.org/10.3389/fpls.2018.01689

Chan, A., Pay, M. L., Christensen, J., He, F., Roden, L. C., Ahmed, H., & Foo, M. (2024). Red, blue or mix: Choice of optimal light qualities for enhanced plant growth and development through *in silico* analysis. *in silico Plants*, *6*(1), Article diae008. https://doi.org/10.1093/insilicoplants/diae008

Choi, H.-G., & Park, K.-S. (2023). Ripening process of tomato fruits postharvest: Impact of environmental conditions on quality and chlorophyll a fluorescence characteristics. *Horticulturae*, *9*(7), Article 812. https://doi.org/10.3390/horticulturae9070812

Clark, M. J., & Slavin, J. L. (2013). The effect of fibre on satiety and food intake: A systematic review. *Journal of the American College of Nutrition*, *32*(3), 200-211. https://doi.org/10.1080/07315724.2013.791194

Costa, D., Moreno, D. S. A., & Alviano, C. S. (2022). Extension of solanaceae food crops shelf life by the use of elicitors and sustainable practices during postharvest phase. *Food and Bioprocess Technology*, *15*, 249-274. https://doi.org/10.1007/s11947-021-02713-z

Craver, J. K., Boldt, J. K., & Lopez, R. G. (2019). Comparison of supplemental lighting provided by high-pressure sodium lamps or light-emitting diodes for the propagation and finishing of bedding plants in a commercial greenhouse. *HortScience*, *54*(1), 52-59. https://doi.org/10.21273/HORTSCI13471-18

de Bruijn, J., Fuentes, N., Solar, V., Valdebenito, A., Vidal, L., Melín, P., Fagundes, F., & Valdés, H. (2023). The effect of visible light on the postharvest life of tomatoes (*Solanum lycopersicum* L.). *Horticulturae*, *9*(1), Article 94. https://doi.org/10.3390/horticulturae9010094

Elliott, C., & Lee, K. (2020). *Adoption of light-emitting diodes in common lighting applications*. U.S. Department of Energy. https://doi.org/10.2172/1669047

Fallik, E., & Ilić, Z. (2021). The influence of physical treatments on phytochemical changes in fresh produce after storage and marketing. *Agronomy*, *11*(4), Article 788. https://doi.org/10.3390/agronomy11040788

Gupta, S., & Agarwal, A. (2017). Artificial lighting system for plant growth and development: Chronological advancement, working principles, and comparative assessment. In *Light emitting diodes for agriculture: Smart lighting* (pp. 1-25). Springer Singapore. https://doi.org/10.1007/978-981-10-5807-3_1

Han, J. W., Ren, Q. S., Ji, Z. T., & Yang, X. T. (2022). Mathematical model of postharvest variation in tomato colour based on optimised response surface methodology. *Journal of the Science of Food and Agriculture*, *102*(7), 2972-2980. https://doi.org/10.1002/jsfa.11637

Huang, Y., Lu, R., Hu, D., & Chen, K. (2018). Quality assessment of tomato fruit by optical absorption and scattering properties. *Postharvest Biology and Technology*, *143*, 78-85. https://doi.org/10.1016/j.postharvbio.2018.04.016

Jürkenbeck, K., Spiller, A., & Meyerding, S. G. H. (2020). Tomato attributes and consumer preferences - a consumer segmentation approach. *British Food Journal*, *122*(1), 328-344. https://doi.org/10.1108/BFJ-09-2018-0628

Kabaş, A., Ercan, U., Kabas, O., & Moiceanu, G. (2024). Prediction of total soluble solids content using tomato characteristics: Comparison of artificial neural network vs. multiple linear regression. *Applied Sciences*, *14*(17), Article 7741. https://doi.org/10.3390/app14177741

Khan, S., Dar, A. H., & Shams, R. (2022). Applications of ultraviolet light-emitting diode technology in horticultural produce: A systematic review and meta-analysis. *Food and Bioprocess Technology*, *15*, 487-497. https://doi.org/10.1007/s11947-021-02742-8

Khoo, H. E., Prasad, K. N., Kong, K. W., Jiang, Y., & Ismail, A. (2011). Carotenoids and their isomers: Colour pigments in fruits and vegetables. *Molecules*, *16*(2), 1710-1738. https://doi.org/10.3390/molecules16021710

Li, R., Wang, J., Yuan, H., Niu, Y., Sun, J., Tian, Q., Wu, Y., Yu, J., Tang, Z., Xiao, X., Xie, J., Hu, L., Liu, Z., & Liao, W. (2023). Exogenous application of ALA enhanced sugar, acid and aroma qualities in tomato fruit. *Frontiers in Plant Science*, *14*, Article 1323048. https://doi.org/10.3389/fpls.2023.1323048

Li, H., Zhang, J., Wang, Y., Li, J., Yang, Y., & Liu, X. (2018). The effects of storage conditions on lycopene content and colour of tomato hot pot sauce. *International Journal of Analytical Chemistry*, *2018*, Article 1273907. https://doi.org/10.1155/2018/1273907

Liu, J., & van Iersel, M. W. (2021). Photosynthetic physiology of blue, green, and red light: Light intensity effects and underlying mechanisms. *Frontiers in Plant Science*, *12*, Article 619987. https://doi.org/10.3389/fpls.2021.619987

Martínez-Zamora, L., Castillejo, N., & Artés-Hernández, F. (2023). Effect of postharvest visible spectrum LED lighting on quality and bioactive compounds of tomatoes during shelf life. *LWT*, *174*, Article 114420. https://doi.org/10.1016/j.lwt.2022.114420

Nájera, C., Guil-Guerrero, J. L., Enríquez, L. J., Álvaro, J. E., & Urrestarazu, M. (2018). LED-enhanced dietary and organoleptic qualities in postharvest tomato fruit. *Postharvest Biology and Technology*, *145*, 151-156. https://doi.org/10.1016/j.postharvbio.2018.07.008

Nassarawa, S. S., Abdelshafy, A. M., Xu, Y., Li, L., & Luo, Z. (2021). Effect of light-emitting diodes (LEDs) on the quality of fruits and vegetables during postharvest period: A review. *Food and Bioprocess Technology*, *14*(3), 388-414. https://doi.org/10.1007/s11947-020-02534-6

Nassarawa, S. S., Belwal, T., & Javed, M. (2022a). Influence of the red LEDs light irradiation on the quality and chemical attributes of postharvest table grape (*Vitis vinifera* L.) during storage. *Food and Bioprocess Technology*, *15*, 1436-1447. https://doi.org/10.1007/s11947-022-02824-1

Nassarawa, S. S., & Luo, Z. (2022b). Effect of light irradiation on sugar, phenolics, and GABA metabolism on postharvest grape (*Vitis vinifera* L.) during storage. *Food and Bioprocess Technology*, *15*, 2789-2802. https://doi.org/10.1007/s11947-022-02919-9

Offiong, U., Jamaludin, D., Nakasha, J., & Khairudin, N. (2023). Impact of photo treatment on tomato physiological qualities during storage and on-shelf display. *Advance and Sustainable Technologies*, *2*(2), Article 335. https://doi.org/10.58915/aset.v2i2.335

Panebianco, S., Van Wijk, E., & Yan, Y. (2024). Delayed luminescence in monitoring the postharvest ripening of tomato fruit and classifying according to their maturity stage at harvest. *Food and Bioprocess Technology*, *17*, 5119-5133. https://doi.org/10.1007/s11947-024-03429-6

Panjai, L., Noga, G., Hunsche, M., & Fiebig, A. (2019). Optimal red light irradiation time to increase health-promoting compounds in tomato fruit postharvest. *Scientia Horticulturae*, *251*, 189-196. https://doi.org/10.1016/j.scienta.2019.03.019

Qin, Y., Gong, A., Liu, X., Li, N., Ji, T., Li, J., & Yang, F. (2024). Testing a simulation model for the response of tomato fruit quality formation to temperature and light in solar greenhouses. *Plants*, *13*(12), Article 1662. https://doi.org/10.3390/plants13121662

Salehi, F. (2022). Application of pulsed light technology for fruits and vegetables disinfection: A review. *Journal of Applied Microbiology*, *132*(4), 2521-2530. https://doi.org/10.1111/jam.15389

Teshome, E., Forsido, S. F., Rupasinghe, H. P. V., & Olika Keyata, E. (2022). Potentials of natural preservatives to enhance food safety and shelf life: A review. *Scientific World Journal*, *2022*, Article 9901018. https://doi.org/10.1155/2022/9901018

Tigist, M., Workneh, T. S., & Woldetsadik, K. (2013). Effects of variety on the quality of tomato stored under ambient conditions. *Journal of Food Science and Technology*, *50*(3), 477-486. https://doi.org/10.1007/s13197-011-0378-0

Tolesa, G. N., & Workneh, T. S. (2017). Influence of storage environment, maturity stage and pre-storage disinfection treatments on tomato fruit quality during winter in KwaZulu-Natal, South Africa. *Journal of Food Science and Technology*, *54*(10), 3230-3242. https://doi.org/10.1007/s13197-017-2766-6

Venkatachalam, K., Lekjing, S., Noonim, P., & Charoenphun, N. (2024). Extension of quality and shelf life of tomatoes using chitosan coating incorporated with cinnamon oil. *Foods*, *13*(7), Article 1000. https://doi.org/10.3390/foods13071000

Wang, D., Wang, Y., Lv, Z., Pan, Z., Wei, Y., Shu, C., Zeng, Q., Chen, Y., & Zhang, W. (2023). Analysis of nutrients and volatile compounds in cherry tomatoes stored at different temperatures. *Foods*, *12*(1), Article 6. https://doi.org/10.3390/foods12010006

Wang, X., Wang, Q., Nguyen, P., & Lin, C. (2014). Cryptochrome-mediated light responses in plants. *The Enzymes*, *35*, 167-189. https://doi.org/10.1016/B978-0-12-801922-1.00007-5

Wang, Y., Li, W., Cai, W., Ma, Y., Xu, Y., Zhao, X., & Zhang, C. (2018). Visible light exposure reduces the drip loss of fresh-cut watermelon. *Journal of Food Science and Technology*, *55*(5), 1816-1822. https://doi.org/10.1007/s13197-018-3096-z

Xiang, F., Xia, Y., Wang, Y., Wang, Y., Wu, K., & Ni, X. (2021). Preparation of konjac glucomannan-based films reinforced with nanoparticles and its effect on cherry tomato preservation. *Food Packaging and Shelf Life*, *29*, Article 100701. https://doi.org/10.1016/j.fpsl.2021.100701

Xu, F., He, S., Zhang, J., Mao, Z., Wang, W., Li, T., Hua, J., Du, S., Xu, P., Li, L., Lian, H., & Yang, H. Q. (2018). Photoactivated CRY1 and phyB interact directly with AUX/IAA proteins to inhibit auxin signalling in *Arabidopsis*. *Molecular Plant*, *11*(4), 523-541. https://doi.org/10.1016/j.molp.2017.12.003

Zhao, Y., Li, L., Gao, S., Wang, S., Li, X., & Xiong, X. (2023). Postharvest storage properties and quality kinetic models of cherry tomatoes treated by high-voltage electrostatic fields. *LWT*, *176*, Article 114497. https://doi.org/10.1016/j.lwt.2023.114497

Zheng, Y., Zou, J., Lin, S., Jin, C., Shi, M., Yang, B., Yang, Y., Jin, D., Li, R., Li, Y., Wen, X., Yang, S., & Ding, X. (2023). Effects of different light intensity on the growth of tomato seedlings in a plant factory. *PLoS ONE*, *18*(11), Article e0294876. https://doi.org/10.1371/journal.pone.0294876

Pertanika J. Trop. Agric. Sci. 49 (S1): 145 - 170 (2026)

PERTANIKA JOURNALS

TROPICAL AGRICULTURAL SCIENCE

Journal homepage: http://www.pertanika.upm.edu.my/

Performance of Green Solvent and Microwave in Developing Sustainable Extraction of Functional Compound and Hydrodistillation Essential Oils from Cinnamon

Devi Yuni Susanti*, Joko Nugroho Wahyu Karyadi, Arifin Dwi Saputro, Rudiati Evi Masithoh, Nanin Agustin, Ella Rofiana, and Salmaa Rosyiidah

Department of Agricultural and Biosystem Engineering, Faculty of Agricultural Technology, Gadjah Mada University, 55281 Yogyakarta, Indonesia

ABSTRACT

Southeast Asian cinnamon contains functional compounds and essential oils that act as natural and beneficial antioxidants. This research developed and evaluated for Microwave-Assisted Hydrodistillation (MAHD) to combine simultaneous extraction of phenolic compounds and distillation of essential oil using a green solvent - Natural Deep Eutectic Solvent: Citric Acid-Sucrose (NADES-CAS). This study aimed to evaluate the performance of NADES-CAS in collecting functional compounds (phenolic and proanthocyanidins) and essential oils using MAHD. The MAHD was conducted using NADES-CAS with a molar ratio of 1:1 in concentrations of 1% under microwave power of 640, 720, and 800 W. The performance was evaluated using Peleg's equation as a kinetic approach. The microwaves increased the value of EC, TDS, and solvent temperature but decreased the density and viscosity, supporting MAHD. Peleg's kinetic model describes an increase in microwave power increase the rate constant (B_0) and capacity constant (C_e). The B_0 values of phenolic and proanthocyanidin compounds were in the range of 0.0264-0.0397 mg/mL.min and 0.0388-0.1117mg/mL.min, respectively. Meanwhile, the C_e value of these compounds were in the range of 0.5349-0.6607 mg/mL and 0.5529-0.9439 mg/mL, respectively. The model accurately predicting the profiles of each compound concentrations during MAHD. The combination of MAHD and NADES successfully distilled essential oils from cinnamon powder with significant components such as Cinnamaldehyde and minor components such as caryophyllene, benzaldehyde, and

ARTICLE INFO

Article history:
Received: 19 July 2025
Accepted: 24 December 2025
Published: 19 March 2026

DOI: https://doi.org/10.47836/pjtas.49.S1.07

E-mail addresses:
deviyunisusanti@ugm.ac.id (Devi Yuni Susanti)
jknugroho@ugm.ac.id (Joko Nugroho Wahyu Karyadi)
arifin_saputro@ugm.ac.id (Arifin Dwi Saputro)
evi@ugm.ac.id (Rudiati Evi Masithoh)
naninagustin@mail.ugm.ac.id (Nanin Agustin)
ella.rofiana0802@mail.ugm.ac.id (Ella Rofiana)
salmaa.rosyiidah@mail.ugm.ac.id (Salmaa Rosyiidah)
* Corresponding author

e-ISSN: 2231-8542

pinene. This innovation is potential to be applied to accelerate the simultaneous extraction of phenolic compounds and distillation of essential oils from cinnamon.

Keywords: Cinnamon, essential oil, green solvent, microwave-assisted hydrodistillation

INTRODUCTION

Cinnamon, a tropical spice native to Southeast Asia, is prized for its aroma and bioactive compounds. It is derived from the inner bark of *Lauraceae* trees and used in both culinary and medicinal contexts (Pages-Rebull et al., 2024). Its compounds exhibit antioxidant, anti-inflammatory, antiparasitic, anticancer, and antidiabetic properties (Zhang et al., 2024), with important benefits in reducing lipids to combat heart disease and high cholesterol (Maierean et al., 2017). Functional compounds in cinnamon can act as natural antioxidants and antimicrobial food preservatives, which can be extracted for use in food products. Additionally, cinnamon bark contains valuable essential oils which can be obtained through distillation (Deshi et al., 2024).

Extraction is a process of separating target compounds from a mixture using suitable solvents, thus facilitating the isolation and preservation of bioactive substances (Wang et al., 2024). Functional antioxidant compounds in cinnamon, such as polyphenols, flavonoids, saponins, tannins, and phenols, can be effectively extracted. Meanwhile, essential oils, which also have high economic and functional value, can be obtained through both extraction and distillation methods (Loto, 2020).

Although conventional extraction is widely applied, it has several limitations, including high energy consumption, longer processing times, and a risk of degrading volatile compounds. Besides conventional extraction, microwave-assisted extraction (MAE) and ultrasound-assisted extraction (UAE) have been widely developed in previous research (Izza et al. 2023; Purdi et al., 2023). Both of these methods are expected to accelerate the extraction process, maximise the diffusion process, use low energy, and maintain the structure of active compounds (Guddi & Sarkar 2024). However, these methods cannot directly separate the essential oils. Thus, the extracted essential oils must be separated using evaporation and condensation in a distillation system.

To save energy and cost, an innovative method combining extraction and distillation simultaneously in a unit called a Microwave-Assisted Hydrodistillation (MAHD) method is proposed. In previous research, Jeyaratnam et al. used MAHD for extracting cinnamon oil. However, it focussed on analysing the results of cinnamon essential oil (Jeyaratnam et al., 2016a; Jeyaratnam et al., 2016b). The present research is proposed with a novelty, which is not only in analysing the simultaneous extraction of bioactive compounds and essential oils from cinnamon using MAHD, but also in exploring the mechanisms and kinetics of extracting bioactive compounds from cinnamon powder while distilling the cinnamon oils simultaneously.

NADES is reported as an environmentally friendly solvent for extracting bioactive compounds, such as phenolic compounds, more effectively than organic solvents (Adeel et al. 2020b). NADES is a green solvent that is safe and non-flammable. It has the right chemical-physical properties for cinnamon extraction (Cravotto et al. 2024b; Mulia et al. 2015). Additionally, NADES can extract both polar and nonpolar compounds. NADES mainly utilises carboxylic acid compounds, choline chloride (ChCl), and hydrogen bond donors (Cravotto, et al. 2024a). A type of NADES used in this MAHD research is citric acid and sucrose (CAS). This solvent is expected to achieve a good synergy and interaction with the microwave, thereby enhancing the extraction process. NADES-CAS has also proven effective in extracting bioactive compounds from sorghum, rice, and others (Susanti et al. 2021). This solvent has also been reported to maintain some functional compounds in cinnamon extract, such as polyphenols, flavonoids, saponins, tannins, and phenols that are susceptible to degradation by the process (Segatto et al. 2022). Research on applying microwaves and utilising green solvents to accelerate the extraction of antioxidant bioactive compounds from sorghum, rice, and other sources has been conducted by previous research (Izza et al. 2023; Susanti et al., 2021).

Additionally, the novelty of this research lies in the design of the MAHD system and the application of Natural Deep Eutectic Solvents-Citric Acid Sucrose (NADES-CAS) as a food-grade, environmentally safe solvent for the extraction of bioactive compounds and cinnamon oils. In this research, the physical characteristics of NADES-CAS are explored, and its effects on extraction performance are analysed, which has not been explicitly addressed in previous studies. Previous research has evaluated and demonstrated the characterisation of NADES-CAS and its potential as a green solvent for extraction (Savi et al., 2019). Furthermore, NADES-CAS has been applied in microwave-assisted extraction of olive oil (Bonacci et al., 2020) and ultrasound-assisted extraction of date sugar (AlYammahi et al., 2023).

The simultaneous extraction and distillation in MAHD using NADES-CAS is expected to be an innovative method that increases energy efficiency and reduces processing time through an environmentally friendly process. The microwave radiation through the solvent likely interacts with the cinnamon powder and solvent, causing uniform heating and vibration, leading to faster and more effective extraction and release of bioactive compounds and essential oils from the cinnamon powder (Adeel et al. 2020a). This research also explores the extraction mechanism using a kinetic approach, which has not been studied in the previous related paper, as a novelty of this paper. MAHD utilises microwaves, and NADES-CAS is expected to accelerate the extraction and distillation processes simultaneously, thereby making them more efficient.

In the current research, the application of green solvent needs to be combined with the right MAHD power to obtain positive synergy and accelerate the collection of functional cinnamon compounds. This study aimed to design and test the performance of MAHD

and green solvent to accelerate the collection of essential oils and bioactive compounds of cinnamon simultaneously by determining the optimal microwave power. First, this research characterised the properties of NADES-CAS under microwave conditions. Then, it was applied to test its performance in MAHD at several microwave powers for the extraction of phenolic and proanthocyanidin compounds, as well as its capability to collect essential oils from cinnamon powder. The extraction performance was evaluated through a kinetic approach using a Peleg model. Additionally, the quality of the resulting essential oil was also evaluated. The result of this research is expected to be applied to enhance the simultaneous extraction of bioactive components and essential oils from cinnamon, compared to conventional methods. It can also serve as a reference for increasing the use of green solvents over organic solvents, which have high toxicity and can harm both health and the environment, thereby supporting sustainable chemistry and pharmacy. The successful integration of NADES-CAS with the MAHD process highlights an environmentally friendly strategy for the extraction of cinnamon compounds.

MATERIALS AND METHODS

Materials and Reagents

The material used in this extraction process was cinnamon obtained from the Beringharjo Market, Yogyakarta, Indonesia. The primary reagents used in this research were citric acid, sucrose, and distilled water to produce NADES-CAS. Other reagents used for the evaluation of phenolic and proanthocyanidin contents were Folin–Ciocalteu reagent, Na_2CO_3, butanol, HCl, iron reagent, and $FeNH_4(SO_4)_2$. All reagents were analytical grade from Merck (Darmstadt, Germany).

Preparation of NADES CAS

The green solvent, 1 M NADES-CAS, was prepared from citric acid (CA) and sucrose (S) in a molar ratio of 1:1 in 1 L of aquadest. Then, the mixture was homogenised using a probe ultrasonic with a power amplitude of 80% at a frequency of 20 Hz to accelerate the homogenous condition using its acoustic power that induced bubbles, compression, and rarefactions in the mixture (Medina-Torres et.al, 2017). The ultrasonic equipment was from Hangzhou Dowell Ultrasound Tech. Co., Ltd. with a model number DW-SD20-1200H, a power of 1.2 kW, and a 220 V / 20 kHz voltage. The initial period of the ultrasonic method was 30 minutes, and then it was stopped temporarily to adjust the environmental temperature to prevent overheating. After that, the process continued for 30 minutes. It was sufficient to ensure a homogenous mixture of NADES-CAS. The mixture of CA and S was diluted in distilled water to reach its concentration of 1%.

The Extraction and Hydrodistillation using MAHD

The extraction and hydrodistillation of volatile compounds from cinnamon powder were conducted in a system of MAHD constructed from the modification of an Electrolux Microwave EMM2308X with a capacity of 23 L, maximum microwave power of 800 W, and a voltage of 220–240 V/ 50 Hz. The microwave had panel control to set the temperature, a magnetic stirrer speed in a microwave flask, microwave power, and time. The extraction temperature was controlled by a temperature controller and a CKC Tinner DH485 (H5CN) indicator. A magnetic stirrer was installed at the bottom of the microwave flask to make stirring. The extraction scheme with MAHD is shown in Figure 1. The extraction was conducted at the stirrer speed of 1600 RPM and a temperature of 100 °C using 1% NADES-CAS. Furthermore, the flask containing the solvent was inserted into the microwave chamber. The temperature profile of the solvent was measured using a thermocouple. This process was conducted at microwave power levels of 640, 720, and 800 W, corresponding to 80%, 90%, and 100% of the maximum microwave power, respectively. The extraction of phenolic compounds, proanthocyanidin compounds, and essential oils was conducted in a flask exposed to microwave radiation. The phenolic and proanthocyanidin compounds, as antioxidant compounds, were measured from the bulk of solvent during the extraction. The essential oil was evaporated and distilled in the distillation system and accommodated in the essential oil container.

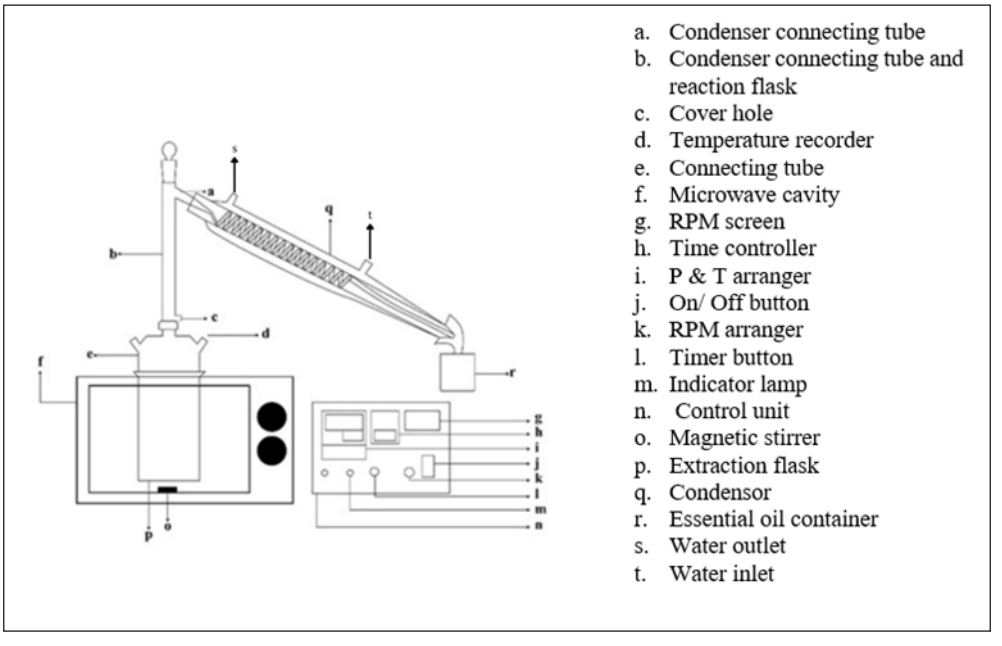

Figure 1. The schematic of Microwave-Assisted Hydrodistillation

Determination of Proanthocyanidins (PA) Content in the Extract

The PA content was determined through the acid butanol assay (de Souza et al., 2018; Susanti et al., 2020). It has been reported as the best method for determining PA concentration and has been widely reviewed in previous studies (Susanti et al. 2020). In this method, a 6 mL acid butanol was mixed with 1 mL of the extract sample and 0.2 mL of $FeNH_4(SO_4)_2.12H_2O$ reagent, then vortexed until homogeneous and incubated at 90 ℃. After 50 minutes, the sample was removed and waited until a normal temperature. The final step was to read the absorbance value using a UV-Vis Spectrophotometer (Mesulab, type N_2S, China) with a wavelength of 550 nm. The result was stated as mg/mL.

Determination of Total Phenolics Content (TPC) in the Extract

Polyphenol content was determined through the Folin-Ciocalteu Test method (Kalpoutzakis et al. 2023). This method has been considered the best method for determining polyphenol content (Yılmaz et al. 2021). This method used seven test tubes containing 15 mL of distilled water and 1 mL of Folin and Ciocalteu's phenol reagent. Each test tube was filled with 1 mL of sample test solution, 1 mL of calibration standard solution, or 1 mL of distilled water. Each test tube was mixed well and left for 6 minutes. Then, 3 mL of sodium carbonate solution was stirred in each tube. Then, the test tubes were placed in the heating block for 120 minutes. As much as 1 mL of solution was transferred into the cuvette and measured for its absorbance at 765 or 760.5 nm after focussing on the spectrophotometer with a blank. The standard solution was measured first, then the sample test solution (Kupina et al. 2019).

The results of cinnamon extraction were tested for polyphenol content. The polyphenol test was carried out using the Folin-Ciocalteu method. The extract of cinnamon (0.5 ml) was reacted with 2.5 mL of 0.2 N Folin Ciocalteau and 2 mL of Na_2CO_3. Next, it was incubated at 50 ºC for 5 minutes, and then its absorbance was tested using a UV-Vis Spectrophotometer (Mesulab, type N_2S, China) at a wavelength of 550 nm.

The Evaluation of Extraction Rate and Maximum Capacity of Extraction using the Peleg Model

The performance of MAHD was analysed using the Peleg kinetic model, which describes the relationship between water content and solute absorption time (Oroian 2017). This model was relevant for predicting TPC and PA concentration in extracts during MAHD. In the Peleg model, the C_0 value indicates the initial TPC and PA concentration, while B_0 (extraction rate constant) and C_e (capacity constant) values indicate the extraction rate and capacity. Additionally, this model was also relevant to releasing solutes into water. Using the Peleg model, the extraction curve (TPC vs time and PA vs time) was fitted to the absorption curve (water content vs time). The equation of the Peleg model is presented in Equation(1). For the initial condition $C_0 - 0$, Equation 1 was rearranged into Equation 2. Equation 2 is expected to provide a reasonable prediction of the PA concentration in the extract during

MAHD. The TPC and PA concentration in the solvent at a given time is denoted as $C(t)$ in mg/mL. The application of the Peleg model as a kinetic approach was evaluated using some validation parameters, namely the Sum Squares of Error (SSE), Root Mean Squared Error (RMSE), Chi-square (X^2), and Coefficient of Determination (R^2) (Azeez et al. 2019).

$$C(t) = C_0 + \frac{t}{\frac{1}{B_0} + \frac{t}{C_e}} \quad [1]$$

$$C(t) = \frac{t}{\frac{1}{B_0} + \frac{t}{C_e}} \quad [2]$$

Determination of Physicochemical Characteristics of Aqueous Extract

Physicochemical characteristics of the resulting aqueous extract were determined, including total dissolved solids (TDS), electrical conductivity (EC), pH, viscosity, and density. During the MAHD process, liquid samples were collected at 30 minutes time of intervals from minute at 30 to 150 to monitor changes in extract properties over time. TDS and EC values in the cinnamon extract were measured using the HORIBA B-173 Conductivity Meter. The EC value indicates the presence of phenolic compounds, while the TDS value indicates the solid material contained in the granules. The density was measured using the ratio between the mass and volume using a pycnometer. Meanwhile, viscosity was determined using a Viscometer Brookfield RTV (Ametec Inc, America) operated at 20 rpm with spindle number 1 (Susanti et al., 2025). The pH value was measured using a Digital pH Meter with mech DrGray.

Gas Chromatography–Mass Spectrometry (GC–MS) Analysis

GC–MS analysis was performed to verify the presence of volatile constituents in the cinnamon essential oils resulting from the best-performing MAHD power treatment. A portion of the extracted oils was introduced into the GC–MS system for compound separation and identification. The instrument was equipped with an Elite-5MS capillary column, and helium served as the carrier gas throughout the run. The detected molecular ion fragments were interpreted by comparing their mass spectra with reference profiles from the NIST Library incorporated in the instrument's software.

RESULTS AND DISCUSSION

Characteristics of the NADES-CAS under the MAHD System

The capability of a solvent to extract bioactive compounds depends on its ability to reach the position of the compound, to bind and bring them out from the inner part of natural resources to the bulk of the solvent. This research evaluated the characteristics of NADES-

CAS as a green solvent in the extraction of bioactive compounds and essential oils from cinnamon through the MAHD method. The parameters of the NADES-CAS characteristics included density, viscosity, total dissolved solids, electric conductivity, and temperature during the MAHD process.

Density of the NADES-CAS

The density of the solvent was evaluated at various MAHD powers, namely 640 W (80%), 720 W (90%), and 800 W (100%). The density is one of the parameters used to evaluate the solvent properties to support the extraction process, besides the solubility in water (Kurniawan et al. 2022). The density of the solvent is shown in Figure 2. It illustrated the relationship between time and density under the MAHD system at various power values of 640, 720, and 800 W.

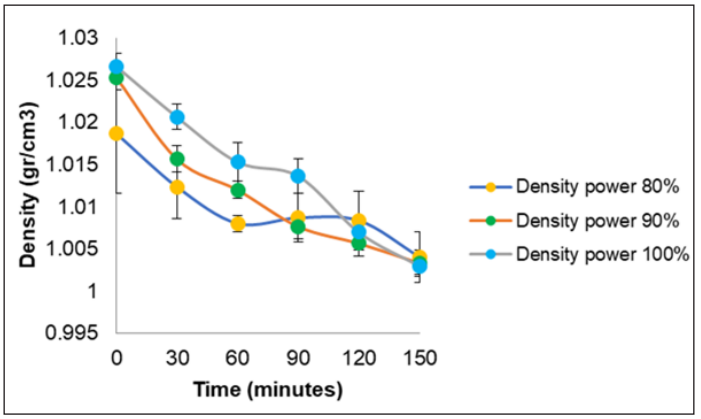

Figure 2. Density value of NADES-CAS during the MAHD process

The density values tended to decrease with increasing extraction time. The longer the extraction time under the microwave, the lower the density of solvent, although the change was not significant. The higher the power of MAHD, the higher the solvent density. The increase in power caused a higher temperature and the evaporation of solvent, which affected its density. This proves that the greater the power used in extraction, the lower the density of the solvent. The results showed that the density value of NADES was higher (1.005 mg/mL to 1.027 mg/mL) than that of pure water (1.0000 mg/mL) (Pires et al., 2022; Susanti et al., 2025).

Viscosity of the NADES-CAS

Viscosity plays a vital role in supporting the solvent's mass transfer into the cinnamon's inner part to collect the substances. Figure 3 shows the profile of the solvent's viscosity

during the MAHD. There was a downward trend in the solvent viscosity corresponding to an increase in the extraction time, although it was not statistically significant. Nevertheless, it was supposed to affect the diffusion of solvent into the pore and internal part of the material to accelerate the extraction.

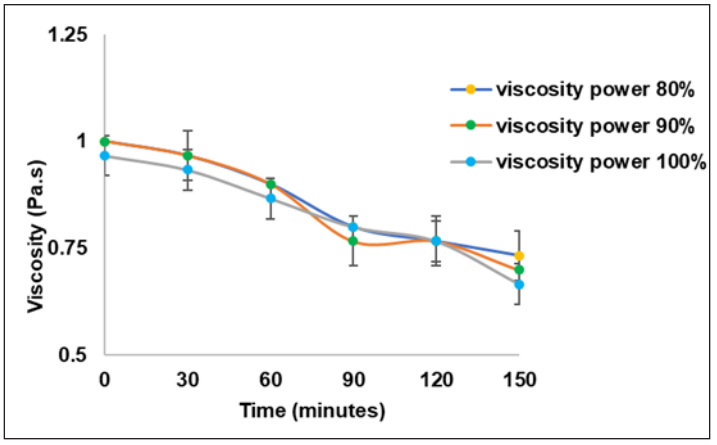

Figure 3. Viscosity value of NADES-CAS during the MAHD process

The decrease in viscosity during the MAHD can be correlated with the increased movement of molecules due to the kinetic energy from microwaves. This particle's movement was expected to accelerate the diffusion of the solvent into the material, thereby extracting the functional compound. The increase in time can cause viscosity to decrease (Mahyati & Azis 2019). The viscosity profiles exhibited similar patterns across the different MAHD power levels. In the extraction method using MAHD with 1% NADES-CAS at various powers, controlling this viscosity is a crucial factor in optimising extraction results to produce essential oils.

Total Dissolved Solids (TDS) of the NADES-CAS

The physical property parameters characterising NADES in this research can be measured by determining the TDS value. Figure 4 shows that the TDS value of NADES-CAS increased significantly with increasing microwave power, with the highest value of 782 mg/L obtained at 800 W and the lowest value of 260.3 mg/L at 640 W. The increase in TDS indicated an increase in the concentration of dissolved solids during extraction. A higher microwave power resulted in more intense heating, thus promoting greater evaporation of water while the solutes remain in the system. When the volume of water decreased, the solution became more concentrated, resulting in higher TDS values. This also reflected the release of more solid compounds from the cinnamon matrix into the NADES solvent during extraction.

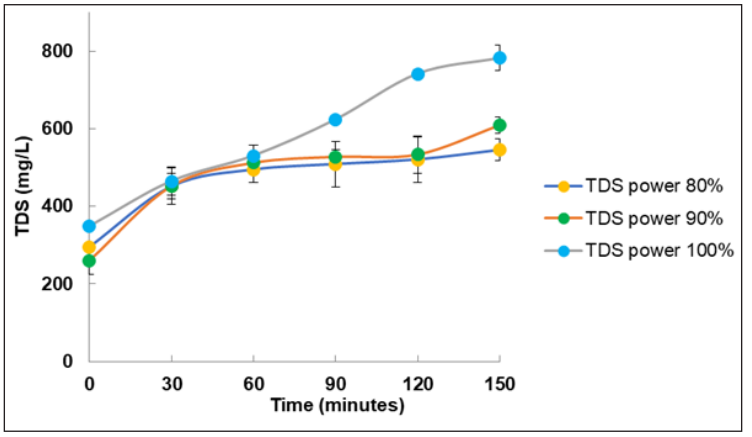

Figure 4. Total dissolved solids of NADES-CAS during the MAHD process

This finding aligns with Várady et al. (2022), who reported that microwave-induced heating enhanced water evaporation, thus increasing solute concentration in extraction systems. Similarly, Igwegbe and Onukwuli (2019) found that higher extraction intensity resulted in higher TDS values due to increased dissolution and release of solid materials into the solvent. Thus, the observed trend was consistent with established mechanisms of microwave-assisted extraction. Overall, the increasing TDS value with higher microwave power confirms that microwave heating promoted both water evaporation and the release of solid compounds into NADES. Therefore, TDS serves as a reliable indicator of the concentration of extracted materials and reflects the efficiency of the MAHD–NADES extraction process.

Electrical Conductivity (EC) of the NADES-CAS

The electrical conductivity (EC) of NADES-CAS increased progressively during the extraction process across all microwave power levels (Figure 5). Additionally, the EC of NADES-CAS increased progressively with increasing power levels.

The increase in EC showed the enhancement of ionic mobility when the internal temperature of the NADES increased under microwave heating. Higher microwave power resulted in faster temperature elevation, which reduced the intermolecular forces in the solvent, promoted ion movement, and ultimately increased conductivity. This heightened ion mobility also improved the ability of NADES-CAS to dissolve polar phenolic compounds from cinnamon, since polar molecules interact more efficiently with highly conductive ionic media. These findings are in line with those of Liu et al. (2018), who reported that temperature was a major determinant of ionic conductivity in liquid systems. Additionally, Fu et al. (2018) demonstrated that an increase in temperature enhanced ion mobility and increased EC of ionic liquid–based solvents, which was consistent with the trend observed

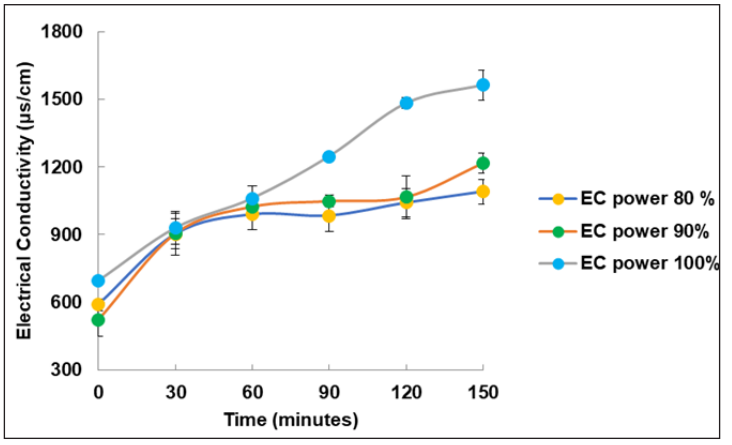

Figure 5. Electrical conductivity of NADES-CAS during the MAHD process

in this study. The increase in EC with increasing microwave power confirms that thermal stimulation significantly enhanced ionic activity in NADES-CAS. This improvement supported more efficient solubilisation of polar phenolics during extraction, indicating that higher microwave power contributed to better extraction performance through increased ionic conductivity.

Solvent Temperature Response at Each Microwave Power

Ionic migration occurs when the electric field generated by microwaves triggers the movement of ions through the process of electrophoresis, where ions move due to changes in the electric field. Heat is generated through friction between ion molecules due to the solvent's resistance to ion migration. Meanwhile, dipole rotation occurs when a continuously fluctuating electric field rotates the dipole molecules in the solvent. In the distillation process using MAHD, the solvent temperature increased along with ion migration activity and dipole rotation, where the rate of temperature increase depends on the dielectric constant and the solvent's response to microwaves. This study used different power variations, starting from 80%, 90% and 100%. The resulting data showed that the power of 80% achieved a temperature of 100 ºC in 14-15 minutes of heating using MAHD. Meanwhile, the power of 90% needed 11-12 minutes, and the power of 100% needed the fastest time, namely 9 minutes, to achieve a temperature of 100 ºC.

Profile of Liquid Extract under MAHD

Electrical Conductivity (EC) of the Extract under MAHD

One of the physical property parameters of the cinnamon extract was EC. The EC value can be seen in Figure 6. The EC value depends on the number of dissolved ions as well as

the type and concentration of ions in the solution. Electrical conductivity (EC) of cinnamon extract is often evaluated to understand its properties in microemulsions, where it interacts with other compounds like tea polyphenols and gallic acid (T. Wang et al. 2023).

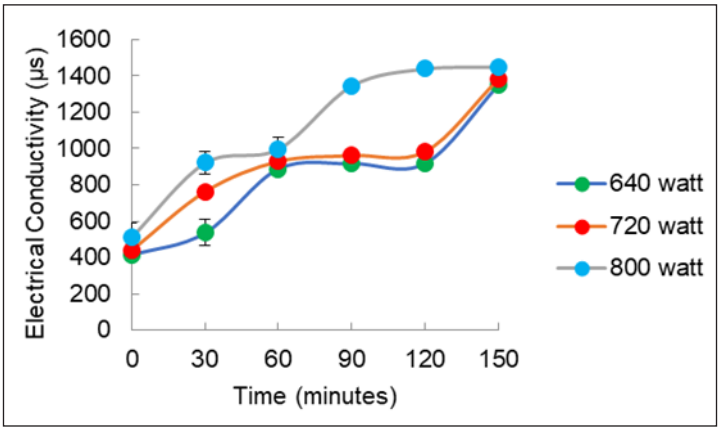

Figure 6. Electrical conductivity (EC) of the extract under MAHD

An increase in EC values with extraction time can be observed in Figure 6, while MAHD at 800 W showed higher EC values compared to the other power levels. This proves that the EC value increased with increasing time and power. In addition, MAHD increased the temperature and pressure on the sample, thereby increasing the number of ions in the solution. The success of an extraction can be seen from the EC value, which was not too high or too low. The EC value obtained in this research was 1450 µs at 800 W, 1383 µs at 720 W, and 1349 µs at 640 W.

Total Dissolved Solids (TDS) of the Extract under MAHD

Besides EC, another physical property parameter of liquid cinnamon extract is the TDS value. The results of TDS values are presented in Figure 7. The high TDS value in the cinnamon extract can identify the presence of compounds such as polyphenols, cinnamaldehyde, and antioxidants. The TDS value of cinnamon extract represents the amount of dissolved substances, such as active and volatile compounds. The value of TDS shows the combination of dissolved organic and inorganic substances as ionised molecules (Rahayu et al. 2019). Based on Figure 7, there was an insignificant increase in the TDS value. TDS value increased with the length of the extraction time. The TDS value obtained from this research was 725 ppm at 800 W, 691 ppm at 720 W, and 674 ppm at power at 640 W. The MAHD at a power of 800 W obtained the highest TDS value because it can increase the temperature and pressure on the sample, accelerating the release of compounds dissolved in the material. The success of an extraction can be seen from the TDS value,

the enhanced release of organic and inorganic constituents from the material resulted in higher TDS values (Izza et al., 2020).

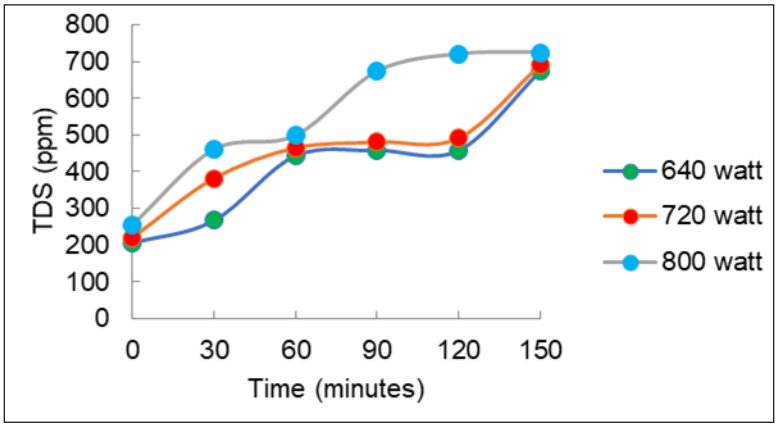

Figure 7. Total dissolved solids (TDS) of the extract under MAHD

Potential of Hydrogen (pH) of the Extract under MAHD

Based on Figure 8, the pH of the extract decreased over time and became more acidic as both the extraction time and microwave power increased. Specifically, the extract exposed to 800 W showed a lower pH value compared to those exposed at 640 W and 720 W. pH measurements were conducted every 30 minutes over 150 minutes at a constant temperature of 100 °C under power levels of 80%, 90%, and 100%. The decrease in pH under higher microwave power can be attributed to enhanced thermal dissociation within the NADES. When the temperature increased, the hydrogen-bonding equilibrium between the hydrogen bond acceptor and donor (HBD, citric acid) shifted, promoting the release of more protons (H^+) into the solution. This increased proton availability resulted in a more acidic (lower pH) environment (Karadendrou et al. 2022). The strength and concentration of hydrogen bonds in the NADES strongly influenced this behavior: a higher HBD content (citric acid) contributed to greater acidity when heated, due to stronger hydrogen-bond interactions and greater dissociation.

These findings are supported by previous studies. Skulcova et al. (2018) stated that the acidity of deep eutectic solvent was significantly influenced by the nature of the HBD, and that pH frequently decreased with temperature increase due to enhanced dissociation of the acid component. A comprehensive review also confirmed that temperature and the chemical identity of the HBD strongly affected the pH behaviour of NADES (Jančíkováet al., 2022). This result observed that increasing microwave power and time led to a more acidic NADES-CAS (lower pH), which was consistent with the known physicochemical behaviour of acid-based eutectic systems. This pH behaviour thereby contributed to the

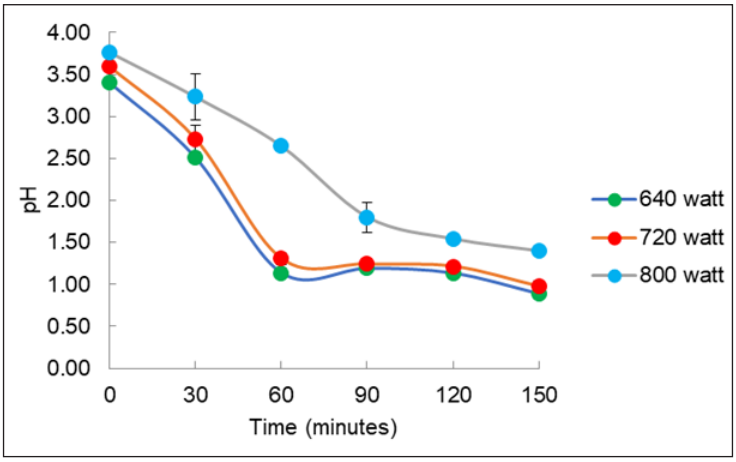

Figure 8. Potential of Hydrogen (pH) of extract under MAHD

enhanced efficiency of phenolic extraction under high-power, high-temperature MAHD conditions.

Total Phenolic Content of the Extract during MAHD

The profile of changes in the amount of Total Phenolic Compound (TPC) extracted in the solvent during the Microwave-Assisted Hydrodistillation (MAHD) process is presented in Figure 9. The TPC value increased with extraction time at all MAHD power levels. At 80% power, TPC increased from approximately 0.30 to 0.40 mg/mL. At higher power levels (90% and 100%), TPC values increased from about 0.45 to 0.65 mg/mL with extraction time. When comparing the power level 90% and 100% at the same extraction time, the difference in TPC values was relatively small, generally within the range of 0.01–0.05 mg/mL The TPC value at a power of 80% was lower than that at powers of 90% and 100% because the energy applied to the cinnamon extract was insufficient to optimally break down the material matrix to limit the release of phenolic compounds. In contrast, higher power levels (90% and 100%) provided greater thermal and microwave-induced molecular movement, enhancing cell wall breakdown and facilitating phenolic diffusion into the solvent. The minimal difference between powers of 90% and 100% indicated that the extraction approached saturation at a power of 90%, where further increases in power no longer produce significant gains. These observations are consistent with prior studies. For example, a microwave extraction study on *Moringa oleifera* leaves (Kheyar et al., 2025), broccoli (Jokićet al., 2025), and *Anoectochilus roxburghii* (Xu et al., 2017) demonstrated that increasing microwave power significantly increased TPC yield. Overall, the TPC extraction profile demonstrated that a microwave power of 90% was sufficient to achieve near-maximum TPC.

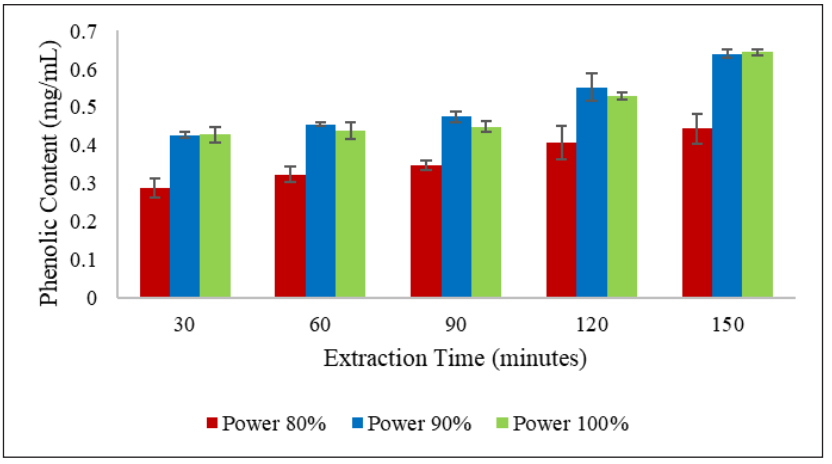

Figure 9. Total phenolic content of the extract during MAHD

The Total Proanthocyanidins Content of Liquid Extract during MAHD

Each solvent has a different dielectric constant, which significantly affects the performance of the extraction process. In this case, the concentration of citric acid and sucrose in distilled water (aquadest) plays an important role in increasing the effectiveness of compound extraction. Citric acid is known to be hygroscopic, allowing it to absorb moisture from its surroundings and thereby maintain the stability of the system. In addition, this compound exhibits good stability against light and air exposure, making it less prone to degradation over time (Luque-Uría et al., 2025). The increase in extraction efficiency is influenced not only by the thermal effects of the solvent but also by the solvent's ability to disrupt and release compounds bound within the material matrix. An effective solvent can enhance the diffusion rate of bioactive constituents, thereby promoting a more efficient release of matrix-bound compounds (Song et al. 2020).

The proanthocyanidin is included in phenolic compounds with many active compounds and was measured using a UV-Vis spectrophotometer. Figure 10 shows that the Total Proanthocyanidin Content (PA) value increased during the Microwave-Assisted Hydrodistillation (MAHD) process, ranging from 0.14 to 0.27 mg/mL. The higher PA results indicated a higher concentration of extracted proanthocyanidin compounds. At a power of 800 W (100%), PA reached a higher value (0.32–0.41 mg/mL), compared to that at powers of 80% and 90%, resulting PA of 0.15–0.26 mg/mL. The PA value of 0.41 mg/mL was achieved at a temperature of 100 °C, a power of 800 W, and an extraction time of 150 minutes. The increase in PA value at high power was due to higher extraction energy, optimal temperature, and better mass transfer efficiency (Izza et al., 2023; Susanti et al., 2020; Susamti et al., 2021). However, power and extraction time must be optimised to ensure energy efficiency and prevent degradation of active compounds.

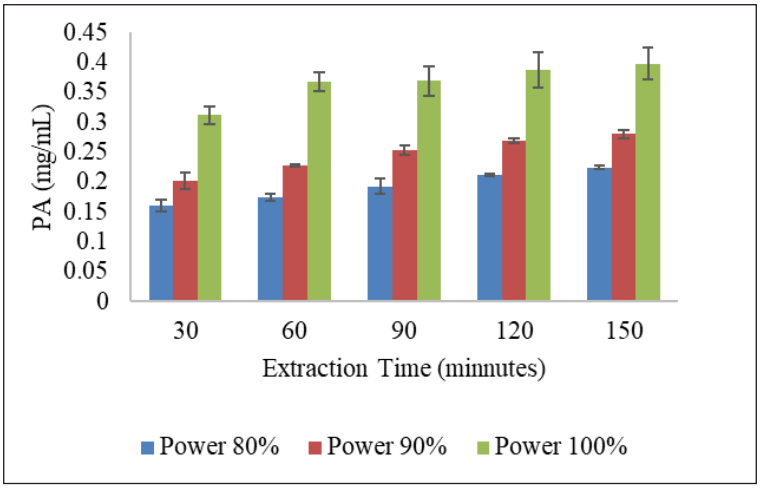

Figure 10. Total proanthocyanidins content of the extract during MAHD

The Application of the Peleg Model in the Extraction

Application of the Peleg Model in the Profile of Total Phenolic Content

The Peleg model interprets the change of TPC during extraction and determines the initial extraction rate constant (B_0) and maximum extraction capacity value (C_e). Table 1 shows that the extraction rate constant (B_0) increased as microwave power rose from 640 W to 800 W. The highest B_0 value was obtained at 800 W (0.03969 mg/mL·min), while the lowest value was obtained at 640 W (0.02642 mg/mL·min). A similar pattern was observed in the equilibrium concentration (C_e), where C_e increased with power, although the difference between 720 W and 800 W was relatively small (0.06785 to 0.066072 mg/mL). Figure 11 further confirms that the Peleg model predictions closely followed the experimental data under all power levels.

The increase in B_0 reflects the faster initial extraction rate when greater microwave power is applied. Higher power enhances internal heating through rapid dipole rotation and ionic conduction, resulting in cell disruption and accelerated release of polyphenols. However, the limited increase from 720 W to 800 W suggests the system approaches thermal saturation, where additional energy no longer significantly accelerates diffusion. The C_e behaviour indicates that 720 W is already sufficient to reach near-maximum extraction capacity. At the lowest power (640 W), both B_0 and C_e were markedly reduced, implying insufficient heat to overcome mass-transfer resistance and fully disrupt the cinnamon matrix.

These observations are in line with previous studies showing that the microwave transmitted to the solvent caused an increasing temperature, causing an increase in the extraction rate value (Sonar & Rathod 2020). The ability of the Peleg model to accurately describe extraction kinetics has also been reported for phenolic extractions from plant

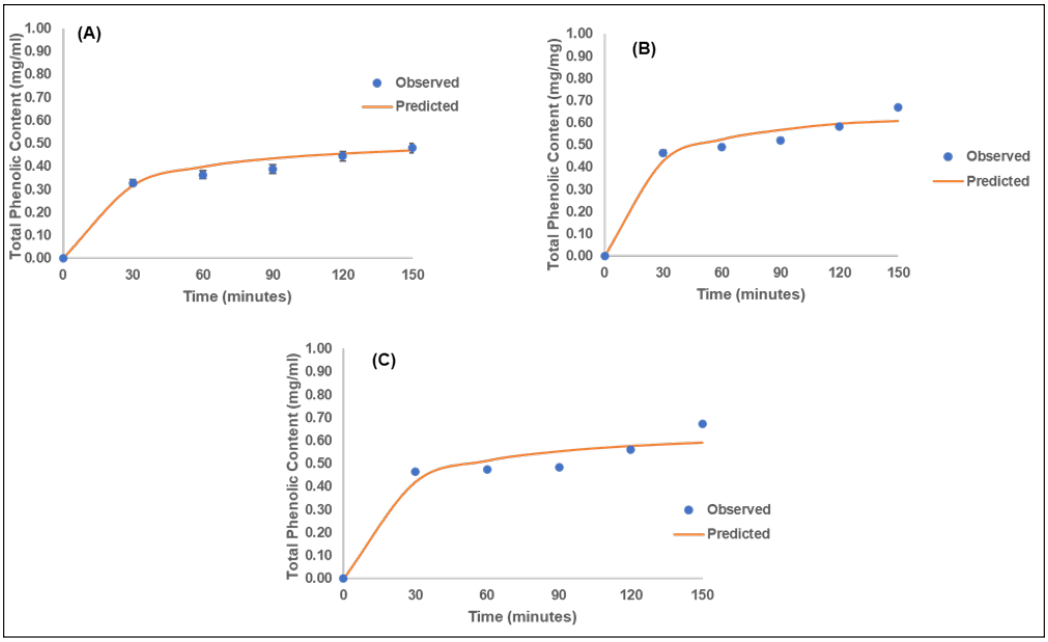

Figure 11. Observed and predicted total phenolic content during MAHD at (A) 640, (B) 720, (C) 800 W

Table 1
Peleg model parameters and validation statistics for the extraction of total phenolic content (TPC) from cinnamon at different microwave-assisted hydrodistillation (MAHD) power levels

The Peleg Model Parameters			Validation Parameters			
Power	B_0	C_e	**SSE**	**RMSE**	**X²**	**R²**
(W)	(mg/mL.min)	(mg/mL)				
640	0.0264	0.5349	0.0079	0.0481	0.0031	0.9810
720	0.0389	0.6785	0.0096	0.0561	0.0038	0.9655
800	0.0397	0.6607	0.0155	0.0718	0.0061	0.9422

matrices, where B_0 correlates with the initial diffusion rate and C_e represents the maximum achievable concentration under given conditions (Pamungkas et al., 2025; Susanti et al., 2025). Overall, the close agreement between predicted and experimental data indicates that the Peleg model is a reliable tool for characterising and forecasting the extraction of TPC from cinnamon behaviour under MAHD conditions.

Application of the Peleg Model in the Profile of Proanthocyanidin Content

Proanthocyanidin (PA) was one of the main target compounds in cinnamon extract due to its strong antioxidant activity (Paquet-Durand et al. 2015). The extraction performance was quantitatively evaluated using the Peleg kinetic model, which provided the extraction rate

constant (B_0) and the maximum extraction capacity (C_e). As shown in Table 2, the highest B_0 value (0.11171 mg/mL·min) was obtained at 800 W, while the lowest B_0 (0.03878 mg/mL·min) was obtained at 640 W. This trend indicates that higher microwave power significantly accelerated the release of PA into the NADES-CAS solvent. As discussed previously, the Peleg model also performed best in predicting the profile of proanthocyanidin during the MAHD. Prediction in each power of MAHD, as shown in Figure 12, illustrated the match value between the predicted proanthocyanidin concentration using the Peleg model and the observed data. It was also supported by the values of several validation parameters, such as SSE, RMSE, X^2, and R^2, presented in Table 2.

Table 2
Peleg model parameters and validation statistics for the extraction of proanthocyanidin (PA) from cinnamon at different microwave-assisted hydrodistillation (MAHD) power levels

The Parameters of the Peleg Model			The Validation Parameters			
Power	B_0	C_e	**SSE**	**RMSE**	**X^2**	**R^2**
(W)	(mg/ mL.min)	(mg/mL)				
640	0.0388	0.5529	0.0024	0.0263	0.0009	0.9939
720	0.0425	0.7300	0.0023	0.0276	0.0009	0.9932
800	0.1117	0.9439	0.0018	0.0214	0.0007	0.9989

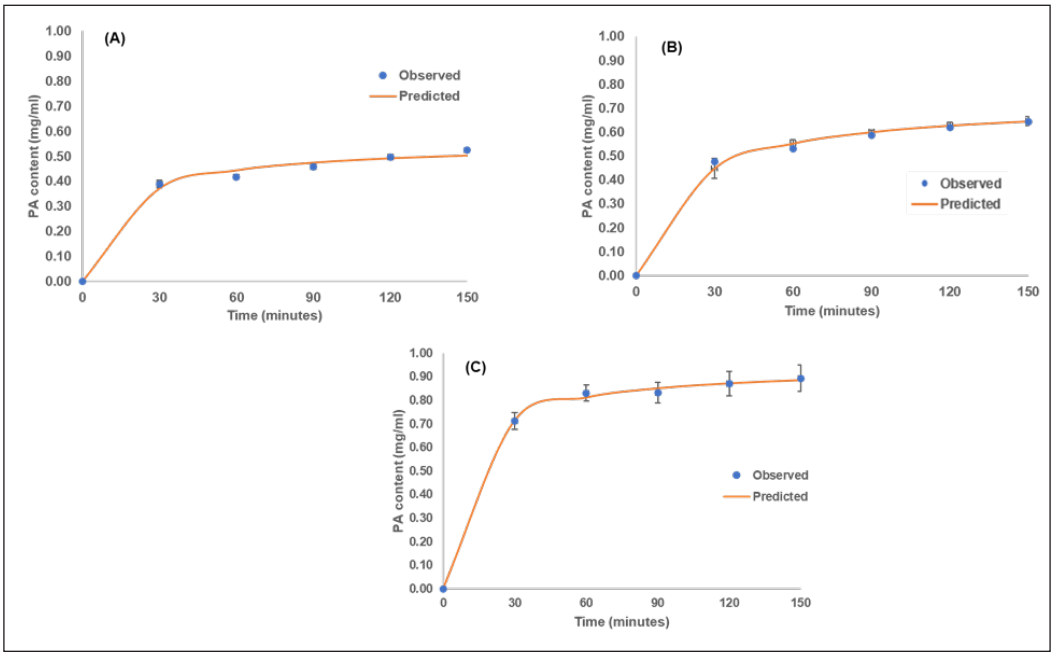

Figure 12. Observed and predicted Proanthocyanidin content during MAHD at (A) 640, (B) 720, (C) 800 W

The increase in B_0 with greater microwave power reflects the enhanced mass-transfer rate during extraction. At 800 W, the rapid internal heating of the solvent and sample matrix allowed the system to reach 100 °C more quickly than at 720 W or 640 W. The elevated temperature enhanced cell wall rupture, reduced solvent viscosity, and accelerated diffusion, enabling more efficient solubilization of PA compounds. Consequently, high power improved both the initial extraction rate and the approach toward the maximum PA concentration. The high extraction temperature increased the diffusion and weakened the plant cell wall and membrane integrity, thereby enhancing solvent penetration and facilitating the release of proanthocyanidins into the extract. Several studies noted that the rise in proanthocyanidin yield at elevated temperatures was associated with greater diffusion rates and the thermal or physical disruption of cell wall structures (Zhang et al., 2018; Thilakarathna et al., 2022; Shi et al., 2022).

The maximum extraction capacity constant (C_e) value was proportional to the initial extraction rate (B_0). At a power of 800 W, the extraction process produced the highest C_e value of 0.9439 mg/mL. It indicates the optimal maximum capacity for releasing proanthocyanidins from cinnamon. The presence of NADES supported the stability of the PA compound at high temperatures, likely due to strong hydrogen-bond interactions between NADES components and the proanthocyanidin molecules, and protected against thermal degradation (Li, 2022; Hikmawati et al., 2021; Silva et al., 2024). At a lower power of 640 W, the extraction resulted in the lowest B_0 value of 0.03878 mg/mL.min, and the lowest C_e value of 0.5529 mg/mL.

The Essential Oil from MAHD

This research assessed the combination of NADES-CAS and microwave for its ability to extract the functional compounds and essential oils from cinnamon. As discussed, the combination proved successful in extracting phenolics, including proanthocyanidins, which are antioxidant compounds in cinnamon. The phenolic compound was released in the bulk of the solvent and remained in the extraction flask. At the same time, the essential oils evaporated with water vapour after they were released from the internal part of the cinnamon. The heat generated from the interaction of the microwave with cinnamon and solvent material supported this evaporation. The evaporation was also supported by the NADES, which created an abrasion and enlarged the pore to support the evaporation of essential oil from the internal part of the cinnamon powder. The essential oil was separated from the water vapour through a distillation process using a cold condenser that settled on the top of the microwave system. The maximum yield of essential oil was achieved at a microwave power of 800 W, which resulted in 0.4% of cinnamon powder. Meanwhile, microwave powers of 720 and 640 W only resulted in 0.22% and 0.18% of cinnamon powder, respectively.

The essential oil extracted from cinnamon bark (*Cinnamomum* spp.) powder has a distinctive aroma due to its several essential oil compounds. The main components are dominated by aromatic aldehyde, terpenoid, and phenylpropane compounds, which play an important role in biological activity and their application in various industries. The essential oil resulting from the MAHD was evaluated to identify the active constituents in the essential oil using the gas chromatography-mass spectrometry (GC-MS) method. The results of GC-MS analysis allow the identification of components based on compound name, molecular weight, and chemical structure, providing detailed information on the chemical profile of cinnamon bark essential oil (Chokkavarapu & Mandla 2019).

Table 3 describes that the essential oil from MAHD of cinnamon essential powder had several main compounds, concluding Cinnamaldehyde (74.982%), Caryophyllene (0.982%), Benzaldehyde (0.438%), and Pinene (0.12%). Cinnamaldehyde is the main component of cinnamon bark, giving a distinctive sweet and spicy aroma. It has antimicrobial and anti-inflammatory activities. The molecular formula in Cinnamaldehyde is C_9H_8O, which consists of 9 carbon atoms, 8 hydrogen atoms, and 1 oxygen atom. The compound contains a benzene (phenyl) ring connected to a carbon-aldehyde chain (CHO) (Friedman, 2017; Guo et al., 20204; Kim et al., 2020). Cinnamaldehyde was the dominant component in the sample, with a total contribution of 74.982%. The presence of two peaks at different retention time (RT) indicates the presence of trans-cinnamaldehyde and cis-cinnamaldehyde isomers. The presence of two peaks can also be caused by heating on the GC-MS device, which can convert some of the trans-cinnamaldehyde to cis-cinnamaldehyde. Cinnamaldehyde was the major compound of the essential oil from cinnamon obtained using MAHD with NADES-CAS solvent. Meanwhile, the others were detected as Caryophyllene, Benzaldehyde, and Pinene.

Table 3
The major volatile compound in the essential oil from cinnamon

No	Retention Time (min)	Name of Compound	Peak Area %
1	12.825; 15.704	Cinnamaldehyde	74.982
2	21.841; 20.606; 22.647	Caryophyllene	0.982
3	7.24; 10.112	Benzaldehyde	0.438
4	7.165; 8.526	Pinene	0.12

CONCLUSION

The combination of Microwave-Assisted Hydrodistillation (MAHD) and the Natural Deep Eutectic Solvent Citric Acid–Sucrose (NADES-CAS) was successfully applied for the simultaneous extraction of phenolic compounds, proanthocyanidins, and essential oils from cinnamon powder. The NADES-CAS (1:1 molar ratio, 1% concentration) demonstrated distinct physicochemical changes under increasing microwave power

(640–800 W), including increased EC, TDS, and temperature, and decreased density, viscosity, and pH. Application of the Peleg model showed high accuracy in predicting the extraction kinetics, with extraction rates (B_0) in the range of 0.0264–0.0397 mg/mL·min for phenolics and 0.0388–0.1117 mg/mL·min for proanthocyanidins, and maximum capacities (C_e) in the range of 0.5349–0.6607 mg/mL for phenolics and 0.5529–0.9439 mg/mL for proanthocyanidins, respectively. Higher microwave power increased both B_0 and C_e values, confirming the acceleration effect on mass transfer during extraction. The MAHD–NADES system also produced cinnamon essential oil with a yield of 0.18–0.40%, dominated by cinnamaldehyde, along with caryophyllene, benzaldehyde, and pinene.

Practically, these findings demonstrated that combining MAHD with a green solvent can shorten extraction time, enhance mass transfer efficiency, and simultaneously recover high-value bioactive compounds and essential oils. This approach offers a scalable, energy-efficient alternative for the extraction industry, particularly for phytochemical and functional ingredient production, enabling faster processing with reduced solvent use and improved yield consistency.

ACKNOWLEDGEMENT

The author would like to thank the "Direktorat Penelitian dan Pengabdian kepada Masyarakat, Direktorat Jenderal Riset dan Pengembangan, Kementerian Pendidikan Tinggi, Sains, dan Teknologi Indonesia and Direktorat Penelitian Universitas Gadjah Mada" for funding the research through "Penelitian Fundamental BIMA" with agreement numbers "048/E5/PG.02.00.PL/2024 and 2694/UN1/DITLIT/PT.01.03/2024".

REFERENCES

Adeel, S., Habib, N., Arif, S., ur Rehman, F., Azeem, M., Batool, F., & Amin, N. (2020). Microwave-assisted eco-dyeing of bio mordanted silk fabric using cinnamon bark (*Cinnamomum verum*) based yellow natural dye. *Sustainable Chemistry and Pharmacy, 17*. https://doi.org/10.1016/j.scp.2020.100306

AlYammahi, J., Darwish, A. S., Almustafa, G., Lemaoui, T., AlNashef, I. M., Hasan, S. W., Taher, H., & Banat, F. (2023). Natural deep eutectic solvents for ultrasonic-assisted extraction of nutritious date sugar: Molecular screening, experimental, and prediction. *Ultrasonics Sonochemistry*, *98*, Article 106514. https://doi.org/10.1016/j.ultsonch.2023.106514

Azeez, L., Adebisi, S. A., Oyedeji, A. O., Adetoro, R. O., & Tijani, K. O. (2019). Bioactive compounds' contents, drying kinetics and mathematical modelling of tomato slices influenced by drying temperatures and time. *Journal of the Saudi Society of Agricultural Sciences*, *18*(2), 120-126. https://doi.org/10.1016/j.jssas.2017.03.002

Bonacci, S., Di Gioia, M. L., Costanzo, P., Maiuolo, L., Tallarico, S., & Nardi, M. (2020). Natural deep eutectic solvent as extraction media for the main phenolic compounds from olive oil processing wastes. *Antioxidants*, *9*(6), Article 513. https://doi.org/10.3390/antiox9060513

Chokkavarapu, N., & Mandla, V. R. (2019). Comparative study of GCMs, RCMs, downscaling and hydrological models: A review toward future climate change impact estimation. *SN Applied Sciences*, *1*(12), 1-15. https://doi.org/10.1007/s42452-019-1764-x

Cravotto, C., Fabiano-Tixier, A. S., Bartier, M., Claux, O., & Tabasso, S. (2024a). Green extraction of hemp seeds cake (*Cannabis sativa* L.) with 2-methyloxolane: A response surface optimisation study. *Sustainable Chemistry and Pharmacy*, *39*, Article 101509. https://doi.org/10.1016/j.scp.2024.101509

Cravotto, C., Grillo, G., Boffa, L., Fabiano-Tixier, A. S., Bartier, M., Jacques, L., & Tabasso, S. (2024b). Microwave-assisted extraction of phytochemicals from *Cannabis sativa* L. inflorescences with 2-methyloxolane. *Sustainable Chemistry and Pharmacy*, *42*, Article 101812. https://doi.org/10.1016/j.scp.2024.101812

de Souza V. B., Thomazini, M., Barrientos, E., Nalin, C. M., Ferro-Furtado, R., Genovese, M. I., & Favaro-Trindade, C. S. (2018). Functional properties and encapsulation of a proanthocyanidin-rich cinnamon extract (*Cinnamomum zeylanicum*) by complex coacervation using gelatin and different polysaccharides. *Food Hydrocolloids*, *77*, 297-306. https://doi.org/10.1016/j.foodhyd.2017.08.006

Deshi, V. V., Awati, M. G., Terdal, D., Patil, S. N., Ghandhe, A. R., Gudigennavar, A. S., Patalli, P., Lata, D., Ram Sing, D., & Siddiqui, M. W. (2024). Cinnamon essential oil incorporated chitosan submicron emulsion as a sustainable alternative for extension of mango shelf life. *Sustainable Chemistry and Pharmacy*, *41*, Article 101736. https://doi.org/10.1016/j.scp.2024.101736

Friedman, M. (2017). Chemistry, antimicrobial mechanisms, and antibiotic activities of cinnamaldehyde against pathogenic bacteria in animal feeds and human foods. *Journal of Agricultural and Food Chemistry*, *65*(48), 10406-10423. https://doi.org/10.1021/acs.jafc.7b04344

Fu, Y., Cui, X., Zhang, Y., Feng, T., He, J., Zhang, X., Bai, X., & Cheng, Q. (2018). Measurement and correlation of the electrical conductivity of the ionic liquid [BMIM][TFSI] in binary organic solvents. *Journal of Chemical & Engineering Data*, *63*(5), 1180-1189. https://doi.org/10.1021/acs.jced.7b00646

Guddi, K., & Sarkar, A. (2024). Optimisation of green extraction technologies for recovering bioactive compounds from *Ixora coccinea* waste flower biomass: A comparative response surface methodology and artificial neural network modelling. *Sustainable Chemistry and Pharmacy*, *42*, Article 101830. https://doi.org/10.1016/j.scp.2024.101830

Guo, J., Yan, S., Jiang, X., Su, Z., Zhang, F., Xie, J., Hao, E., & Yao, C. (2024). Advances in pharmacological effects and mechanism of action of cinnamaldehyde. *Frontiers in Pharmacology*, *15*, Article 1365949. https://doi.org/10.3389/fphar.2024.1365949

Igwegbe, C. A., & Onukwuli, O. D. (2019). Removal of total dissolved solids (TDS) from aquaculture wastewater by coagulation-flocculation process using *Sesamum indicum* extract: Effect of operating parameters and coagulation-flocculation kinetics. *The Pharmaceutical and Chemical Journal, 6*(4), 32-45.

Izza, H. F., Susanti, D. Y., Mariyam, S., & Saputro, A. D. (2023). Performance of microwave-assisted extraction of proanthocyanidins from red sorghum grain in various power and citric acid concentration. *Journal of the Saudi Society of Agricultural Sciences, 22*(7), 480-492. https://doi.org/10.1016/j.jssas.2023.05.002

Jančíková, V., Jablonský, M., Voleková, K., & Šurina, I. (2022). Summarising the effect of acidity and water content of deep eutectic solvent-like mixtures—A review. *Energies*, *15*(24), Article 9333. https://doi.org/10.3390/en15249333

Jeyaratnam, N., Nour, A. H., Kanthasamy, R., Nour, A. H., Yuvaraj, A. R., & Akindoyo, J. O. (2016a). Essential oil from *Cinnamomum cassia* bark through hydrodistillation and advanced microwave-assisted hydrodistillation. *Industrial Crops and Products, 92*, 57-66. https://doi.org/10.1016/j.indcrop.2016.07.049

Jeyaratnam, N., Nour, A. H., & Akindoyo, J. O. (2016b). The potential of microwave-assisted hydrodistillation in extraction of essential oil from *Cinnamomum cassia* (cinnamon). *ARPN Journal of Engineering and Applied Sciences, 11*(4), 2179-2183.

Jokić, S., Cvjetko, M., Božić, Đ., Fabek, S., Toth, N., Vorkapić-Furač, J., & Redovniković, I. R. (2012). Optimisation of microwave-assisted extraction of phenolic compounds from broccoli and its antioxidant activity. *International Journal of Food Science and Technology*, *47*(12), 2613-2619. https://doi.org/10.1111/j.1365-2621.2012.03143.x

Kalpoutzakis, E., Chatzimitakos, T., Athanasiadis, V., Mitakou, S., Aligiannis, N., Bozinou, E., Gortzi, O., Skaltsounis, L. A., & Lalas, S. I. (2023). Determination of the total phenolics content and antioxidant activity of extracts from parts of plants from the Greek island of Crete. *Plants, 12*(5), Article 1092. https://doi.org/10.3390/plants12051092

Karadendrou, M. A., Kostopoulou, I., Kakokefalou, V., Tzani, A., & Detsi, A. (2022). L-proline-based natural deep eutectic solvents as efficient solvents and catalysts for the ultrasound-assisted synthesis of aurones via Knoevenagel condensation. *Catalysts, 12*(3), Article 249. https://doi.org/10.3390/catal12030249

Kheyar, F., Kheyar, N., Amiali, M., Boulekbache-Makhlouf, L., Kadi, A., Benchabane, A., & Bitam, A. (2025). Impacts of microwave-assisted extraction parameters on total phenolic compounds yield from Algerian Moringa oleifera leaves, using response surface methodology. *Natural Product Research*, *39*(14), 4126-4134. https://doi.org/10.1080/14786419.2024.2333044

Kim, N. Y., Trinh, N. T., Ahn, S. G., & Kim, S. A. (2020). Cinnamaldehyde protects against oxidative stress and inhibits the TNF-α-induced inflammatory response in human umbilical vein endothelial cells. *International Journal of Molecular Medicine*, *46*(1), 449-457. https://doi.org/10.3892/ijmm.2020.4582

Kupina, S., Fields, C., Roman, M. C., & Brunelle, S. L. (2019). Determination of total phenolic content using the Folin-C assay: Single-laboratory validation, first action 2017.13. *Journal of AOAC International, 102*(1), 320-321. https://doi.org/10.1093/jaoac/102.1.320

Kurniawan, N. I., Lujala, P., Rye, S. A., & Vela-Almeida, D. (2022). The role of local participation in the governance of natural resource extraction. *Extractive Industries and Society, 9*, 26-29. https://doi.org/10.1016/j.exis.2021.101029

Li, D. (2022). *Natural deep eutectic solvents in phytonutrient extraction and other applications*. *Frontiers in Plant Science, 13,* Article 1004332. https://doi.org/10.3389/fpls.2022.1004332

Liu, Y., Friesen, J. B., McAlpine, J. B., Lankin, D. C., Chen, S. N., & Pauli, G. F. (2018). Natural deep eutectic solvents: Properties, applications, and perspectives. *Journal of Natural Products, 81*(3), 679-690. https://doi.org/10.1021/acs.jnatprod.7b00945

Loto, R. T. (2020). Evaluation of the corrosion inhibition effect of the combined admixture of rosemary and cinnamon cassia oil on mild steel in weak acid electrolyte. *Sustainable Chemistry and Pharmacy, 17*, Article 100298. https://doi.org/10.1016/j.scp.2020.100298

Mahyati, & Azis, A. (2019). Optimisation of temperature and time in carrageenan extraction of seaweed (*Kappaphycus alvarezii*) using ultrasonic wave extraction methods. *IOP Conference Series: Earth and Environmental Science, 370*(1), Article 012076. https://doi.org/10.1088/1755-1315/370/1/012076

Maierean, S. M., Serban, M. C., Sahebkar, A., Ursoniu, S., Serban, A., Penson, P., & Banach, M. (2017). The effects of cinnamon supplementation on blood lipid concentrations: A systematic review and meta-analysis. *Journal of Clinical Lipidology, 11*(6), 1393-1406. https://doi.org/10.1016/j.jacl.2017.08.004

Medina-Torres, N., Ayora-Talavera, T., Espinosa-Andrews, H., Sánchez-Contreras, A., & Pacheco, N. (2017). Ultrasound assisted extraction for the recovery of phenolic compounds from vegetable sources. *Agronomy, 7*(3), Article 47. https://doi.org/10.3390/agronomy7030047

Mulia, K., Krisanti, E., Terahadi, F., & Putri, S. (2015). Selected natural deep eutectic solvents for the extraction of α-mangostin from mangosteen (*Garcinia mangostana* L.) pericarp. *International Journal of Technology, 6*(7), 1211-1220. https://doi.org/10.14716/ijtech.v6i7.1984

Oroian, M. (2017). The temperature hydration kinetics of *Lens culinaris*. *Journal of the Saudi Society of Agricultural Sciences, 16*(3), 250–256. https://doi.org/10.1016/j.jssas.2015.08.004

Pages-Rebull, J., Pérez-Ràfols, C., Serrano, N., & Díaz-Cruz, J. M. (2024). Analytical methods for cinnamon authentication. *Trends in Food Science and Technology, 146*, Article 104388. https://doi.org/10.1016/j.tifs.2024.104388

Pamungkas, K. D., Karyadi, J. N. W., Setyaningsih, W., & Susanti, D. Y. (2025). Microwave-Assisted Extraction's Kinetics of Phycobiliprotein from Spirulina Platensis: Influence of Citric Acid Concentration. *Trends in Sciences*, *22*(7), Article 10042. https://doi.org/10.48048/tis.2025.10042

Paquet-Durand, O., Zettel, V., Kohlus, R., & Hitzmann, B. (2015). Optimal design of experiments and measurements of the water sorption process of wheat grains using a modified Peleg model. *Journal of Food Engineering, 165*, 166-171. https://doi.org/10.1016/j.jfoodeng.2015.06.025

Pires, I.V., Sakurai, Y. C. N., Ferreira, N. R., Moreira, S. G. C., da Cruz Rodrigues, A. M., & da Silva, L. H. M. (2022). Elaboration and characterisation of natural deep eutectic solvents (NADESs): Application in the extraction of phenolic compounds from pitaya. *Molecules*, *27*(23), Article 8310. . https://doi.org/10.3390/molecules27238310

Purdi, T. S., Setiowati, A. D., & Ningrum, A. (2023). Ultrasound-assisted extraction of *Spirulina platensis* protein: Physicochemical characteristic and techno-functional properties. *Journal of Food Measurement and Characterisation, 17*(5), 5474-5486. https://doi.org/10.1007/s11694-023-02051-y

Rahayu, S., Alsuhendra, & Ridawati. (2019). The pH value, total dissolved solid and sensory profile of silky pudding with 'Secang' wood extract (*Caesalpinia sappan* L.). *KnE Social Sciences, 3*(12), 428-437. https://doi.org/10.18502/kss.v3i12.4110

Savi, L. K., Dias, M. C. G. C., Carpine, D., Waszczynskyj, N., Ribani, R. H., & Haminiuk, C. W. I. (2019). Natural deep eutectic solvents (NADES) based on citric acid and sucrose as a potential green technology: a comprehensive study of water inclusion and its effect on thermal, physical and rheological properties. *International Journal of Food Science and Technology*, *54*(3), 898-907. https://doi.org/10.1111/ijfs.14013

Segatto, M. L., Schnarr, L., Olsson, O., Kümmerer, K., & Zuin, V. G. (2022). Ionic liquids vs. ethanol as extraction media of algicidal compounds from mango processing waste. *Frontiers in Chemistry, 10*, Article 986987. https://doi.org/10.3389/fchem.2022.986987

Shi, L., Zhao, W., Yang, Z., Subbiah, V., & Suleria, H. A. R. (2022). Extraction and characterisation of phenolic compounds and their potential antioxidant activities. *Environmental Science and Pollution Research, 29*(54), 81112-81129. https://doi.org/10.1007/s11356-022-23337-6

Silva, C. N. d., Silva, R. M. d., Lemes, A. C., & Ribeiro, B. D. (2024). *Recovery of phenolic compounds by deep eutectic solvents in orange by-products and spent coffee grounds. Sustainability, 16*(17), Article 7403. https://doi.org/10.3390/su16177403

Skulcova, A., Russ, A., Jablonsky, M., & Sima, J. (2018). The pH behavior of seventeen deep eutectic solvents. *BioResources*, *13*(3), 5042-5051. https://doi.org/10.15376/biores.13.3.5042-5051

Sonar, M. P., & Rathod, V. K. (2020). Extraction of type II antidiabetic compound corosolic acid from *Lagerstroemia speciosa* by batch extraction and three phase partitioning. *Biocatalysis and Agricultural Biotechnology, 27,* Article 101694. https://doi.org/10.1016/j.bcab.2020.101694

Song, P., Hsu, C. H., Vignale, G., Zhao, M., Liu, J., Deng, Y., Fu, W., Liu, Y., Zhang, Y., Lin, H., Pereira, V. M., & Ping Loh, K. (2020). Coexistence of large conventional and planar spin Hall effect with long spin diffusion length in a low-symmetry semimetal at room temperature. *Nature Materials, 19*(3), 292-298. https://doi.org/10.1038/s41563-019-0600-4

Susanti, D. Y., Sediawan, W. B., Fahrurrozi, M., & Hidayat, M. (2020). Optimisation of agitation and kinetic studies on proanthocyanidin compound extraction from red sorghum grains in agitated vessel. *IOP Conference Series: Materials Science and Engineering, 778*(1), Article 012085. https://doi.org/10.1088/1757-899X/778/1/012085

Susanti, D. Y., Sediawan, W. B., Fahrurrozi, M., & Hidayat, M. (2021). The effects of ultrasound wave on the extraction of proanthocyanidins from red sorghum grain using green solvent and a kinetics model of the extraction. *Key Engineering Materials, 884*, 212-219. https://doi.org/10.4028/www.scientific.net/KEM.884.212

Susanti, D. Y., Kalyani, N. F., Astuti, F. P., Purwandari, F. A., Kurniawan, M. P., Kistanti, A., Pamungkas, K.D., & Setyaningsih, W. (2025). Characterisation and performance evaluation of NADES-CAF in ultrasound and microwave extraction of phycocyanin from *Arthrospira platensis*. *International Journal of Design & Nature and Ecodynamics*, *20*(1), 21-30. *https://doi.org/10.18280/ijdne.200103*

Thilakarathna, W. P. D. W., & Rupasinghe, H. P. V. (2022). Optimisation of the extraction of proanthocyanidins from grape seeds using ultrasonication-assisted aqueous ethanol and evaluation of anti-steatosis activity in vitro. *Molecules, 27*(4), Article 1363. https://doi.org/10.3390/molecules27041363

Várady, M., Tauchen, J., Klouček, P., & Popelka, P. (2022). Effects of total dissolved solids, extraction yield, grinding, and method of preparation on antioxidant activity in fermented specialty coffee. *Fermentation, 8*(8), Article 375. https://doi.org/10.3390/fermentation8080375

Wang, J. D., Yang, S. L., Liu, G. S., Zhou, Q., Fu, L. N., Gu, Q., Cai, Z. H., Zhang, S., & Fu, Y. J. (2024). A degradable multi-functional packaging based on chitosan/silk fibroin via incorporating cellulose

nanocrystals-stabilised cinnamon essential oil Pickering emulsion. *Food Hydrocolloids, 153*, Article 109978. https://doi.org/10.1016/j.foodhyd.2024.109978

Wang, T., Xu, H., Dong, R., Wu, S., Guo, Y., & Wang, D. (2023). Effectiveness of targeting the NLRP3 inflammasome by using natural polyphenols: A systematic review of implications on health effects. *Food Research International, 165*, Article 112567. https://doi.org/10.1016/j.foodres.2023.112567

Xu, M., Shao, Q., Ye, S., Li, S., Wu, M., Ding, M., & Li, Y. (2017). Simultaneous extraction and identification of phenolic compounds in *Anoectochilus roxburghii* using microwave-assisted extraction combined with UPLC-Q-TOF-MS/MS and their antioxidant activities. *Frontiers in Plant Science*, *8*, Article 1474. https://doi.org/10.3389/fpls.2017.01474

Yılmaz, F. M., Görgüç, A., Uygun, Ö., & Bircan, C. (2021). Steviol glycosides and polyphenols extraction from *Stevia rebaudiana* Bertoni leaves using maceration, microwave-, and ultrasound-assisted techniques. *Separation Science and Technology, 56*(5), 936-948. https://doi.org/10.1080/01496395.2020.1743311

Zhang, K. X., Ye, W. Q., Yun, S. J., Zhou, Z. Y., Yu, S., Piao, X. C., Jiang, J., & Lian, M. L. (2024). Green flash extraction optimisation of *Cynanchum wilfordii* adventitious roots and evaluation of their cancer cell inhibition. *Sustainable Chemistry and Pharmacy, 42*, Article 101859. https://doi.org/10.1016/j.scp.2024.101859

Zhang, Q.-W., Lin, L.-G., & Ye, W.-C. (2018). Techniques for extraction and isolation of natural products: A comprehensive review. *Chinese Medicine, 13*(1), Article 20. https://doi.org/10.1186/s13020-018-0177-x

Pertanika J. Trop. Agric. Sci. 49 (S1): 171 - 192 (2026)

PERTANIKA JOURNALS

TROPICAL AGRICULTURAL SCIENCE

Journal homepage: http://www.pertanika.upm.edu.my/

Physical Properties and Mass Modelling of Matoa Fruit (*Pometia pinnata*) at Different Varieties

Mohd Hafizz Wondi[1]*, Nur Izzah Nabilah Haris[2], Maimunah Mohd Ali[3], Sharifah Raina Manaf[1], Abdul Rahman Saili[4], Akmal Shafiq Badarul Azam[5], Bernard Maringgal[6], Muhammad Hazwan Hamzah[7], and Muhammad Shahimi Ariffin[5]

[1]Faculty of Plantation and Agrotechnology, Universiti Teknologi MARA Sarawak Branch, 96400 UiTM Mukah, Sarawak, Malaysia
[2]Department of Chemical and Environmental Engineering, Faculty of Engineering, University Putra Malaysia, 43400 UPM Serdang, Selangor, Malaysia
[3]Department of Food Sciences, Faculty of Science and Technology, Universiti Kebangsaan Malaysia, 43600 UKM Bangi, Selangor, Malaysia
[4]Faculty of Plantation and Agrotechnology, Universiti Teknologi MARA Cawangan Sarawak, 94300 UiTM Kota Samarahan, Sarawak, Malaysia
[5]Center of Mathematical Sciences, Faculty of Computer and Mathematical Sciences, Universiti Teknologi MARA Sarawak Branch, 96400 UiTM Mukah, Sarawak, Malaysia
[6]Faculty of Resource Science and Technology, Universiti Malaysia Sarawak, 94300 UNIMAS Kota Samarahan, Sarawak, Malaysia
[7]Department of Biological and Agricultural Engineering, Faculty of Engineering, Universiti Putra Malaysia, 43400 UPM Serdang, Selangor, Malaysia

ABSTRACT

Matoa fruit is a tropical fruit with a native background of Southeast Asia that is very promising in terms of specific flavour and nutrient properties, yet is under a poor usage by the groups because of the lack of post-harvest studies. There are two types of mass modelling discussed in this paper to facilitate post-harvest handling, sorting, and grading: purple and red Matoa. The average mass, primary diameter, Surface Area (SA), and sphericity of purple Matoa were 42.86 g, 54.22 mm, 7133 mm², and 0.85, in comparison to 17.55 g, 40.95 mm, 3610 mm², and 0.78 of red Matoa, respectively. It is worth noting that the dimensions, SA, and volume have been used as independent parameters to come up with regression models. The quadratic model proved to have the best predictive potential. The most suitable predictor of mass was the equivalent mean diameter (D_e) with a $R^2 = 0.962$ and

ARTICLE INFO

Article history:
Received: 19 July 2025
Accepted: 12 December 2025
Published: 19 March 2026

DOI: https://doi.org/10.47836/pjtas.49.S1.08

E-mail addresses:
mohdhafizz@uitm.edu.my (Mohd Hafizz Wondi)
izzahnabilah@upm.edu.my (Nur Izzah Nabilah Haris)
maimunahmma@ukm.edu.my (Maimunah Mohd Ali)
sharifahraina@uitm.edu.my (Sharifah Raina Manaf)
arsaili@uitm.edu.my (Abdul Rahman Saili)
akmalshafiq@uitm.edu.my (Akmal Shafiq Badarul Azam)
mbernard@unimas.my (Bernard Maringgal)
hazwanhamzah@upm.edu.my (Muhammad Hazwan Hamzah)
mshahimi@uitm.edu.my (Muhammad Shahimi Ariffin)
* Corresponding author

Standard Error of Estimate (SEE) = 0.689. In line with this, the quadratic model was very good in explaining the case of SA, where $R^2 = 0.960$ and SEE = 0.714. Likewise, the model of the volume of an ellipsoid had a high predictive accuracy ($R^2 = 0.960$, SEE = 0.709). The results indicate that quadratic models are reliable in forecasting the mass of Matoa fruit, which can be used to design effective automated grading systems. This research would help to commercialise Matoa fruit in a sustainable way by removing the labour-intensive operations and increasing the value of the fruit in commercial and industrial use. Future research may focus on scalability and integration with machine vision systems.

Keywords: Mass modelling, mass prediction model, Matoa fruit, physical properties, post-harvest

INTRODUCTION

Matoa fruit (*Pometia pinnata Forst & Forst)* is a tropical tree species indigenous to the Southeast Asian region, with native populations and wide distribution across Borneo, Sumatra, and Papua New Guinea. *Pometia pinnata* trees typically reach heights of 12 to 20 metres and produce fruit that matures approximately 10 weeks after anthesis (Figure 1). The fruit is generally to in diametre and exhibits high morphological variability, occurring in several varieties distinguished by pericarp colour, such as purple, brown, yellow, red, and green. Its distinct flavour, reminiscent of longan, rambutan, and durian, has gained popularity beyond its native areas, particularly in Malaysia, where its nutritional and culinary values are increasingly acknowledged.

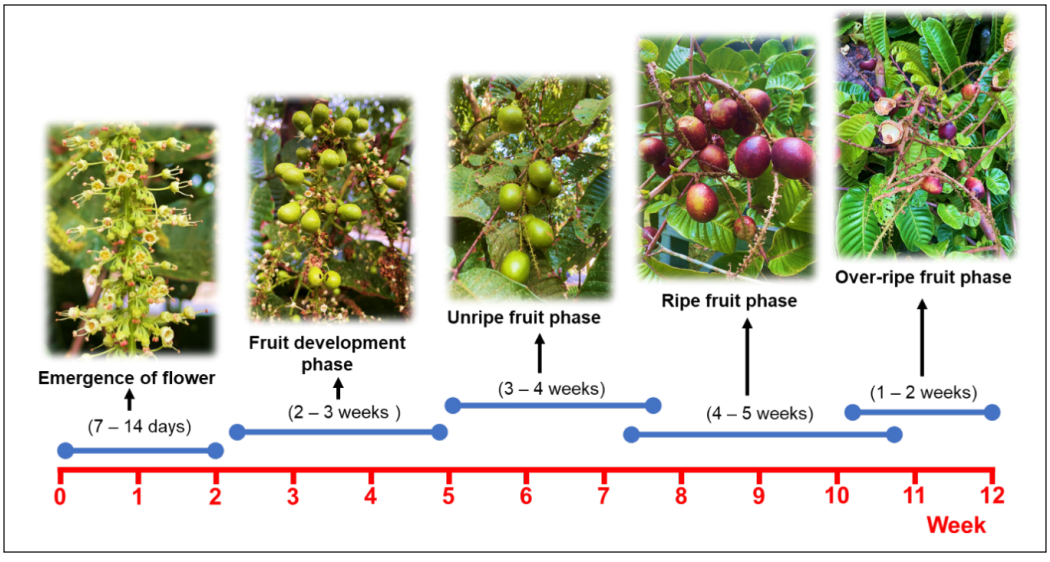

Figure 1. Timeline of Matoa fruit maturation process

Matoa fruit is rich in provitamin A carotenoids, particularly beta-carotene, which the human body metabolises into active vitamin A. Vitamin A is a powerful antioxidant, protecting cells from oxidative stress and slowing ageing. In the same manner, vitamin E enhances the circulation of the blood, thus making sure the oxygen and nutrients circulate well all over the body. Mataoa fruit has been associated with improved cardiovascular health and has been a target among health-conscious consumers when it is consumed frequently. Moreover, Matoa fruit also has bioactive substances, such as saponins, which have an antifungal, antibacterial, and larvicidal effect (Chapagain et al., 2008; Faustina & Santoso, 2017; Ghazzawi et al., 2023; Jomova et al., 2023; Mohammad et al., 2012; Sauriasari et al., 2017; Sholiha et al., 2024; Wahedi et al., 2024; Warraich et al., 2020; Wondi et al., 2025). These positive characteristics underline that it can be applied in agriculture and in the pharmaceutical industry. Nevertheless, the potential of the fruit is not fully exploited because few studies have been conducted on post-harvest processing and handling technologies.

As the popularity of Matoa fruit increases, it is important to conduct research on its physical characteristics to improve post-harvest management and realise its commercial potential. The main physical traits like colour, porosity, sphericity, aspect ratio, dimensions and mass are vital in coming up with effective packaging, grading, sorting, washing and transportation systems (Bhushan et al., 2022; Chandegara & Varshney, 2014; Lorestani et al., 2012; Mahawar et al., 2019; Wondi et al., 2024). Uniformity of size and shape is important in ensuring that automated grading and sorting systems are developed based on homogeneous physical features in order to maximise efficiency (Ahemen & Raji, 2017; Viana de Araujo et al., 2020). Hence, mass-based grading systems have become integral to post-harvest management due to their cost-effectiveness and efficiency, especially for fruits with irregular shapes. Accurate mass grading is effective to improve packaging configurations, decrease the expenses of transportation, and increase storage factors due to the assurance of uniformity (Mahawar et al., 2019; Wondi et al., 2023). Thus, it is necessary to learn the correlations between the physical properties of Matoa fruit and the distribution of its mass in order to design effective post-harvest systems that will minimise losses and maximise the market value.

Previous studies have successfully applied mass prediction models referring to the physical characteristics of various fruits, including strawberries (Birania et al., 2022), Sohiong (Vivek et al., 2018), oil palm fruitlets (Sanganamoni et al., 2024; Wondi et al., 2021), *Terminalia chebula* (Sumit Sudhir et al., 2019); pepper berries (Megat Ahmad Azman et al., 2020), dabai (Afiqah et al., 2024), wood apple (Grover et al., 2024; Murakonda et al., 2022), coconut (Pandiselvam et al., 2019), and banana (Kamble et al., 2021). Although similar research has been successful on other fruits, no published research can be found to determine the physical properties and the mass modelling of the Matoa fruit. However,

Matoa does not have uniformly spherical fruits. Instead, it has a characteristic, thick pericarp and an irregular ellipsoid shape, which differs considerably among varieties (purple vs. red). Normal spherical models do not work well when it comes to estimating the mass of such irregular agricultural products. Thus, this research paper aims to address this gap by: (1) creating a detailed database of physical properties of purple and red Matoa, and (2) creating and testing variety-specific quadratic regression models. These contributions are essential to the design of low-cost, automated grading systems capable of managing the morphological irregularities of the *Sapindaceae* family.

MATERIALS AND METHODS

Materials

Two ripe Matoa fruits (Figure 2) with different varieties (purple and red) were harvested from a Mukah, Sarawak farm. Harvesting of the fruits was at the commercial maturity (ripe) stage. After the harvesting, the fruits were washed in order to remove foreign material, dust, and remnants of floral. A total of 60 samples (N=60) of 30 purple and 30 red fruits were randomly chosen to be analysed in terms of physical properties. Before measuring it, samples were screened to exclude all defects, physical damage, and pest infestation. It is important to note that all the experiments were carried out on the same day when the fruits were picked at room temperature.

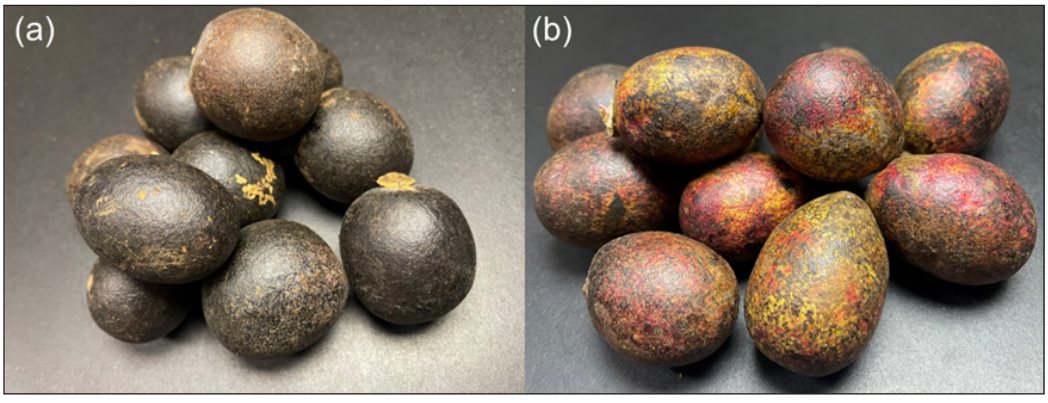

Figure 2. Matoa fruit (*Pometia pinnata*): (a) purple Matoa and (b) red Matoa

Determination of Matoa Fruit Dimension Properties

The test of physical properties was carried out on randomly picked fruits. The palm fruitlets' dimensions, the primary diametre (L), intermediate diametre (W) and minor diametre (T) were taken and recorded on a digital vernier calliper (Mitutoyo, Japan) with a precision of 0.01 mm. The visual observation showed that Matoa fruits are not exactly spherical but

assume the shape of an ellipsoid. Therefore, the volume of the fruit was modeled using three geometric approximations (ellipsoid, prolate spheroid, and oblate spheroid) because their geometric shapes are more rigorous mathematical approximations of fruits that do not have equal axes (L, W and T). The physical properties, such as fruit's equivalent mean diametre (D_e), geometric mean diametre (D_g), and arithmetic mean diametre (D_a), were calculated following standard agricultural engineering protocols established by relationships (Mohsenin, 1986), which serve as the fundamental benchmark for characterising biological materials. The Da, Dg, and De were calculated using Equations 1, 2, and 3, respectively.

$$D_a = \frac{(L + W + T)}{3} \quad [1]$$

$$D_g = (L \times W \times T)^{1/3} \quad [2]$$

$$D_e = \left[\frac{[L \times (W \times T)^2]}{4}\right]^{1/3} \quad [3]$$

where D_a denotes the arithmetic mean diametre, D_g represents the geometric mean diametre, D_e portrays the equivalent mean diametre, L stands for the primary diametre (mm), W signifies the intermediate diametre (mm), and T illustrates the minor diametre (mm).

Determination of Matoa Fruit Surface Area

The geometric shapes of the fruitlet s are represented as ellipsoidal and spherical with their corresponding equations as shown below, using which the formula of Surface Area (SA) was calculated as indicated by Equation 4 (Pradhan et al., 2008):

$$SA = \pi {D_g}^2 \quad [4]$$

where SA represents the fruit's SA (mm^2), D_g stands for geometric mean diametre.

The Criteria Projected Area (CPA) of the entire fruit was calculated using the formulae 5, 6, 7, and 8 applied by (Vivek et al., 2018):

$$PA_L = \frac{\pi \times \mathrm{L} \times W}{4} \quad [5]$$

$$P_{AW} = \frac{\pi \times W \times W}{4} \quad [6]$$

$$PA_T = \frac{\pi \times T \times W}{4} \quad [7]$$

$$CPA = \frac{P_L + P_W + P_T}{3} \quad [8]$$

where PA_L depicts the projected area perpendicular to the primary diametre (mm^2), PA_W portrays the projected area perpendicular to the intermediate diametre (mm^2), PA_T signifies the projected area perpendicular to the minor diametre (mm^2), and CPA illustrates the criteria projected area (mm^2).

The sphericity ∅ and A_r demonstrate that the fruit's aspect ratio was determined using the following expression Equations 9 and 10, respectively (Goyal et al., 2007; Mohsenin, 1986):

$$\emptyset = \frac{(L \times W \times T)^{1/3}}{L} \quad [9]$$

$$R_a = \frac{W}{L} \quad [10]$$

where ∅ the sphericity (dimensionless) and Ra are the aspect ratios.

Determination of Matoa Fruit Gravimetric Properties

The bulk density of the fruitlets was used to calculate the weight density of the fruits in a 1000 ml cylindrical container by filling it with the fruits, but not compacted and weighing the content using a digital weighing balance (AY120, Shimadzu Corporation, Japan) whose accuracy was set at 0.001 g (Gupta & Das, 1997; Sirisomboon et al., 2007). The density of the bulk was determined using the mass of the fruits and the volume of the container using Equation 11:

$$\rho_b = \frac{m_b}{V_b} \quad [11]$$

where ρ_b demonstrates the fruits' bulk density (kg/m^3), m_b represents the fruitlets' bulk mass (kg), and V_b signifies the container's volume (m^3).

The actual density is calculated as the average weight of the individual fruitlets of the fruits divided by the correct volume as given in Equation (12). The specific weight of fruitlets (AY120, Shimadzu Corporation, Japan) was measured using a digital weighing balance. This meant that the volume of the fruitlets was ascertained using the water displacement method that had been embraced by (Mohsenin, 1986). The water displaced

weight was measured, inserted, and used in Equation (12) to calculate the fruitlets' volume. Besides, the volume of an ellipsoid (V_{ellip}), the volume of the prolate spheroid (V_{pro}), and the volume of an oblate spheroid (V_{osp}) were further calculated using Equations 13 – 16 Sanganamoni et al., (2024):

$$V = \frac{m_w}{\rho_w} \quad [12]$$

$$\rho_t = \frac{m_s}{V_s} \quad [13]$$

$$V_{ellip} = \frac{4\pi}{3} \times \left[\frac{a}{2}\right] \times \left[\frac{b}{2}\right] \times \left[\frac{c}{2}\right] \quad [14]$$

$$V_{pro} = \frac{4\pi}{3} \times \left[\frac{a}{2}\right]^2 \times \left[\frac{b}{2}\right] \quad [15]$$

$$V_{osp} = \frac{4\pi}{3} \times \left[\frac{a}{2}\right] \times \left[\frac{b}{2}\right]^2 \quad [16]$$

where V is the volume of individual fruitlets (mm^3), ρ_t represents the fruit's actual density(kg/m^3), m_w demonstrates the water displaced mass (kg), ρ_w signifies the water's density (1000 kg/m^3), V_{ellip} stands for volume of an ellipsoid (mm^3), V_{pro} portrays volume of prolate spheroid (mm^3), and V_{osp} illustrates volume of an oblate spheroid (mm^3).

Porosity, ε, portrays the pores' amount in a bulk material. It is determined using Equation 17 (Mohsenin, 1986):

$$\varepsilon = \left[1 - \frac{\rho_b}{\rho_t}\right] \times 100 \quad [17]$$

where ε represents the porosity, ρ_b stands for the bulk density of fruits (kg/m^3), and ρ_t demonstrates the proper density of fruits (kg/m^3).

Determination of Matoa Fruit Frictional Properties

The static friction coefficients of the fruits were examined on a Mild Steel (MS) and Stainless Steel (SS) surfaces. Thus, the friction angle was calculated utilising a piece of tilting equipment that could be increased by a screw device to alter the tilting angle. An open-ended plastic box (50 mm x 50 mm x 50 mm) was placed horizontally on an adjustable tilting plate and filled with the fruit sample. Hence, the box was lifted slightly

to prevent direct contact with the plate surface. Besides, the angle of tilt was measured using a protractor on the side as the plate's inclination was gradually raised by adjusting the screw until the box began to slide down. This was carried out on three different samples. Equation 18 was applied to determine the coefficient of static friction:

$$\mu = \tan \alpha \quad [18]$$

where μ represents the friction's coefficient, α stands for the angle of tilt (º).

Determination of Matoa Fruit Colour Properties

Colour is one of the main sensory properties, and in many cases, the presence of anthocyanins (Radunić et al., 2015). To measure the colour value of Matoa fruit in other varieties (purple and red), an UltraScan Pro spectrophotometer (D65 HunterLab) was used to determine the colour values of Matoa pericarp. The intensity of colour was indicated by *L*-value (ranging from 0 for darkness to 100 for lightness), *a*-value (from +a for redness to −a for greenness), and *b*-value (from +b for yellowness to −b for blueness) (Wondi et al., 2020). Meanwhile, Chroma (C) and Hue angle (H) were computed from the *L*, a*,* and *b** values employing formulas 19 and 20 (Grover et al., 2024):

$$C = \sqrt{(a*)^2 + (b*)^2} \quad [19]$$

$$C = \sqrt{(a*)^2 + (b*)^2} \quad [20]$$

Mass Modelling

The mass of Matoa fruit was predicted based on the calculated physical properties (such as dimensional measurements, volume, and projected area) using five respective model equations outlined in Table 1. Mass modelling was categorised into three approaches: (1) Linear Dimensions, (2) Projected Area, and (3) Calculated Volume:

1. Development of a single-variable regression model for fruit mass referring to the linear dimensions, including D_e, D_g, D_a, thickness (T), width (W), and length (L).
2. Development of a multiple-variable regression model for fruit mass using projected areas, including CPA, projected area perpendicular to minor diameter (PA_T), projected area perpendicular to intermediate diameter (PA_W), projected area perpendicular to primary diametre (PA_L), and SA.
3. Development of a single-variable regression model for fruit mass considering measured ellipsoid volume (V_{ellip}), Oblate spheroid volume (V_{osp}), and Prolate spheroid volume (V_{pro}).

Based on experimental observations, five regression models; linear, quadratic, S-curve, power, and logarithmic, were applied to predict the mass of purple and red variety Matoa fruits. Consequently, the equations for these models are provided in Table 1. In these equations, M represents the mass of the fruit in grams, X denotes the physical parameter used to predict its relationship with mass, and a, b, and c are the curve-fitting constants specific to each model. Thus, the Coefficients of Determination (R^2) value for each model, which approaches 1.00, indicates the best-fit model. Note that a high SEE indicates an unstable dataset model, while a low SEE indicates a reliable model.

Table 1

Mathematical mass models for Matoa fruit

No.	Model	Equations
1	Linear	$M = a + bX$
2	Quadratic	$M = a + bX + cX^2$
3	S-curve	$M = a + (b/X)$
4	Power	$M = aX^b$
5	Logarithmic	$M = a + b \ln(X)$

RESULTS AND DISCUSSION

Physical Properties of Matoa Fruits

Table 2 presents the average, maximum, and minimum values of the physical characteristics of Matoa fruit in different varieties (purple and red varieties). The mean mass values for the purple variety were 42.86 g ± 3.13 for mass (M), 54.22 mm ± 2.64 for primary diameter (L), 45.22 mm ± 0.91 for intermediate diametre (T), and 44.10 mm ± 0.88 for minor diametre (W). For the red variety, the mean values were 17.55 g ± 3.32 for mass, 40.95 mm ± 5.38 for primary diametre, 30.88 mm ± 3.10 for intermediate diametre, and 30.31 mm ± 3.05 for minor diametre. The purple Matoa fruit had higher mass, primary, intermediate, and minor diametre values than the red variety. These dimensional differences resulted in substantially larger arithmetic (D_a = 47.84 mm ± 1.37), geometric (D_g = 47.63 mm ± 1.30), and equivalent diametre (D_e = 47.63 mm ± 1.30) for purple Matoa, whereas the corresponding values for red Matoa ranged between 33.71 and 34.04 mm.

Shape-related parameters further differentiated the two varieties. Purple Matoa exhibited an aspect ratio of 0.88 ± 0.02 and sphericity of 0.85 ± 0.03, indicating a shape closer to spherical. Sphericity, which describes how closely a shape approximates that of a sphere, is ideal when the value is 1.00 (Megat Ahmad Azman et al., 2020; Wondi et al., 2021). Being a Sapindaceae, Matoa has similar morphological features to Lychee (Litchi chinensis) and Longan (Dimocarpus longan). In this case, the value of sphericity is 0.85 (purple) and 0.78 (red), which

are similar to those observed with Lychee (0.73–0.76) but not so high as Longan, which is generally more spherical (>0.90) (Jalgaonkar et al., 2017). Nevertheless, the red Matoa has an aspect ratio indicating a more rounded form, unlike the rest of its round relatives. It means that although Longan can be easily placed with the help of rolling mechanisms, red Matoa might need to be placed on the belt sorting to avoid excessive sliding or unbalanced rotations. Actual density and porosity are essential factors in the design of hoppers and in regulating flow rates for fruit processing, grading, conveyance, and packaging equipment. Red Matoa showed a true density of 790 kg/m3 ± 0.06 while the corresponding value for purple Matoa was 660 kg/m3 ± 0.09. Porosity was also slightly higher for red Matoa, indicating a looser packing structure that may facilitate better aeration during storage and transportation (Barbhuiya et al., 2020; Wondi et al., 2021). Porosity is also a valuable characteristic that determines the best fruit storage temperature.

Table 2
Physical properties of Matoa fruit in different varieties (purple and red)

Properties	Variety					
	Purple			Red		
	Min.	Max.	Mean	Min.	Max.	Mean
M (g)	38.44	47.31	42.86 ± 3.13	13.72	24.66	17.5 ± 3.32
L (mm)	50.42	58.70	54.22 ± 2.64	34.28	53.56	40.95±5.38
W (mm)	43.83	46.63	45.22±0.91	27.54	38.37	30.88±3.10
T (mm)	42.66	45.69	44.10±0.88	27.29	37.71	30.31±3.05
D_a	46.05	50.34	47.84±1.37	29.70	43.21	34.04±3.83
D_g	45.89	50.01	47.63±1.30	29.53	42.63	33.71±3.72
D_e	45.89	50.01	47.63±1.30	29.53	42.63	33.71±3.72
R_a	0.85	0.91	0.88±0.02	0.80	0.86	0.83±0.02
S	0.81	0.89	0.85±0.03	0.74	0.82	0.78±0.02
ρ_t (kg/m^3)	540	800	660±0.09	720	880	790±0.06
ε (%)	33.41	55.32	43.71±7.92	42.36	52.9	46.07±3.95
SA (mm^2)	6615	7858	7133±3.90	2741	5711	3610±8.74
V (mm^3)	55520	79250	66420±0.92	17600	32880	22500±0.50
PA_L (mm^2)	1754	2150	1927±1.27	742	1614	1005±2.47
PA_W, (mm^2)	1509	1708	1607±0.65	596	1156	756±1.61
PA_T, (mm^2)	1469	1674	1568±0.61	590	1137	742±1.58
CPA (mm^2)	1586	1844	1700±0.81	643	1302	834±1.88
V_{ellip}, (mm^3)	50590	65490	56690±0.47	13490	40580	20760±0.78
V_{pro}, (mm^3)	42920	52020	47260±0.28	10840	29070	15570±0.53

Table 2 (*continued*)

Properties	Variety					
	Purple			Red		
	Min.	Max.	Mean	Min.	Max.	Mean
V_{osp}, (mm^3)	47380	60630	52940±0.40	12610	36880	19010±0.70
μ (°) MS	10.50	12.30	11.31±0.62	10.80	11.70	11.92±0.65
μ (°) SS	9.82	12.98	11.19 ± 1.31	7.67	8.75	8.09±0.55
*L**	24.04	27.00	25.22 ± 0.96	27.54	30.72	29.01±1.02
*a**	1.47	3.48	2.13±0.61	5.46	15.40	11.40±2.69
*b**	-0.47	2.31	0.52±1.03	2.66	9.75	5.91±2.30
Chroma	1.54	4.18	2.33 ± 0.84	7.86	17.79	13.01±2.80
Hue	-17.73	38.23	8.20 ± 21.22	14.24	46.03	27.57 ± 10.43

Note. Data are expressed as: Mass, M; Major diametre, L; Intermediate diametre, W; Minor diametre, T; Arithmetic mean diametre, D_a; Geometric mean diametre, D_g; Equivalent mean diametre, D_e; Sphericity, S; Aspect ratio, R_a; True density, ρ_t; Porosity, ε; Surface area, SA; Volume, V; Projected area perpendicular to L, PA_L; Projected area perpendicular to W, PA_W; Projected area perpendicular to T, PA_T; Criteria projected area, CPA; Ellipsoid volume, V_{ellip}; Prolate spheroid volume, V_{pro}; Oblate spheroid volume, V_{osp}; Coefficient of friction, μ; MS, Mild steel; SS, Stainless steel

Purple Matoa also recorded substantially higher surface area (7133 mm^2 ± 3.90) and volume (66420 mm^3 ± 0.92). These parameters are particularly important for thermal and mass transfer processes such as drying, cooling, and aeration. Projected area measurements followed similar trends. Purple Matoa showed larger projected areas in all orientations, with mean PA_L, PA_W, PA_T, and CPA values of 1927 mm^2 ± 1.27, 1607 mm^2 ± 0.65, 1568 mm^2 ± 0.61, and 1700 mm^2 ± 0.81, respectively, compared with 1005 mm^2 ± 2.47, 756 mm^2 ± 1.61, 742 mm^2 ± 1.58, and 834 mm^2 ± 1.88 for red Matoa. Among these, CPA was the highest for both varieties, highlighting its relevance in estimating respiration rate and heat and mass transfer during postharvest handling (Mahawar et al., 2019; Megat Ahmad Azman et al., 2020). The mean values for the V_{ellip}, V_{pro} and V_{osp} for purple Matoa were recorded as 56690 mm^3 ± 0.47, 47260 mm^3 ± 0.28, and 52940 mm^3 ± 0.40, respectively. The mean values for red Matoa fruit were as follows: V_{ellip}, 20760 mm^3 ± 0.78; V_{pro}, 15570 mm^3 ± 0.53; and V_{osp}, 19010 mm^3 ± 0.70. The physical properties play a very important role in the design and development of machine vision-based grading systems (Dono et al., 2024; Saikumar et al., 2023). Volume estimates based on ellipsoidal, prolate, and oblate spheroidal models further confirmed the consistently larger size of the purple variety.

The frictional behaviour of Matoa fruits varied with surface material. On mild steel surfaces, the mean friction angles were comparable for purple (11.31° ± 0.62) and red Matoa (11.92° ± 0.65). However, lower friction angles were observed on stainless steel surfaces,

particularly for red Matoa (8.09° ± 0.55), indicating reduced resistance to movement and suggesting stainless steel as a more suitable material for smooth conveying applications. Colour parametres (*L*, a*,* and *b**) also revealed distinct varietal differences. Purple Matoa exhibited lower lightness (*L** = 25.22 ± 0.96), chroma (2.33 ± 0.84), and colour intensity, whereas red Matoa showed higher values of *L** (29.01 ± 1.02), *a** (11.40 ± 2.69), *b** (5.91 ± 2.30), chroma (13.01 ± 2.80), and hue angle (27.57° ± 10.43), indicating brighter and more saturated pigmentation. These differences are particularly relevant for machine vision-based grading and automated quality assessment systems.

Mass Modelling

Mass modelling was done on the average dimensions, volumes, weights, SA and projected areas of the various Matoa fruit varieties. Tables 3, 4 and 5 show the summary of the best-performing models that are found, R^2, SEE, F-value and significance level (Sig.) of the predictor of mass of dimension, SA and volume-based model. The selection of the model was largely based on the maximum value of R^2 (nearer to 1.00). Nevertheless, the F-value was used as a secondary measure to evaluate the robustness of the model. The higher the F-value, the higher the signal-to-noise ratio and the greater predictive efficiency. Importantly, the SEE values of Power, S-curve and logarithmic models are on the basis of log-transformed data, and they can not be directly compared to the linear-scale SEE of the Quadratic models. The analysis showed that the quadratic regression model always gave the highest coefficient of determination (R^2) and the lowest Standard Error of Estimate (SEE) on a comparison of linear, S-curve, power, and logarithmic models. This is due to a superior performance, which is a result of the geometric association between the linear dimensions of a fruit and its mass. Volume is intrinsically associated with mass, and it is a three-dimensional property (approximately proportional to L x W x T). Therefore, the correlation between one linear (1D) and mass (3D) is non-linear in nature. This geometric curvature is better represented by the quadratic model ($M = a + bX + cX^2$). Nonetheless, in the case of the Red, more elongated species, which appears more of an ellipsoidal form, the models of logarithms were often more successful at stable volumetric parameters, indicating a different mass distribution of morphological phenomena of volumetric parameters of the spherical purple variety.

Models Based on Dimensions

Table 3 depicts the best-performing mass model that has been determined by a dimension-based method, which includes independent parameters that include: sphericity (S), arithmetic mean diametre (D_a), geometric mean diametre (D_g), minor diametre (W), intermediate diametre (T), and major diametre (L). In addition, the findings showed that the purple and red Matoa varieties are the best fit in the quadratic model. The purple Matoa variety was

Table 3
Mass models of Matoa fruit in different varieties (purple and red) are based on dimension

Independent Parameter	Variety	Best Model	Regression Constant			Statistical Parameters			
			a	b	c	R^2	SEE	Sig.	F-value
L	Purple	Logarithmic	-198.105	60.364	-	0.883	1.134	< 0.05	60.504
	Red	Quadratic	-13.135	0.901	-0.004	0.883	1.287	< 0.05	26.367
W	Purple	Quadratic	-26.892	-9.873	0.034	0.806	1.462	< 0.05	33.230
	Red	Quadratic	-46.593	3.021	-0.030	0.929	0.999	< 0.05	46.127
T	Purple	Quadratic	613.941	-28.648	0.356	0.617	2.195	< 0.05	5.638
	Red	Quadratic	-48.629	3.210	-0.034	0.917	1.081	< 0.05	38.849
D_a	Purple	Quadratic	-559.413	22.886	-0.215	0.962	0.689	< 0.05	89.227
	Red	Quadratic	-31.469	1.990	-0.016	0.911	1.124	< 0.05	35.664
D_g	Purple	Quadratic	-613.483	25.152	-0.239	0.959	0.720	< 0.05	81.546
	Red	Logarithmic	-89.259	30.405	-	0.913	1.039	< 0.05	83.682
S	Purple	Quadratic	717.350	-1502.366	832.450	0.641	2.126	< 0.05	6.241
	Red	Quadratic	719.638	-1697.979	1021.565	0.608	2.355	< 0.05	5.421

Note. Data are expressed as: Major diameter (L); Intermediate diameter (W); Minor diameter (T); Arithmetic mean diameter (D_a); Geometric mean diameter (D_g); Sphericity (S)

well fitted by the quadratic model. D_a and D_g were among the dimensional parameters that provided very precise predictions, with which a single-dimensional predictor can be relied upon to predict the grading. D_a model was the best predictor (Figure 3), with the highest coefficient of determination (R^2=0.962) and F-value (F=89.23, $p < 0.001$) of the purple variety. A residual analysis was done to identify any form of systematic bias. As depicted in Figure 4, the random scatter of standardised residuals around the zero axis confirms homoscedasticity and the absence of any systematic bias, validating the model's reliability for mass grading of the spherical purple fruit. This indicates that the arithmetic average of axes will provide the mass distribution of the spherical purple fruit well. Another model that performed well was the D_g model with an R^2 of 0.959 and an F-value of 81.55. D_g is a theoretically acceptable predictor, although slightly less than D_a, as it explains the geometric product of the three axes. The best-fitting equations for the purple variety are presented in Equations 21 and 22:

$$M = -559.41 + 22.89D_a - 0.22\,{D_a}^2 \quad [21]$$

$$M = -613.48 + 25.152D_g - 0.24\,{D_g}^2 \quad [22]$$

For the red Matoa fruit, the linear dimensions specifically intermediate diametre (W) and minor diametre (T) yielded the most accurate predictions among the raw dimensions. The Width (W) quadratic model achieved the highest accuracy with an R^2 of 0.929 (*F = 46.13*). However, a distinct deviation was observed for the mean diametre. The Logarithmic model provided the best fit for the D_a, achieving an R^2 of 0.945 and a remarkably high F-value of 137.09. This reinforces the observation that the elongated red variety scales differently than the spherical purple variety. The best-fitting equations for the red variety are presented in Equations 23 and 24:

$$M = -46.59 + 3.12W - 0.03\,W^2 \quad [23]$$

$$M = -389.38 + 111.89\ln(D_a) \quad [24]$$

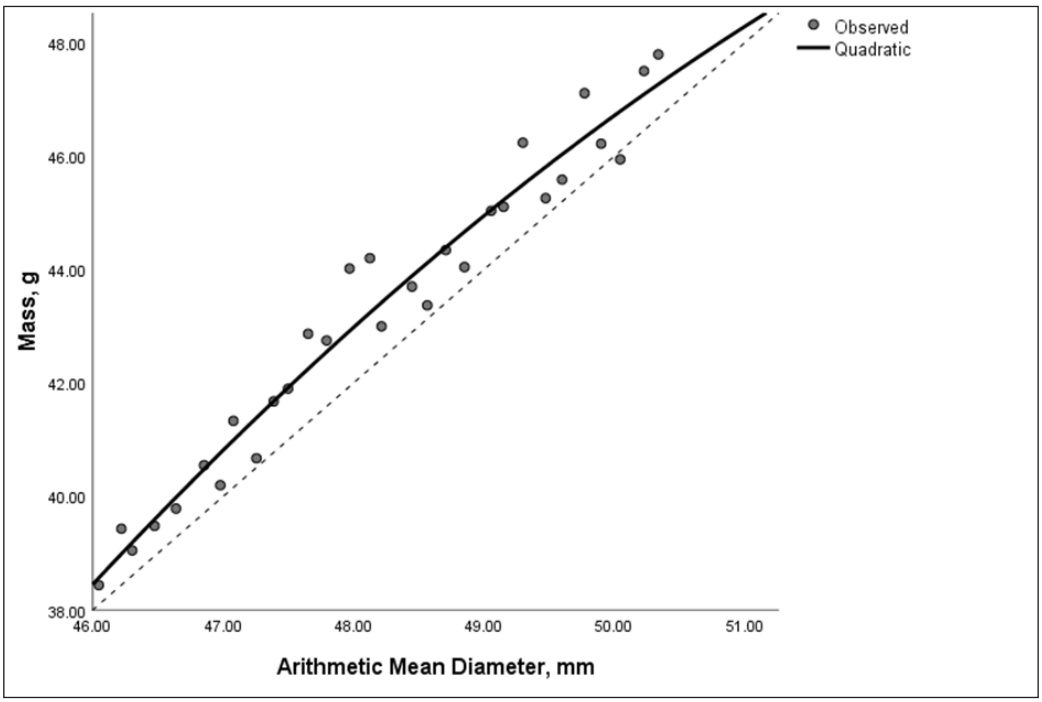

Figure 3. Best-fitting quadratic regression models for purple variety Matoa fruit mass prediction based on Arithmetic Mean Diametre (D_a), showing the highest single-dimensional accuracy (R^2=0.962)

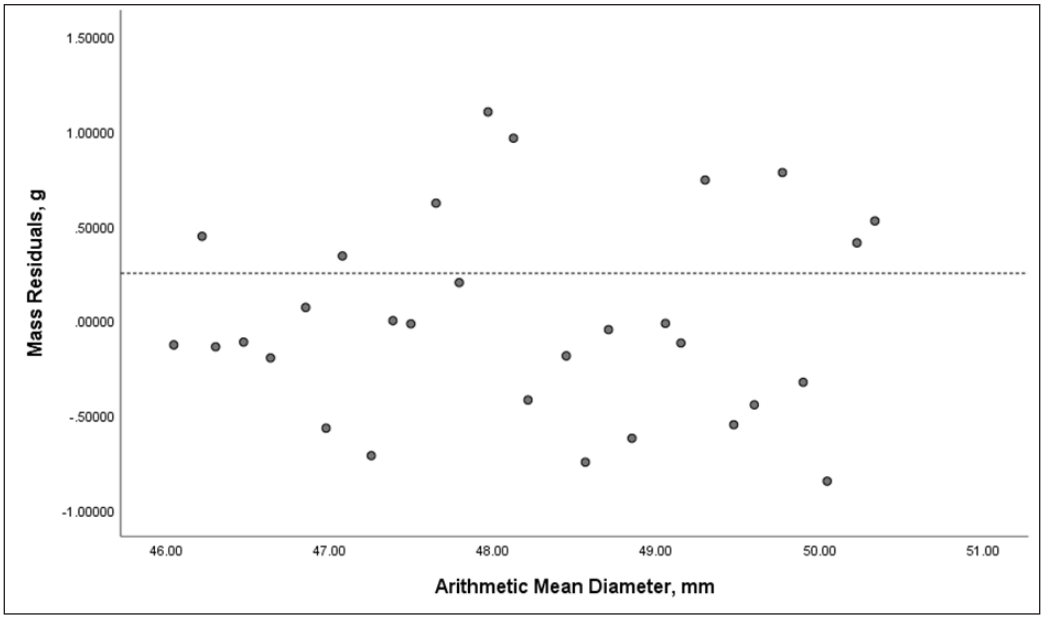

Figure 4. Residual diagnostics for the quadratic mass model of purple variety Matoa based on the Arithmetic Mean Diametre, D_a. The random scatter of the standardised residuals around the zero-line visually confirms constant variance of errors and demonstrates the absence of any systematic bias in the model predictions across the entire range of observed mass values

Model Based on Surface Area

A quadratic model provided the best fit for predicting the mass of Matoa fruit based on Surface Area (SA) parameters (Table 4). The SA-based modelling has been used to predict the mass of both purple and red Matoa fruits using Criteria Projected Area (CPA), PA_T, PA_W, PA_L, and SA. In the purple fruits, the most accurate predictions were obtained by the total Surface Area (SA) and Projected Area (PA_L). The SA model achieved an R^2 of 0.960 and a high F-value of 82.93 ($p < 0.001$). Equally, the PA_L model demonstrated an R^2 of 0.945. Such strong correlations affirm that optical systems that quantify the projected area are capable of estimating mass. This is a better performance ($R^2 = 0.94$) than that shown with Sohiong fruit ($R^2 = 0.88$), presumably because the pericarp of Matoa is smoother and thus more area can be measured in this case than with the rough-skinned fruits. The best parameters, together with the associated model equations, are as follows stated in Equations 25 and 26:

$$M = -163.06 + 0.05SA - 35.16\,SA^2 \quad [25]$$

$$M = -73.69 + 0.097PA_L - 23.9\,{PA_L}^2 \quad [26]$$

On the other hand, the red variety had a high affinity to SA using the Logarithmic models as in Equation 27. The Logarithmic model of SA had an R^2 value of 0.940 and a very significant F-value of 126.3 against the Quadratic model (R^2=0.914). Mechanically, this verifies the fact that the mass distribution of the red variety in relation to the surface area involves a logarithmic trend due to its lower sphericity. However, for lateral projections (PA_W), as in Equation 28, the Quadratic model remained optimal:

$$M = -305.57 + 46.08\, ln\,(SA) \quad [27]$$

$$M = -10.42 + 0.05PA_W - 22.91\, PA_W{}^2 \quad [28]$$

Models Based on Volume

Table 5 shows the best-performing model parameters determined by use of a volume model, which took into account Oblate (V_{osp}), Prolate (V_{pro}) and Ellipsoid (V_{ellip}) volumes in estimating the mass of the purple and red Matoa fruits. These findings indicate that a quadratic model best fits the mass of the purple fruit, given the Vellip, with the highest R^2 of 0.960. This is consistent with the physical fact that in spherical fruits, the distribution of densities is relatively constant and hence volume is an almost ideal predictor of mass as indicated in Equation 29:

$$M = -67.28 + 0.003V_{ellip} - 30.32\, V_{ellip}{}^2 \quad [29]$$

In agreement with the area models, the red variety was found to respond to the Logarithmic model in predicting mass using V_{ellip} with a higher R^2 of 0.913 with a much higher F-value (F=83.9) than the Quadratic model. But in the case of V_{osp}, the Quadratic model fit best (R^2=0.914). This finding corresponds to the results of Sumit Sudhir et al. (2019) with dried *Terminalia chebula*, who found that, depending on the aspect ratio of the fruit, the plotted geometric approximation (Oblate vs. Ellipsoid) would dramatically change their best-fitting regression curve. Equation 30, the quadratic model, is as follows:

$$M = -86.61 + 0.004V_{osp} - 39.14\, V_{osp}{}^2 \quad [30]$$

CONCLUSION

This study successfully characterised the physical parameters of various Matoa fruit varieties and established their robust association with fruit mass. The study revealed that purple and red Matoa varieties are highly differentiated in terms of size, mass, and shape, where the purple one is always more massive and spherical. The mass modelling that followed identified that the quadratic regression model is the best mathematical tool that

Table 4
Mass models of Matoa fruit in different varieties (purple and red) based on area

Independent Parameter	Variety	Best Model	Regression Constant			Statistical Parameters			
			a	b	c	R^2	SEE	Sig.	F-value
SA	Purple	Quadratic	-163.060	0.050	-35.16	0.960	0.714	< 0.05	82.931
	Red	Logarithmic	-106.669	15.203	-	0.913	1.038	< 0.05	83.888
P_{AL}	Purple	Quadratic	-73.686	0.097	-23.90	0.945	0.835	< 0.05	59.679
	Red	Logarithmic	-82.285	14.490	-	0.908	1.066	< 0.05	79.065
P_{AW}	Purple	Quadratic	163.395	-0.194	7.394×10^{-5}	0.813	1.534	< 0.05	15.212
	Red	Quadratic	-10.420	0.051	-22.91	0.930	0.996	< 0.05	46.416
P_{AT}	Purple	Quadratic	111.634	-0.132	5.598×10^{-5}	0.745	1.790	< 0.05	10.244
	Red	Quadratic	-10.780	0.053	-24.13	0.925	1.028	< 0.05	43.359
CPA	Purple	Quadratic	-149.207	0.189	-49.49	0.923	0.983	< 0.05	42.110
	Red	Quadratic	-7.686	0.041	-17.53	0.921	1.054	< 0.05	41.015

Note. Data are expressed as: Surface area (SA); Volume (V); Projected area perpendicular to L (PA_L); Projected area perpendicular to W (PA_W); Projected area perpendicular to T (PA_T); Criteria projected area (CPA)

Table 5
Mass models of Matoa fruit in different varieties (purple and red) based on volume

Independent Parameter	Variety	Best Model	Regression Constant			Statistical Parameters			
			a	b	c	R^2	SEE	Sig.	F-value
V_{ellip}	Purple	Quadratic	-67.278	0.003	-30.320	0.960	0.709	< 0.05	84.042
	Red	Logarithmic	-82.707	10.136	-	0.913	1.038	< 0.05	83.889
V_{pro}	Purple	Quadratic	53.926	-0.001	-33.830	0.776	1.678	< 0.05	12.135
	Red	Quadratic	-0.115	0.002	-28.670	0.927	1.013	< 0.05	44.729
V_{osp}	Purple	Quadratic	-86.606	0.004	-39.140	0.934	0.911	< 0.05	49.567
	Red	Quadratic	2.096	0.001	-17.910	0.914	1.103	< 0.05	37.187

Note. Data are expressed as: Ellipsoid volume (V_{ellip}); Prolate spheroid volume (V_{pro}); Oblate spheroid volume (V_{osp})

can be used to predict fruit mass of all the tested physical characteristics. The implication of these results in practical terms is that the design of automated grading systems cannot be neglected as the correlation between projected area and mass is very high which guarantees that low-cost machine vision systems can be calibrated to substitute slower and more expensive load-cell-based weighing systems providing a feasible pathway to high-speed, non-contact grading that will have a strong impact on economic efficiency and labour intensity. In addition, the calculated coefficients of friction and the data of sphericity offer invaluable information in dealing with the design, namely the use of stainless steel surfaces to reduce damage, and it would require a particular conveyor design to deal with the more ellipsoidal red one due to its rolling instability. The resulting quadratic models with fruit dimension and approximated volume as the measure of mass prediction have been suggested to be adopted in designing and optimising the post-harvesting machinery to be used in the handling, cleaning, conveying, and storage of Matoa fruit. The scalability and robustness of these quadratic models in a continuous, high-speed industrial sorting environment are therefore worth future research to prove their validity.

ACKNOWLEDGEMENT

This work was supported by the Universiti Teknologi MARA (UiTM) through the Excellence Research Fund (DKCM), Reference No: 600-TNCPI 5/3/DDN (13) (003/2024).

REFERENCES

Afiqah, N., Abdul, H., Shamsudin, R., & Ariffin, S. H. (2024). Physical properties of full-ripe dabai (*canarium odontophyllum miq. variety song*) at different fractions. *Pertanika Journal of Science and Technology*, *32*(2), 725-739. https://doi.org/https://doi.org/10.47836/pjst.32.2.13

Ahemen, S. A., & Raji, A. O. (2017). Moisture-dependent physical properties of Tacca involucrata tubers. *Journal of Food Process Engineering*, 1-8. https://doi.org/10.1111/jfpe.12541

Barbhuiya, R. I., Nath, D., Singh, S. K., & Dwivedi, M. (2020). Mass modelling of indian coffee plum (*Flacourtia Jangomas*) fruit with its physicochemical properties. *International Journal of Fruit Science*, *20*(3), 1-24. https://doi.org/10.1080/15538362.2020.1775161

Bhushan, B., Manoj Kumar, M., Kirti, J., Vijay, S. M., & Dattatreya, M. K. (2022). Mass modelling of guava (*cv. Allahabad safeda*) fruit with selected dimensional attributes: Regression analysis approach. *Journal of Food Process Engineering*, *45*(3), 1-10. https://doi.org/https://doi.org/10.1111/jfpe.13978

Birania, S., Attkan, A. K., Kumar, S., Kumar, N., & Singh, V. K. (2022). Mass modelling of strawberry (Fragaria Ananasa) based on selected physical attributes. *Journal of Food Process Engineering*, *February*, 1-12. https://doi.org/10.1111/jfpe.14023

Chandegara, V. K., & Varshney, A. K. (2014). Design and development of leaf splitting unit for aloe vera gel expulsion machine. *Journal of Food Process Engineering*, *37*(4), 427-437. https://doi.org/10.1111/jfpe.12098

Chapagain, B. P., Saharan, V., & Wiesman, Z. (2008). Larvicidal activity of saponins from Balanites aegyptiaca callus against Aedes aegypti mosquito. *Bioresource Technology*, *99*(5), 1165-1168. https://doi.org/10.1016/j.biortech.2007.02.023

Dono, F. X., Baatuuwie, B. N., Abagale, F. K., & Borgen, P. (2024). Application of computer vision and machine learning in morphological characterisation of Adansonia digitata fruits. *Smart Agricultural Technology*, *9*(June), 1-11. https://doi.org/10.1016/j.atech.2024.100528

Faustina, F. C., & Santoso, F. (2017). Extraction of fruit peels of *Pometia pinnata* and its antioxidant and antimicrobial activities. *Jurnal Penelitian Pascapanen Pertanian*, *11*(2), 80-88. https://doi.org/10.21082/jpasca.v11n2.2014.80-88

Ghazzawi, H. A., Hussain, M. A., Raziq, K. M., Alsendi, K. K., Alaamer, R. O., Jaradat, M., Alobaidi, S., Al Aqili, R., Trabelsi, K., & Jahrami, H. (2023). Exploring the relationship between micronutrients and athletic performance: A comprehensive scientific systematic review of theliterature in sports medicine. *Sports*, *11*(6). https://doi.org/10.3390/sports11060109

Goyal, R. K., Kingsly, A. R. P., Kumar, P., & Walia, H. (2007). Physical and mechanical properties of aonla fruits. *Journal of Food Engineering*, *82*(4), 595-599. https://doi.org/10.1016/j.jfoodeng.2007.03.019

Grover, R., Kumar, A., & Kumar, S. (2024). Physical characterisation and mass modelling of Wood apple (Aegel marmelos L.). *Food Physics*, *1*(May), 100013. https://doi.org/10.1016/j.foodp.2024.100013

Gupta, R. K., & Das, S. K. (1997). Physical properties of sunflower seeds. *Journal of Agricultural and Engineering Research*, *66*(1), 1-8. https://doi.org/10.1006/jaer.1996.0111

Jalgaonkar, K., Mahawar, M. K., Bibwe, B., Dukare, A., Kannaujia, P., & Bhushan, B. (2017). Moisture dependent physical properties of Litchi seeds (Litchi chinensis). *Food & Nutrition Journal*, *5*(6). https://doi.org/10.29011/2575-7091.100048

Jomova, K., Raptova, R., Alomar, S. Y., Alwasel, S. H., Nepovimova, E., Kuca, K., & Valko, M. (2023). Reactive oxygen species, toxicity, oxidative stress, and antioxidants: chronic diseases and aging. *Archives of Toxicology*, *97*(10), 2499-2574. https://doi.org/10.1007/s00204-023-03562-9

Kamble, M. G., Singh, A., Mishra, V., Meghwal, M., & Prabhakar, P. K. (2021). Mass and surface modelling of green plantain banana fruit based on physical characteristics. *Computers and Electronics in Agriculture*, *186*, Article 106194. https://doi.org/10.1016/j.compag.2021.106194

Lorestani, A. N., Jaliliantabar, F., & Gholami, R. (2012). Mass modelling of caper (Capparis spinosa) with some engineering properties. *Quality Assurance and Safety of Crops & Foods*, *4*, 38-42. https://doi.org/10.1111/qas.12004

Mahawar, M. K., Bibwe, B., Jalgaonkar, K., & Ghodki, B. M. (2019). Mass modeling of kinnow mandarin based on some physical attributes. *Journal of Food Process Engineering*, *42*(5), 1-11. https://doi.org/10.1111/jfpe.13079

Megat Ahmad Azman, P. N., Shamsudin, R., Che Man, H., & Ya'acob, M. E. (2020). Some Physical Properties and Mass Modelling of Pepper Berries (Piper nigrum L.), Variety Kuching, at Different Maturity Levels. *Processes*, *6*(1314), 1-15. https://doi.org/10.3390/pr8101314

Mohammad, F. V., Noorwala, M., Ahmad, V. U., Zahoor, A., & Lajis, N. H. J. (2012). A new monodesmosidic triterpenoid saponin from the leaves of *Pometia pinnata*. *Natural Product Communications*, *7*(11), 1423-1426. https://doi.org/10.1177/1934578x1200701105

Mohsenin, N. N. (1986). *Physical Properties of Agricultural Materials and Food Products* (1st ed.). Gordon and Breach Science Publishers.

Murakonda, S., Patel, G., & Dwivedi, M. (2022). Characterisation of engineering properties and modelling mass and fruit fraction of wood apple (Limonia acidissima) fruit for post-harvest processing. *Journal of the Saudi Society of Agricultural Sciences*, *21*(4), 267-277. https://doi.org/10.1016/j.jssas.2021.09.005

Pandiselvam, R., Manikantan, M. R., Balasubramanian, D., Beegum, P. P. S., Mathew, A. C., Ramesh, S. V., Hebbar, K. B., & Niral, V. (2019). Mechanical properties of tender coconut (Cocos nucifera L.): Implications for the design of processing machineries. *Journal of Food Process Engineering*, 1-8. https://doi.org/10.1111/jfpe.13349

Pradhan, R. C., Naik, S. N., Bhatnagar, N., & Vijay, V. K. (2008). Moisture-dependent physical properties of jatropha fruit. *Industrial Crops & Products*, *29*, 341-347. https://doi.org/10.1016/j.indcrop.2008.07.002

Radunić, M., Jukić Špika, M., Goreta Ban, S., Gadže, J., Díaz-Pérez, J. C., & Maclean, D. (2015). Physical and chemical properties of pomegranate fruit accessions from Croatia. *Food Chemistry*, *177*, 53-60. https://doi.org/10.1016/j.foodchem.2014.12.102

Saikumar, A., Nickhil, C., & Badwaik, L. S. (2023). Physicochemical characterization of elephant apple (Dillenia indica L.) fruit and its mass and volume modelling using computer vision. *Scientia Horticulturae*, *314*, Article 111947. https://doi.org/10.1016/j.scienta.2023.111947

Sanganamoni, S., Kancherla, S., Pedapati, A., Akki, S., & Patel, J. (2024). Physical characterisation and development of mathematical models for predicting mass and area of oil palm fruits. *Journal of Food Process Engineering*, *47*(1), 1-24. https://doi.org/10.1111/jfpe.14512

Sauriasari, R., Azizah, N., & Basah, K. (2017). Tyrosinase inhibition, 2,2-diphenyl-1-picrylhydrazyl radical scavenging activity, and phytochemical screening of fractions and ethanol extract from leaves and stem bark of Matoa (*Pometia pinnata*). *Asian Journal of Pharmaceutical and Clinical Research*, *10*(Special Issue), 85-89. https://doi.org/10.22159/ajpcr.2017.v10s5.23105

Sholiha, F. U., Yuniastuti, E., & Hartati, S. (2024). The matK gene analysis in five types of Matoa (*Pometia pinnata J. R. Forst. & G. Forst*) based on the pericarp colour. *Journal of Applied Biology & Biotechnology*, *12*(3), 54-58. https://doi.org/10.7324/JABB.2024.167495

Sirisomboon, P., Kitchaiya, P., Pholpho, T., & Mahuttanyavanitch, W. (2007). Physical and mechanical properties of Jatropha curcas L. fruits, nuts and kernels. *Biosystems Engineering*, *97*, 201-207. https://doi.org/10.1016/j.biosystemseng.2007.02.011

Sumit Sudhir, P., Rama Chandra, P., & Sabyasachi, M. (2019). Physical characterisation and mass modelling of dried Terminalia chebula fruit. *Journal of Food Process Engineering*, *December 2018*, 1-10. https://doi.org/10.1111/jfpe.12992

Viana de Araujo, M. E., Guimarães Barbosa, E., Oliveira, A. C. L., Milagres, R. S., Carvalho Pinto, F. de A., & Corrêa, P. C. (2020). Physical properties of yellow passion fruit seeds *(Passiflora edulis)* during the drying process. *Scientia Horticulturae*, *261*, Article 109032. https://doi.org/10.1016/j.scienta.2019.109032

Vivek, K., Mishra, S., & Chandra, R. (2018). Physicochemical characterisation and mass modelling of Sohiong (Prunus nepalensis L.) fruit. *Journal of Food Measurement and Characterization*, *12*, 923-936. https://doi.org/10.1007/s11694-017-9708-x

Wahedi, J. A., Vincent, V. M., Pukuma, S. M., Bawa, I. S., Agboola, O. O., Aju-Ahmeh, C. O., Filgona, J., & Olowoyo, J. O. (2024). Phytochemical screening and larvicidal activities of Cymbopogon citratus and Annona senegalensis against Culex quinquefasciatus. *Scientific African*, *23*(May 2022), e02057. https://doi.org/10.1016/j.sciaf.2024.e02057

Warraich, U. e. A., Hussain, F., & Kayani, H. U. R. (2020). Aging - Oxidative stress, antioxidants and computational modelling. *Heliyon*, *6*(5), e04107. https://doi.org/10.1016/j.heliyon.2020.e04107

Wondi, M. H., Haris, N. I. N., Shamsudin, R., Yunus, R., Mohd Ali, M., & Iswardi, A. H. (2024). Development and testing of an oil palm (Elaeis guineensis Jacq.) fruit digester process for kernel free in crude palm oil production. *Industrial Crops & Products*, *208,* Article 117755. https://doi.org/10.1016/j.indcrop.2023.117755

Wondi, M. H., Johar, N., Haris, N. I. N., Manaf, S. R., Sulaiman, M. N., Mohd Ali, M., Talip, M. S. A., Kadir, A. R. A., & Fikry, M. (2025). Borneo's Indigenous Fruits as Natural Sources for Nano-Coating Applications: Nutritional and Antioxidant Insights. *Journal of Advanced Research in Micro and Nano Engineering*, *42*(1), 151-176.

Wondi, M. H., Shamsudin, R., Yunus, R., Alsultan, G. A., & Iswardi, A. H. (2020). Centrifugal separation-assisted and extraction of crude palm oil from separated mesocarp fiber: Central composite design optimisation. *Journal of Food Process Engineering*, *43*(7). https://doi.org/10.1111/jfpe.13426

Wondi, M. H., Shamsudin, R., Yunus, R., Baharudin, M. S., Arnan, M. Z., & Rahman, A. F. A. (2021). Physical and mechanical properties of sterilised oil palm fruits at different component. *AMA, Agricultural Mechanization in Asia, Africa and Latin America*, *52*(3), 3985-a3997.

Wondi, M. H., Shamsudin, R., Yunus, R., Mohd Ali, M., & Haris, N. I. N. (2023). Design of a separator machine for oil palm fruit mesocarp and nut using computer-aided design and linear finite element analysis. *Journal of Food Process Engineering*, Article e14457. https://doi.org/10.1111/jfpe.14457

Pertanika J. Trop. Agric. Sci. 49 (S1): 193 - 209 (2026)

PERTANIKA JOURNALS

TROPICAL AGRICULTURAL SCIENCE

Journal homepage: http://www.pertanika.upm.edu.my/

Effects of Cooking Methods and Time on the Physical Properties of Cooked Glutinous Rice

Puteri Nurain Megat Ahmad Azman[1], Rosnah Shamsudin[1,*], Norhashila Hashim[2], Hasfalina Che Man[2], Muhammad Hazwan Hamzah[2], and Maimunah Mohd Ali[3]

[1]Department of Process and Food Engineering, Faculty of Engineering, Universiti Putra Malaysia, 43400 UPM Serdang, Selangor, Malaysia

[2]SMART Farming Technology Research Centre, Department of Biological and Agricultural Engineering, Faculty of Engineering, Universiti Putra Malaysia, 43400 UPM Serdang, Selangor, Malaysia

3Department of Food Sciences, Faculty of Science and Technology, Universiti Kebangsaan Malaysia, 43600 UKM Bangi, Selangor, Malaysia

ABSTRACT

Glutinous rice is primarily grown in Southeast Asia, and it is highly diversified in uses. There is a limited study on the effects of different cooking methods on the physical properties and cooking time of glutinous rice. This study aims to evaluate the effects of different cooking methods on the physical properties and cooking time of glutinous rice. Before cooking, the glutinous rice obtained was stored for two months under 4°C and 28°C to represent chilled and ambient storage conditions. For the steaming method, 250 g of glutinous rice from the two conditions were soaked at room temperature for 3 hours, then cooked using an electric steamer. Meanwhile, the unsoaked glutinous rice was used for the boiling method in an electric rice cooker. This study uses soaked and unsoaked glutinous rice to represent the two common cooking methods consumers use. Based on the results, the cooked glutinous rice from storage condition B had the significantly (p<0.05) highest increment in apparent density (2086.14kg/m^3) and cooking time (34.07 minutes). Also, they had the highest reduction in length (8.68 mm), equivalent diametre (2.95mm), projected area (0.23), surface area (25.69mm^2), volume (13.45mm^3), and weight (0.0279g) when compared to storage condition A. The size of cooked glutinous rice is greater than that of steamed glutinous rice, which shows more expansion. Boiling produced greater swelling and water uptake, while steaming resulted in more compact grains with lower expansion. Hence, this study contributes to improving quality control in product development and guides on optimal cooking practices for consumers.

ARTICLE INFO

Article history:
Received: 19 July 2025
Accepted: 15 December 2025
Published: 19 March 2026

DOI: https://doi.org/10.47836/pjtas.49.S1.09

E-mail addresses:
puteri.nurain@ymail.com (Puteri Nurain Megat Ahmad Azman)
norhashila@upm.edu.my (Norhashila Hashim)
hasfalina@upm.edu.my (Hasfalina Che Man)
hazwanhamzah@upm.edu.my (Muhammad Hazwan Hamzah)
maimunahmma@ukm.edu.my (Maimunah Mohd Ali)
* Corresponding author

Keywords: Cooking methods, grain expansion, glutinous rice, physical properties, steaming

INTRODUCTION

In many Southeast Asian countries, glutinous rice is the main foodstuff and is used in a variety of traditional and modern recipes. About 90% of Asia's global production and consumption was contributed by rice (Naomi & Lewis, 2019). Cooking is a key process for rice before eating. The whole cooking process involves water washing, pre-soaking, and cooking with the proper method. Pre-soaking is a traditional pretreatment before cooking. It would result in uniform cooking and less cooking time (Hu et al., 2020). Water soaking prior to cooking is common for cooking this rice form for better eating quality. Understanding the impact of the cooking method on the quality of these marketable rice varieties is beneficial to consumers (Krongworakul et al., 2020). In this study, the sample preparations were conducted prior to cooking (unsoaked and soaked processes based on the cooking methods). Generally, heating starchy meals can cause starch granules to gelatinise, losing their amylose and amylopectin crystallinity and creating a disordered structure that makes starch more prone to enzymatic hydrolysis (Ngo et al., 2023). Employing advanced processing and cooking technologies can enhance the quality and overall acceptability of glutinous rice (Ali & Hashim, 2024).

Grain dimensions are one of the crucial characteristics that need to be included in measuring the physical properties of rice (Bhattacharya, 2011). Measuring the grain dimensions is the first step to characterise the rice shape, and those values are also further used for several dimensional calculations (Nádvorníková et al., 2018). Physical properties such as dimensions, aspect ratio, projected area, surface area, volume, weight, and density are those properties that can be measured and observed without altering the material composition. Dimensions are an important property for designing the soaking system. Weight measurement is an external criterion that is mostly used for more valuable foods (Azman et al., 2020). Cooking time is essential for evaluating and interpreting how different cooking methods affect the physical properties of rice (Ojediran et al., 2020). Physical properties and cooking time are the most important aspects, which are the first expressions that will be observed by the consumers. Most of the previous studies investigated the physical properties of non-glutinous rice, including Díaz et al. (2015), Meena et al. (2010), Oli et al. (2016), Ravi et al. (2014), Smanalieva et al. (2015), Thakur & Gupta (2006), and Varnamkhasti et al. (2008). Most recent published studies on investigating nutritional, thermal, and pasting properties and potential products of glutinous rice. However, there is a limited study related to the effects of steaming and boiling methods on physical properties changes and cooking time of glutinous rice. Also, it has a lack of investigation into the effects of storage time on the cooking properties of glutinous rice. Most previous studies either focus on non-glutinous varieties or evaluate only selected physicochemical properties, leaving important gaps in understanding how direct versus indirect heating affects cooking properties. Moreover, this study contributes to improving quality control

in glutinous rice-based product development, supports standardisation in food preparation, and provides guidance on optimal cooking practices for consumers.

Therefore, this study aims to (1) evaluate the effects of cooking methods (steaming and boiling) on the physical properties and cooking time of glutinous rice, and (2) investigate the correlations between physical properties and cooking methods combined with storage conditions before cooking. Hence, this study provides knowledge and a theoretical basis for both home cooks and the food industry regarding the best practices for preparing glutinous rice.

MATERIALS AND METHODS

Materials Preparation

The local glutinous rice cultivar (Siding) was purchased from the local farm (Kuala Selangor, Selangor, Malaysia). Only head glutinous rice grains, free from any physical defects or insect infestations, were chosen for analysis. Once brought to the laboratory, the glutinous rice samples were stored under conditions A (4°C) and B (28°C) for 2 months, as shown in Figure 1. These two storage conditions were chosen to represent chilled and ambient storage conditions, which are commonly used in glutinous rice handling. The stored raw glutinous rice samples were taken from each condition to evaluate the changes in dimensions, aspect ratio, surface area, volume, weight, and cooking time of glutinous rice under different cooking methods for five replications.

Preparation of Steamed and Cooked Glutinous Rice

The stored glutinous rice was cooked using both the steaming and boiling methods. Glutinous rice samples (1.5 kg) from two storage conditions, A (4°C) and B (28°C), were washed once with tap water before cooking to remove dirt and foreign objects. Two hundred and fifty grammes of washed samples from each storage condition were used for both the steaming and boiling methods. For the steaming method, the glutinous rice samples were soaked at room temperature for 3 hours with a glutinous rice-to-water ratio of 1:1.5 to ensure that the glutinous rice was completely immersed in the water and had uniform heat transfer and evaporation process. After soaking, the glutinous rice was cooked using an electric steamer. About seven hundred millilitres of water was used in the steamer, and the steaming temperature was 110.00 ±2.00°C. Meanwhile, the unsoaked glutinous rice was used for the boiling method in an electric rice cooker with a glutinous rice-to-water ratio of 1:1.5. This study uses soaked and unsoaked glutinous rice to represent the two common cooking methods consumers use, aiming to determine their influence on the physical properties of glutinous rice.

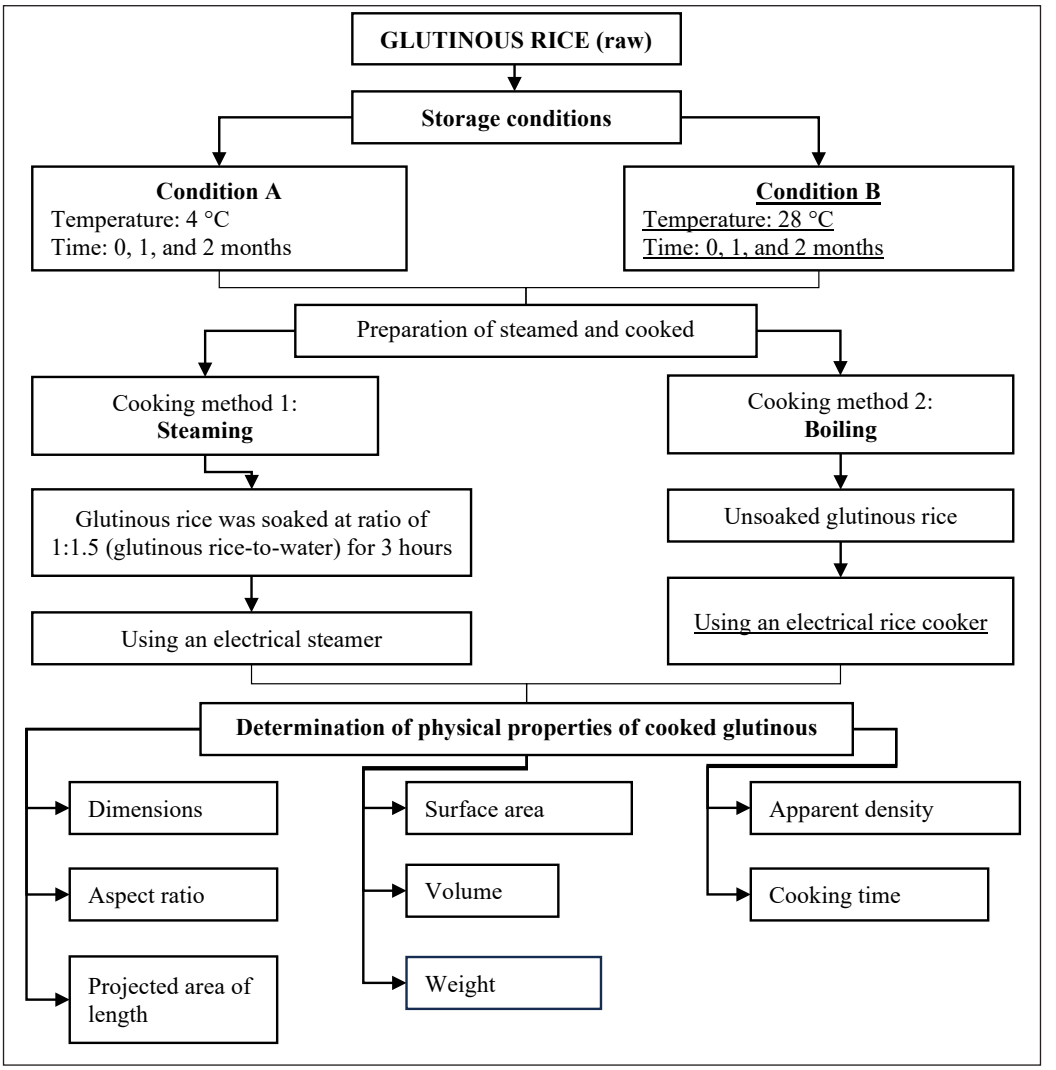

Figure 1. Flowchart for the preparation of steamed and cooked glutinous rice samples and determination of physical properties

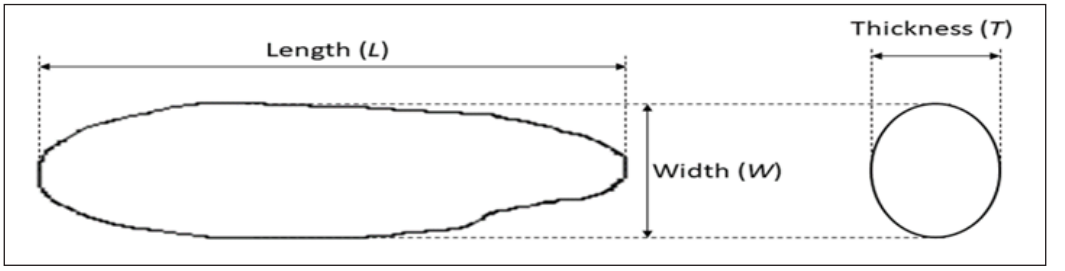

Figure 2. Dimensions of glutinous rice grain

Determination of Dimensions

As shown in Figure 2, the length (L), width (W), and thickness (T) of the steamed and cooked glutinous rice grains were measured using a digital vernier calliper (Series 500, Mitutoyo, Japan) with an accuracy of 0.01 mm. For each condition, glutinous rice grains were randomly selected, and their dimensions were measured and recorded 10 times to ensure accuracy (Hoque et al., 2022).

The equivalent diametre (De) of the steamed and cooked glutinous rice was determined as Equation 1 based on the measured length, width, and thickness (Hoque et al., 2022; Othman & Oma, 2017):

$$\mathrm{De\ (mm)} = \left(\frac{\mathrm{L(W+T)^2}}{4}\right)^{\frac{1}{3}} \quad [1]$$

Determination Aspect Ratio

The Equation 2 used to calculate the aspect ratio (R_a) of the steamed and cooked glutinous rice is as follows (Hoque et al., 2022):

$$\mathrm{R_a} = \frac{\mathrm{W}}{\mathrm{L}} \quad [2]$$

Determination of the Projected Area of Length

Projected area of length (PA_L) is defined as the projected area of steamed and cooked glutinous rice in a perpendicular direction to the length. An Equation 3 was used to calculate the projected area of the length (Azman et al., 2025).

$$\mathrm{PA_L} = \left(\frac{\pi \mathrm{WL}}{4}\right) \quad [3]$$

Determination of Surface Area

The surface area (SA) was calculated by using the measurements of length, width, and thickness of the steamed and cooked glutinous rice. The calculation followed the Equation 4 as follows (Hoque et al., 2022; Othman & Oma, 2017):

$$\mathrm{SA\ (mm^2)} = \frac{\pi \times \mathrm{B} \times \mathrm{L}^2}{2\mathrm{L} - \mathrm{B}} \quad [4]$$

$$\text{Where } \mathrm{B} = (\mathrm{W} \times \mathrm{T})^{\frac{1}{2}}$$

Determination of Volume

The volume (V) of the steamed and cooked glutinous rice was determined by Equation 5 (Hoque et al., 2022; Zainal & Shamsudin, 2021):

$$V\ (mm^3) = 0.25 \times [(\pi/6) \times L \times (W + T)^2] \quad [5]$$

Determination of Weight

The 100 glutinous rice grain weight was obtained for a sample of individual grains from each condition, which were selected randomly and weighed on a digital electronic scale (JA203P, Xingyun, China) with a precision of 0.001 g, and the result was expressed in grammes.

Determination of Apparent Density

The apparent density (ρ_{app}) The density of a grain is defined as the ratio of the mass of a grain to its volume. The apparent density of a grain was calculated using Equation 6:

$$\rho_{app} = \frac{M_i}{V_i} \quad [6]$$

Determination of Cooking Time

Head rice (250 g) samples were put into some aluminium cups from each storage condition and steamed in the electric steamer. Cooking time was assessed by taking out a few grains during various time intervals of cooking and pressing them until no white core was left. The steps were repeated for the boiling methods of glutinous rice five times

Statistical Analysis

Data analyses were done using the Minitab Statistic 16 Edition to conduct a Tukey's test to differentiate and determine the significant difference between the means. Both mean and standard deviation were reported from data of five replications for each analysis. The limits of confidence were taken as 95% (p<0.05). Pearson correlation coefficient analysis for the relationships between different cooking methods in some storage times and the dimensions, aspect ratio, surface area, volume, weight, and cooking time of glutinous rice.

RESULTS AND DISCUSSION

Dimensions

The dimensions (length, width, thickness, and equivalent diametre) of cooked glutinous rice grains, prepared using steaming and boiling methods from various storage conditions

(4 °C and 28 °C) for 0, 1, and 2 months, are presented in Table 1. The shape and size of glutinous rice grains are important physical properties. Glutinous rice exhibits significant variation across storage conditions and cooking methods. It was steamed in an electrical steamer at 110.00 ±2.00 °C. After 2 months of storage in conditions A and B, the glutinous rice was steamed, and the length was significantly (p<0.05) decreased from 9.39 ±0.10 mm to 8.43 ±0.30 mm. The steamed glutinous rice was insignificantly decreased from 1.92 ±0.09 mm to 1.87 ±0.08 mm in width, and 1.67 ±0.08 mm to 1.61 ±0.03 mm in thickness for the first- and second-month storage, respectively. Meanwhile, the cooked glutinous rice dimensions using a rice cooker were significantly decreased at p<0.05, from 9.46 ±0.30 mm to 8.68 ±0.09 mm in length, and 1.93 ±0.07 mm to 2.10 ±0.09 mm in width for 2 months storage conditions A and B. However, the cooked glutinous rice had insignificantly decreased from 1.52 ±0.08 mm to 1.46 ±0.05 mm in thickness, for the first- and second-months storage, respectively.

According to Table 1, the length, width, and thickness of steamed glutinous rice for the 2-month storage condition B were the highest compared to other conditions. The cooked glutinous rice of 2 months storage condition B had the greatest change in length, width, and thickness compared to other conditions. Furthermore, the results showed that the equivalent diameters of steamed and cooked glutinous rice varied from 3.12 ±0.06 mm to 2.94 ±0.05 mm and from 3.04 ±0.07 mm to 2.95 ±0.04 mm, respectively.

During gelatinisation of cooking, the cell structure of glutinous rice started to rupture, which caused amylopectin to be leached. Moreover, the utilisation of heat and water during cooking breaks down the double helical and crystalline structures within starch granules, as it allows water to diffuse more easily into glutinous rice, and it expands in size (Liang et al., 2025). Generally, the dimensions of cooked glutinous rice will be increased due to gelatinisation of starch. However, this study revealed different results due to the effects of storage conditions prior to cooking and different cooking methods used. Therefore, this study shows that the cooked glutinous rice using an electric rice cooker has the greatest change in length, width, and equivalent compared to the steamed glutinous rice using a steamer.

This is due to direct contact with water during cooking compared to the steaming method, which uses vapour contact on the glutinous rice.

Projected Area of Length

The projected area of steamed glutinous rice under storage conditions A and B decreased from 14.16 ±0.64 to 12.67 ±0.76 and 14.16 ±0.64 to 12.38 ±0.65 when the length and width decreased. A similar trend was indicated for the projected area of cooked glutinous rice under storage conditions A and B, with the values from 14.34 ±0.52 to 13.75 ±0.75 and 14.34 ±0.52 to 13.50 ±0.39, respectively.

Table 1
Dimensions of each 100 steamed and cooked glutinous rice

Storage Condition	Storage Time (Months)	Cooking Method	L (mm)	W (mm)	T (mm)	De (mm)	PA_L	Ra	SA (mm^2)
	0		9.39 ±0.10[a]	1.92 ±0.09[a]	1.67 ±0.08[a]	3.12 ±0.06[a]	14.16 ±0.64[a]	0.20 ±0.01[b]	29.17 ±0.88[a]
A	1		8.57 ±0.54[b]	1.92 ±0.09[a]	1.64 ±0.05[a]	3.00 ±0.09[b]	12.93 ±1.04[b]	0.22 ±0.02[a]	26.64 ±1.61[b]
	2	Steaming	8.49 ±0.43[b]	1.90 ±0.07[a]	1.63 ±0.05[a]	2.98 ±0.06[b]	12.67 ±0.76[b]	0.22 ±0.01[a]	26.17 ±1.16[b]
	0		9.39 ±0.10[a]	1.92 ±0.09[a]	1.67 ±0.08[a]	3.12 ±0.06[a]	14.16 ±0.64[a]	0.20 ±0.01[b]	29.17 ±0.88[a]
B	1		8.48 ±0.41[b]	1.92 ±0.09[a]	1.62 ±0.04[a]	2.98 ±0.06[b]	12.79 ±0.84[b]	0.23 ±0.02[a]	26.20 ±1.17[b]
	2		8.43 ±0.30[b]	1.87 ±0.08[a]	1.61 ±0.03[a]	2.94 ±0.05[b]	12.38 ±0.65[b]	0.22 ±0.01[a]	25.61 ±0.90[b]
	0		9.46 ±0.08[a]	1.93 ±0.07[b]	1.52 ±0.08[a]	3.04 ±0.07[ab]	14.34 ±0.52[ab]	0.20 ±0.01[b]	27.98 ±1.09[a]
A	1		8.98 ±0.09[b]	2.10 ±0.09[a]	1.49 ±0.06[a]	3.07 ±0.05[a]	14.81 ±0.72[a]	0.23 ±0.01[a]	27.66 ±0.71[a]
	2	Boiling	8.71 ±0.10[c]	2.01 ±0.11[ab]	1.48 ±0.08[a]	2.98 ±0.05[b]	13.75 ±0.75[b]	0.23 ±0.01[a]	26.16 ±0.64[b]
	0		9.46 ±0.08[a]	1.93 ±0.07[a]	1.52 ±0.08[a]	3.04 ±0.07[a]	14.34 ±0.52[a]	0.20 ±0.01[b]	27.98 ±1.09[a]
B	1		8.91 ±0.06[b]	1.99 ±0.06[a]	1.51 ±0.07[a]	3.01 ±0.07[ab]	13.93 ±0.44[ab]	0.22 ±0.01[a]	26.87 ±0.96[b]
	2		8.68 ±0.09[c]	1.98 ±0.06[a]	1.46 ±0.05[a]	2.95 ±0.04[b]	13.50 ±0.39[b]	0.23 ±0.01[a]	25.69 ±0.50[c]

Note. Data are expressed as mean ±SD; L, length (mm); W, width (mm); T, thickness (mm); De, equivalent diameter (mm); PA_L, projected area of length; Ra, aspect ratio; SA, surface area (mm^2); A, storage of glutinous rice at 4°C before cooking; B, storage of glutinous rice at 28°C before cooking. Different letters indicate statistically significant differences exist, $p<0.05$ for each column within each condition. Means that those that do not share a letter are significantly different. The Tukey test was applied with 95% simultaneous confidence intervals

Based on the results in Table 1, the steamed glutinous rice under storage condition B had the greatest change in projected area of length when compared to other conditions. The relationship between projected area and length was shown significantly.

Aspect Ratio

The aspect ratio of steamed and cooked glutinous rice varied from 0.20 ±0.01 to 0.23 ±0.02 for 2 months storage conditions A and B. As can be seen, they were increased when compared to the cooked glutinous rice without storage. As indicated, the aspect ratio of steamed and cooked glutinous rice was affected by the storage conditions A and B in 2 months. Thus, storage condition B has the most impact on the aspect ratio increment of cooked glutinous rice.

Surface Area

The surface area of steamed glutinous rice has decreased gradually, with the values of 26.64 ±1.61 mm^2 and 26.17 ±1.16 mm^2 for the first and second months after storage conditions A, respectively. Meanwhile, it was also decreased gradually from 26.20 ±1.17 mm^2 to 25.61 ±0.90 mm^2 for the first and second months after storage condition B. The surface area of cooked glutinous rice attained on the first and second months of storage condition A was 27.66 ±0.71 mm^2 and 26.16 ±0.64 mm^2. For storage condition B, the surface area values of cooked glutinous rice were 26.87 ±0.96 mm^2 and 25.60 ±0.50 mm^2 for the first and second months, respectively. Therefore, the surface area of cooked glutinous rice using an electric rice cooker was higher when stored in condition A.

Volume

The mean volume values of steamed glutinous rice were varied from 13.85 ±0.85 mm^3 to 15.85 ±0.90 mm^3 (storage condition A) and 13.37 ±0.70 mm^3 to 15.85 ±0.90 mm^3 (storage condition B). The volume values of cooked glutinous rice ranged from 13.89 0.72 mm^3 to 15.16 ±0.76 mm^3 and 13.45 ±0.48 mm^3 to 14.75 ±0.97 mm^3 after 2 months of storage conditions A and B, respectively. As indicated, the volume of steamed and cooked glutinous rice was affected by the storage conditions A and B in 2 months. The volume is directly proportional to the dimensions of glutinous rice, as the volume is reduced when the dimensions decrease. Thus, storage condition B has the most impact on volume reductions of steamed and cooked glutinous rice.

Weight

The weight of glutinous rice was determined for all steamed and cooked glutinous rice after 2 months of storage conditions A and B. The weight of a steamed glutinous rice

decreased until it reached 0.0239 ±5.5x10-5 g, while the cooked glutinous rice reached 0.0279 ±5.5x10-5 g after 2 months of storage. As indicated, the weight of steamed and cooked glutinous rice was affected by the storage conditions A and B in 2 months. Thus, storage condition B has the most impact on weight reductions of steamed and cooked glutinous rice. In general, the weight of glutinous rice increased after cooking. However, the results differed in this study due to the effect of storage conditions prior to cooking, where the weight of glutinous rice reduced during storage.

Apparent Density

Table 2 presents the results of the apparent density of glutinous rice that was stored for 2 months and then cooked using steaming and boiling methods. The apparent density values obtained for steamed glutinous rice were increased for both storage conditions A (1642.20 ±31.94 to 1792.30 ±49.28 kg/m^3) and B (1642.20 ±31.94 to 1784.13 ±45.39 kg/m^3). Meanwhile, the apparent density values for the cooked glutinous rice were decreased and then increased for both storage conditions A and B. The increment in density is affected by the reduction in the volume of glutinous rice at increasing moisture content levels (Anjali et al., 2023).

Table 2
Some physical properties of steamed and cooked glutinous rice

Storage Condition	Storage Time (Months)	Cooking Method	V (mm^3)	Weight (g)	ρ_{app} (kg/m^3)	Cooking Time (Min)
A	0	Steaming	15.85 ±0.90^{a}	0.0254 ±7×10^{-6a}	1642.20±31.94^{b}	25.21 ±0.03^{c}
	1		14.22 ±1.22^{b}	0.0248 ±8×10^{-6b}	1704.63 ±30.78^{b}	25.52 ±0.06^{b}
	2		13.85 ±0.85^{b}	0.0246 ±8×10^{-6c}	1792.30 ±49.28^{a}	26.17 ±0.06^{a}
B	0		15.85 ±0.90^{a}	0.0254 ±7×10^{-6a}	1642.20 ±31.72^{b}	25.21 ±0.03^{c}
	1		13.91 ±0.89^{b}	0.0242 ±4.42×10^{-4b}	1801.95 ±75.21^{a}	27.07 ±0.05^{b}
	2		13.37 ±0.70^{b}	0.0239 ±5.5×10^{-5b}	1784.13 ±45.39^{a}	29.16 ±0.08^{a}
A	0	Boiling	14.75 ±0.97^{ab}	0.0294 ±7×10^{-6a}	2024.61 ±55.40^{a}	30.19 ±0.04^{c}
	1		15.16 ±0.76^{a}	0.0286 2.9×10^{-5b}	1869.19 ±43.86^{b}	32.04 ±0.02^{b}
	2		13.89 ±0.72^{b}	0.0282 ±3.18×10^{-4c}	2054.48 ±31.29^{a}	33.23 ±0.05^{a}
B	0		14.75 ±0.97^{a}	0.0294 ±7×10^{-6a}	2024.62 ±55.92^{ab}	30.19 ±0.04^{c}
	1		14.30 ±0.88^{ab}	0.0282 ±4.42×10^{-4b}	1957.91 ±53.74^{b}	34.07 ±0.05^{b}
	2		13.45 ±0.48^{b}	0.0279 ±5.5×10^{-5b}	2086.14 ±43.85^{a}	36.19 ±0.03^{a}

Note. Data are expressed as mean ±SD; V, volume (mm^3); ρ_{app}, apparent density (g/mm^3); A, storage of glutinous rice at 4°C before cooking; B, storage of glutinous rice at 28°C before cooking. Different letters indicate statistically significant differences exist, p<0.05 for each column. Means that those that do not share a letter are significantly different. The Tukey test was applied with 95% simultaneous confidence intervals

Cooking Time

As can be seen in Table 1, the cooking methods (steaming or boiling) affect the cooking time significantly at $p<0.05$. For steamed glutinous rice, the cooking time increased from 25.21 ±0.03 mins to 26.17 ±0.06mins and 25.21 ±0.03mins to 29.16 ±0.08mins, respectively, for conditions A and B. It has the same trend as the cooked glutinous rice, which increased until reaching 33.23 ±0.05mins and 36.19 ±0.03mins for conditions A and B, respectively. As indicated, the cooking time of steamed and cooked glutinous rice was affected by the storage conditions A and B in 2 months. The glutinous rice stored in condition B and then cooked using the boiling method showed that it required a longer time to cook when compared to the steaming method. This is due to the boiling method of using an electric rice cooker, which involves a more gradual cooking process compared to steaming, where the glutinous rice is soaked first before being cooked, resulting in faster gelatinisation and cooking. According to the previous study of Thomas et al. (2013), the glutinous rice from Thailand had a minimum cooking time of 22.67 ±0.00mins. Patria et al. (2020) stated that the cooking time of Japonica Rice ranged from 3.00 to 10.33 mins. These previous studies showed the difference in their determination of cooking time because there is no storage condition prior to cooking included, and the laboratory procedure cooking methods used, rather than replicating the common cooking methods used by consumers.

Correlations for Physical Properties of Glutinous Rice After Cooking using the Steaming and Boiling Methods

Table 3 indicates a significant ($p<0.05$) correlation analysis of some physical properties of glutinous rice that are affected by storage conditions (A and B) combined with the selected cooking methods (steaming and boiling). For storage condition A and steaming method, length was highly positively correlated with the equivalent diameter (r=0.999, $p<0.05$) and surface area (r=0.998, $p<0.05$). The correlation coefficients between thickness and volume and weight were highly positive, with the values of 0.998 ($p<0.05$) and 1.000 ($p<0.001$), respectively. The equivalent diameter was highly positively correlated with surface area (r=1.000, $p<0.05$) and volume (r=0.999, $p<0.05$). The correlation coefficient between surface area and volume was highly positive with the value of 1.000 ($p<0.05$), while the volume was highly positively correlated with weight (r=0.998, $p<0.05$). Under storage condition B and steaming method, the thickness was highly positively correlated with the equivalent diameter (r=0.998, $p<0.05$), surface area (r=1.000, $p<0.001$), volume (r=0.999, $p<0.05$), and weight (r=0.999, $p<0.05$). The correlation coefficients between equivalent diameter and surface area, volume, and weight were highly positive with the values 0.998 ($p<0.05$), 1.000 ($p<0.05$), and 1.000 ($p<0.05$), respectively. The surface area was highly positively correlated with the volume and weight (r=0.999, $p<0.05$), while the

correlation coefficient between volume and weight was highly positive with the value of 1.000 (p<0.05).

As shown in Table 3, the length of cooked glutinous rice under storage condition A and boiling method was highly positively correlated with the weight (r=1.000, p<0.05). Meanwhile, the correlation coefficient between equivalent diametre and volume was 1.000 (p<0.05). However, the length of cooked glutinous rice under storage B and the boiling method was highly negatively correlated with aspect ratio (r=−0.999, p<0.05). The correlation coefficient between equivalent diametre and volume was highly positive, with a value of 1.000 (p<0.05). Thus, the results showed that the storage conditions combined with the cooking methods using steaming and boiling have different trends of correlations with some physical properties of steamed and cooked glutinous rice.

Principal Component Analysis for Physical Properties of Steamed and Cooked Glutinous Rice

Principal component analysis (PCA) was performed to determine the clustering length, width, thickness, equivalent diametre, aspect ratio, surface area, volume, and weight within the cooking methods (steaming and boiling). According to Figure 3, PC1 explained the total variance of length, width, thickness, equivalent diametre, aspect ratio, surface area, volume, and weight. In PCA, PC1 was dominant when compared to PC2. Figure 3 shows the PCA score plot used to illustrate the PCA results. They specified a clear and scattered separation between the two cooking methods based on the length, width, thickness, equivalent diametre, aspect ratio, surface area, volume, and weight of steamed and cooked glutinous rice. Theoretically, the PCA results illustrated that storage conditions prior to cooking and cooking methods influenced these physical properties. Hence, their changes were verified by classifying the two cooking methods and four storage conditions.

The PCA loading plot of length, width, thickness, equivalent diametre, aspect ratio, surface area, volume, and weight is illustrated in the Figure 4. The correlations among these physical properties and cooking methods, combined with storage conditions, can be seen in the loading plot. Based on Figure 4 the thickness and surface were loaded positively on PC1 and PC2. Meanwhile, width and aspect ratio were loaded negatively on PC1 and PC2.

CONCLUSION

The study revealed that both steaming and boiling methods affect the dimensions, projected area, aspect ratio, surface area, volume, weight, apparent density, and cooking time of glutinous rice. In this study, the glutinous rice Siding cultivar was used in storage, steaming, and boiling methods. The effects of different cooking methods on the physical properties and cooking time of glutinous rice were investigated. Due to storage conditions (before

Table 3
Correlation matrix for some physical properties of glutinous rice after cooking using the steaming and boiling methods

	Condition A (Steaming method)							Condition B (Steaming method)						
	L	**W**	**T**	**De**	**Ra**	**SA**	**V**	**L**	**W**	**T**	**De**	**Ra**	**SA**	**V**
W	0.568*							0.540*						
T	0.987*	0.693*						0.994*	0.629*					
De	0.999**	0.610*	0.994*					0.986*	0.672*	0.998**				
Ra	-0.997*	-0.500*	-0.971*	-0.991*				-0.929*	-0.189*	-0.882*	-0.854*			
SA	0.998**	0.621*	0.995*	1.000**	-0.989*			0.994*	0.628*	1.000***	0.998**	-0.883*		
V	0.996*	0.643*	0.998**	0.999**	-0.985*	1.000**		0.987*	0.668*	0.999**	1.000**	-0.857*	0.999**	
Weight	0.987*	0.693*	1.000***	0.994*	-0.971*	0.995*	0.998**	0.990*	0.655*	0.999**	1.000**	-0866*	0.999**	1.000**
	Condition A (Boiling method)							**Condition B (Boiling method)**						
	L	**W**	**T**	**De**	**Ra**	**SA**	**V**	**L**	**W**	**T**	**De**	**Ra**	**SA**	**V**
W	-0.605*							-0.902*						
T	0.993*	-0.697*						0.825*	-0.500*					
De	0.526*	0.359*	0.419*					0.912*	-0.645*	0.984*				
Ra	-0.935*	0.849*	-0.971*	-0.189*				-0.999**	0.882*	-0.849*	-0.929*			
SA	0.869*	-0.131*	0.803*	0.878*	-0.636*			0.969*	-0.767*	0.939*	0.985*	-0.978*		
V	0.536*	0.348*	0.430*	1.000**	-0.200*	0.884*		0.918*	-0.656*	0.982*	1.000**	-0.934*	0.988*	

Note. Data are expressed as L, length; W, width; T, thickness; De, equivalent diametre; Ra, aspect ratio; SA, surface area; V, volume
*Not significant, **Significant at $p<0.05$, ***Significant at $p<0.001$

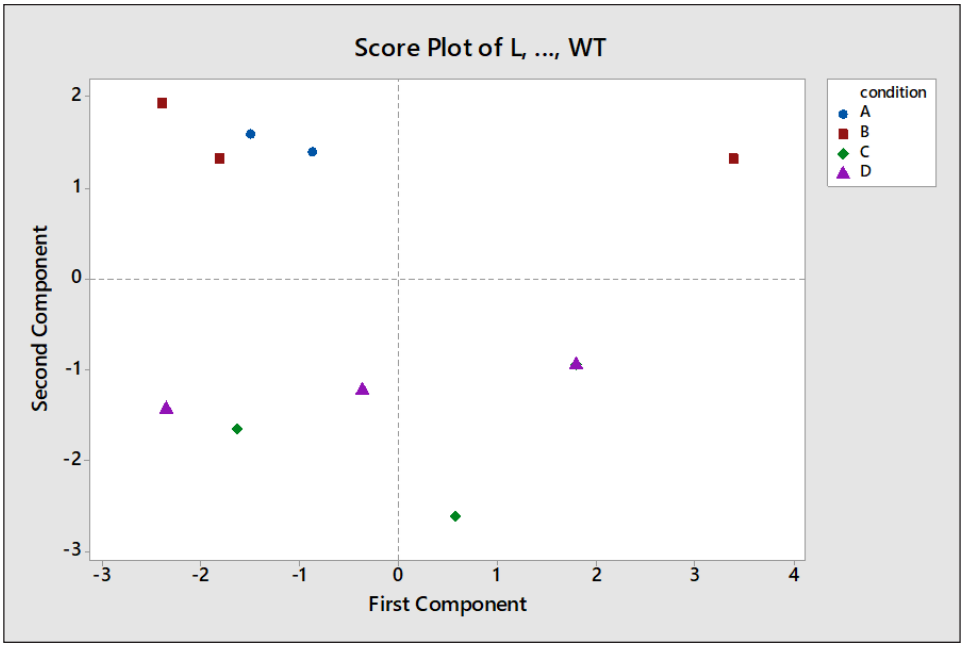

Figure 3. The score plot of the physical properties of steamed and cooked glutinous rice. The yellow circle shows the steaming method, while the blue circle shows the boiling method. Storage conditions are labelled as A: 4 °C storage before steaming, B: 28 °C storage before steaming, C: 4 °C before boiling, and D: 28 °C before boiling of glutinous rice

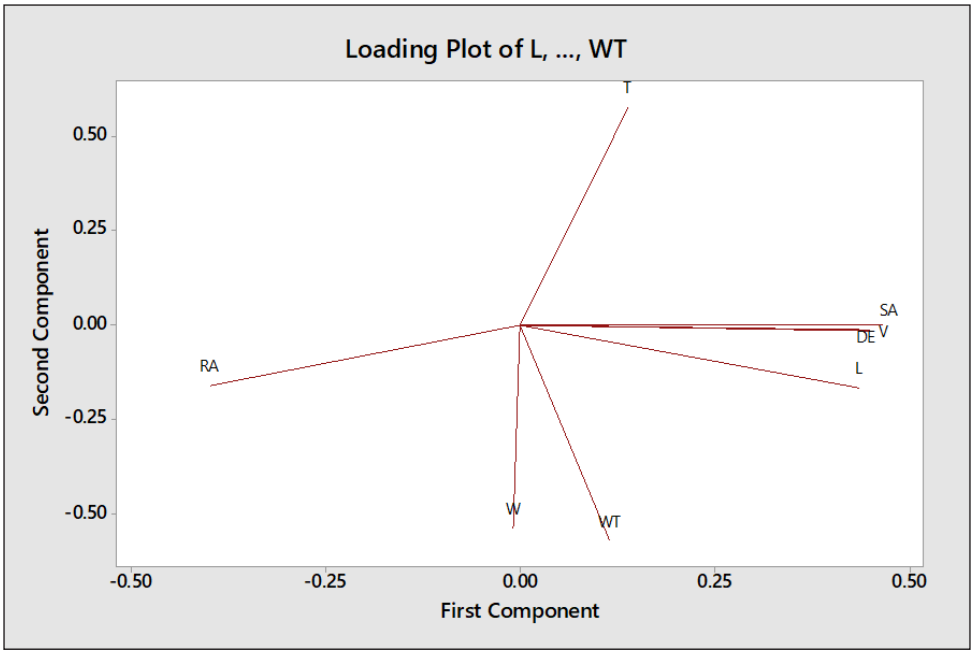

Figure 4. The loading plot of the physical properties of steamed and cooked glutinous rice

cooking) and cooking methods, significant changes in the physical properties of glutinous rice were observed. A reduction in length, equivalent diametre, projected area, surface area, volume, and weight of the steamed glutinous rice was determined, along with a notable increase in aspect ratio, apparent density, and cooking time. For the steaming method, the steamed glutinous rice from storage condition A had the highest increment in apparent density (1792.30 ±49.28 kg/m3), while the steamed glutinous rice from storage condition B had the highest in cooking time (29.16 ±0.08 mins). The steamed glutinous rice from storage condition B had reduced in length (8.43 ±0.30 mm), equivalent diametre (2.94 ±0.05 mm), projected area (12.38 ±0.65), surface area (25.61 ±0.90 mm^2), volume (13.37 ±0.70 mm^3), and weight (0.0239 ±5.50×10^{-5} g) when compared to storage condition A. In the boiling method, the cooked glutinous rice also led to a reduction in length, equivalent diametre, projected area, surface area, volume, and weight. However, it had an increase in aspect ratio, apparent density, and cooking time. For the boiling method, the cooked glutinous rice from storage condition B had the highest increment in apparent density (2086.14 ±43.85 kg/m^3) and cooking time (36.19 ±0.03 mins). Also, they had the highest reduction in length (8.68 ±0.09 mm), equivalent diametre (2.95 ±0.04 mm), projected area (0.23 ±0.01), surface area (25.69 ±0.50 mm^2), volume (13.45 ±0.48 mm^3), and weight (0.0279 ±5.50×10^{-5} g) when compared to storage condition A. The size of cooked glutinous rice is greater than that of steamed glutinous rice, which shows more expansion. Nevertheless, steamed glutinous rice is generally preferred over the cooked glutinous rice using the boiling method, which tends to result in glutinous rice that is slightly soggy and more prone to sticking together compared to steaming. This is due to the direct water absorption during cooking using the boiling method. Overall, the findings highlight that storage conditions (A and B) together with the selected cooking methods (steaming and boiling) significantly influence the physical properties and cooking behaviour of glutinous rice. Hence, this study provides knowledge and a theoretical basis for both home cooks and the food industry regarding the best practices for preparing glutinous rice. It provides meaningful insights for both consumers and food processors by evaluating cooking approaches that optimise the desired quality attributes of glutinous rice. Based on this study's findings, some key areas for future research that can be identified include the determination of the longer-term storage effects' influence on physical and functional changes of glutinous rice, evaluation of cooking methods' effect on the chemical properties, microstructural analysis, and investigation of sensory perception and consumer acceptability.

ACKNOWLEDGEMENT

The authors express their appreciation to the Ministry of Higher Education of Malaysia for providing financial support under the Trans-disciplinary Research Grants Scheme (TRGS)

with Project Number: TRGS/1/2020/UPM/02/7. They also express their gratitude to the Universiti Putra Malaysia for the technical support to conduct this research.

REFERENCES

Ali, M. M., & Hashim, N. (2024). Exploring nutritional compositions, volatile compounds , health benefits, emerging processing technologies, and potential food products of glutinous rice : A review. *Rice Science*, *31*(February). https://doi.org/10.1016/j.rsci.2024.02.002

Anjali, K. U., Kamatchi, A. R., Haripriya, S., Kumar, A., & Reddy, C. K. (2023). Varietal differences in the physical and engineering attributes of underutilised pigmented and non-pigmented paddy and rice landraces. *Food Science and Engineering*, 248-264. https://doi.org/10.37256/fse.4220232342

Azman, P. N. M. A., Shamsudin, R., Che Man, H., & Ya'acob, M. E. (2020). Effect of soaking process on physical properties of mature pepper berries (Piper nigrum L.). *Food Research*, *4*(S1), 116-123. https://doi.org/10.26656/fr.2017.4(s1).s04

Azman, P. N. M. A., Shamsudin, R., Hashim, N., & Che Man, H. (2025). Kinetics of Dimensional Changes in Glutinous Rice at Different Rice-Water Ratio and Soaking Time. *Journal of Engineering and Sustainable Development*, *29*(03), 289-296.

Bhattacharya, K. R. (2011). *Rice quality: A guide to rice properties and analysis* (First Edit). Woodhead Publishing. https://doi.org/https://doi.org/10.1533/9780857092793

Díaz, E. O., Kawamura, S., & Koseki, S. (2015). Physical properties of rough and brown rice of Japonica, Indica, and NERICA types. *Agricultural Engineering International: CIGR Journal*, 274-85.

Hoque, N., Islam, M. Z., Rahman, F., Mahmud, N., Rahman, M., & Biswas, B. (2022). Grain physical properties analysis of some improved rice varieties. *Asian Journal of Crop, Soil Science, and Plant Nutrition*, *6*(2), 242-250. https://doi.org/10.18801/ajcsp.060222.29

Hu, X., Lu, L., Guo, Z., & Zhu, Z. (2020). Volatile compounds, affecting factors, and evaluation methods for rice aroma: A review. *Trends in Food Science & Technology*, *97*(January), 136-146. https://doi.org/10.1016/j.tifs.2020.01.003

Krongworakul, N., Naivikul, O., Boonsupthip, W., & Wang, Y. J. (2020). Effect of conventional and microwave heating on physical and chemical properties of Jasmine brown rice in various forms. *Journal of Food Process Engineering*, *43*(10), 1-12. https://doi.org/10.1111/jfpe.13506

Liang, C., Han, Y., Xu, H., Liu, D., & Jiang, C. (2025). The high molecular weight and large particle size and high crystallinity of starch increase gelatinisation temperature and retrogradation in glutinous rice. *Carbohydrate Polymers*, *348*(PA), 122756. https://doi.org/10.1016/j.carbpol.2024.122756

Meena, S. K., Vijayalakshmi, D., & Ravindra, U. (2010). Physical and cooking characteristics of selected aromatic rice varieties. *Asian Journal of Dairy and Food Research*, *29*, 227-231.

Nádvorníková, M., Banout, J., Herák, D., & Verner, V. (2018). Evaluation of physical properties of rice used in traditional Kyrgyz Cuisine. *Food Science and Nutrition*, *6*(6), 1778-1787. https://doi.org/10.1002/fsn3.746

Naomi, K. F., & Lewis, H. Z. (2019). Rice: Importance for Global Nutrition. *Journal of Nutritional Science and Vitaminology*, *65*, 2-3. https://doi.org/https://doi.org/10.3177/jnsv.65.s2

Ngo, T. Van, Kunyanee, K., & Luangsakul, N. (2023). Insights into recent updates on factors and technologies that modulate the glycemic index of rice and its products. *Foods*, *12*(19). https://doi.org/10.3390/foods12193659

Ojediran, J. O., Okonkwo, C. E., Olayanju, T. A., Hussain, S. Z., Olaniran, A. F., & Adewumi, A. D. (2020). Effect of polishing duration on physical, milling, cooking, and sensory properties of a novel mix-colored Nigerian parboiled rice. *Cereal Chemistry*, *97*(6), 1172-1182. https://doi.org/10.1002/cche.10337

Oli, P., Ward, R., Adhikari, B., & Torley, P. (2016). Colour change in rice during hydration : Effect of hull and bran layers. *Journal of Food Engineering*, *173*, 49-58. https://doi.org/10.1016/j.jfoodeng.2015.10.036

Othman, R. S., & Oma, K. A. (2017). Study starch content and a variety of physical characteristics of rice (Oryza sativa L.). *Polytechnic Journal*, *7*(3). https://doi.org/10.25156/ptj.2017.7.3.38

Patria, D. G., Sutrisno, A., Hsu, J. L., & Lin, J. (2020). Physical properties and cooking quality of extruded restructured rice: impact of water temperature and water level. *Food Research*, *4*(5), 1616-1622. https://doi.org/10.26656/fr.2017.4(5).141

Ravi, U., Menon, L., Madhavan, R., Priyadharshini, S., & Dhivya, M. E. (2014). Determination of quality characteristics of indigenous organic Asian Indian rice variety - Neelam samba. *Agricultural Science Digest*, *34*(3), 177-182. https://doi.org/https://doi.org/10.5958/0976-0547.2014.00997.5

Smanalieva, J., Salieva, K., Borkoev, B., Windhab, E. J., & Fischer, P. (2015). Investigation of changes in chemical composition and rheological properties of Kyrgyz rice cultivars (Ozgon rice) depending on long- term stack-storage after harvesting. *LWT - Food Science and Technology*, 1-7. https://doi.org/10.1016/j.lwt.2015.03.045

Thakur, A. K., & Gupta, A. K. (2006). Water absorption characteristics of paddy, brown rice and husk during soaking. *Journal of Food Engineering*, *75*(2), 252-257. https://doi.org/10.1016/j.jfoodeng.2005.04.014

Thomas, R., Wan-Nadiah, W. A., & Bhat, R. (2013). Physiochemical properties, proximate composition, and cooking qualities of locally grown and imported rice varieties marketed in Penang, Malaysia. *International Food Research Journal*, *20*(3), 1345-1351.

Varnamkhasti, M. G., Mobli, H., Jafari, A., Keyhani, A. R., Soltanabadi, M. H., Rafiee, S., & Kheiralipour, K. (2008). Some physical properties of rough rice (Oryza Sativa L.) grain. *Journal of Cereal Science*, *47*(3), 496-501. https://doi.org/10.1016/j.jcs.2007.05.014

Zainal, N., & Shamsudin, R. (2021). Physical Properties of Different Cultivar Local Glutinous rice (susu and siding) and Commercial Thai Cultivar. *Advances in Agricultural and Food Research Journal*, *2*, 1-10. https://doi.org/10.36877/aafrj.a0000178

Pertanika J. Trop. Agric. Sci. 49 (S1): 211 - 233 (2026)

PERTANIKA JOURNALS

TROPICAL AGRICULTURAL SCIENCE

Journal homepage: http://www.pertanika.upm.edu.my/

Review Article

Adoption of Smart Farming Technologies (SFTs) among Young Farmers: A Systematic Literature Review

Nurul Aziemah Majid, Nur Bahiah Mohamed Haris[1]*, Jasmin Arif Shah[1], Nik Norasma Che'Ya[1], and Mohd Mursyid Arshad[2]

[1]Department of Agriculture Technology, Faculty of Agriculture, Universiti Putra Malaysia, 43400 UPM Serdang, Selangor, Malaysia

[2]Professional Development and Continuing Education, Faculty of Educational Studies, Universiti Putra Malaysia, 43400 UPM Serdang, Selangor, Malaysia

ABSTRACT

The concept of smart farming is increasingly being applied in the agricultural industry to enhance efficiency, boost productivity and strengthen food security. It also contributes to achieving sustainable farming practices. Young farmers who are more digitally literate and adaptable to new technologies are often more inclined to explore and adopt smart farming solutions. This systematic literature review article on the adoption of smart farming technologies, particularly among young farmers, examines the factors influencing their adoption. A comprehensive search was conducted in databases such as Scopus, IEEE Xplore, ScienceDirect, ProQuest, and Google Scholar, focussing on peer-reviewed studies published between 2019 and 2024. The review adopted the Preferred Reporting Items for Systematic Reviews and Meta-Analyses (PRISMA) guidelines. A total of 213 articles were retrieved during the identification process, and after the screening, eligibility assessment, and quality appraisal, only 15 articles were selected for inclusion in this SLR. The review identified six key themes, including individual factors, social influences, knowledge and experience, technology factors, institutional support, and economic factors. Further analysis of these themes resulted in the identification of 13 sub-themes. Findings suggest that perceived usefulness, followed by psychological factors, are the primary factors of smart farming technology adoption among young farmers. However, economic factors, particularly cost, remain a significant barrier. Finally, the study presents several recommendations at the end of this research for the reference of future scholars.

Keywords: Adoption, smart farming technologies, systematic literature review (SLR), young farmers

ARTICLE INFO

Article history:
Received: 19 July 2025
Accepted: 30 December 2025
Published: 19 March 2026

DOI: https://doi.org/10.47836/pjtas.49.S1.10

E-mail addresses:
nurulaziemahmajid@gmail.com (Nurul Aziemah Majid)
nurbahiah@upm.edu.my (Nur Bahiah Mohamed Haris)
jasmin.arifshah@upm.edu.my (Jasmin Arif Shah)
niknorasma@upm.edu.my (Nik Norasma Che'ya)
m_mursyid@upm.edu.my (Mohd Mursyid Arshad)
* Corresponding author

e-ISSN: 2231-8542

INTRODUCTION

According to the United Nations, the global population is projected to increase to between 9.4 and 10.1 billion by 2050, creating significant challenges for food production. In response, the concept of smart farming is increasingly recognised as a solution to address these challenges. Smart farming technologies (SFTs) are transforming agriculture by integrating advanced technologies into farming practices (Dias et al., 2022). The adoption of SFTs has become essential to address critical challenges in the agriculture sector, including climate change, extreme weather, pest and disease outbreaks, and the issue of an ageing farming population (Alotaibi, 2023; Talaviya et al., 2020; Yoe, 2017). These technologies have the potential to enhance productivity and efficiency by automating farm activities, improving agricultural output and strengthening food security. In addition, SFTs play an important role in promoting sustainable farming practices. These practices include precision agriculture, efficient irrigation systems and reduced chemical usage, all of which contribute to long-term environmental sustainability and soil health (Hadi Suzer et al., 2024; Sharma et al., 2024). Therefore, the integration of SFTs not only modernises agriculture but also aligns with global sustainability goals.

SFTs represent an innovative solution for overcoming challenges in the agricultural sector. By integrating technology into farming practices, smart farming modernises agriculture and enables farmers to remotely monitor crops (Zaman et al., 2023). SFTs refers to the use of technologies such as Internet of Things (IoT), cloud storage, robotics, big data analysis, and Artificial Intelligence (AI) to manage agricultural activities (Dhanaraju et al., 2022; Wee & Ting, 2023). Through precise resource utilisation, SFTs help farmers optimise agricultural inputs and improve data authenticity by providing accurate weather forecasts, yield predictions and disease mapping based on reliable meteorological and climate data networks (Amiri-Zarandi et al., 2022). Beyond their direct impact on farming practices, SFTs can also attract young individuals to the agricultural industry, addressing the ageing workforce issue (Kwakye et al., 2021).

To sustain the agricultural industry and achieve sustainable development, youth involvement in the sector must be encouraged. One approach to achieving this is by utilising SFTs in farm management, as these innovations can attract youth to pursue careers in agriculture, particularly in agribusiness (Harisudin et al., 2023; Kwakye et al., 2021). Osabohien (2023) highlighted that improved access to technology and ICT serves as a potential catalyst for increasing youth involvement in agriculture. Furthermore, an analysis by Jaafar et al. (2021) revealed that Malaysia's internet usage reached 88.7% in 2020, with a significant youth presence, as 85.9% of users fell within this demographic. This underscores the potential for technology-driven approaches in engaging young people in agriculture.

Despite the growing body of research on SFTs, most existing studies focus on examining adoption among the general farming population without considering age differences. What remains unclear is how these factors influence young farmers, given that their technological readiness and motivations might differ from older generation farmers. As youth play an important role in sustaining the future agriculture sector, a clearer understanding of their adoption patterns is needed. This SLR therefore addresses the gap by systematically identifying existing evidence on the determinants of SFT adoption among young farmers.

The Need for a Systematic Review

Systematic Literature Review (SLR) has been widely used in the social sciences for many decades, primarily to support practice and policy decisions and to guide future research efforts (Petticrew & Roberts, 2006). SLR is a literature review process that applies principles of empirical research to enhance transparency at every stage of the review and minimise the risk of bias (Lame, 2019). It is a methodical approach for identifying, reviewing, and synthesising all relevant studies available to address a specific research question. An SLR is particularly crucial compared to traditional literature reviews. It addresses issues such as transparency, author bias, retrieval bias, and publication bias.

The adoption of SFTs among young farmers is increasingly recognised as an important area of research due to its potential impact on sustainable agriculture. While many studies have explored the adoption of SFTs, the majority focus on the general farming population, with youth often included as a subset of respondents rather than the primary focus. Examples include the studies from Chuang et al. (2020a), Kwapong et al. (2023), Erokhin et al. (2024), Isma Addi et al. (2024) and Wee and Lim (2022). On the other hand, several studies have examined the adoption of SFTs specifically among young farmers, such as Chuang et al. (2020a) and Kwakye et al. (2021). These studies highlight the need for an SLR to better understand factors influencing SFT adoption among young farmers.

Existing SLRs on IoT and smart farming adoption largely emphasize the general farming population (Bashiru et al., 2024; Omar, 2021), leaving the perspectives of young farmers underexplored. To address this gap, an SLR focussed on the adoption of SFTs among young farmers is essential. Using a systematic approach, an SLR ensures a more objective and comprehensive review of the literature. The current literature review is structured around the research question: What are the key factors influencing young farmers' adoption of smart farming technologies? This review primarily focussed on factors affecting human adoption.

METHODOLOGY

This section discusses the four main sections, which are PRISMA, resources, process for selecting articles, and data abstraction and analysis.

Prisma

This paper adopts the PRISMA approach, also known as the Preferred Reporting Items for Systematic Reviews and Meta-Analyses, to guide the SLRs process. PRISMA serves as a publication standard, providing a structured framework for authors to conduct SLRs by including the necessary information to evaluate and assess the quality of the review (Mohamed Shaffril et al., 2019). It is widely used to facilitate the development of SLRs and meta-analyses (Abbasi et al., 2022). Page et al. (2021) emphasised that PRISMA is particularly suitable for systematic reviews in various fields, including social sciences. They highlighted its ability to help academic authors produce comprehensive and well-structured systematic analyses that are highly relevant to the research community. PRISMA provides a detailed checklist of guidance for reporting literature searches within systematic reviews, with its core component being a flow diagram that outlines the process from initial search through selection and screening (Haddaway et al., 2022).

Information Sources and Search Strategy

The first step in developing the SLR is formulating suitable research questions. Given the focus of this SLR on the adoption of SFTs among young farmers, the following research questions were identified:

> What are the key factors influencing young farmers' adoption of smart farming technologies?

Building on these research questions, the review methods for this study were implemented using several databases accessible through the Universiti Putra Malaysia library's website. The databases utilised include Scopus, IEEE Xplore and ProQuest. These databases were selected because they cover topics related to agriculture, technology and multidisciplinary studies. Additionally, to maximise the likelihood of retrieving relevant articles, manual searches were performed on established resources such as ScienceDirect and Google Scholar.

The Systematic Review Process for Selecting Articles

Identification

Identification is the process of determining and selecting various relevant keywords to facilitate the SLR search process. This stage is essential, as appropriate keywords ensure the selection of studies directly related to the research questions and address the specific issues of interest outlined in the review. Based on the research questions, the primary

keywords identified were adoption, smart farming technology, and youth. To expand the range of relevant studies, additional and related keywords were identified, resulting in a more comprehensive set of search terms. Furthermore, various agricultural technologies, such as Internet of Things (IoT), Machine Learning (ML), Artificial Intelligence (AI), robotics, and Big Data, were also included as keywords when searching for articles (Refer to Table 1). Then, the keywords were combined into a search sentence using Boolean operators (OR and AND) to optimise the search strategy.

Table 1
Primary and expanded keywords

Primary Keywords	Expanded Keywords
Adoption	Acceptance
	Intention
Smart farming technology	Smart farming
	Smart agriculture
	Digital farming
	Intelligent farming
	Internet of Things (IoT)
	Machine Learning (ML)
	Artificial Intelligence (AI)
	Robotics
	Big data
Youth	Young farmers

The article search was conducted across five databases: Scopus, IEEE Xplore, ScienceDirect, ProQuest, and Google Scholar, chosen for their relevance and coverage. Scopus, the largest abstract and indexing database, offers extensive coverage of subjects such as agriculture, technology, and life sciences (Burnham, 2006). IEEE Xplore focuses on computer science and technology, making it relevant for SFTs. ScienceDirect and ProQuest provide multidisciplinary coverage, including agriculture and social sciences. Google Scholar was used for manual searches due to its accessibility and widespread use.

Advanced search techniques were applied, including Boolean operators (AND, OR), phrase searching, field codes, filtering and selected keywords. Since each database has its own syntax and functionality, the search strings were specifically tailored to align with the capabilities of each database (Refer to Table 2). Based on the searching techniques employed, a total of 213 articles were retrieved.

Table 2
The search strings

Database	Search String
Scopus	ALL ("smart farming" OR "Internet of Things" OR "IoT" OR "AI" OR "ML" OR "Robotics") AND ("adoption" OR "acceptance") AND ("youth" OR "young farmer?") AND (LIMIT-TO (SUBJAREA, "SOCI") OR LIMIT-TO (SUBJAREA , "AGRI")) AND (LIMIT-TO (DOCTYPE , "ar")) OR LIMIT-TO (EXACTKEYWORD, "Technology Adoption") OR LIMIT-TO (EXACTKEYWORD, "Technology") OR LIMIT-TO (EXACTKEYWORD, "Internet Of Things") OR LIMIT-TO (EXACTKEYWORD, "Agriculture") OR LIMIT-TO (EXACTKEYWORD , "Agricultural Technology") OR LIMIT-TO (EXACTKEYWORD , "Adoption"))
IEEE Xplore	("All Metadata":adoption) OR ("All Metadata":acceptance) AND ("All Metadata":smart farming) OR ("All Metadata":technology) OR ("All Metadata":IoT) OR ("All Metadata":Internet of Things) OR ("All Metadata":Artificial intelligence) AND ("All Metadata":youth) OR ("All Metadata":young farmers)
ScienceDirect	adoption of smart farming technologies among young farmers
Proquest	("Internet of Things" OR IoT) AND ("farm management" OR "agriculture management" OR "smart farming") AND ("adoption" OR "acceptance" OR "implementation" OR "utilisation") AND ("young farmers" OR "youth farmers" OR "youth in agriculture")
Google Scholar	adoption of smart farming technologies among young farmers

Screening

The 213 articles retrieved during the identification process underwent a screening process to select those suitable for the systematic review, guided by predefined inclusion and exclusion criteria (Mohamed Shaffril et al., 2021). Only articles published between 2019 and 2024, written in English, and peer-reviewed were considered. Additionally, only empirical research articles were included, while review articles were excluded, as the SLR aims to synthesize original research findings. Relevance was another key criterion: selected studies had to provide findings specifically related to the adoption of smart farming technologies (SFTs), ensuring alignment with the review's objectives. Following the screening process, 153 articles were excluded as they did not meet the inclusion criteria. The inclusion and exclusion criteria are detailed in Table 3. Consequently, 60 articles remain and will proceed to the next stage of the systematic review process.

Eligibility

All 60 remaining articles underwent a second screening process, referred to as eligibility. This eligibility process involved manual screening by the researchers to minimize errors made by the database (Mohamed Shaffril et al., 2021). During this phase, the titles,

Table 3
Inclusion criteria

Criterion	Inclusion	Exclusion
Publication year	Published within the last 5 years (2019-2024)	Published before 2019
Publication type	Peer-reviewed journal articles (Research articles)	Review articles, books, or non-peer-reviewed sources
Language	English	Non-English
Findings type	Empirical data	Review data
Findings focus	Adoption of SFTs in farming practices; young farmers included as a respondents	Topics unrelated to adoption

abstracts, and the main contents, such as methodology, results and discussion, were thoroughly examined. As a result, 40 articles were excluded because their focus was not on SFTs adoption, they were review articles, or they did not include young farmers as a respondent. Thus, only 20 articles were deemed eligible to proceed to the next stage: data abstraction and analysis. Figure 1 illustrates the flow of the systematic review process for selecting articles.

Quality Appraisal

These 20 articles were then subjected to quality appraisal. Two researchers independently examined each article considered suitable for inclusion in the SLR. The quality of the articles was assessed by adapting the Mixed Method Appraisal Tool (MMAT) developed by Pace et al. (2012), which is designed to appraise qualitative, quantitative, and mixed methods studies. In this process, each selected article from the eligibility phase was further examined based on three criteria: 1) whether the study presented a clear research objective; 2) whether the collected data adequately addressed the stated research objective; 3) whether data, analysis and interpretations were coherent. Each criterion was rated as "Yes," "No," or "Cannot tell." A minimum cut-off of two out of three criteria rated as "Yes" was applied for inclusion. After independently reviewing the quality of the articles, the researchers discussed their findings and decided which articles should remain in this SLR and which should be excluded. As a result, 15 articles were selected for further analysis in this SLR.

Data Abstraction and Analysis

The next step was data abstraction from the articles that had been assessed for quality. This process was carried out by two researchers. As the focus of this SLR was to examine previous findings on the adoption of SFTs among young farmers, data abstraction focussed on three main sections of each article: the abstract, results and discussion.

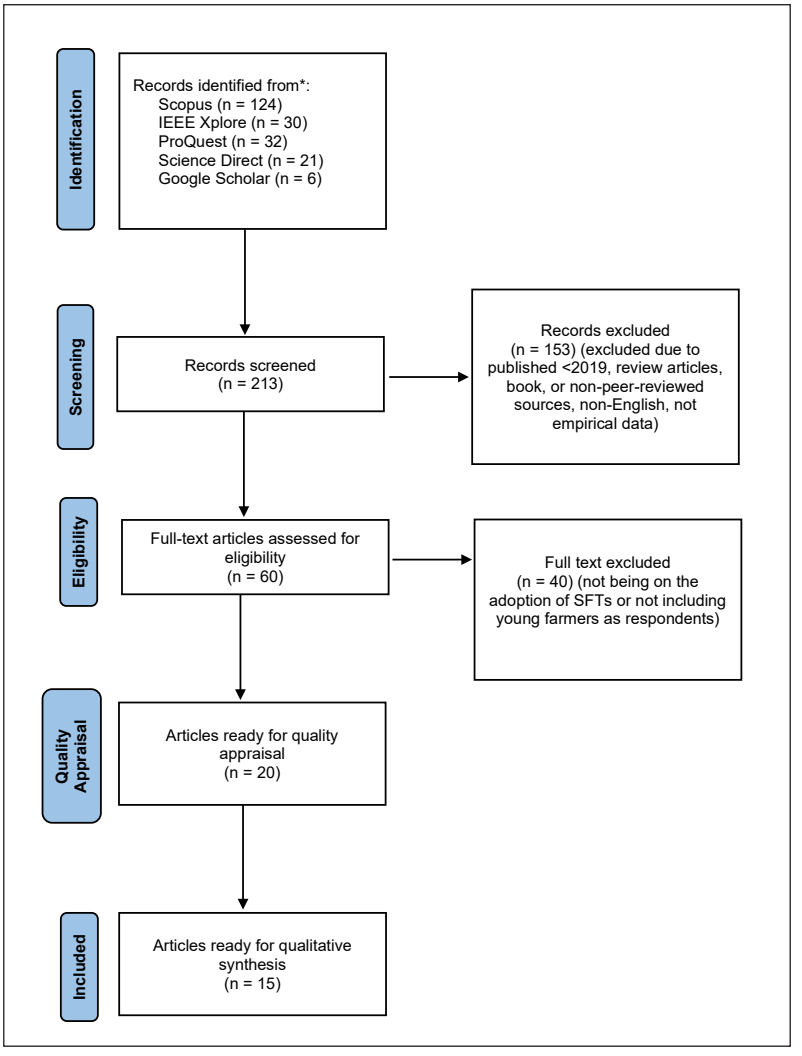

Figure 1. Flow diagramme of the systematic review process (adapted from Mohamed Shaffril et al. (2020))

After extracting the necessary data from the selected articles, the next step involved analysing the data. Since this SLR follows an integrative review approach that incorporates diverse methodologies (quantitative, qualitative, and mixed methods), qualitative synthesis was employed, as it is suitable for both quantitative and qualitative studies (Mohamed Shaffril et al., 2021). Qualitative synthesis is a method of systematically reviewing and integrating findings from various studies, making it particularly useful for understanding experiences, perceptions and social phenomena. For this synthesis, thematic analysis was utilised as the analytical method, as it was the most appropriate for synthesising mixed research design (Flemming et al., 2019). Thematic analysis is a systematic process for

identifying and organising key themes from qualitative data (Bearman & Dawson, 2013). This approach allows the synthesis of findings into coherent themes, offering deeper insights into the research topic.

To identify the appropriate themes, the extracted data were analysed one by one. Data with similarities were grouped, and each group was assigned a theme that represented its core idea. This process resulted in the identification of six main themes: (1) Individual factors, (2) Social Influences, (3) Knowledge and Experience, (4) Technology Factors, (5) Institutional Support, and (6) Economic Factors. Subsequently, the findings within each theme were analysed again to develop sub-themes, resulting in the identification of 14 sub-themes. The process of selecting the themes was discussed and agreed upon by two researchers to ensure accuracy and validity.

RESULTS

Background of the Studies included in the Review

Before discussing the main findings, this section provides background information on the selected articles for the SLR. Among the 15 selected articles, one was published in 2019 (Jithin Das et al., 2019), three were published in 2020 (Ali et al., 2020; Chuang et al., 2020a; Chuang et al., 2020b), two in 2022 (Giua et al., 2022; Wee & Lim, 2022), six in 2023 (Acharya et al., 2023; Dixit et al., 2023; Harisudin et al., 2023; Hassan et al., 2023; Irawan et al., 2023; Kwapong et al., 2023), and the remaining three in 2024 (Erokhin et al., 2024; Isma Addi et al., 2024; Mishra et al., 2024). Figure 2 presents the year of publication of the articles.

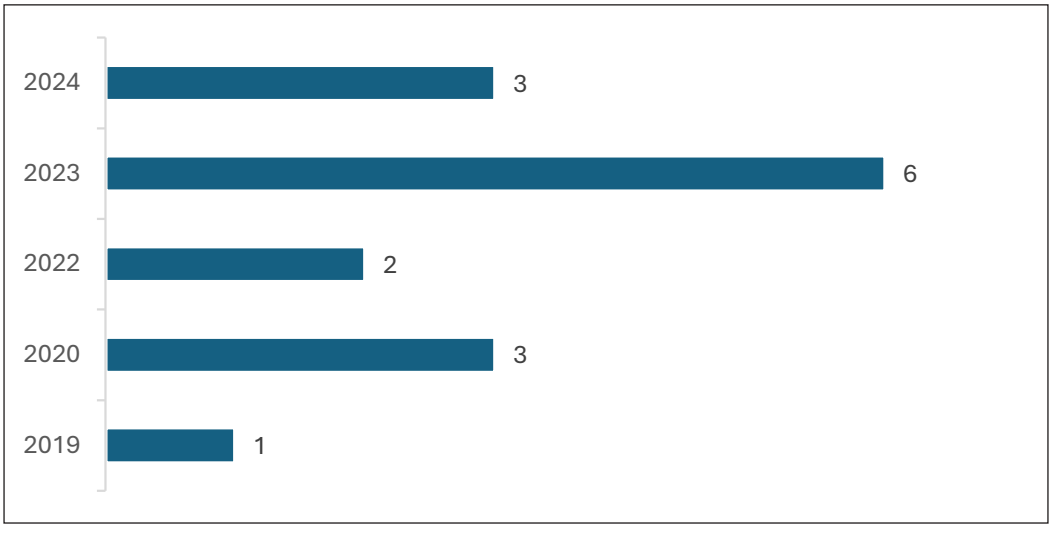

Figure 2. Year of publication

Additionally, the articles are published in various journals, including two in Technology in Society, one in Pakistan Journal of Agricultural Research (M. Ali et al., 2020), one in Agraris (Irawan et al., 2023), one in International Food and Agribusiness Management Review (Chuang et al., 2020a), one in Frontiers in Sustainable Food Systems (Kwapong et al., 2023), one in the International Journal of Environmental Research and Public Health (Chuang et al., 2020b), one in Sustainability (Switzerland) (Erokhin et al., 2024), one in PLoS One (Mishra et al., 2024), one in the International Journal of Academic Research in Business and Social Sciences (Isma Addi et al., 2024), one in AIMS Agriculture and Food (Harisudin et al., 2023), one in AgriEngineering (Jithin Das et al., 2019), one in ASEAN Journal on Science and Technology for Development (Hassan et al., 2023), and one in Journal of Agribusiness Marketing (Wee & Lim, 2022).

Out of the 15 articles, four specifically focussed on on young farmers as their respondents (Chuang et al., 2020a; Harisudin et al., 2023; Hassan et al., 2023; Irawan et al., 2023). For the remaining 11 articles, the percentage of young farmers among respondents was above 30%. Regarding the technology coverage across the 15 articles (Figure. 3), six examined the general adoption of SFTs (Chuang et al., 2020b; Dixit et al., 2023; Giua et al., 2022; Irawan et al., 2023; Mishra et al., 2024; Wee & Lim, 2022). Four articles focussed specifically on IoT adoption (Acharya et al., 2023; Chuang, Wang, & Liang, 2020; Harisudin et al., 2023; Isma Addi et al., 2024). Additionally, two articles explored Climate Smart Agriculture Technology (CSAT) adoption (Hassan et al., 2023; Kwapong et al., 2023), while one article investigated ICTs adoption (M. Ali et al., 2020). Furthermore, one article studied cloud computing adoption (Jithin Das et al., 2019), and another examined adoption of water-smart farming technologies (Erokhin et al., 2024).

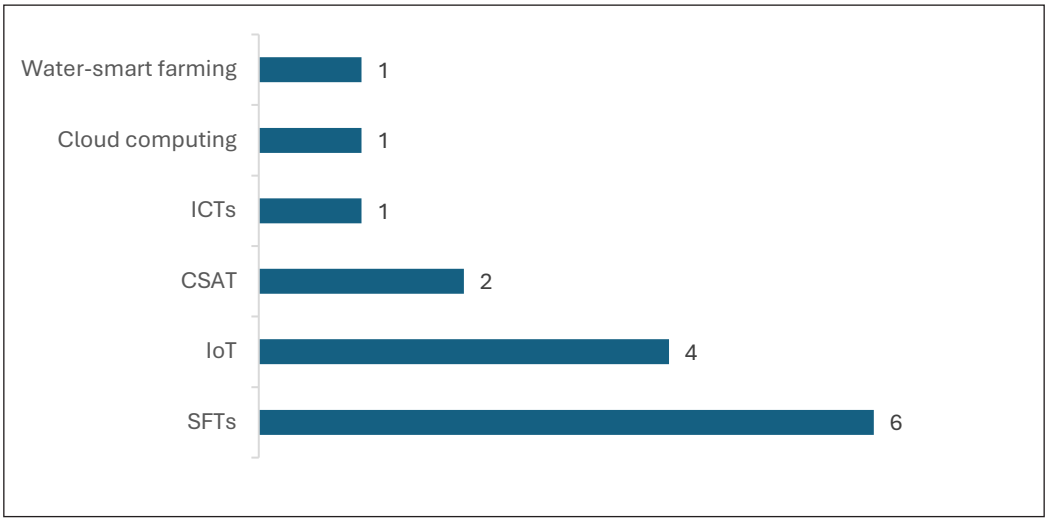

Figure 3. Technology coverage across the articles

Main Findings

In this section, the discussion synthesises the findings of the systematic literature review, highlighting six main themes influencing the adoption of SFTs among young farmers. The prominence of these themes varies significantly across the reviewed literature: Technology Factors emerged as the most frequently cited theme, supported by 12 out of 15 studies. This is followed by Individual Factors and Social Influences, each supported by 8 studies. Knowledge and Experience were supported by 7 studies, while Institutional Support and Economic Factors each received support from 4 studies. Additionally, the 14 sub-themes will also be discussed (Table 4).

Individual Factors

One of the main themes identified in this SLR is individual factors, comprise elements such as attitude, behaviour, motivation and perception. These elements play a crucial role in shaping their intention and willingness to adopt SFTs. Based on the analysis, individual factors are categorised into two sub-themes: psychological (P) and perception and belief (PB).

Psychological (P)

The adoption of SFTs among young farmers appears to be influenced by their psychological factors, supported by seven studies (Dixit et al., 2023; Erokhin et al., 2024; Isma Addi et al., 2024; Jithin Das et al., 2019; Kwapong et al., 2023; M. Ali et al., 2020). Specifically, positive attitude plays a positive role in encouraging young farmers to adopt SFTs in their farming practices. One key reason for their positive attitude is young farmers' concerns for food security and the environmental impact of farming, as emphasised by Kwapong et al. (2023). Furthermore, Isma Addi et al. (2024) found that young farmers perceive the use of IoT in agriculture as highly convenient, which positively influences their attitude. This, in turn, encourages a high level of behavioural intention to adopt IoT technologies in their agricultural practices.

Perception and Belief (PB)

PB sub-theme, derived from three studies (Irawan et al., 2023; Isma Addi et al., 2024; Mishra et al., 2024), underscores how individual worldviews shape adoption. These factors significantly affect young farmers' decisions to adopt such technologies. A study conducted by Irawan et al. (2023) revealed that young farmers believe digital farming contributes to making agriculture more sustainable, which further motivates their adoption of CSAT. Moreover, Isma Addi et al. (2024) found that young farmers believe using IoT can enhance

Table 4
Themes and sub-themes identified in the reviewed articles

Authors	Research Design	Individual Factors		Social Influences		Knowledge and Experience			Technology Factors			Institutional Support		Economic Factors	
		P	PB	IF	TSS	KA	PE	TB	PU	IA	FC	GS	OS	COE	EG
(Acharya et al., 2023)	Quantitative								/			/		/	
(M. Ali et al., 2020)	Quantitative	/		/											/
(Chuang et al., 2020a)	Quantitative				/				/				/		/
(Chuang et al., 2020b)	Quantitative					/									
(Dixit et al., 2023)	Quantitative	/							/	/		/	/		/
(Erokhin et al., 2024)	Quantitative	/				/			/						/
(Giua et al., 2022)	Quantitative			/						/					
(Harisudin et al., 2023)	Mixed method			/					/						
(Hassan et al., 2023)	Mixed method	/									/	/			/
(Irawan et al., 2023)	Mixed method		/			/		/							
(Isma Addi et al., 2024)	Quantitative	/	/			/			/						/
(Jithin Das et al., 2019)	Mixed method	/		/	/	/			/					/	/
(Kwapong et al., 2023)	Qualitative	/		/	/		/	/	/				/		/
(Mishra et al., 2024)	Quantitative		/	/					/						
(Wee & Lim, 2022)	Quantitative			/			/			/	/				

Note. "/" indicates that the corresponding theme or sub-theme was identified or reported in the article.

Individual Factors	Social Influences	Knowledge and Experience	Technology Factors	Institutional Support	Economic Factors
P = Psychological	IF = Interpersonal Factors	KA = Knowledge & Awareness	PU = Perceived Usefulness	GS = Government Support	COE = Cost and Operational Efficiency
PB = Perception & Belief	TSS = Trust & Support	PE = Practical Exposure	IA = Innovation Attribute	OS = Organisational Support	EG = Economic Gains
		TB = Technology Benefits	FC = Facilitating Conditions		

their productivity. Furthermore, Mishra et al. (2024) emphasised that young farmers with high self-efficacy are more likely to adopt agricultural technologies, demonstrating the importance of confidence in their abilities to successfully use these tools.

Social Influence

Another theme identified is social influences. The analysis categorises social influences into two sub-themes: Interpersonal Factors (IF) and Trust and Support (TSS).

Interpersonal Factors (IF)

The adoption of SFTs among young farmers is significantly influenced by IF, supported by seven studies (Giua et al., 2022; Harisudin et al., 2023; Jithin Das et al., 2019; Kwapong et al., 2023; Mishra et al., 2024; Wee & Lim, 2022). IF refer to the consideration young farmers give to others' perceptions of their actions in adopting SFTs. This also includes cases where young farmers adopt SFTs because their peers or relatives have already done so, indicating that their decisions are influenced by others' actions. Adoption is heavily influenced by social influence from peers and relatives (Giua et al. 2022; Mishra et al. 2024; Wee & Lim 2022). Technology adoption among farmers is positively influenced by active peer communication, trusted social groups, and young farmers' social interactions (Harisudin et al., 2023; Jithin Das et al., 2019; Kwapong et al., 2023).

Trust and Support (TSS)

TSS sub-theme, derived from three studies (Chuang et al., 2020a; Jithin Das et al., 2019; Kwapong et al., 2023), emphasises the importance of reliable external guidance. A study by Jithin Das et al. (2019) highlighted that Irish farmers benefit from knowledge transfer through agricultural extension services and participate in discussion groups to share information about these technologies. Similarly, research by Kwapong et al. (2023) found that young farmers place confidence in the information provided by the agricultural extension agents. Furthermore, Chuang et al. (2020a) emphasised that a sense of trust is a crucial factor that encourages young farmers to adopt IoT-based technologies.

Knowledge and Experience

Individuals with knowledge and experience are more confident in adopting SFTs. Therefore, knowledge and experience are one of the themes identified in this SLR. This theme is divided into three sub-themes: Knowledge and Awareness (KA), Practical Exposure (PE) and Technology Benefits (TB:).

Knowledge and Awareness (KA)

KA sub-theme, supported by four studies (Chuang et al., 2020b; Erokhin et al., 2024; Irawan et al., 2023; Isma Addi et al., 2024; Jithin Das et al., 2019), reveals that a high level of knowledge about SFTs and their applications significantly increases the likelihood of adoption. Farmers who actively seek information through digital platforms (Jithin Das et al., 2019) and have a strong knowledge of smart agriculture, show higher adoption rates (Chuang et al., 2020b; Isma Addi et al., 2024). Specific knowledge, such as acknowledging the need to reduce water waste, can also directly motivate the adoption of targeted technologies like water-smart systems (Erokhin et al., 2024).

Practical Exposure (PE)

PE sub-theme highlights that hands-on experience with technologies plays a crucial role in building young farmers' confidence to adopt SFTs. According to Kwapong et al. (2023), young farmers often start by experimenting with the technologies on a small scale first, then once they confirm the innovation was beneficial, they gradually scale up its implementation across their entire farm. Similarly, Wee & Lim (2022) found that practical exposure serves as the initial step toward developing the behavioural intention to adopt SFTs.

Technology Benefit (TB)

The sub-theme of TB explores young farmers' knowledge and understanding of the benefits SFTs. Young farmers who have a high level of understanding of these technology benefits are more likely to adopt SFTs in their farming practices. A study by Kwapong et al. (2023) found that young farmers' willingness to adopt CSAT was driven by their desire to increase yields, soil fertility and conserve water for plant use. Additionally, Irawan et al. (2023) highlighted that young farmers' understanding of the benefits and outcomes of digital farming practices strongly influences their adoption decision.

Technology Factors

Technological factors become another key theme in this SLR. These technological factors include the ease of use, the benefits to users, and the innovation in technology itself. There are three sub-themes under this theme: Perceived Usefulness (PU), Innovation Attribution (IA) and Facilitating Conditions (FC).

Perceived Usefulness (PU)

PU sub-theme is a dominant predictor in SFTs adoption, supported by nine studies (Acharya et al., 2023; Chuang et al., 2020a; Dixit et al., 2023; Erokhin et al., 2024; Harisudin et

al., 2023; Isma Addi et al., 2024; Jithin Das et al., 2019; Kwapong et al., 2023; Mishra et al., 2024). Nine out of fifteen articles identified perceived usefulness as one of the factors influencing young farmers to adopt SFTs. This sub-theme aggregates perceived usefulness, ease of use, and relative advantage. This indicates that young farmers are more likely to adopt SFTs when the technologies contribute to simplifying and easing their farming activities (Jithin Das et al., 2019; Kwapong et al., 2023), contribute to agricultural production and field management (Chuang et al., 2020a) and easy to handle (Acharya et al., 2023; Dixit et al., 2023; Isma Addi et al., 2024; Mishra et al., 2024). The relative advantage, such as increased productivity at a lower cost, is a significant motivator, driving an openness to change (Dixit et al., 2023; Harisudin et al., 2023).

Innovation Attribution (IA)

IA sub-theme, including characteristics such as compatibility, technological complexity and performance expectancy, as identified across three studies (Dixit et al., 2023; Giua et al., 2022; Wee & Lim, 2022). SFTs that are compatible with existing farming techniques encourage adoption among young farmers (Dixit et al., 2023). Furthermore, performance expectancy, what the technology is expected to achieve, has been identified as a key driver of adoption intention (Giua et al., 2022; Wee & Lim, 2022).

Facilitating Conditions (FC)

FC sub-theme, supported by two studies (Hassan et al., 2023; Wee & Lim, 2022), refers to the necessary infrastructure and resources, such as internet access and necessary skills. These technological aspects are crucial in encouraging young farmers to adopt advanced technologies. According to Hassan et al. (2023), the technology dimension of FC, which includes the perceived benefits that address farmers' needs and the ease of implementation, significantly encourages young farmers' intention to adopt CSAT. Furthermore, Wee & Lim (2022) found that FC are the factor driving young farmers' behavioural intention to adopt SFTs.

Institutional Support

Adopting a technology requires consideration of multiple factors, therefore, support from related institutions is necessary. As a result, institutional support becomes another main theme. The sub-themes under institutional support are government support (GS) and organisational support (OS).

Government Support (GS)

GS sub-theme, supported by three articles (Acharya et al., 2023; Dixit et al., 2023; Hassan et al., 2023), is crucial for enhancing young farmers' confidence. This aligns with the findings of Hassan et al. (2023), who stated that youth are motivated to adopt CSAT with government support such as technology rental, access to land and infrastructure. Such support reassures them when facing any challenges in adopting the technology. Similarly, Dixit et al. (2023) emphasised that government support significantly influences the adoption of SFTs. In addition, Acharya et al. (2023) highlighted that the government should equip young farmers with sufficient knowledge and training on the technical aspects of SFTs, as well as provide standardised guidelines and frameworks for the adoption of SFTs.

Organisational Support (OS)

OS sub-theme, also derived from three articles (Chuang et al., 2020a; Dixit et al., 2023; Kwapong et al., 2023), centres primarily on the role of the Department of Agriculture and Agricultural Extension. Effective communication between extension officers and farmers positively influences adoption (Dixit et al., 2023). The active involvement of extension officers in meetings and field demonstrations is essential for transferring knowledge and information about SFTs (Kwapong et al., 2023), and this support is a significant factor in adoption decisions (Chuang et al., 2020a).

Economic Factors

Technology adoption involves financial considerations, including initial costs, ongoing expenses and maintenance fees. The financial aspects, such as the cost of technology implementation and the expected economic returns, impact their willingness to invest in these technologies. This theme is categorised into two sub-themes: Cost and Operational Efficiency (COE) and Economic Gains (EG).

Cost and Operational Efficiency (COE)

COE sub-theme, supported by three articles (Acharya et al., 2023; Jithin Das et al., 2019; Kwapong et al., 2023), presents a contradicting finding based on adoption status. For non-adopters, high costs are a major barrier to embracing new technologies (Jithin Das et al., 2019), and young farmers are more likely to adopt with a lower initial cost (Kwapong et al., 2023). However, adopters acknowledge that while the initial investment is high, the long-term operational efficiency and financial returns make it a worthwhile and profitable decision (Jithin Das et al., 2019; Kwapong et al., 2023).

Economic Gains (EG)

EG sub-theme, supported by three articles (Chuang et al., 2020a; Hassan et al., 2023; Jithin Das et al., 2019), highlights that anticipated returns are a primary concern given the high financial investment required. Jithin Das et al. (2019) highlighted that young farmers are willing to adopt a cloud computing system if they perceive the technology as profitable. Additionally, Chuang et al. (2020a) found that high average annual turnover increases young farmers' willingness to invest in SFTs. Furthermore, Hassan et al. (2023) emphasised that the economic dimension is a strong motivation for adoption. Young farmers, specifically those concerned about employment opportunities, view SFTs as capable of creating new jobs and enhancing financial stability.

DISCUSSION

This SLR has identified six main themes (individual factors, social influences, knowledge and experience, technology factors, institutional support, and economic factors) influencing the adoption of SFTs among young farmers. Each theme consists of various sub-themes, indicating that adoption decisions are shaped by a combination of psychological, technological, and structural conditions. The strongest factor is PU, followed by psychological, interpersonal factors, and knowledge. Additionally, economic factors, particularly the cost of adoption, are discussed as a barrier that hinders young farmers from integrating these technologies.

Among all the identified factors, PU is the strongest determinant influencing the adoption of SFTs among young farmers. Almost all the reviewed articles in this SLR emphasise the significance of PU, indicating that young farmers are more inclined to adopt SFTs when they perceive them as beneficial and capable of enhancing their farming practices (Acharya et al., 2023; Chuang et al., 2020a; Dixit et al., 2023; Erokhin et al., 2024; Harisudin et al., 2023; Isma Addi et al., 2024; Jithin Das et al., 2019; Kwapong et al., 2023; Mishra et al., 2024). These findings align with the Technology Acceptance Model (TAM), which highlights the crucial role of perceived usefulness in technology adoption.

Furthermore, TAM also posits that perceived ease of use influences the intention to use technology. However, in this SLR, only Dixit et al. (2023) highlighted perceived ease of use as a significant factor affecting young farmers' decisions. This suggests that young farmers prioritise the actual benefits of SFTs over their ease of use. However, studies outside this SLR, such as Kamrath et al. (2018) and El Bilali et al. (2021), also support the principles of TAM. Their findings indicate that both perceived usefulness and perceived ease of use influence technology adoption, suggesting that individuals are more likely to adopt technology that is both effective and easy to use.

Psychological factors are the second most frequently discussed in the articles selected for this SLR. Among these, young farmers' attitude towards SFTs stands out as a key

motivator. However, these attitudes stem from various motivations: environmental concerns (Erokhin et al., 2024; Kwapong et al., 2023), anticipated long-term profitability (Dixit et al., 2023; Jithin Das et al., 2019), and the alignment of SFTs with sustainable farming practices. While TPB suggests that positive attitudes should translate into intention and behaviour (Ajzen, 1991), many studies examine attitude or intention only, without assessing actual adoption behaviour (Ali et al., 2023; Erokhin et al., 2024). Similar emphasis on psychological factors by Cui and Wang (2023) is found in reviews of general farmers in China, but the evidence remains limited for the young farmers population.

To encourage SFTs adoption, government and industry stakeholders must highlight the benefits of these technologies through targeted training programs, demonstrations and guidance on their operation. These initiatives not only shape a positive attitude but also enhance young farmers' knowledge, increasing their confidence to adopt SFTs. This is relevant as knowledge and experience have been identified as factors influencing their willingness to adopt. Additional studies support that higher knowledge and understanding of technology will increase an individual's willingness to adopt innovations (Kwakye et al., 2021; Osei et al., 2022; Zhang & Zhu, 2023).

Social influence also plays a crucial role in influencing the willingness of young farmers to adopt SFTs. These factors include interpersonal interactions, external perception, and trust. Moreover, trust and relationship with the external expert further enhance young farmers' confidence in adopting SFTs (Jithin Das et al., 2019; Kwapong et al., 2023). These findings suggest that, beyond individuals' motivation, social factors also play a role in reinforcing young farmers' confidence in adopting SFTs. Therefore, the government or companies providing SFTs should highlight success stories of adopters who have effectively implemented these technologies to inspire and encourage wider adoption among non-adopters.

Economic factors play a decisive role in young farmers' adoption of SFTs because these technologies require high upfront investment, which many young farmers cannot afford due to limited capital. Although cost is widely reported as a major barrier (Jithin Das et al., 2019), this reluctance also reflects uncertainty about financial returns. Notably, several studies show that adopters do experience long-term economic benefits once they begin using SFTs (Chuang et al., 2020a; Kwapong et al., 2023), suggesting a gap between perceived and actual value. This indicates that the challenge is not only affordability but also limited financial knowledge and confidence in managing investment risk. Therefore, financial support mechanisms such as subsidies or rental schemes should be complemented with financial education to help young farmers evaluate long-term returns and view SFTs as viable investments rather than financial burdens.

The findings of this review generally align with earlier SLRs (Cui & Wang, 2023; Thomas et al., 2023), emphasising the central role of PU and the influence of economic, social, and knowledge-related factors. Yet, several patterns are uniquely pronounced among young farmers: ease of use is less influential and financial barriers are more restrictive. These observations highlight the value of considering youth-specific contexts when applying technology adoption frameworks, suggesting that existing models may benefit from adjustments to better capture the motivations and constraints of younger farmers.

CONCLUSION

In conclusion, this SLR on the adoption of SFTs among young farmers provides an understanding of the factors influencing their adoption. A key contribution of this review is the identification and synthesis of six major themes and 14 sub-themes, offering a more structured and comprehensive categorization of adoption determinants. This SLR contributes to young farmers' focussed perspectives, who play a crucial role in sustaining future crop production systems. The review also contributes to the field by highlighting technological factors, particularly PU, as the most influential factors across the studies reviewed (12 studies). In contrast, economic factors and institutional support were found to be the least explored (4 studies each), despite being well-recognised barriers for young farmers. This imbalance indicates a gap in existing research and underscores the need for future empirical studies to examine economic constraints more rigorously, given their potential to directly hinder SFTs' adoption.

Therefore, policies or interventions should be designed to specifically encourage the adoption of SFTs among young farmers. Initiatives that enhance young farmers' exposure to the tangible benefits of SFTs, such as demonstrations and training programs, may significantly improve adoption rates. Furthermore, targeted financial supports, such as subsidies, rental schemes and low-interest loans, with stronger institutional support, are essential to reduce the upfront financial burden that affects young farmers. Additionally, highlighting how these technologies contribute to sustainable and efficient farming practices can strengthen the alignment with young farmers' values and encourage their sustained commitment to sustainable agriculture.

This study recommends that future research focus specifically on young farmers to better understand their motivations and decision-making in adopting SFTs, particularly related to the agriculture sector. Further studies should also examine key barriers to adoption among young farmers, including individual, social, technological, institutional, knowledge, and economic factors. Additionally, future research should conduct region- or country-specific comparisons, as SFT adoption patterns and influencing factors may vary across different geographical contexts.

ACKNOWLEDGEMENT

This research was supported by the Putra IPM Grant (GP-IPM/2023/9769800), Universiti Putra Malaysia (UPM). The authors would like to express their sincere gratitude for the financial support provided, which made this study possible.

REFERENCES

Abbasi, R., Martinez, P., & Ahmad, R. (2022). The digitisation of agricultural industry – a systematic literature review on agriculture 4.0. *Smart Agricultural Technology, 2*, 100042. https://doi.org/10.1016/j.atech.2022.100042

Acharya, U., Kate, N., Ramaprasad, B. S., & Srivastava, A. (2023). The adoption of smart agriculture technologies based on the perception of the farmers in the Indian context. *2023 2nd International Conference on Smart Technologies for Smart Nation (SmartTechCon)*, (pp. 586-593). https://doi.org/10.1109/SmartTechCon57526.2023.10391525

Ajzen, I. (1991). The theory of planned behaviour. *Organisational Behaviour and Human Decision Processes, 50*(2), 179-211. https://doi.org/10.1016/0749-5978(91)90020-T

Ali, M., Man, N., Muharam, F. M., & Omar, S. Z. (2020). Factors influencing behavioral intention of farmers to use ICTs for agricultural risk management in Malaysia. *Pakistan Journal of Agricultural Research, 33*(2), 295-302. https://doi.org/10.17582/journal.pjar/2020/33.2.295.302

Ali, Md. A., Dhanaraj, R. K., & Nayyar, A. (2023). A high performance-oriented AI-enabled IoT-based pest detection system using sound analytics in large agricultural field. *Microprocessors and Microsystems, 103*, 104946. https://doi.org/https://doi.org/10.1016/j.micpro.2023.104946

Alotaibi, M. (2023). Climate change, its impact on crop production, challenges, and possible solutions. *Notulae Botanicae Horti Agrobotanici Cluj-Napoca, 51*(1), 13020. https://doi.org/10.15835/NBHA51113020

Bashiru, M., Ouedraogo, M., Ouedraogo, A., & Läderach, P. (2024). Smart farming technologies for sustainable agriculture: A review of the promotion and adoption strategies by smallholders in Sub-Saharan Africa. *Sustainability, 16*(11), Article 4817. https://doi.org/10.3390/su16114817

Bearman, M., & Dawson, P. (2013). Qualitative synthesis and systematic review in health professions education. *Medical Education, 47*(3), 252-260. https://doi.org/10.1111/medu.12092

Burnham, J. F. (2006). Scopus database: A review. *Biomedical Digital Libraries, 3*, Article 1. https://doi.org/10.1186/1742-5581-3-1

Chuang, J.-H., Wang, J.-H., & Liang, C. (2020). Implementation of Internet of Things depends on intention: Young farmers' willingness to accept innovative technology. *International Food and Agribusiness Management Review, 23*(2), 253-266. https://doi.org/10.22434/IFAMR2019.0121

Chuang, J.-H., Wang, J.-H., & Yu-Chang, L. (2020). Farmers' knowledge, attitude, and adoption of smart agriculture technology in Taiwan. *International Journal of Environmental Research and Public Health, 17*(19), 7236. https://doi.org/https://doi.org/10.3390/ijerph17197236

Cui, L., & Wang, W. (2023). Factors affecting the adoption of digital technology by farmers in China: A systematic literature review. *Sustainability, 15*(20), 14824. https://doi.org/10.3390/su152014824

Dias, J. P., Restivo, A., & Ferreira, H. S. (2022). Designing and constructing Internet of Things systems: An overview of the ecosystem. *Internet of Things, 19*, 100529. https://doi.org/10.1016/J.IOT.2022.100529

Dixit, K., Aashish, K., & Kumar Dwivedi, A. (2023). Antecedents of smart farming adoption to mitigate the digital divide – extended innovation diffusion model. *Technology in Society, 75*, 102348. https://doi.org/https://doi.org/10.1016/j.techsoc.2023.102348

Erokhin, V., Mouloudj, K., Bouarar, A. C., Mouloudj, S., & Gao, T. (2024). Investigating farmers' intentions to reduce water waste through water-smart farming technologies. *Sustainability, 16*(11), 4638. https://doi.org/https://doi.org/10.3390/su16114638

Flemming, K., Booth, A., Garside, R., Tunçalp, Ö., & Noyes, J. (2019). Qualitative evidence synthesis for complex interventions and guideline development: clarification of the purpose, designs and relevant methods. *BMJ Global Health, 4*(Suppl 1), e000882. https://doi.org/10.1136/bmjgh-2018-000882

Giua, C., Materia, V. C., & Camanzi, L. (2022). Smart farming technologies adoption: Which factors play a role in the digital transition? *Technology in Society, 68*, 101869. https://doi.org/https://doi.org/10.1016/j.techsoc.2022.101869

Haddaway, N. R., Page, M. J., Pritchard, C. C., & McGuinness, L. A. (2022). PRISMA2020: An R package and Shiny app for producing PRISMA 2020-compliant flow diagrams, with interactivity for optimised digital transparency and Open Synthesis. *Campbell Systematic Reviews, 18*(2). https://doi.org/10.1002/cl2.1230

Hadi Suzer, M., Şenbayram, M., & Ali Çullu, M. (2024). Sustainable farming through precision agriculture: Enhancing nitrogen use and weed management. *IntechOpen*. https://doi.org/10.5772/intechopen.114256

Harisudin, M., Kusnandar, Riptanti, E. W., Setyowati, N., & Khomah, I. (2023). Determinants of the Internet of Things adoption by millennial farmers. *AIMS Agriculture and Food, 8*(2), 329–342. https://doi.org/10.3934/AGRFOOD.2023018

Hassan, R., Suhaili, W. S., Nore, B. F., & Basunia, M. A. (2023). Youth resilience toward climate smart agriculture technology adoption in Brunei Darussalam. *ASEAN Journal on Science and Technology for Development, 40*(3), 195-202. https://doi.org/10.61931/2224-9028.1545

Irawan, N. C., Mulyo, J. H., & Suryantini, A. (2023). Unleashing the power of digital farming: Local young farmers' perspectives on sustainable value creation. *Agraris, 9*(2), 316-333. https://doi.org/10.18196/agraris.v9i2.239

Isma Addi, J., Mohamad Alias, M. R., Fauzan, F., Ismail, A. F. @ M. F., Widjajanti, K., Kurnianingrum, D., & Karmagatri, M. (2024). Awareness and acceptance of the Internet of Things (IOT) among agropreneurs. *International Journal of Academic Research in Business and Social Sciences, 14*(9). https://doi.org/10.6007/IJARBSS/v14-i9/22699

Jaafar, N. R. N., Bahar, N., Ibrahim, N., Baharudin, A., Ismail, W. S. W., Sim, S. T., Aziz, M. A., & Tan, K. A. (2021). Are Malaysian youths overdependent on the internet?: A narrative review. *Frontiers in Psychiatry, 12*, Article 710790. https://doi.org/10.3389/fpsyt.2021.710790

Jithin Das, V., Sharma, S., & Kaushik, A. (2019). Views of Irish farmers on smart farming technologies: An observational study. *AgriEngineering, 1*(2), 164-187. https://doi.org/10.3390/agriengineering1020013

Kwakye, B. D., Brenya, R., Cudjoe, D. A., Sampene, A. K., & Agyeman, F. O. (2021). Agriculture technology as a tool to influence youth farming in Ghana. *Open Journal of Applied Sciences, 11*(08), 885-898. https://doi.org/10.4236/ojapps.2021.118065

Kwapong, N. A., Whitfield, S., Ambuko, J., Ankrah, D. A., & Swanepoel, F. (2023). Using participatory videos in understanding farmers experiences with climate smart agricultural practices: reflections from Ghana. *Frontiers in Sustainable Food Systems, 7,* Article 1282993. https://doi.org/10.3389/fsufs.2023.1282993

Lame, G. (2019). Systematic literature reviews: An introduction. In *Proceedings of the International Conference on Engineering Design (ICED 2019)* (pp. 1633-1642). https://doi.org/10.1017/dsi.2019.169

Mishra, N., Bhandari, N., Maraseni, T., Devkota, N., Khanal, G., Bhusal, B., Basyal, D. K., Paudel, U. R., & Danuwar, R. K. (2024). Technology in farming: Unleashing farmers' behavioural intention for the adoption of agriculture 5.0. *PLoS One, 19*(8), e0308883. https://doi.org/https://doi.org/10.1371/journal.pone.0308883

Mohamed Shaffril, H. A., Ahmad, N., Samsuddin, S. F., Samah, A. A., & Hamdan, M. E. (2020). Systematic literature review on adaptation towards climate change impacts among indigenous people in the Asia Pacific regions. *Journal of Cleaner Production, 258*, 120595. https://doi.org/10.1016/j.jclepro.2020.120595

Mohamed Shaffril, H. A., Samah, A. A., Samsuddin, S. F., & Ali, Z. (2019). Mirror-mirror on the wall, what climate change adaptation strategies are practiced by the Asian's fishermen of all? *Journal of Cleaner Production, 232*, 104-117. https://doi.org/10.1016/j.jclepro.2019.05.262

Mohamed Shaffril, H. A., Samsuddin, S. F., & Abu Samah, A. (2021). The ABC of systematic literature review: the basic methodological guidance for beginners. *Quality & Quantity, 55*(4), 1319-1346. https://doi.org/10.1007/s11135-020-01059-6

Omar, S. (2021). Internet of Things (IoT) for smart farming: A systematic review. *International Journal of Computer Applications, 174*(27), 47-54. https://doi.org/10.5120/ijca2021921182

Osabohien, R. (2023). ICT adoption and youth employment in Nigeria's agricultural sector. *African Journal of Economic and Management Studies*, Advance online publication. https://doi.org/10.1108/AJEMS-03-2022-0111

Osei, R., Adusei-Antwi, J., Gyabaah, V., & Yeboah, R. A. (2022). Assessing youth perceptions and knowledge of modern agriculture: A case of youth in Tano North municipality of Ahafo. *International Journal of All Research Writings, 5*(7).

Pace, R., Pluye, P., Bartlett, G., Macaulay, A. C., Salsberg, J., Jagosh, J., & Seller, R. (2012). Testing the reliability and efficiency of the pilot Mixed Methods Appraisal Tool (MMAT) for systematic mixed studies review. *International Journal of Nursing Studies, 49*(1), 47-53. https://doi.org/10.1016/j.ijnurstu.2011.07.002

Page, M. J., McKenzie, J. E., Bossuyt, P. M., Boutron, I., Hoffmann, T. C., Mulrow, C. D., Shamseer, L., Tetzlaff, J. M., Akl, E. A., Brennan, S. E., Chou, R., Glanville, J., Grimshaw, J. M., Hróbjartsson, A., Lalu, M. M., Li, T., Loder, E. W., Mayo-Wilson, E., McDonald, S., … Moher, D. (2021). The PRISMA 2020 statement: An updated guideline for reporting systematic reviews. *International Journal of Surgery, 88,* 105906. https://doi.org/10.1016/j.ijsu.2021.105906

Petticrew, M., & Roberts, H. (2006). *Systematic reviews in the social sciences: A practical guide.* Blackwell Publishing.

Sharma, P., Sharma, P., & Thakur, N. (2024). Sustainable farming practices and soil health: a pathway to achieving SDGs and future prospects. *Discover Sustainability, 5*(1), 250. https://doi.org/10.1007/s43621-024-00447-4

Talaviya, T., Shah, D., Patel, N., Yagnik, H., & Shah, M. (2020). Implementation of artificial intelligence in agriculture for optimisation of irrigation and application of pesticides and herbicides. *Artificial Intelligence in Agriculture, 4*, 58-73. https://doi.org/10.1016/j.aiia.2020.04.002

Thomas, R. J., O'Hare, G., & Coyle, D. (2023). Understanding technology acceptance in smart agriculture: A systematic review of empirical research in crop production. *Technological Forecasting and Social Change, 189*, 122374. https://doi.org/10.1016/J.TECHFORE.2023.122374

Wee, G. W. E., & Lim, A. S. S. (2022). Factors influencing the behavioural intention for smart farming in Sarawak, Malaysia. *Journal of Agribusiness Marketing, 9*(1), 37-56. https://doi.org/10.56527/jabm.9.1.4

Wee, G. W. E., & Ting, I. S. H. (2023). Development of smart farming technologies in Malaysia: Insights from bibliometric analysis. *Journal of Agribusiness Marketing, 10*(1). https://doi.org/10.56527/fama.jabm.10.1.3

Yoe, H. (2017). Smart farming: ICT based agriculture (Keynote address). In *2017 18th International Conference on Software Engineering, Artificial Intelligence, Networking and Parallel/Distributed Computing (SNPD)* (p. 3). https://doi.org/10.1109/SNPD.2017.8022651

Zaman, N. B. K., Raof, W. N. A. A., Saili, A. R., Aziz, N. N., Fatah, F. A., & Vaiappuri, S. K. N. (2023). Adoption of smart farming technology among rice farmers. *Journal of Advanced Research in Applied Sciences and Engineering Technology, 29*(2), 268-275. https://doi.org/10.37934/araset.29.2.268275

Zhang, Z., & Zhu, L. (2023). A review on unmanned aerial vehicle remote sensing: Platforms, sensors, data processing methods, and applications. *Drones, 7*(6), 398. https://doi.org/10.3390/drones7060398

REFEREES FOR THE PERTANIKA
JOURNAL OF TROPICAL AGRICULTURAL SCIENCE

Vol. 49 (S1) 2026

The Editorial Board of the Pertanika Journal of Tropical Agricultural Science wishes to thank the following:

Aida Safina Aridi
(UTHM, Malaysia)

Aimi Athirah Aznan
(UNIMAP, Malaysia)

Bernard Maringgal
(UNIMAS, Malaysia)

Darius El Pebrian
(UiTM, Malaysia)

Dayang Norulfairuz Abang Zaidel
(UTM, Malaysia)

Mariam Firdaus Mad Nordin
(UTM, Malaysia)

Mohammad Effendy Ya'acob
(UPM, Malaysia)

Ngadisih Ngadisih
(UGM, Indonesia)

Noor Akhmazillah Mohd Fauzi
(UTHM, Malaysia)

Norliza Abd.Rahman
(UKM, Malaysia)

Nurul Aqilah Mohd Zaini
(UKM, Malaysia)

Nur Huda Faujan
(USIM, Malaysia)

Nurfatimah Mohd Thani
(UKM, Malaysia)

Rashidah Ruslan
(UNIMAP, Malaysia)

Shamsul Anuar
(UPM, Malaysia)

Siti Amni Ismail
(UiTM, Malaysia)

Zurina Zainal Abidin
(UPM, Malaysia)

UiTM - *Universiti Teknologi Mara*
UKM - *Universiti Kebangsaan Malaysia*
USIM - *Universiti Sains Islam Malaysia*
UTHM - *Universiti Tun Hussein Onn Malaysia*
UGM - *Universitas Gadjah Mada*
UPM - *Universiti Putra Malaysia*
UNIMAP - *Universiti Malaysia Perlis*
UNIMAS - *Universiti Malaysia Sarawak*
UTM - *Universiti Teknologi Malaysia*

While every effort has been made to include a complete list of referees for the period stated above, however if any name(s) have been omitted unintentionally or spelt incorrectly, please notify the Chief Executive Editor, *Pertanika* Journals at executive_editor.pertanika@upm.edu.my

Any inclusion or exclusion of name(s) on this page does not commit the *Pertanika* Editorial Office, nor the UPM Press Centre or the university to provide any liability for whatsoever reason.

Pertanika Journal of Tropical Agricultural Science
Vol. 49 (S1) 2026

Content

Pertanika Editorial Office, Journal Division,
Putra Science Park,
1st Floor, IDEA Tower II,
UPM-MTDC Center,
Universiti Putra Malaysia,
43400 UPM Serdang,
Selangor Darul Ehsan
Malaysia

http://www.pertanika.upm.edu.my
Email: executive_editor.pertanika@upm.edu.my
Tel. No.: +603- 9769 1622

http://penerbit.upm.edu.my
Email: penerbit@upm.edu.my
Tel. No.: +603- 9769 8855

e-ISSN 2231-8542